Physics Reports 843 (2020) 1–81

Contents lists available at ScienceDirect

Physics Reports

journal homepage: www.elsevier.com/locate/physrep

A review of recent advances in thermophysical properties at the nanoscale: From solid state to colloids

Lin Qiu [a,b], Ning Zhu [a], Yanhui Feng [a,*], Efstathios E. Michaelides [c], Gaweł Żyła [d], Dengwei Jing [e], Xinxin Zhang [a], Pamela M. Norris [b], Christos N. Markides [f], Omid Mahian [g,*]

[a] School of Energy and Environmental Engineering, University of Science and Technology Beijing, Beijing 100083, China
[b] Department of Mechanical and Aerospace Engineering, University of Virginia, Charlottesville, VA, 22904-4746, USA
[c] Department of Engineering, Texas Christian University, Fort Worth, TX 76129, USA
[d] Department of Physics and Medical Engineering, Rzeszów University of Technology, 35-959 Rzeszów, Poland
[e] International Research Center for Renewable Energy, Xi'an Jiaotong University, Xi'an, Shanxi 710049, China
[f] Clean Energy Processes (CEP) Laboratory, Department of Chemical Engineering, Imperial College London, London SW7 2AZ, UK
[g] School of Chemical Engineering and Technology, Xi'an Jiaotong University, Xi'an, Shanxi 710049, China

ARTICLE INFO

Article history:
Received 5 December 2019
Accepted 5 December 2019
Available online 12 December 2019
Editor: I. Procaccia

Keywords:
Nanomaterial
Colloids
Solid state
Thermophysical properties
Data mining

ABSTRACT

Nanomaterials possess superior optical, electrical, magnetic, mechanical, and thermal properties, which have made them suitable for a multitude of applications. The present review paper deals with recent advances in the measurement and modeling of thermophysical properties at the nanoscale (from the solid state to colloids). For this purpose, first, various techniques for the measurement of the solid state properties, including thermal conductivity, thermal diffusivity, and specific heat capacity, are introduced. The main factors that affect the solid state properties are grain size, grain boundaries, surface interactions, doping, and temperature, which are discussed in detail. After that, methods for the measurement and modeling of thermophysical properties of colloids (nanofluids), including thermal conductivity, dynamic viscosity, specific heat capacity, and density, are presented. The main parameters affecting these properties, such as size, shape, and concentration of nanoparticles, aggregation, and sonication time are studied. Furthermore, the properties of not only simple nanofluids but also hybrid nanofluids (which are composed of more than one type of nanoparticles) are investigated. Finally, the main research gaps and challenges are listed.

Contents

* Corresponding authors.
E-mail addresses: yhfeng@me.ustb.edu.cn (Y. Feng), omid.mahian@xjtu.edu.cn (O. Mahian).

https://doi.org/10.1016/j.physrep.2019.12.001

1. Introduction

1.1. Nanotechnology background

To understand the unique specifications of nanomaterials, it is best to begin with the origins of nanotechnology. In 1959, a new concept-nanotechnology was first proposed by Nobel award winner physicist Richard Feynman. Then, in 1981, the atomic cluster was first observed by scanning tunneling microscopy, which marked the birth of nanotechnology. In 1991, carbon nanotubes (CNTs) were first discovered by Iijima [1]. Since then, the study of thermal, electrical and mechanical properties of CNTs has become a hot spot in the nanotechnology field. It is believed that the most promising nano-based technologies in the current century will be the results of multi-disciplinary efforts involving physics, nanobiology, nanochemistry, nanoelectronics, nanofabrication, nanomechanics, engineering technology and medical science, etc. [2–4]. Therefore, the first and foremost challenge at this stage is to create more novel nanomaterials and devices with a wide range of applications, such as nanomedicine, nano-generator and nanoelectronics. With the introduction of the seminal idea of nanotechnology, nanomaterials that render unique specifications compared with traditional engineered materials have attracted great attention. Nanomaterials are defined as materials with at least one dimension at the nanoscale. At present, the research on nanotechnology mainly involves nanomaterial preparation and performance characterization for applications in microelectronics and computer technology, medical and health technology, aerospace, energy and the environment, biotechnology and agriculture. Nowadays, researchers are working on modifying the properties of nanomaterials to adopt them for utilizing in various fields.

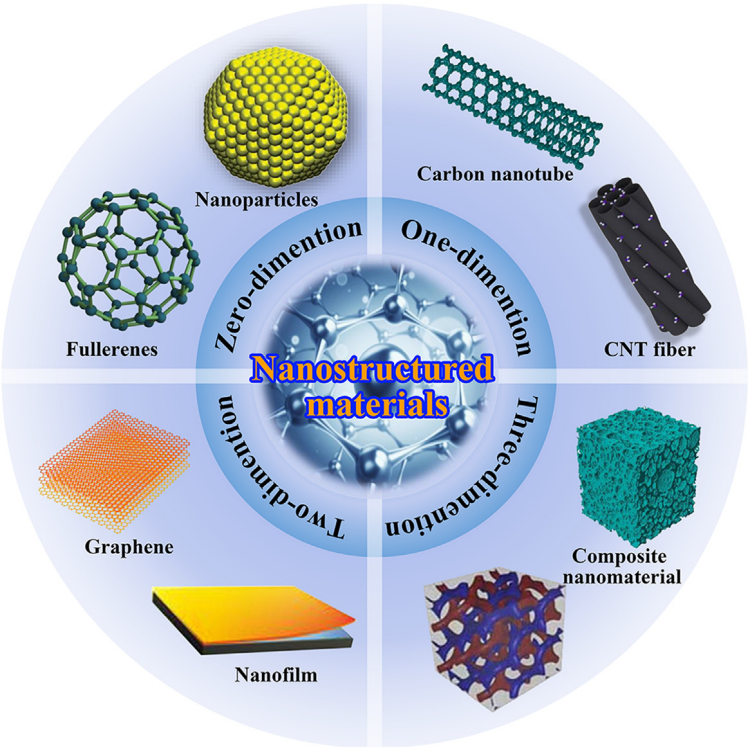

Fig. 1. Schematic diagram of solid nanostructured materials with different dimensions [5–7].
Source: Reprinted with permission from Elsevier and Royal Society of Chemistry.

1.2. What are solid and colloidal nanostructured materials?

Solid nanostructured materials are the most common nanomaterials. They can be roughly classified into four groups according to their appearance: powder, fiber, film, and bulk. According to the dimensions, nanomaterials are divided into:
(i) Zero-dimensional (0-D) nanostructures, which have all three dimensions on the nanometer length scale, such as nanoparticles (NPs) and fullerenes;
(ii) One-dimensional (1-D) nanostructures, which only have one dimension at the nanoscale, such as nanowires, nanofibers and nanotubes;
(iii) Two-dimensional (2-D) nanostructures, which have two dimensions at the nanoscale, such as graphene and nanofilms; and
(iv) Three-dimensional (3-D) nanomaterials, also known as bulk nanomaterials, which have the characteristics of nanomaterials, such as composite nanomaterials, nanocrystalline (NC) materials.

Fig. 1 presents the classification of nanostructured materials in solid state.

In thermal systems such as heat exchangers which are used in various applications such as car radiators or cooling of electronic devices, the working fluid plays a vital role as the heat carrier. If the working fluid has not possessed adequate capabilities for heating or cooling of the thermal equipment, the equipment may be severely damaged. One approach for modifying the potential of conventional liquids is the addition of solid nanoparticles to increase the liquids effective thermal conductivity (k_{eff}). In practice, the research on nanofluids has begun in 1993 when a report was published on the thermal conductivity (k) and dynamic viscosity (μ) of water-based suspensions containing Al_2O_3, TiO_2, and SiO_2 particles with sizes in the range of 1–100 nm [8]. However, the term "nanofluid" was first introduced by Choi in 1995 [9]. A colloidal suspension consisting of one type of nanoparticle and a conventional liquid such as water is called a simple (or mono) nanofluid. In contrast, hybrid nanofluids are composed of more than one type of nanoparticles into a base fluid. Ceramic nanofluids are an example of one of the simple nanofluids prepared by the Argonne National Laboratory (ANL) group. Soon afterwards, the emergence of metal-based nanofluids marked a new step in the field of nanofluid. For this first time, Xuan and Li [10] used a metal-based nanoparticle, i.e. copper, for making transformer oil based nanofluids. Since then, nanofluids have become a hot topic of research. Nanofluids could be mixtures of metals (*e.g.*, Au, Ag, Cu, Fe), metal and non-metal oxides (*e.g.*, Al_2O_3, TiO_2, CuO, SiO_2), carbon-based nanomaterials (carbon nanotubes (CNTs), fullerene, graphene), carbides (SiC) or polymers. Fig. 2 illustrates the classification of nanoparticles and an overview of nanofluids preparation approach. Water, ethylene glycol and oil are the most common base fluids which have poor

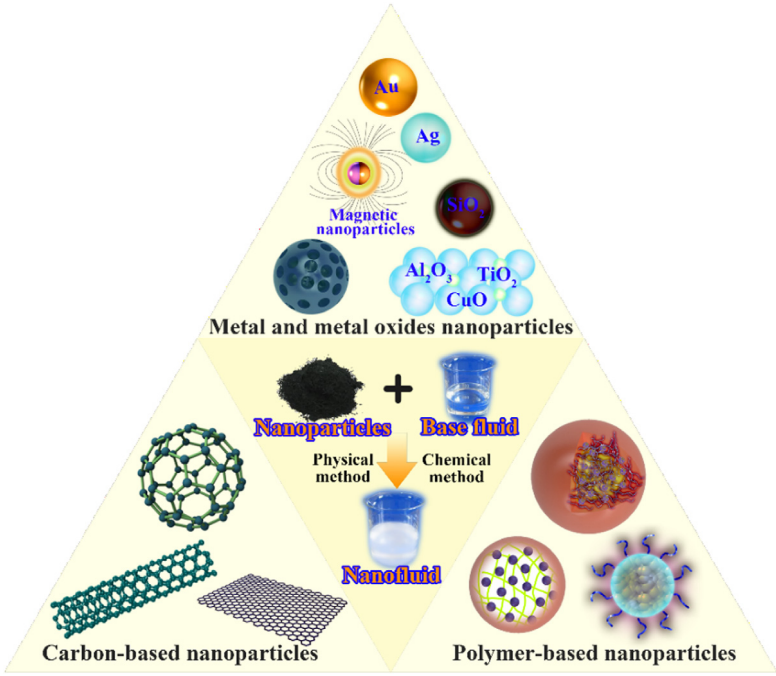

Fig. 2. Schematic diagram of nanoparticles classification and overview of nanofluids preparation approach.

k [11,12]. Numerous studies have shown that nanofluids exhibit an enhanced k and convective heat transfer coefficient (h) compared to common fluids [13–15]. In addition, the specific heat capacity (c_p), density (ρ) and dynamic viscosity (μ) are also important thermophysical properties for nanofluids [16–18].

1.3. What are the advantages and disadvantages of nanostructured materials?

In general, nanostructured materials render excellent properties compared to conventional materials, and this endows them with broad application prospects. Fig. 3 summarizes the advantages and disadvantages of some typical solid nanostructured materials and nanofluids. For example, in solid nanostructured materials, carbon nanomaterials exhibit high surface to volume ratio, high electrical conductivity (σ), high thermal conductivity, high mechanical strength and good chemical stability. For nano-porous materials, aerogels are the most representative because they have ultra-high porosity (95% or greater) and ultra-low ρ (0.02–0.32 g/cm^3). Since the internal pore size is on the nanoscale, which is even smaller than the mean free path (MFP) of the energy carriers, aerogels have ultra-low k (0.02–0.036 W/m K). Hence, aerogels are considered as one of the most promising new high-efficiency insulation materials [19]. In addition, the high specific surface area characteristics of nano-porous materials also determine their excellent gas storage characteristics [20]. There are also some disadvantages of solid nanostructured materials, mostly related to cost and processing.

The cost of synthesizing nanostructured materials is much higher than that of conventional materials. As for some special nanomaterials, the synthesis and processing technology are still not mature enough to produce on a large scale. Therefore, commercial applications have been limited.

In addition, there are some disadvantages of nanofluids, which are listed below:

- High cost of preparation and a relatively complicated preparation process.
- A key issue is how to avoid the aggregation and sedimentation of nanoparticles.
- Nanofluids have a higher dynamic viscosity than conventional fluids, so they consume more pumping power during transport.
- Nanofluids are prone to corrosion of components in contact with them.

1.4. What are the application fields of nanostructured materials?

After understanding how nanostructured materials are different from conventional materials, the question arises on what fields these materials can be applied to and how can they help us in our daily life? Generally, nanostructured

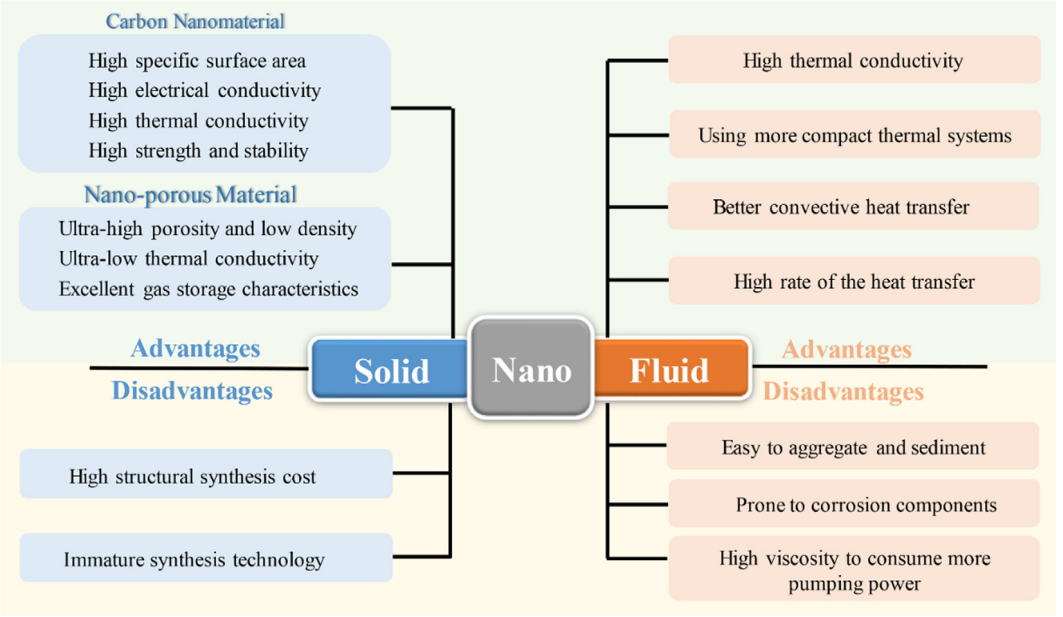

Fig. 3. Advantages and disadvantages of some typical solid and colloidal nanofluids.

materials have exhibited great application prospects in the fields of energy, aerospace, environmental science, microelectronics, bioengineering, medicine, and other fields [3,21,22]. Nanofluids are used in heat exchangers [23], solar energy systems [24–28], engine cooling systems [29], refrigerators, as porous media [30], and in many flow processes that require cooling or heating [31], hence they all have a primary scientific and industrial interest. Fig. 4 illustrates a general overview of the application fields of nanomaterials.

1.5. Aim of this review article

In this article, a comprehensive state-of-the-art review of the thermophysical properties of nanoscale materials is provided. The review is presented in two parts, the first part (Part I) mainly introduces the latest research progress on thermophysical properties of solid nanostructured materials, which includes theoretical and experimental research advances in k, c_p, and thermal diffusivity (α), focusing on the experimental measurement techniques, theory vs. experiments and the main factors affecting various thermophysical properties. The second part (Part II), mainly introduces the latest research progress on the thermophysical properties of nanofluids, including various mathematical models (from classical to advanced models), experimental measurement techniques, theory vs. experiments and the main factors affecting the k, c_p, ρ, μ and heat transfer rate of nanofluids. In addition, studies on molecular dynamic (MD) simulation that is used for modeling the properties at the nanoscale are reviewed. The review ends with a summary of the applications of data mining in the study of thermal properties of nanomaterials, and a brief discussion of the challenges and gaps in the research at the present stage, with future research hotspots and directions proposed.

2. Solid state

This section focuses on the thermophysical properties of solid nanomaterials especially carbon nanotubes, fibers, nanowires, nanofilms, graphene and nanocomposites. State-of-the-art measurement techniques for thermophysical properties are exposed, including the T-type probe method, the 3ω method, and their combination form called 3ω-T type method, the comprehensive T-type method, the H-type method and the laser flash Raman spectroscopy. For crystalline nanomaterials, the dominant energy carriers are crystal vibrations, phonons which have characteristic lengths on the order of nanometers. There are several factors that affect their k, c_p and α, such as the intrinsic electron–phonon and phonon–phonon scatterings, grain boundaries, surface interactions, grain size and temperature [32]. In amorphous nanomaterials, which are completely disordered in structure, the phonons no longer satisfy the intrinsic thermal transport mechanism. All phonon vibration modes are localized, and the corresponding disordered diffusion between high-energy localized vibrational modes (LVMs) is the primary means of thermal transport. Therefore, the disorder and temperature of amorphous materials are the main factors affecting their k [33]. Knowledge of the phonon transport mechanisms and adjacent LVMs in solid nanomaterials is a prerequisite for accurately description of the thermal transport processes. A broader range of phonon transport mechanisms and LVMs are the theoretical basis for studying the thermophysical

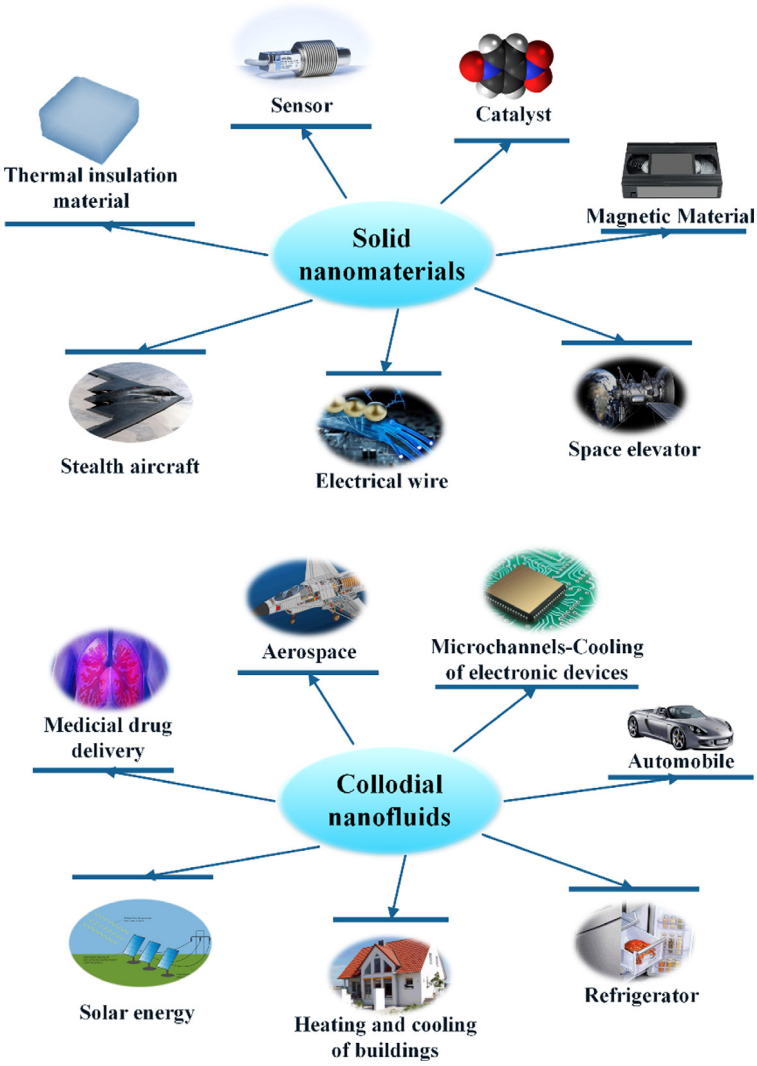

Fig. 4. Widespread application fields for nanomaterials: From solid state to colloids.

properties of solid nanomaterials, such as phonon dispersion, correlated scattering, ballistic transport and low-frequency propagating and diffusive vibrational modes [34]. A schematic diagram of the research on thermophysical properties of solid materials is shown in Fig. 5.

2.1. Thermal conductivity

In general, the main purpose of research on the nanomaterials thermal conductivity is to make their conductivity as high or low as possible depending on the application. For the study of thermal conductivity, we will focus on theory, experimental measurement techniques, MD simulation and the key influencing factors on thermal conductivity value.

2.1.1. Theory

In order to better understand the thermophysical properties and thermal transport mechanisms in nanoscale materials, theoretical research is essential [35–49]. It is well known that electrons and phonons are the energy carrier in metallic nanomaterials while in non-metal crystalline materials, phonons are the primary energy carriers responsible for thermal transport [35]. Therefore, studying the phonon MFP distribution is critical to recognize the internal thermal transport mechanisms of crystalline materials [41]. In nanostructured materials, the wave vectors and MFP of phonons carrying a large amount of energy are at the nanoscale. Therefore, finding the MFP distribution of phonons is a key to understand the thermal transport characteristics of phonons as carriers. Fig. 6 displays a flow chart for the theoretical study of k for solid nanostructured materials.

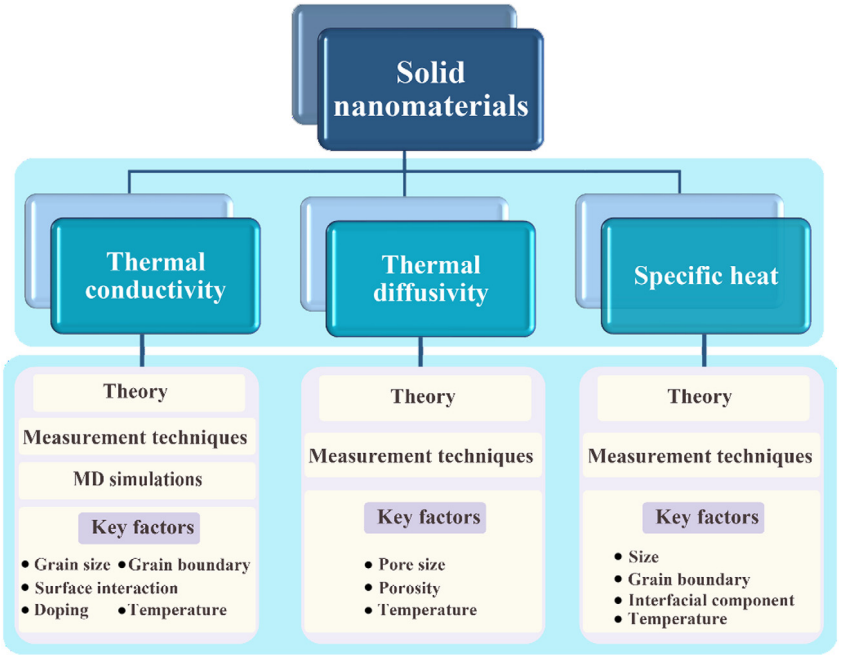

Fig. 5. Schematic diagram of the overall framework of thermophysical properties of solid nanomaterials.

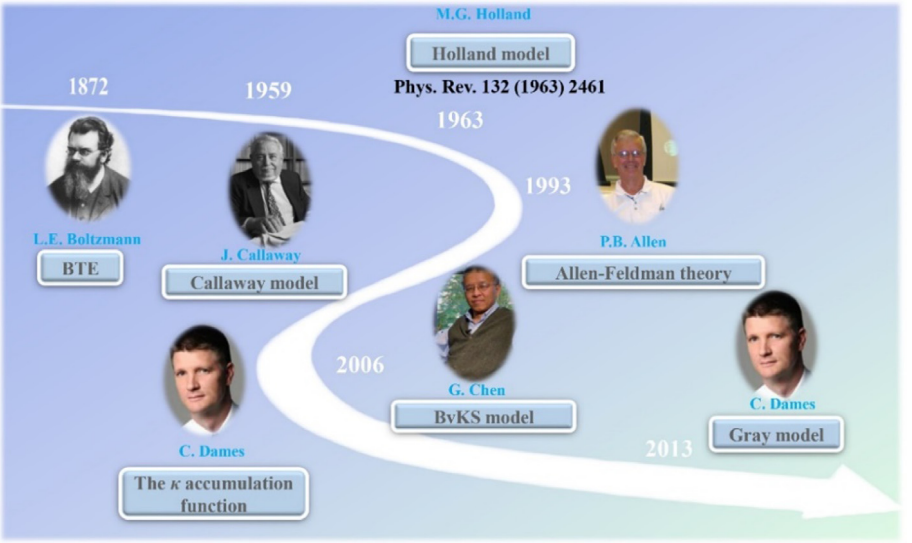

Fig. 6. Flow chart of the theoretical study for the thermal conductivity of solid nanostructured materials.

Compared with its bulk materials, the scattering of nanomaterials at the interface greatly reduces the k. The key factor determining the scattering of nanostructure interfaces lies in the relationship between the characteristic length of the nanostructures and the MFP of the carriers. In 2013, Yang and Dames [35] have studied the k of bulk materials and nanostructures through MFP spectrum and thermal conductivity accumulation function (k_{acc}), the advantage is that it can specifically quantitate the contribution of each MFP to the bulk thermal conductivity. Based on the kinetic theory and Boltzmann transport equation (BTE) in the relaxation time approximation, the k of an isotropic bulk material can be expressed as [36]:

$$k_{\mathrm{bu}} = \sum_{P} \int_{0}^{\infty} \frac{1}{3} c\,(\omega)\, \nu\,(\omega)\, \Lambda_{\mathrm{bu}} \mathrm{d}\omega \tag{1}$$

where ω and v represent the phonons frequency and the phonons group velocity, respectively, $c(\omega)$ represents the volumetric specific heat capacity per unit phonon frequency, Λ_{bu} is the bulk phonon MFP and P indexes the polarizations. The above equation is derived on the assumption that the dispersion relation under the relaxation time approximation is isotropic.

In order to focus on the bulk MFP, Λ_{bu} and reflect its contribution to k, the integral variable is changed from ω to Λ_{bu} and exchanges the order of integration and summation, Eq. (1) can be expressed by [35,36]:

$$k_{\mathrm{bu}} = \int_0^{\infty} \left(-\sum_P \frac{1}{3} c\left(\omega\right) v\left(\omega\right) \Lambda_{\mathrm{bu}} \frac{\mathrm{d}\omega}{\mathrm{d}\Lambda_{\mathrm{bu}}} \right) \mathrm{d}\Lambda_{\mathrm{bu}} = \int_0^{\infty} k_{\Lambda_{\mathrm{bu}}} \mathrm{d}\Lambda_{\mathrm{bu}} \tag{2}$$

where $k_{\Lambda_{\mathrm{bu}}}$ is the contribution to k per MFP. Subsequently, Yang and Dames [35] applied the concept of bulk MFP distribution to the calculation of k of nanostructured materials (k_{nano}). And here are some necessary assumptions: ignoring the effect of the wave confinement, the group velocity (v) and spectral heat capacity $c(\omega)$ of the nanostructures are approximately the same as that of bulk. Thus, compared to the thermal transport inside the bulk, the nanostructures exhibit a significantly reduced MFP due to the scattering of energy carriers at the boundaries and interfaces, and the k_{nano} is written by [37–39]:

$$k_{\mathrm{nano,\,type}} = \sum_P \int_0^{\infty} \frac{1}{3} c\left(\omega\right) v\left(\omega\right) \Lambda_{\mathrm{nano}} \mathrm{d}\omega \tag{3}$$

where the subscript "type" represents the type of nanomaterials, such as nanowire or nanofilm, Λ_{nano} is the nanostructure effective MFP. The scattering from boundaries and interfaces results in $\Lambda_{\mathrm{nano}} < \Lambda_{\mathrm{bu}}$, which again changes the integral variable from ω to Λ_{bu} and exchanged the order of integration and summation [35]:

$$k_{\mathrm{nano,\,type}} = \int_0^{\infty} \left[-\sum_P \frac{1}{3} c\left(\omega\right) v\left(\omega\right) \Lambda_{\mathrm{bu}} \left(\frac{\mathrm{d}\Lambda_{\mathrm{bu}}}{\mathrm{d}\omega} \right)^{-1} \right] \frac{\Lambda_{\mathrm{nano}}}{\Lambda_{\mathrm{bu}}} \mathrm{d}\Lambda_{\mathrm{bu}} = \int_0^{\infty} k_{\Lambda_{\mathrm{bu}}} \frac{\Lambda_{\mathrm{nano}}}{\Lambda_{\mathrm{bu}}} \mathrm{d}\Lambda_{\mathrm{bu}} \tag{4}$$

where Λ_{nano} strongly depends on the characteristic length (L_{c}) and the type of nanostructure.

Alternatively, another perspective different from bulk MFP spectrum is k_{acc}. In terms of the normalized k_{acc}, it can be defined as [40]:

$$k_{\mathrm{acc}}\left(\Lambda_{\mathrm{bu}}\right) = \frac{1}{k_{\mathrm{bu}}} \int_0^{\Lambda_{\mathrm{c}}} k_{\Lambda_{\mathrm{bu}}} \mathrm{d}\Lambda_{\mathrm{bu}} \tag{5}$$

which represents the fraction of the total k due to carriers with MFPs less than Λ_{bu}. Eq. (5) was first proposed by Dames and Chen [40]. Eq. (4) has a counterpart related to the k_{acc}, thus the k_{nano} can be obtained by using Eqs. (4) and (5):

$$k_{\mathrm{nano,type}} = -k_{\mathrm{bu}} \int_0^{\infty} k_{\mathrm{acc}}\left(\Lambda_{\mathrm{bu}}\right) \frac{\mathrm{d}B_{\mathrm{type}}}{\mathrm{d}\Lambda_{\mathrm{bu}}} \mathrm{d}\Lambda_{\mathrm{bu}} \tag{6}$$

where B_{type} is a function related to the ratio $\Lambda_{\mathrm{bu}}/L_{\mathrm{c}}$, and it depends on the type of nanostructure and Knudsen number (Kn). When $\Lambda_{\mathrm{bulk}} = 0$, $B_{\mathrm{type}} \to$ as $\Lambda_{\mathrm{bulk}} \to \infty$, $k_{\mathrm{acc}}(\Lambda_{\mathrm{bulk}}) = 0$, which can be interpreted as an enormous interfacial thermal resistance caused by boundary scattering.

In addition, the gray model is another common simple approximation approach for predicting the effect of the MFP spectrum on k. Traditionally, based on a single lumped "gray" or effective MFP, the contribution of MFP distribution to thermal transport can be described as [35]:

$$\Lambda_{\mathrm{Gr}} = \frac{k_{\mathrm{bu}}}{\sum_P \int_0^{\infty} \frac{1}{3} c\left(\omega\right) v\left(\omega\right) \mathrm{d}\omega} \tag{7}$$

which assumes that the bulk MFP distribution is not affected by a given temperature, it always uses the same gray value. Therefore, the calculation formula of k_{nano} of the gray model can be obtained using Eqs. (6) and (7) [35]:

$$k_{\mathrm{nano,Gr}} = k_{\mathrm{bu}} B_{\mathrm{type}} \left(\frac{\Lambda_{\mathrm{Gr}}}{L_{\mathrm{c}}} \right) = k_{\mathrm{bu}} B_{\mathrm{type}}\left(\mathrm{Kn}_{\mathrm{Gr}}\right) \tag{8}$$

where $\mathrm{Kn}_{\mathrm{Gr}}$ is the Knudsen number of the gray medium. Although this approximation method is relatively simple, its applicability is rather limited. It exhibits a good approximation for a system with a narrow distribution of real MFPs. However, for other widely distributed systems, the gray model is not valid. The above mentioned models are summarized in Table 1.

Early in 1959, Callaway [41] proposed a theoretical model for calculating the k of the lattice at low temperatures, which is named the Callaway model. It is assumed that the phonon scattering process can be represented by a relaxation time related to ω, and that there is no dispersion and isotropy in the crystal vibrational spectrum. Assuming identical contributions from longitudinal and transverse phonons to the heat conduction, phonon scattering mechanisms involved in (i) normal three-phonon processes (N processes), (ii) boundary scattering, (iii) point impurities and (iv) Umklapp

Table 1
Summary of some models for thermal conductivity of bulk and nanostructured materials.

Materials	Equation	Ref.
Bulk	$k_{\mathrm{bu}} = \sum_P \int_0^\infty \frac{1}{3} c\,(\omega)\, v\,(\omega)\, \Lambda_{\mathrm{bu}} \mathrm{d}\omega$	[36]
Bulk	$k_{\mathrm{bu}} = \int_0^\infty \left(-\sum_P \frac{1}{3} c\,(\omega)\, v\,(\omega)\, \Lambda_{\mathrm{bu}} \frac{\mathrm{d}\omega}{\mathrm{d}\Lambda_{\mathrm{bu}}} \right) \mathrm{d}\Lambda_{\mathrm{bu}} = \int_0^\infty k_{\Lambda_{\mathrm{bu}}} \mathrm{d}\Lambda_{\mathrm{bu}}$	[35,36]
Nanostructure	$k_{\mathrm{nano,\,type}} = \int_0^\infty \left[-\sum_P \frac{1}{3} c\,(\omega)\, v\,(\omega)\, \Lambda_{\mathrm{bu}} \left(\frac{\mathrm{d}\Lambda_{\mathrm{bu}}}{\mathrm{d}\omega} \right)^{-1} \right] \frac{\Lambda_{\mathrm{nano}}}{\Lambda_{\mathrm{bu}}} \mathrm{d}\Lambda_{\mathrm{bu}} = \int_0^\infty k_{\Lambda_{\mathrm{bu}}} \frac{\Lambda_{\mathrm{nano}}}{\Lambda_{\mathrm{bu}}} \mathrm{d}\Lambda_{\mathrm{bu}}$	[35,37–39]
Nanostructure	$k_{\mathrm{nano,type}} = -k_{\mathrm{bu}} \int_0^\infty k_{\mathrm{acc}}\,(\Lambda_{\mathrm{bu}}) \frac{\mathrm{d}B_{\mathrm{type}}}{\mathrm{d}\Lambda_{\mathrm{bu}}} \mathrm{d}\Lambda_{\mathrm{bu}}$	[35,40]
Nanostructure (gray model)	$k_{\mathrm{nano,Gr}} = k_{\mathrm{bu}} B_{\mathrm{type}} \left(\frac{\Lambda_{\mathrm{Gr}}}{L_{\mathrm{c}}} \right) = k_{\mathrm{bu}} B_{\mathrm{type}}\,(\mathrm{Kn_{Gr}})$	[35]

processes (U processes) are all considered. Through these assumptions and approximations, Callaway obtained the following integral expression for k [41]:

$$k = cT^3 \int_0^{\theta_{\mathrm{D}}/T} \frac{x^4 e^x \left(e^x - 1\right)^{-2} \mathrm{d}x}{v_b/L + Ix^4T^4 + (\varsigma_1 + \varsigma_2)\, x^2T^5} + k_2 \tag{9}$$

where T is temperature, $c = \left(\frac{k}{2\pi^2 v_{\mathrm{s}}}\right)\left(\frac{k}{\hbar}\right)^3$, v_{s} is an average phonon velocity, $I = A\left(\frac{k}{\hbar}\right)^4$-isotope scattering contribution, A is a coefficient, subscript $i = 1$ and 2 represent the N and U processes, respectively. ς_{i} denotes three phonons scattering, $\hbar$ is the reduced Planck constant, θ_{D} is Debye temperature, k_2 is a correction term, and $x = \frac{\hbar\omega}{k_{\mathrm{B}}T}$. Based on the above analysis, Allen [42] revisited the Callaway model and improved, corrected and simplified it. Based on the Debye-type phonon model, the relative roles of the N and U processes are reanalyzed. He postulated that Callaway underestimated the suppression of the N processes in relaxing thermal current and proposed a new calculation result of k by elongating the relaxation time. The Callaway model based on the Debye approximation is [42]:

$$k = k_{\mathrm{RTA}} \left(1 + \frac{\overline{\tau_{\mathrm{C}}\,(\omega, T)\,/\tau_{\mathrm{N}}\,(\omega, T)}}{\overline{\tau_{\mathrm{C}}\,(\omega, T)\,/\tau_{\mathrm{U}}\,(\omega, T)}} \right) \tag{10}$$

where k_{RTA} is the k corresponding to the relaxation-time approximation (RTA), τ is the relaxation time.

An analytical model of crystal k different from the Callaway model was proposed by Holland [43]. It fully considers the effect of longitudinal and transverse phonons on heat conduction, and proposed a new theoretical model for k, consisting of two parts:

$$k = k_{\mathrm{T}} + k_{\mathrm{L}} \tag{11}$$

where

$$k_{\mathrm{T}} = \frac{2}{3} \int_0^{\theta_{\mathrm{T}}/T} \frac{cT^3 x^4 e^x \left(e^x - 1\right)^{-2} \mathrm{d}x}{\tau_{\mathrm{T}}^{-1}} \tag{11a}$$

$$k_{\mathrm{L}} = \frac{1}{3} \int_0^{\theta_{\mathrm{L}}/T} \frac{cT^3 x^4 e^x \left(\mathrm{e}^x - 1\right)^{-2} \mathrm{d}x}{\tau_{\mathrm{L}}^{-1}} \tag{11b}$$

and subscripts T and L indicate the transverse and longitudinal phonons, respectively. The k of silicon in the temperature range of 1.7–1300 K is calculated by this model, which is in good agreement with experimental data [43].

Slack [44] first discussed the scattering of Born–von Karman dispersion in 1964. Based on the Born–von Karman dispersion theory, the Born–von Karman–Slack (BvKS) model was proposed by Dames and Chen [40]. In the BvKS model, the frequency ω is expressed as:

$$\omega = \omega_0 \sin\left(\frac{\pi q}{2q_0}\right) \tag{12}$$

where q_0 is the Debye cutoff wave vector, which is determined by the number density of original unit cells, and ω_0 is the frequency parameter. The BvKS dispersion theory includes a reduced wave vector group velocity close to the first Brillouin zone boundary. The calculation results of the BvKS model are most consistent with the numerical results [35]. This suggests that the BvKS model is more accurate and superior for studies involving phonon boundary scattering compared to the Holland model, the modified Callaway model and the gray model.

Based on the above theoretical concept, Yang and Dames [35] calculated the phonon contributed k of silicon by six models: the three most common analytical models (Callaway model [41], Holland model [43] and Born–von Karman–Slack

(BvKS) model [40]), MD simulation, first-principles (1stP) calculation and a simple gray model. For bulk Si, the calculation results of the three analytical models agree well with the experimental data as the relative error is less than 10%. For an individual silicon nanowire with diameter of 115 nm, the calculation results of the BvKS model fit better with the experimental data than the other models. Furthermore, based on the assumption of diffusion boundary scattering, the normalized k of silicon nanowires and the normalized in-plane k of silicon thin films were calculated based on the above integral transformation.

Cuffe et al. [45] conducted a theoretical and experimental study on the contributions of reconstructing the MFP distribution to k for Si nanofilms. To verify the accuracy of the experiments, they used the phonon BTE to calculate k for Si nanofilms by assuming an approximate isotropic dispersion:

$$k_{\mathrm{mem}} = \sum_S \int_0^\infty \frac{1}{3} c\left(\omega\right) \nu S\left(\frac{\Lambda_{\mathrm{bu}}}{d}\right) \Lambda_{\mathrm{bu}} \mathrm{d}\omega \tag{13}$$

where d is the thickness of the nanofilm and S is a function representing the contribution to the heat flux of a phonon with a particular MFP and is given by [45]:

$$S\left(\frac{\Lambda_{\mathrm{bu}}}{d}\right) = 1 - \frac{3}{8}\frac{\Lambda_{\mathrm{bu}}}{d} + \frac{3}{2}\frac{\Lambda_{\mathrm{bu}}}{d}\int_1^\infty \left(\frac{1}{t^3} - \frac{1}{t^5}\right) e^{-\frac{d}{\Lambda_{\mathrm{bu}}}t} \mathrm{d}t \tag{14}$$

and the $c(\omega)$ is defined as [36]:

$$c\left(\omega\right) = \frac{\partial}{\partial T} D\left(\omega\right) g_{\mathrm{BE}} \hbar\omega = \frac{q\left(\omega\right)^2}{2\pi^2} \frac{\mathrm{d}q\left(\omega\right)}{\mathrm{d}\omega} \hbar\omega \frac{\partial g_{\mathrm{BE}}}{\partial T} \tag{15}$$

Here, $D(\omega)$ is the density of states, g_{BE} is the Bose–Einstein distribution and $q(\omega)$ is the polarization-dependent phonon wave vector. Based on the normalized accumulated MFP distribution in Eq. (5), we can obtain the relationship between k_{mem} and k_{bu}, which is given by Eq. (16) [45]:

$$\frac{k_{\mathrm{mem}}}{k_{\mathrm{bu}}} = \int_0^\infty k_{\mathrm{acc}}\left(\Lambda_{\mathrm{bu}}\right) \frac{\mathrm{d}S\left(\frac{\Lambda_{\mathrm{bu}}}{d}\right)}{\mathrm{d}\Lambda_{\mathrm{bu}}} \mathrm{d}\Lambda_{\mathrm{bu}} \tag{16}$$

However, it is difficult to invert this equation to obtain k_{acc} as a function related to d from experimental measurements (k_{mem}). The reconstruction of the k_{acc} can be implemented by imposing some constraints on it. Using an algorithm based on a convex optimization procedure, the result of the reconstruction is obtained, which is in good agreement with the distribution calculated from first principles and the MD calculations.

For amorphous nanomaterials, the dominant factor affecting their k is the degrees of disorder (ε). As is well known, the most common materials (such as silica, silicon, graphene) have several different stable structures, *i.e.*, single crystal, polycrystalline, amorphous. The biggest difference between these structures is the different ε. As an important structural parameter, ε is a strong indicator of the thermal transport properties of materials. Specifically, an ultra-low ε indicates a very orderly internal structure of the material, which is considered as a single crystal structure with various excellent properties, such as extremely high k up to 5300 W/m K [46]. A relatively high ε indicates disordered internal structure or the called amorphous structure. The k is close to that of an insulator which is typically below 1 W/m K [47]. For amorphous nanomaterials with high ε, the phonon velocity and polarization direction inside the structure are not clear, and the related concept of a phonon cannot be used to evaluate the thermophysical properties any more. When the value of ε is within 0–1, the heat conduction mainly depends on both phonons and diffusons. Diffusons contribute to k by harmonic coupling with other modes due to the disorder. Therefore, for nanostructures with a certain degree of disorder, the total vibrational k consists of two parts [47]:

$$k = k_{\mathrm{P}} + k_{\mathrm{D}} \tag{17}$$

where k_{P} denotes the k contributed by phonons from propagating modes, and k_{D} represents the k contributed by diffusons from nonpropagating modes given by the Allen–Feldman (AF) theory [48,49]. The k_{P} can be derived from the c_{p} in different modes and vibrational density of states (VDOS) of phonons [47]. During the derivation of Eq. (18), the system is assumed to be isotropic and has a single polarization, so that mode properties are only related to ω [48,49]:

$$k_{\mathrm{P}} = \frac{1}{V_{\mathrm{s}}} \int_0^{\omega_{\mathrm{cut}}} D\left(\omega\right) c\left(\omega\right) \alpha\left(\omega\right) \mathrm{d}\omega \tag{18}$$

where V_{s} is the system volume, and ω_{cut} is the phonon cutoff frequency. When the frequency is less than ω_{cut}, phonons contribute to transport, and at higher frequencies diffusions contribute. $D(\omega)$, $c(\omega)$ and $\alpha\left(\omega\right) = {s_{\mathrm{s}}}^2 \tau\left(\omega\right)/3$ are the vibrational density of states, mode specific heat capacity and mode thermal diffusivity of the vibration mode related to ω, respectively. $\tau(\omega)$ is the phonon lifetime and s_{s} is the sound speed. For phonons, the DOS of the material can be described by the Debye model [47]:

$$D\left(\omega\right) = \frac{3V\omega^2}{2\pi^2 {s_{\mathrm{s}}}^3} \tag{19}$$

Thus, we can judge the ω_{cut} and s_s of the material according to whether the VDOS of the material satisfies the Debye model. The quantum expression for the $c(\omega)$ is given by:

$$c(\omega) = k_B \left[\frac{\hbar\omega/2k_BT}{\sinh(\hbar\omega/2k_BT)} \right]^2 \tag{20}$$

where k_B is the Boltzmann constant. Similar to the contribution of phonons to k, the contribution of diffusons to k can also be derived from the c in different modes and α [48,49]:

$$k_D = \frac{1}{V} \sum_{\omega>\omega_{cut}} c(\omega_i)\,\alpha(\omega_i) \tag{21}$$

where ω_i is the vibration frequency of the ith localized mode, $c(\omega_i)$ is the diffuson isobaric specific heat capacity, and $\alpha(\omega_i)$ is the diffuson diffusivity of the ith localized mode. The thermal diffusivity of the localized mode can be derived from the AF theory [48]:

$$\alpha(\omega_i) = \frac{\pi V^2}{\hbar^2 \omega_i^2} \sum_{j\neq i} |M_{ij}|^2 \delta(\omega_i - \omega_j) \tag{22}$$

where M_{ij} is the thermal coupling between ith modes and jth modes, which can be calculated by the modal frequencies and the spatial overlap of mode vectors.

In this section, we have summarized and combed the theoretical models for the k of solid nanomaterials. For crystal materials, the wave vector of phonons carrying a large amount of energy and the MFP at the nanoscale are the key factors determining the k. Here we first introduce the theoretical models for the k of the bulk based on the BTE; then, based on the bulk theoretical models, the model for the k of nanomaterials was proposed, and the process and principle of this evolution were described in detail. Finally, the Callaway model, the Holland model, the BvKS model and a simple gray model were introduced. For amorphous nanomaterials, the k is dominated by phonons and diffusons. The contribution of diffusons comes from their harmonic coupling with other modes, which can be obtained by the AF theory.

2.1.2. Experimental measurement techniques

2.1.2.1. T type probe method (for nanotubes, nanowires). The T-type probe method is an effective method to measure the k of individual micro/nanoscale fibrous materials, such as nanotubes and nanowires. Zhang et al. [50] first developed this steady-state measurement method based on the heat conduction principle of the pin fin when it is attached to a hot wire. A platinum wire with known electrical and thermal properties is used as the heating wire, and the two ends of the wire are welded to the heat sink. When a direct current is applied to the wire from both ends, the uniform heat flux creates a parabolic temperature distribution in the metal wire. Fixing one end of the individual fibrous material on the heat sink while the other end is overlapped at the middle of the heating wire, heat will flow from the heating wire into the fibrous material and results in a parabolic temperature distribution within the test structure. According to the evolution of the temperature distribution, the axial k of the fibrous material is extracted [51]. It is to be noted that the measurement uncertainty of this method is less than 7% in the vacuum condition. A key issue affecting the measurement accuracy is the thermal contact resistance at the connection between the fibrous materials and the hot wire. Wang et al. [51] separated the axial thermal conductivity of the fibrous sample from the thermal contact resistance by measuring the fibrous samples with a series of different lengths while maintaining the same contact conditions.

In addition to the measurement of a single fibrous sample with micrometer diameter, Fujii et al. [52] implemented the measurement of the k using the T-type probe method for a single CNT with diameter of tens of nanometers. A unique sample holder consisting of suspended platinum film nanosensors was fabricated by electron beam etching on a multilayer film. Under the scanning electron microscope (SEM), a single CNT grown by the arc discharge evaporation method was suspended on the electrode of the nanosensors with two ends fixed by locally focused electron beam irradiation. The k of the CNT was obtained by measuring the average temperature rise and the heat generation rate of the nanosensors. It was observed that the k of the single CNT decreased with increasing diameter. Specifically, for a single CNT with the diameter of 9.8 nm (CNT I), k exceeded 2000 W/m K. For a single CNT (grown in the same process of CNT I) with the diameter of 16.1 nm (CNTII), k decreased to 1600 W/m K. For an individual CNT (still grown in the same process of CNT I and CNT II) with the diameter of 28.2 nm (CNT III), the k decreased to 500 W/m K. Furthermore, the k no longer increased with the increasing temperature when the temperature reached 320 K, which can be explained noting that phonon scattering became the dominate mechanism of thermal transport.

2.1.2.2. 3ω method (for nanotubes, nanowires, nanofilms). The traditional 3ω method is based on a micrometer-sized metal strip with four pads on the surface of the material to be tested. The strip is used as both a heater and a temperature sensor. Driven by a sinusoidal alternating current with an angular frequency of 1ω, the strip produces a temperature fluctuation of 2ω. In a small temperature range, the resistance of the strip also fluctuates with frequency of 2ω. The resulting third harmonic voltage ($U_{3\omega}$) contains information related to the thermophysical properties of the sample. Cahill [53,54] first proposed this method for k measurement of solid bulks and films. At present, this method has been applied to the k measurement for a wide range of micro/nanoscale materials [6,48–59].

Ahmed et al. [55] first measured k (~26 W/m K) of an ultrathin nano crystalline diamond film with a thickness of 16 μm using the frequency range up to 1 MHz. In addition to a single layer film, Olson et al. [56] extended the 3ω method for multilayer structures. This work uses a non-approximate analytical solution to extract the k of multilayer film structures in the form of thermal impedance, and the α of the material can be obtained at the same time. For microfilms with anisotropic k values, Qiu et al. [57] shear pressed and polished the top of a vertically aligned CNT (VACNT) array to a horizontally aligned CNT (HACNT) film, then deposited a group of sensors with different widths and directions on it. Through analyzing the variant temperature rise versus frequency curves, the anisotropic k values along x (in-plane along the CNT axes), y (in-plane perpendicular to the CNT axes) and z (out-of-plane) directions are extracted to 127 W/m K, 42 W/m K and 4 W/m K, respectively.

Qiu et al. [60] then applied the similar test structure to measure the k of a single conductive carbon fiber (CF) and CNT fiber, respectively, both of which accurately reflected the axial thermal transport performance of individual fibrous samples. Since this method uses the fiber itself as the heater and thermometer, its feasibility strongly relies on the highly conductive properties of the materials [61,62] in the previous reports. To handle the challenge of measurements on non-conductive fiber, Qiu et al. [63] modified the 3ω method by depositing a platinum conductive layer on the surface of the non-conductive fiber to secure the electrical current passing through the fiber, achieving k measurement of individual porous polyimide fibers.

Another milestone on the development path of the 3ω method is the freestanding sensor-based 3ω technique, which ensures the porous material with uneven surfaces can be measured even in on-site situations [5,64]. An advantage of this method which needs to be pointed out is this modified method can achieve the simultaneous measurement of k and contact thermal resistance between the sample-sensor interface [65] or even the nanoscale interfacial thermal transport characteristics within nanoparticle-decorated graphene layers [66], which is a hotspot in micro/nanoscale thermal transport studies.

2.1.2.3. 3ω-T type method (for nanotubes, nanowires). For most materials, but especially for thermoelectric materials, there is a need to extract multiple physical parameters (k, α, c_p, σ, temperature coefficient of resistance, Seebeck coefficient) simultaneously in order to evaluate their specific characteristics. When the material size goes down to micrometers or even nanometers, two problems are frequently encountered: one is the remarkable difference between the individual samples, hence it is better to measure all of the properties from the same individual sample; the other is that multiple transfer of samples during the separate measurements for different physical properties lead to damage to the morphologies of the microscale samples, thus affecting their intrinsic physical properties. To solve these problems, Ma et al. [67] developed the so-called comprehensive 3ω-T type method, which successfully realized the in-situ measurement of multiple parameters, as given above, for individual Bi_2S_3 nanowires.

The conventional DC T-type method can be applied to measure the thermal contact resistance and thermal impedance of nanowires. It can also be used to measure the thermal effusivity (b) of the nanowire, and then the k is obtained by the formula $k = b^2/\rho c$. The 3ω-T type method has an advantage over the 3ω method in that it can measure the thermophysical properties of both metallic and non-metallic nanowires, that is to say, the 3ω-T type method is not limited to conductive samples. Compared with the conventional DC T-type method, the thermal penetration depth of the hot wire in the 3ω-T type method can be changed by adjusting the frequency of sinusoidal alternating current. Thereby, the separation of the thermal resistance of the test wire from the junction can be implemented [68]. For the 3ω-T method, the relative uncertainty of the α is 6% for microscale samples and 18% for nanoscale samples.

2.1.2.4. H-type method (for nanofilms). The H-type method is one of the most common methods for measuring the k of nanofilms. The measurement principle is to sandwich the nanofilm between two metallic sensors, and then control the temperature of the metallic sensor by regulating the heating power of the metallic sensor. The temperature difference between the sensor and the nanofilm determines the k of the nanofilm. Typically, a larger temperature difference between the film and the metal sensor indicates a lower k of the film. Wang et al. [69] discovered the existence of thermal rectification in various asymmetric monolayer graphene nanostructures by the H-type method. By preparing asymmetric single-layer defect-engineered graphene rectifiers by electron beam lithography and ion etching, the k of the thermal rectifiers was measured by monitoring the temperature change of the graphene sandwiched between the metal sensors caused by heat conduction. A two-dimensional heat conduction model for the H-type method was also established, combined with the COMSOL multiphysics software for thermodynamic process analysis. It can be observed that the k for the defect-engineered graphene thermal rectifier was significantly lowered, accompanied by the average thermal rectification factor ξ_{ave} of 26%. It was also concluded that the asymmetric structure of the single-layer graphene thermal rectifier has higher k and lower thermal rectification factor than the defect-engineered graphene thermal rectifier.

2.1.2.5. Raman spectroscopy method (for nanofilms). Although ideal 2-D graphene is predicted to possess an extremely high k, experimental data have not been reported yet since conventional thermal measurement methods, such as the laser flash method and the thermal bridge method, are not enable to measure the thermal conductivity of graphene with the single atomic layer thickness. Due to the strong temperature dependence on Raman G peak frequency, Balandin et al. [46] proposed to carry out the measurement of k for suspended single-layer graphene (SLG) based on Raman spectroscopy. The results suggested that the k of SLG was 4840–5300 W/m K at room temperature (RT), which was slightly higher than the reported single-walled CNT (SWCNT) value [70,71]. In the same year, Ghosh et al. [72] reported the extremely high

k of a set of graphene flakes suspended across trenches in a Si/SiO_2 wafer also through the Raman spectroscopy method. The graphene flakes rendered k in the range of 3080–5150 W/m K while the phonon MFP was about 775 nm. This work further explored the mechanism of high thermal transport. In addition, it proposed that graphene multilayer films can be well applied in micro/nano thermal management since they are prone to interface with the heat sink.

For accurate measurement of graphene thermal conductivity, researchers have focused on the Raman spectroscopy method, in order to actualize non-contact, non-destructive and fast thermal property measurement. Faugeras et al. [73] measured large-area monolayer graphene and obtained k of about 630 W/m K, which is significantly different from the previous report of the extremely high k up to 5000 W/m K. The authors believed that this huge deviation was mainly due to the different assumptions which are made for optical absorbance efficiency of graphene samples. By considering the effect of environment, Chen et al. [74] placed the SLG in a vacuum, air and CO_2 gas, respectively to compare differences in k of SLG by Raman spectroscopy. The large differences in k among different environments indicated that the heat loss to the surrounding gas should be considered to avoid the measurable errors in k. To eliminate the effect of substrate, Cai et al. [75] grew the graphene monolayer over a hole substrate, and obtained k of about 630 W/m K at 660 K for the suspended graphene without a substrate. Yan et al. [76] extended the samples from carbon materials to molybdenum disulfide (MoS_2), and measured multiple types of monolayer MoS_2 including suspended, Si_3N_4-supported and sapphire-supported with k of 34.5 ± 4 W/m K, which agreed well with simulation results. The accurate characterization of the single-layer MoS_2 in this work provided important data for its optical and electronic applications. In addition, inspired by Balandin's work, Doerk et al. [77] proposed the thermal measurement method of single nanowires by the Raman thermography technology, which greatly expanded material categories based on Raman measurements.

2.1.2.6. Time-domain thermoreflectance. Time-domain thermoreflectance (TDTR) is a powerful method to measure the k because it has a high accuracy and wide applicability for various materials, especially for micro/nano-scale materials. However, because of the long platform displacement required for the temporal delay, it is difficult to maintain the size and position of the laser spot as it is focused on the sample, which limited application and further development. This was true until Costescu et al. [78] found the measurement error due to small spot sizes and unchanged position can be reduced once the ratio of the in-phase signal to the inverted signal is used as the fitting signal. Hence, scholars began to use this technique to measure the thermal conductance (G) at solid interfaces. Then, Cahill [79] focused on how to use TDTR for layered structure measurements. During this study period, he found the accurate heat transfer model for the metal interfaces is much more complicated due to the additional effect caused by electrons. In order to break through the limitations of the materials' types, Gundrum et al. [80] heightened the sensitivity and accuracy by using the ratio of in-phase signal to out-of-phase signal to replace the in-phase signal, and successfully extended the G measurement to typical metal interfaces such as Cu–Al interfaces. Lyeo and Cahill [81] further studied G of an intriguing an-harmonic scattering interface formed by the interface of low and high Debye temperature materials, *i.e.*, bismuth/hydrogen-terminated diamond interface. It was not surprising to find that G was extremely low which even significantly exceeded the radiation limit. These results illustrated that there was an additional thermal transport channel by the three phonon processes owing to the highly dissimilar lattice vibrations. The exploration of the TDTR method implemented by Cahill has laid a solid foundation for TDTR's application in micro and nanoscale thermophysical measurement and provided new ideas for further development of the TDTR method.

Other scientists have also contributed a lot to the TDTR technique. Li et al. [82] proposed the Asymmetric-Beam Time-Domain Thermoreflectance (AB-TDTR) technique based on the controllable elliptical ratio and spot size. Utilizing the significantly different sensitivity of the out-of-plane or in-plane signals, k in the direction of interest can be obtained. This technology can be used for k measurement of isotropic (boron phosphide, boron nitride and silicon), transversely isotropic (sapphire, quartz and graphite) and anisotropic materials (black phosphorus). Jiang et al. [83] achieved high-accuracy k measurement (uncertainty $< 10\%$) of thin films ($\sim$400 nm) by developing the dual-frequency TDTR. They [84] also pointed out that rough surfaces could be measured once the artificial signals were eliminated by avoiding the pump beam leaking into the photodetector. Jang et al. [85] completed the measurement of k in different directions of black phosphorus by using the low frequency to extend the laser's thermal penetration depth for out-of-plane measurement and the beam-offset method for in-plane measurement. Jiang et al. [86] reported a new TDTR technique based on a variable spot size approach which overcame the measurement problem associated with strongly anisotropic materials, and this technique has been used on a wide variety of materials including molybdenum disulfide, rutile titania, and highly ordered pyrolytic graphite. Fig. 7 shows a schematic diagram of the k measurement methods mentioned above for nanostructured materials [50,61,65,69,86–88].

2.1.3. Experimental studies

In the previous section we have detailed the various techniques for measuring k of solid nanostructured materials, including their measurement principles and the selection for different nanomaterials. Since some typical nanomaterials, such as CNT, graphene, fullerene, nanofilms and nanowires, have a certain crystal structure, grain size, grain boundary, interfacial interaction, defect concentration, and doping degree, these features, together with the temperature, will play a major role in the determination of k [89] Here, we will discuss in detail how these factors affect the k.

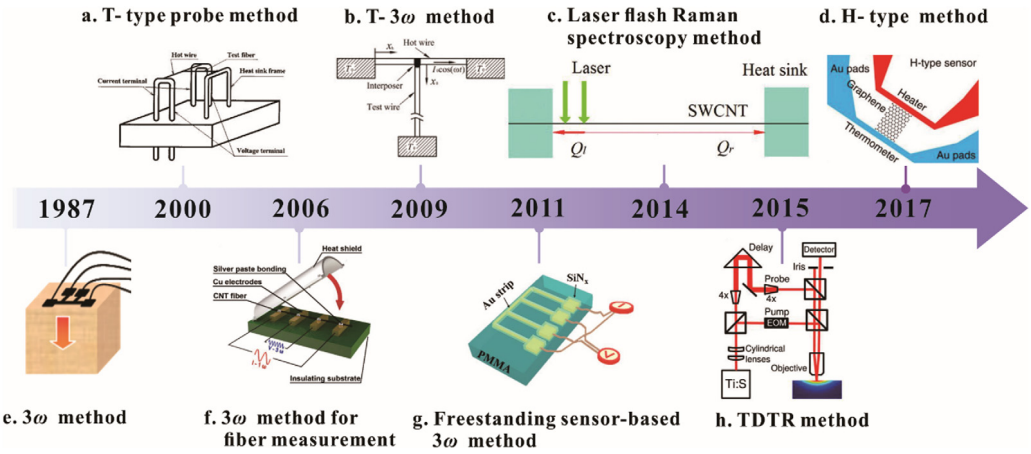

Fig. 7. Schematic diagrams of measurement techniques for: (a) T-type probe method [50] (Reprinted with permission from Springer Nature), (b) 3ω-T type probe method [87] (Reprinted with permission from Springer Nature), (c) Laser flash Raman spectroscopy method [88] (Reprinted with permission from RSC Pub), (d) H-type probe method [69], (e) 3ω method, (f) 3ω method for fiber measurement [61] (Reprinted with permission from Elsevier), (g) freestanding sensor-based 3ω method [65] (Reprinted with permission from Elsevier) and (h) TDTR method [86] (Reprinted with permission from AIP Publishing).

2.1.3.1. Effect of grain size. It is widely recognized that the effect of grain size (L) on the k of polycrystalline solid materials is not negligible. In the 1980s, scientists began to pursue knowledge of how grain size would affect the thermophysical properties of polycrystalline materials. A good example is an Australian material scientist Savvides [90], who experimentally confirmed the k of polycrystalline $Ge_{30}Si_{70}$ is negatively linearly correlated with $L^{-1/2}$ for L exceeding 10 μm, which is perfectly consistent with theoretical predictions. Zhang et al. [91] experimentally corroborated that the k of polycrystalline platinum nanofilms is mainly reduced by grain boundary scattering instead of surface scattering. Since the in-plane grain size (L_i) determines the grain boundary scattering rate, increasing L_i helps reduce the scattering. Dong et al. [92] demonstrated when L is large enough in nanocrystal materials, the internal thermal resistance is close to that of the single crystal, and the thermal resistance between the crystals approaches zero. The size effect is greater than the grain boundary effect on the k for the nanocrystal material. A study by Wang et al. [38] also confirmed this point. Similarly, Soyez et al. [93] also corroborated that increasing the nanoparticle size is another effective way to boost k.

Notice the above-mentioned studies mostly focused on nanofilm materials, which are representative of NC materials. It is worth mention that a study by Qiu et al. [94] experimentally confirmed the grain size effect on k also existed in carbon fibers (CFs) after graphitization treatment. This case is special because although the fiber size is not at the nanoscale, the inner structure is composed of nanocrystals. This was the first time that macroscopic materials can also render size effects on k. In brief, the reciprocal of in-plane coherence length (L_a^{-1}) can reflect the number of grain boundaries, which adversely and linearly related to the k ($k \propto -L_a^{-1}$). In marked contrast, some studies have found k might be dominated by defects instead of L. An example is from a study by Watari et al. [95], who claimed the k of polycrystalline Si_3N_4 was determined by internal defects, such as dislocation, while L seemed to have no obvious effect on k.

2.1.3.2. Effect of grain boundary. As mentioned above, grain boundaries are another important factor that affects the k of NC materials. A wide variety of nanostructures have now been introduced into materials, which fuels the enormous amount of research on phonon grain boundary scattering to boost thermoelectric performance [38]. It is generally believed that NC boundaries can effectively scatter short-wave phonons, which reduces the lattice k of the material in the low temperature region. To harness this feature, scientists chose NC-silicon instead of single crystal silicon as an ideal thermoelectric material, since the k of NC-silicon is two to three orders of magnitude lower than that of single crystal silicon, indicating a high figure of merit (ZT) value [96].

Mohr et al. [97] studied the effect of grain boundaries on the k of nanodiamond films. The study found that the k due to grain boundary scattering is an index of the cohesive energy of the grain boundaries. Furthermore, the structure, width and chemical composition of the grain boundaries also have a non-negligible impact on the k of the nanodiamond film. Grain boundaries with a higher sp^3/sp^2 ratio show a higher k. In addition, the grain boundary elastic modulus affects k more than the elastic behavior. Anaya et al. [98] confirmed that the in-plane k of polycrystalline diamond film is strongly inhomogeneous, which is a result of the limitation of the MFP of phonons at the grain interface. The above researches have provided new ideas for controlling the heat transfer by means of controlling grain boundaries.

2.1.3.3. Effect of surface interactions. How to use surface interactions to modulate the thermophysical properties is always a research hotspot for thermal functional materials. It is experimentally corroborated by Qiu et al. [61] that decorating noble nanoparticles (Au, Pd, Pt) onto CNT surfaces can induce low-frequency vibrations of C atoms at the CNT interface, which contribute to interfacial heat transport. By decorating 10% (wt%) Au nanoparticles between CNTs, the axial k of

the assembled fibers gets boosted by 70%. Similarly, small halogen molecules added into CNT interfaces also improve the interfacial thermal transport by introducing low-frequency phonons and providing additional thermal channels [62].

Another general method for surface interaction modification is functionalization of the surfaces. Li et al. [99] studied the k of hybrid graphene nanoribbons by reverse NEMD and reported that graphene with gradient hydrogen arrangement showed a remarkable thermal rectification without the chirality and length dependence. Qiu et al. [61] prepared CNT fibers with inter-tube functionalized surfaces, and the k of the fibers got diametrically boosted owing to the improved interfacial heat transfer.

Since surface interaction is dominated by the non-bonded van der Waals force which generally leads to weak energy transport, novel interfacial structures with stronger bonding and enhanced heat transfer have been sequentially reported. Losego et al. [100] modified the interfacial force from van der Walls to covalent bonding by the self-assembled monolayer and realized ∼80% boost of the interfacial thermal conductance (G) between Au and z-cut quartz surfaces. Based on the above work, O'Brien et al. [101] strongly bonded copper and silica surfaces by the organic nanomolecular monolayer (NML). The G was controllable by choosing different terminated-groups of NMLs, such as CH_3–NML and SH–NML, with a maximum G of 430 MW/m^2 K. This novel idea inspired the interest of researchers. Majumdar et al. [102] carried out a study on the phonon mismatch level between the bonded SAM and metal leads, and discovered the relation between the mismatch level and the thermal transport. According to their results, the higher the phonon matching level, the stronger the interfacial thermal transport capability. Zheng et al. [103] extended the samples to polymers. Different from the previous work, the interfacial thermal transport was linearly dependent on the solubility between the polymer and SAM.

The above work provided three general methods for heat transfer enhancement and modulation, *i.e.*, the surface functionalization, interface decoration and surface bonding strength. It was confirmed that k is significantly affected by the surface functionalization. Research in this field so far has many benefits for the exploration of heat transfer mechanisms and design of micro/nano-scale thermal management materials.

2.1.3.4. Effect of doping. Due to the limitations of CNT preparation techniques, short CNTs are easier to prepare. However, studies have revealed that when short CNTs are assembled into CNT fibers, their thermophysical properties are much lower than predicted theoretical values. Conversely, long CNTs have superior thermophysical properties compared to short CNTs. Aiming at the contradiction between the length and performance of CNTs, Behabtu et al. [104] addressed this problem very well. By using the high-throughput wet spinning method, ultra-long CNTs were obtained. Then, the CNTs were assembled into CNT fibers with excellent thermophysical properties. In order to study the effect of doping on the thermal transport mechanism, they studied the effects of acid doping, annealing and iodine doping on the k of CNT fibers. The average k of the acid-doped fibers was measured to be 380 W/m K, while the k of the iodine doped CNT fibers was doubled to 635 W/m K. This evident boost of k resulted from improved inter-tube contact and greatly reduced impurity and defect scattering resulting from the annealing process of iodine doping.

Another representative example of defect influenced thermophysical properties comes from ideal 2-D structured graphene. It is frequently reported that structurally defective graphene renders a remarkably reduced k, primarily due evidently to increased phonon scattering [105]. Due to the fact that substitutional doping of atoms does not destroy the hexagonal lattice structure of graphene, the thermophysical properties of graphene with doping atoms attract much attention these days. Studies have shown that the k of doped graphene has a strong relation with the mass and concentration of the dopants, specifically the difference in the mass between the dopant and the C atom (ΔM). Hu et al. [106] studied the effect of isotope doping (^{13}C, $\Delta M = 1$) on the k of graphene. The results revealed that the isotope doping leads to a behavior of decreased phonon relaxation times and weakens the k dependence of isotope-doped graphene on temperature. It is to be noted that the normalized accumulative k of doped graphene is not much different from that of pristine graphene, owing to the fact that the relaxation time of high-frequency phonons is slightly reduced and that of the low-frequency phonons remains basically the same.

Mortazavi et al. [107] studied the effect on k of replacing the carbon atoms in single-layer graphene with boron atoms (B, $\Delta M = 1.2$). The results indicate that when the concentration of doped boron atoms in single layer graphene is 0.75%, the k of graphene along both chiral directions is reduced by more than 60%. In addition, when the concentration of boron atoms doped in graphene reached 1%, the chirality no longer affected the k of graphene. Phonon scattering was regarded as the most likely key factor for the decrease of the k for graphene and the disappearance of chirality in the structure. Similar results were reported by Goharshadi et al. [108] and Zhang et al. [109], who concluded that a very low nitrogen-doped concentration (0.5%–1%) is powerful enough to induce a sharp decrease in the k of graphene. Furthermore, Zhang et al. [109] believed that some studies only considered the effect of nitrogen configurations (graphite-N) on k of graphene, while most nitrogen atoms are pyridinic-like structures (pyridinic-N) in reality. They compared the thermophysical properties between graphite-N and pyridinic-N-doped graphene. The results have implied that in addition to the influence of nitrogen concentration on the k of graphene, the type of nitrogen atoms doped should also be highlighted. The inhibition of the k by pyridinic-N-doping is more significant than the graphite-N doping for graphene.

The above studies were all theoretical work typically around substitutional dopants with a small ΔM. To study the effect of heavy dopants (high ΔM) on the k of graphene, Lee et al. [110] used the same group of silicon dopant (Si, $\Delta M = 16$) as the substitutional dopants for C. High quality Si-doped graphene was synthesized by a low pressure chemical vapor deposition (CVD) method. The results emphasized that the inhibitory effect of heavy dopants on the k of graphene is more significant, typically by 1–2 orders of magnitude. The main reasons for this phenomenon were due to the large mass difference between the C atoms and the Si atoms and the presence of Si atoms reduces the phonon MFP.

2.1.3.5. Effect of defects. It is inevitable that nanomaterials have defects, which could be vacancies, impurity atoms, or rough edges. Low-dimensional nanomaterials such as graphene and nanowires provide an ideal platform for exploring the effect of defects on k [106,111–118]. For vacancy defects, Li et al. [111] constructed a perfect crystal β-SiC with single point defect structure in the earlier study. The local density of states (LDOS) calculation results described that the presence of the point defect caused a change in the thermal transport mechanism from one dictated by phonon–phonon collisions to one dictated by phonon-defect scattering. Malekpour et al. [112] verified this conclusion experimentally by electron beam irradiation to generate defects. Furthermore, Haskins [113] pointed out that a single point vacancy is a high-energy defect, which would result in the formation of a double-coordination of three carbon atoms, thereby destroying the sp^2 bond of the surrounding crystal lattice. Quantitative analysis using the Green–Kubo method has shown that the introduction of a 0.42% vacancy defect in graphene results in a significant decrease in k from 2903 W/m K to 118.1 W/m K [114]. Since low frequency phonons with a long MFP contribute to heat conduction and are strongly inhibited by defect scattering [106], the increase in the defect concentration weakens the k dependence on temperature, besides the suppression of the k itself. The most common vacancies are Stone-Thrower-Wales vacancy, double vacancy and monovacancy. Feng et al. [115] observed that graphene with monovacancy and long MFP renders the lowest k, which can be explained by the presence of vacancies enhancing the effect of long-wavelength phonon scattering on k. At the same concentration, the monovacancy has larger total cross-sectional area than the other two defects, which induces scattering of long-wavelength phonons, leading to the strongest reduction in k.

Impurity atom is another structural defect. Hu et al. [116] studied the mixture of graphene nanoribbons (GNR) and isotopes, which demonstrated that the presence of impurity atoms caused the inter-atomic bond length and bond energy to be distorted, destroying the lattice symmetry and causing phonon scattering. Later, Chien et al. [117] applied 1.25% functional coverage to GNRs, which reduced the k by 50%. This is since functionalized sp^3 bonds are not bound and only supported by the surface of the GNR. In addition, the surface supported rotating functional group interacts with the surrounding low-energy phonons, which causes phonon scattering.

Moreover, Chen et al. [118] studied the effect of defects on nanowire materials. At low temperatures, the phonon zero acoustic mode plays a leading role in thermal transport. The calculation results of the scattering matrix method indicate that the larger the vacancy defect, the stronger the zero acoustic mode scattering and the smaller the effect of defects on the k. This is caused by additional phonon scattering due to the localization of phonons near the defect. Therefore, controlling defects in materials are extremely important for the regulation of k.

2.1.3.6. Effect of temperature. It is well known that the temperature effect on the k is critical for the study of the thermophysical properties of nanoscale materials, especially at high temperatures. The temperature effect of nanoscale materials has been studied widely, such as that in carbon nanomaterials, aerogels and composite phase change materials (PCM). Results have exhibited remarkably different temperature dependences and their potential for thermal management applications.

Graphene is a hot nanomaterial due to its unique thermal transport properties in multiple aspects. Scientists have found the temperature dependence of k is representative to illustrate some new microscopic thermal transport mechanisms. Fang et al. [119] studied the temperature dependence of k of armchair and zigzag nano-porous graphene, and found that the k decreased with increasing temperature ranging from 300 K to 1000 K. The underlying mechanism was explained by the fact that the higher temperatures result in a decrease in the phonon MFP. Pop et al. [120] obtained the trend of k in graphene at low temperatures, indicating that low frequency phonons dominate heat transfer at low temperatures. Moreover, the low-frequency phonons of zigzag graphene are more dispersive than that of armchair graphene [121], which results in the k of armchair graphene being higher than that of zigzag graphene at 100 K. Renteria et al. [122] found that the in-plane k of freestanding reduced graphene oxide (rGO) films increased from 3 W/m K at RT to 61 W/m K at 1000 K, while the out-of-plane k was only 0.09 W/m K at 1000 K. This strong anisotropy of k provided a new idea for use of graphene as a thermal management material for electronic devices.

Silica aerogel is a promising excellent thermal insulation material, which is almost transparent to 3–8 μm near-infrared radiation. Thus, thermal radiation seriously affects the thermal insulation properties of silica aerogel at high temperatures. Xie et al. [123] studied the relationship between k and temperature of silica aerogel. The results emphasized that the k rose slowly with temperature at low temperatures, while it increased rapidly with the increase of temperature at high temperatures. This is due to contributions of radiation heat transfer at high temperatures.

Carbon nanomaterials are commonly used as core materials for composite phase change materials (PCMs) to enhance thermal transport due to their high k and low ρ [124,125]. Fan et al. [126] studied the temperature dependence of k for paraffin-based composite PCMs filled with various carbon nanomaterials (CNTs, carbon nanofibers, and graphene). The results suggested that k is almost constant when the temperature was lower than the solid phase transition point, while the k increased significantly with increasing temperature when the temperature was close to the solid–liquid phase change point (melting point). Notice that the k of the composite PCMs filled with graphene is the weakest in temperature dependence according to these reports.

Based on the above discussion, we have obtained some meaningful conclusions. For NC materials, the grain size effect is greater than the grain boundary effect on the k. NC boundaries can scatter short-wave phonons, which reduces the lattice k of the material in the low temperature region. By decorating a noble metal (Au, Pd and Pt) between the interfaces, we can cause low-frequency vibration of the C atoms, and the addition of small molecules of halogen between the interfaces creates an additional hot channel that facilitates heat transfer. Different doping and defect concentrations have

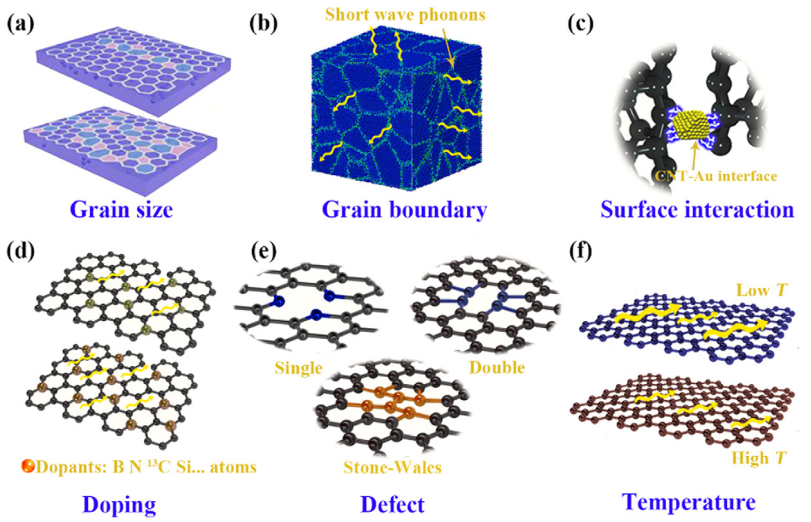

Fig. 8. Schematic diagram of the effect of different factors on the thermal conductivity of nanomaterials. The effect of: (a) grain size [127], (b) grain boundary [92], (c) surface interactions [61] (Reprinted with permission from Elsevier), (d) doping, (e) defects and (f) temperature.

certain effects on the k of nanomaterials, owing to increases in the phonon scattering. The difference in the mass of the doping atoms is also one of the key factors for the sharp decline in k. The k of different nanomaterials has different degrees of dependence on temperature. Fig. 8 illustrates a schematic diagram of the effect of different factors on the k of nanomaterials. It is clearly seen from the graph that different factors exhibit different influences on the crystal structure, either causing k to increase or decrease.

2.1.4. Molecular dynamics (MD) simulations

Although state-of-the-art thermophysical measurement techniques have achieved k characterization on the micro-scale of even nanoscale materials, such as porous polyimide fiber [63] and an individual CNT [128], the thermal transport mechanisms of the heat carriers cannot be well explained by existing experimental observations. Hence, molecular-level simulation has become an important tool for exploring the thermal transport mechanism in simple materials [129]. The representative simulation methods include MD, BTE, thermal diffusion equation and non-equilibrium Green's function. The MD method is based on Newton's law which describes the position and momentum space trajectories of particles in the system. It obeys the ergodic hypothesis and implements the calculation of a vast number of particles. In consideration of the computational domain, MD is the most commonly used method as an atomic-level simulation, which can fully reflect the thermal behavior of materials.

Owing to the nanoscale nature and the outstanding thermal transport properties, carbon nanomaterials have attracted researchers' attention recently. Various simulation methods are being used to reveal the novel mechanisms behind the exceptional thermal transport phenomena. Xu et al. [130] found the remarkably boosted G between individual CNTs by modifying the molecular structure with higher phonon mode coupling. This study described that the electron–phonon coupling effect at heterogeneous carbon–metal interfaces yields extremely high G compared with other nanoscale interfaces. Varshney et al. [131] proposed a new 3-D carbon network which was the combination of graphene sheets and CNTs, and the CNTs were situated between layers of graphene as the pillars. Due to phonon scattering at the carbon–graphene junctions, the heat transfer was dominated by the length of the CNT pillars.

In addition, the thermal transport properties of silicon nanowires (SiNW) have been studied by Yang et al. [132] to verify the low-dimensional phonon transport mechanisms. The results implied that the phonon–phonon interaction can be neglected when the SiNW length is less than its MFP, while the phonon–phonon interaction dominates the thermal transport when the SiNW length is much longer than the MFP. They also verified that Fourier's law is invalid for low-dimensional thermal transport. The relationship between the diameter and k has been studied by Zhou et al. [133]. Based on a combination of Normal scattering process and Umklapp scattering processes of acoustic phonons, they verified the nonmonotonic diameter dependence of k for thin SiNW and the critical diameter was 2–3 nm. Soleimani et al. [134] studied the thermal transport of SiNW and evaluated phonon transport by comparing Equilibrium Molecular Dynamics (EMD) and Non-Equilibrium Molecular Dynamics (NEMD) methods. The results propose that the k is a function of length, cross section width and temperature. The enhancement of k can be achieved by increasing the length, increasing the cross section and decreasing the temperature.

With the rapid development of nanoscale devices and nanocomposite materials, there has been an increasing interest in interfacial thermal transport. The thermal transport mechanisms at the materials' interface have been studied for the purpose of producing suitable micro/nanoscale structures for heat transfer for various situations. The effects of

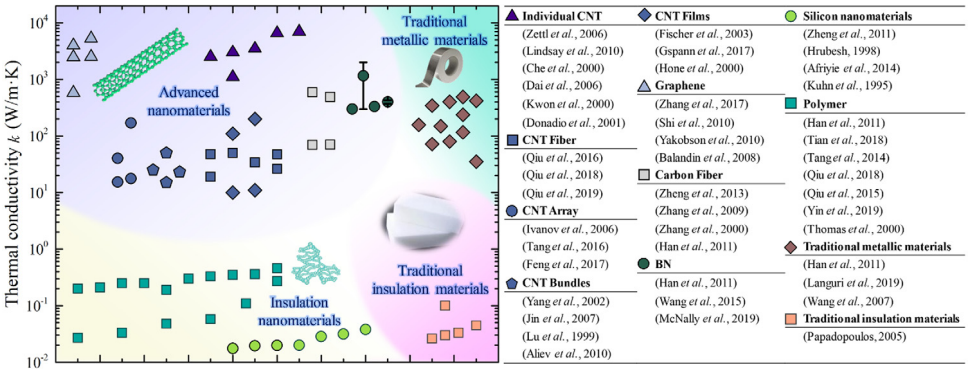

Fig. 9. Schematic diagram of the reported thermal conductivity values of some representative nanomaterials versus traditional materials.

temperature and disorder of solid interfaces have been studied by Stevens et al. [135]. Their NEMD results indicate good agreement with the diffuse mismatch model (DMM) for high mismatch interfaces at a temperature approximately half of the melting temperature. However, the obvious disagreement happened at highly matched interfaces, since significant temperature dependence is included in the MD calculations by Stevens et al. while not in the DMM, which only considers elastic scattering. Moreover, defects exert a great effect on highly matched interfaces but a negligible effect on highly mismatched interfaces. Hence, interface mixing was proposed to be an effective approach to boost the interfacial heat transfer, which was confirmed to result in a doubling of G.

Similarly, Liang and Tsai [136] studied thermal transport between two phonon mismatch solids and reported a novel finding that the introduction of intercalation within a highly mismatched solid–solid interfaces can increase G by 60% at a specific Debye temperature. Comparison between the simulation results and the classical model has been carried out by Merabia and Termentzidis [137]. It was found that the EMD results are consistent with DMM, while NEMD results agree well with results of AMM. This work is very useful for researchers seeking to choose a simulation method. In addition, the k of superlattices is another hotspot in the field of nanomaterial thermophysical properties. Termentzidis et al. [138] reported the interfacial geometry dependence of k for superlattices determined by both EMD and NEMD simulations. If the MFP and superlattice period are on the same order of magnitude, the height and roughness govern thermal transport of superlattices. Specifically, the in-plane k is dominated by the ratio of height to roughness and superlattice period, while the out-of-plane k monotonically increases due to interfacial phonon scattering.

In addition to the effects of phonon transport, in some metal-containing structures, the contribution of electrons to the thermal transport cannot be ignored, since the effect of electron–phonon (e–p) coupling has been confirmed in the previous work [61]. The first detailed study of e–p coupling for thermal transport at metal–nonmetal interfaces was reported by Majumdar and Reddy [139] based on the DMM named Two-Temperature Model (TTM). The results indicate that G strongly depends on the e–p coupling factor and the lattice k of the metal. Since this report, it has been accepted that in the study of nanoscale heat transfer MD results need to be combined with the TTM for calculation of G [140]. The e–p coupling also has been considered for metal–dielectric interfaces [141], which is different from ordinary metal–nonmetal interfaces. It is generally believed that the contribution of e–p coupling to interfacial thermal transport is quite limited for metal–dielectric interfaces. Results from current simulation of thermal transport mechanisms at the micro/nanoscale still fail to agree perfectly with experimental results. With continual improvements in computing capabilities, simulation results are getting closer and closer to reality and MD simulation of micro/nano thermal transport will be more widely adopted in future research.

In the end, we summarize the k of some representative nanomaterials, such as individual CNTs [71,142–146], CNT fibers [60–62], CNT arrays [57,65,147], CNT bundles [148–151], CNT films [152–154], graphene [46,69,75,155], CFs [50,51,94,156], BN [156–158], silicon nanomaterials [159–162], and polymers [5,64,156,163–166], and we compare with k of traditional materials (metal, glass and water, etc.) [156,167–169], with the purpose of emphasizing the superior performance of nanomaterials in heat dissipation or thermal insulation. It is clearly that nanomaterials exhibit excellent thermophysical properties compared with traditional materials, not only for high k, but also for thermal insulation, as shown in Fig. 9.

2.2. Thermal diffusivity

It is well known that k represents the ability of a material to transfer heat, while α corresponds to the rate of heat transfer in a material. In other words, α is considered as the rate of diffusion from the hot end to the cold end in the material, which is independent of the amount of energy during heat conduction, and it is a transient value. Since k and α have a certain relation, in some cases, we will further determine the k of the material by measuring the α, and thus theoretical and experimental research on α of solid nanostructured materials is essential. Here below we will focus

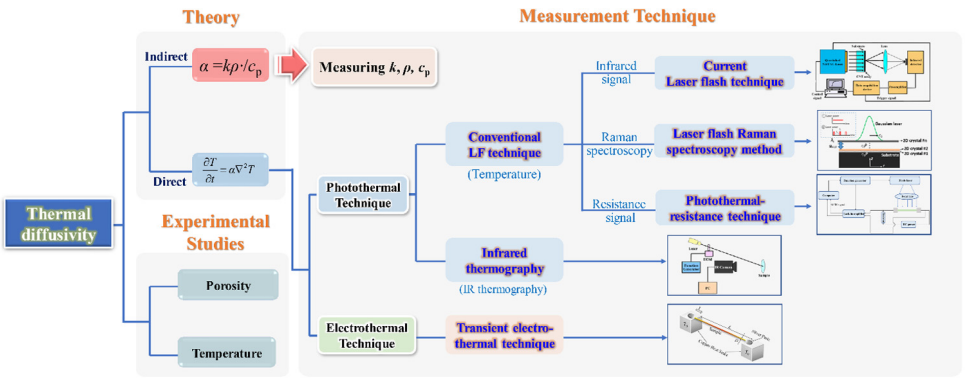

Fig. 10. Schematic diagram of research on thermal diffusivity of solid nanomaterials [170–173].
Source: Reprinted with permission from Elsevier and AIP Publishing.

on theoretical and experimental measurement methods of α for solid nanostructured materials. The laser flash Raman spectroscopy method and transient electro-thermal (TET) technique are widely used for measurement of α. The factors affecting α will also be discussed and summarized in detail. Fig. 10 displays a high-level overview of the study of α of solid nanomaterials.

2.2.1. Theory

The relation between k, ρ and c_p is defined as:

$$\alpha = k/\rho \cdot c_p \tag{23}$$

The higher the α, the stronger the ability of the medium to balance its internal temperature o, so α is an indicator of the ability of the medium to propagate energy. Direct theoretical calculation of α is relatively rare and difficult. In theory, we usually calculate k and c_p to obtain α using Eq. (23). We have already discussed the use of BTE for theoretical calculation of k. The specific heat capacity includes mainly phonon specific heat capacity and electron specific heat capacity. However, for some nanomaterials, c_p is primarily dominated by phonons, as will be described in detail in Section 2.3.

Purely theoretical studies of thermal diffusivity are limited, hence α and the involved transport mechanisms are generally studied using experimental techniques. Direct measurements of α based on another form of α, which describes the simple relationship between time and temperature, are defined as follows:

$$\frac{\partial T}{\partial t} = \alpha \Delta^2 T \tag{24}$$

Since α describes the rate of heat transfer from heat source to heat sink, a rapid heating technique should be utilized in the measurement. The first characterization of α was done using laser flash technology to heat the sample with a laser pulse and the temperature change in a short distance from the heating location was analyzed [174]. Under one-dimensional adiabatic conditions, α is generally defined as follows:

$$\alpha = 0.1388 \times d^2/t_{0.5} \tag{25}$$

where d is the thickness and $t_{0.5}$ is the half maximum of time. Since the measurement of α requires rapid heating, measurement techniques are mostly based on laser heating, like the laser flash Raman spectroscopy method. Here we introduce some typical measurement methods.

2.2.2. Experimental measurement techniques

2.2.2.1. Laser flash technique. The laser flash technique as a classical thermophysical property measurement technique was first proposed by Parker et al. in 1961 [174]. It is a high sensitivity, transient, non-contact measurement technique and is widely applied in the measurement of the α for homogeneous materials [175]. During testing, a short laser pulsed is irradiated onto the front side of the sample, and then the temperature rise of the sample at the back surface is recorded in real time. The α is obtained by fitting the temporal temperature profile. An important feature of this technique is the energy and the width of the pulse laser can be easily adjusted. Based on this measurement principle, Lin et al. [176] characterized the thermophysical properties of vertically aligned MWCNTs. For their measurement analysis, they made some assumptions. First, when the laser was irradiated onto the surface of the sample, the thin gold coating which facilitated the rapid planar distribution of heat was considered to undergo ideal 1-D heat transfer. Second, the surface of the sample was opaque due to the gold coating, and thus the penetration depth of the incident laser was regarded to be negligible. Therefore, a very small change in temperature was required during each measurement. It was confirmed that

α is independent of the thickness of the sample and the metal coating on the bottom of the MWCNT film improved the measurement accuracy. Xie et al. [170] used nanosecond pulsed lasers to achieve non-contact heating of MWCNT arrays, and the α was obtained by fitting for temperature versus time. Measured α value for the MWCNT arrays were as high as 4.6×10^{-4} m^2/s at RT, which is much larger than that of some known excellent thermal conductors, such as copper and silver. Furthermore, Akoshima et al. [177] synthesized a high-purity super growth SWNT forest with a length of 1 mm. It was found that the α of SWCNT forests is not much different from isotropic graphite and has a strong dependence on temperature. Specifically, the α was within the range of 0.47–0.77 $\times10^{-4}$ m^2/s at RT, which was higher than 0.2–0.6$\times10^{-4}$ m^2/s at 1000 K.

2.2.2.2. Laser flash Raman spectroscopy method. As a non-contact, non-destructive and fast thermal property measurement method, the Raman spectroscopy method is ideal for measuring microscale materials and has been applied for graphene [72], bilayer MoS_2 [178] and 3-D nanofoams [179]. This method is based on the temperature dependent Raman band shift and generally defines the thermal properties by the combination of absorbed laser power and the steady-state heat conduction model. However, it is difficult to accurately determine the absorbed laser power of materials, which limits the application on micro/nano-scale materials measurement. To solve this problem, Li et al. [180] have reported a new method, referred to as the Laser flash-Raman spectroscopy method. By using a pulsed laser with two independent steady-state and unsteady-state heat conduction models, they eliminated the influence of the absorbed laser power parameter in the analysis of thermal properties. After verifying the accuracy of the technique by comparing with α results from measurements made using the 3ω method, they completed α measurements of CFs and CNTs. An additional advantage of this technique is the sample can be non-electrical, which is suitable for the thermophysical property characterization of insulating materials. Later, Li et al. [180] extended the materials to 2-D nanomaterials and further explored the difference between the 2D nanomaterial measurements with and without a supporting substrate. They reported the measurement of thermal properties of 2-D van der Waals heterostructures by using variable spot sizes, which ensured the simultaneous measurement of k, α and interfacial resistance [171].

2.2.2.3. Transient electro-thermal (TET) technique. The transient electro-thermal technique (TET) is an effective method for measuring the α of fibers or narrow strips, which overcomes the shortcomings of other methods such as long test time and weak signals [181]. Briefly, a direct current is applied to a suspended fiber which sets on the heat sinks. The generated Joule heat will increase the temperature of the fiber, and the transient temperature response at each moment is used to determine the α of the material.

During derivation of the thermal conduction model for the TET method, Guo et al. [168] ignored the heat loss on the sample surface and assumed that the sample was heated constantly. The stability of sample heating power was maintained by increasing the impedance of the circuit in the experimental setup. The average α of the SWCNT bundle in this work was measured to be 2.73×10^{-5} m^2/s. At the same time, the α of the non-conductive material was measured using a polyester fiber coated with a gold layer, which was 5.26×10^{-7} m^2/s. Given the effect of convection and radiation and non-constant power heating under low vacuum, Xing et al. [182] established a dimensionless model under surface heat transfer and non-constant heating conditions. The α was obtained using the Levenberg–Marquardt algorithm by analyzing the temperature response in the full model. It was found that a linear relation exists between the dimensionless parameter model and the measurement error, which provides an evaluation method for the impact of different conditions on the measurement error. Besides the fibrous material, Feng et al. [183] studied the α of poly(3-hexylthiophene) narrow strips by the TET method to complete the calibration of the temperature and resistance relationship. This study provided a technical reference for the measurement of α of film materials.

It is also intriguing to note that the α in the TET method is extracted from the transition state before the temperature reaches the steady state. Huang et al. [184] extended the electrothermal method to obtain α from the initial transient change to the final steady state. The advantage of this approach is there is no need to know the c_p and ρ of the material itself. A more accurate α can be obtained by global fitting of the normalized temperature curve over time. In a follow-up study, Huang et al. [185] used the TET method to study the thermophysical properties of a natural fiber, *i.e.*, spider silk. The results exhibited that both α and k increased under stretching. Specifically, α was increased by 50% with a 20% strain. Xing et al. [181] measured α of spider silk by both the TET method and the 3ω method to compare the advantages and disadvantages between these two techniques. It was demonstrated that the TET method had a significant time advantage when measuring the α of large diameter long fibers. However, in other cases, the TET method is inferior to the 3ω method in measurement accuracy.

2.2.2.4. Photothermal resistance technique. The photothermal resistance technique, also known as the optical heating and electrical thermal sensing (OHETS) technique was first proposed by Hou et al. [172] in 2006. It can be used to characterize the thermophysical properties of 1-D micro/nanoscale conductive and non-conductive materials. In brief, the sample to be tested is suspended on two electrodes and irradiated with a periodic laser beam. Due to the heating of the laser beam, the temperature of the sample changes periodically, so that the electrical resistance of the sample also produces periodic variation. Then the variation in electrical resistance is reflected by the change of voltage via applying a direct current to the sample, which is used to derive the thermophysical property parameters of the sample. Based on the above-mentioned measurement principle, Hou et al. [186] verified the reliability of this technique by measuring a platinum wire of 25.4 μm diameter as the reference sample, and pointed out that the measured k of the platinum wire was consistent with the

reference value. Subsequently, they measured the α of three different SWNT bundles, human hair and clothing fibers. Since SWNT bundles are conductors, while human hair and clothing fibers are non-conductors, a metal film was deposited onto the non-conductive sample surface to ensure that the temperature can be accurately extracted after applying an electrical voltage signal. The results found that the α of three different SWNT bundles was 2.98×10^{-5} m^2/s, 4.41×10^{-5} m^2/s and 6.64×10^{-5} m^2/s. For non-conductive human hair and clothing fibers, the α was on the order of 10^{-6} m^2/s, which further demonstrated the excellent thermophysical properties of CNTs compared to traditional materials.

Moreover, Hou et al. [187] measured the α of single submicron ($\sim$800 nm) polyacrylonitrile (PAN) fibers. During the measurement, since PAN fibers are non-conductive, an Au film with a thickness of nanometers was coated on the surface of the PAN fibers and a periodic laser beam pulse was irradiated on the suspended individual fibers. The periodic variation of the sample temperature was derived by the change of the electrical resistance of the nanoscale Au film. By measuring the α of three samples coated Au films with different thicknesses, it was concluded that if the thickness of the Au film is reasonable (approximately nanometer level), this technique can be used to successfully measure the α of low k, non-conductive 1-D micro/nanoscale materials.

2.2.2.5. Infrared thermography. Another effective method for measuring α is infrared thermography, which was first proposed by Welch et al. [188] to measure the α of metal and graphite-epoxy plates. The measurement principle is also based on the variation of temperature caused by photothermal excitation, and the distribution of temperature is recorded by an infrared camera. During the measurement process, the sinusoidal laser beam is irradiated on the surface of the sample, when the heat propagates along the radial direction, the amplitude and the phase of the thermal wave are modulated by adjusting the frequency of the laser to ensure that the sample remains thermally thin. At that time, the thermal response can be represented by the 1-D heat conduction equation. Although the α is related to both the amplitude and the phase change of the heat wave, the phase signal is more suitable for the local variation of the surface temperature and the emissivity of the sample to be tested. Therefore, Giri et al. [173] proposed a new method to estimate α by only using the phase information. They reported that active infrared thermography techniques can be used to characterize α in the direction perpendicular to the axial direction of the templated Bi_2Te_3 nanowires obtained by electrodeposition on anodized aluminum (AAO) templates. The results showed that the α perpendicular to the axial direction of the nanowire of AAO templates with different pore sizes is within the range of $8.8–9.2\times10^{-7}$ m^2/s, while the α of the AAO/Bi_2Te_3 nanocomposite was slightly lower, 6.7×10^{-7} m^2/s.

Moreover, Mendioroz et al. [189] measured the α of thin plates and filaments by means of a lock-in thermography technique. The experimental factors affecting the α were analyzed and the experimental conditions for accurate measurement were established. The results indicated that the infrared thermography technique could be used to effectively measure α of various isotropic and anisotropic thin samples under a vacuum environment. Notice that the sample needs to be large enough to eliminate the influence of boundary effects. It was further confirmed that the 1-D heat flux loss model overestimates the α of the sample, which proves that some α values reported in the literature were higher than the true value. The α of polyether-ether-ketone (PEEK) films with thicknesses of 25, 75, 125, and 250 μm was measured in the air and vacuum, respectively. The results argued that the α in a vacuum was lower than the α in the air, owing to the elimination of heat flow loss in the vacuum.

2.2.3. Experimental studies

2.2.3.1. Effect of porosity. To study the effect of porosity (ζ) on α, we need to pay attention to highly porous solids which render excellent thermal insulation properties. It is generally believed that the thermal insulation performance is largely determined by the pore structure [190]. Wahsh et al. [191] studied the α of nanoporous spinel/forsterite/zirconia composite ceramics, which revealed that the ζ increases with increasing zirconia content, resulting in the decrease of α. This can be attributed to the tetragonal to monoclinic phase transition of zirconia and the thermal expansion mismatch between the different phases in different ceramic composites. Some studies suggest the use of density ρ instead of ζ to construct the relation with α. This is reasonable as ρ is inversely correlated with ζ in the form of $\zeta = 1-\rho/\rho_s$. Here ρ_s denotes the density of dense materials without ζ. Venkataraman et al. [192] studied the relationship between ρ and α of aerogel-based nano-porous fibrous materials. The results indicate that the higher the ρ, the greater the k. Hirata et al. [193] studied the α and k of porous mullite ceramics from both theoretical and experimental aspects. The results claim that α and k have similar dependence on ζ. These conclusions are intuitive because higher ρ or lower ζ suggest high mass fraction of solid components, which construct the heat conduction network of the porous material.

Similarly, Mayr et al. [194] measured the α of CF reinforced polymers (CFRP) using active infrared technology and discussed the effects of pore shape and ζ on α. Interestingly, it was found that the α of CF decreases linearly with an increase of ζ, and is lower than that of spherical pores under the same ζ. Wu et al. [195] also confirmed that the α of CFRP is closely related to the pore shape and ζ. As ζ increases, the α of CFs decreases correspondingly. In addition, the α of CFRP in three directions was studied, and was the largest along the direction of the fiber bundle, which demonstrated the remarkably anisotropy in thermophysical properties.

2.2.3.2. Effect of temperature. In general, the temperature-dependent α relies on two factors, one is the lattice wave and the phonon transfer energy, the other is the free electron transfer energy. When the temperature rises, the collision probability between phonons is larger, resulting in stronger lattice scattering and reduced phonon MFP, and thus the effect of phonons on the α is reduced.

Graphene is a typical anisotropic thermally conductive material which is widely used for heat dissipation in electronic devices. Many scientists have studied the influence of temperature on graphene thermophysical properties [196]. Pan et al. [197] prepared reduced graphene oxide/multiwalled carbon nanotubes (rGO/CNT) films and studied the effect of temperature on their α. The results emphasized that both in-plane and cross-plane α values of the rGO/CNT increase with increasing temperature, because higher phonon vibration frequencies and larger amplitudes led to faster heat transfer at higher temperatures [198]. However, others reported the opposite trend, which could be explained by Umklapp phonon scattering [110]. Tuan et al. [199] bonded graphene to an alumina substrate and measured its α. It was found that the α of graphene decreased with the increasing temperature and the in-plane α of graphene was as high as 7.5×10^{-6} m^2/s at RT. This is 400 times that of the cross-plane α of graphene. From the above studies, we can see that graphene and its composite films demonstrate a great potential in thermal management applications.

CNT-based composites are also nanocomposites with excellent thermal transport properties. Jackson et al. [200] studied the α of CF/CNT composites. The α of the composites tends to decrease with increasing temperature. The higher the CNT volume fraction, the higher the α of the composites, at constant temperature. Xie et al. [170] measured the α of MWCNT in the temperature range of −55 to 200 °C. The results supported the finding that the α increases with increasing temperature in the range of −55 to 70 °C. This trend is consistent with that previously obtained via the 3ω method [150], but the results were an order of magnitude higher than the α value measured with 3ω. The reason for this disparity is that longer CNTs were used in Ref. [150], which typically have more defects that leads to an increase in the phonon scattering probability and thus result in reduced heat transfer capability. In the temperature range of 70–200 °C, the α does not change much, which was said to be due to the fact that the phonon scattering mechanisms were unclear and need to be further clarified [150].

The temperature effect on thermophysical properties has also been widely studied, in nanopowders, which are common matrix materials for nanocomposites due to their scale effect. Similarly, Voges et al. [201] studied the thermophysical properties of SiO_2/Al_2O_3/carbon black composite powder tablets. Their results suggest that the thermophysical properties of powder tablets are comparable to those of aerogels, and their α values decrease with increasing temperature. This is due to enhanced Umklapp scattering of phonons with increased temperature resulting in decreased α. Zhan and Mukherjee [202] found that the α of CNT-reinforced Al_2O_3-based ceramics decrease with increasing temperature, which is also due to the effect of Umklapp scattering and thus reduced phonon MFPs.

Thus far, we have summarized and discussed research on α of solid nanomaterials. Since there are great difficulties in the theoretical calculation of α, the more common practices are calculated indirectly by using k, c_p and ρ, which are obtained by experimental measurement techniques at this stage.

Most measurement techniques are transient, and can be categorized into photothermal techniques and electrothermal techniques. The most classic photothermal technology is the traditional laser flash method. With the development of technology, more advanced measurement techniques have emerged, including the current laser flash method (the main difference is temperature measurement technique compared with the traditional laser flash method), laser Raman flash method, photothermal resistance method and infrared thermography. For electrothermal techniques, we focus on the transient electrothermal technique. In addition, the factors affecting the α of solid nanomaterials mainly involve in ζ and temperature. The results have demonstrated that α and k have similar dependence on ζ, while the temperature-dependent α relies on two factors: one is the lattice wave and the phonon transfer energy, the other is the free electron transfer energy. Fig. 11 summarizes the α values of some representative nanomaterials (individual CNTs [168,170,177], CNT fibers [60–62], CNT array [57,172,203,204], CNT films [148,205], CNT bundles [206,207], CNT composites [202,208], silicon nanomaterials [159], graphene [209–211], polymer [181,212–214] and aerogel [215–217]) and traditional materials (metal, air, foam, etc. [218]) from the literature, which is convenient to intuitively understand the superior thermophysical properties of nanomaterials compared with traditional materials.

2.3. Isobaric specific heat capacity

2.3.1. Theory

Assuming that the atoms in the solid are simple harmonic oscillators and the vibrational degrees of freedom are fully excited, the high temperature limit of c_p of a monoatomic solid is defined as [219]:

$$\overline{c_p} = 3\overline{R} = 3N_A k_B \tag{26}$$

This is the Dulong–Petit law, which can be explained by the energy equipartition theorem in classical statistical mechanics. This law cannot predict the materials' behavior at low temperatures but overestimate the c_p of many materials such as graphite and diamond. It has been observed that the c_p of some solids decreases with decreasing temperature, which does not agree with the Dulong–Petit law. Einstein explained this trend based on quantum theory. And he also used harmonic oscillators to describe atomic vibrations and some new assumptions: energy quantization and atomic vibration at the same frequency [220]. The c_p in the Einstein model is defined by:

$$c_p = 3N_A k_B f_E \left(\frac{T_E}{T}\right) \tag{27}$$

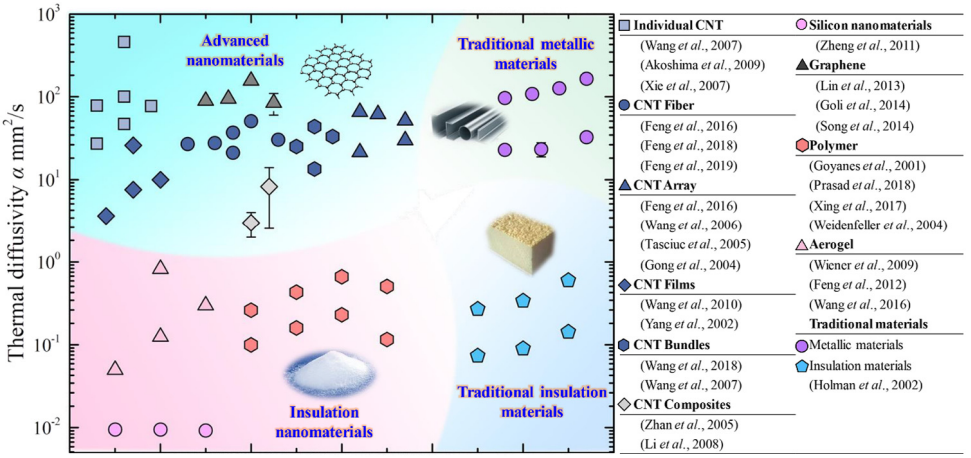

Fig. 11. Schematic diagram of the reported thermal diffusivity values with some reported representative nanomaterials versus traditional materials from the literature.

where $T_E = \frac{\hbar\omega_E}{k_B}$ is the Einstein temperature and $f_E\left(\frac{T_E}{T}\right)$ is the Einstein heat capacity function. When $T \gg T_E$, the Einstein c_p can be expressed as $c_{p,E} = 3N_A k_B$, which agrees well with the results of the Dulong–Petit law.

Later, Debye [221] introduced the concept of collective vibrations of the lattice. It is assumed that the crystal is an isotropic continuum and the thermal motion of the atom occurs in the form of elastic waves. Each elastic wave vibration mode is equivalent to a harmonic oscillator. Debye adopted the concept of Einstein's energy quantization and corrected the assumption of atomic single frequency vibration to consider all the vibrations below the Debye frequency. The Debye frequency is the upper limit of the specified elastic wave frequency. The expression of the Debye model is:

$$c_p = 9N_A k_B \left(\frac{T}{T_{De}}\right)^3 \int_0^{T_D} \frac{x^4 e^x}{(e^x - 1)^2} dx \tag{28}$$

where $x = \frac{\hbar\omega_E}{k_B T}$. At high temperature $T \gg T_{De}$, which is in good agreement with the Einstein model and the Dulong–Petit law. At low temperature $T \ll T_{De}$, the c_p of the Debye model is $c_p = \frac{12}{5} N_A k_B \left(\frac{T}{T_{De}}\right)^3$, which is referred to as the Debye-T^3 law. This is a good fit to experimental curves since only the low frequency modes are excited by thermal excitation. Fig. 12 provides a general idea of the theoretical study of c_p of solid nanomaterials, which clearly reflects the connections and differences between the above-mentioned three theoretical computational models.

2.3.2. Experimental measurement techniques

2.3.2.1. 3ω method. The 3ω method can be used to measure the c_p for a wide variety of nanomaterials. In the limited reports on the c_p values of nanomaterials, the traditional 3ω method has been applied to the measurement of millimeter-long aligned MWCNT arrays [150,222,223], CNT fibers [61,62], and nanofilms [224,225]. Notice, these nanomaterials are generally in limited amounts, which makes conventional c_p measurement techniques such as differential scanning calorimetry (DSC) ineffective. Lu et al. [222] completed c_p measurements of MWCNT arrays within the 10–300 K temperature range under vacuum conditions. The results confirm that c_p is linearly dependent on temperature and is nearly 500 J/kg K at RT, which is mainly attributed to the behavior of phonons. According to the theoretical calculations, c_p is related to the integral of phonon spectrum and temperature. The phonon spectrum is constant over the experimental temperature range (far lower than the Debye temperature), which results in the linear dependence of c_p on temperature. Hu et al. [223] reported the c_p of 13 μm-thick vertically aligned CNT arrays is 312 J/kg K around RT, and climbs to 375 J/kg K when the temperature increases to 325 K. These values are much lower than the previous reports [50,62,222], which could be explained by the effect of the extremely low c_p value of the trapped air in the CNT array.

Lu et al. also used the 3ω method to measure the c_p of a typical filament sample, such as a high-purity platinum wire with a diameter of 20 μm and a length of 8 mm as used in their study [223]. A significant contribution of their study is the air convection-induced heat loss was quantitatively estimated for the first time, and the proper vacuum condition was given to ensure the measurement uncertainty of c_p was less than 4%. Furthermore, the sample quantity required for the c_p measurement can be much less than other techniques. Specifically, the filament sample can be as light as 0.00001 mg, such as a 1 mm long CNT bundle, which is 10^5 times lighter than that required for commercial DSC techniques which basically require quantities in mg. Therefore, it is safe to say the 3ω method provides the possibility of c_p measurement of trace-level nanomaterials, which is of great significance since the quantity of novel nanomaterials is always limited. Qiu et al. attained the c_p of the functionalized and densified CNT fibers [60], Au nanoparticle-decorated CNT fibers [61], and

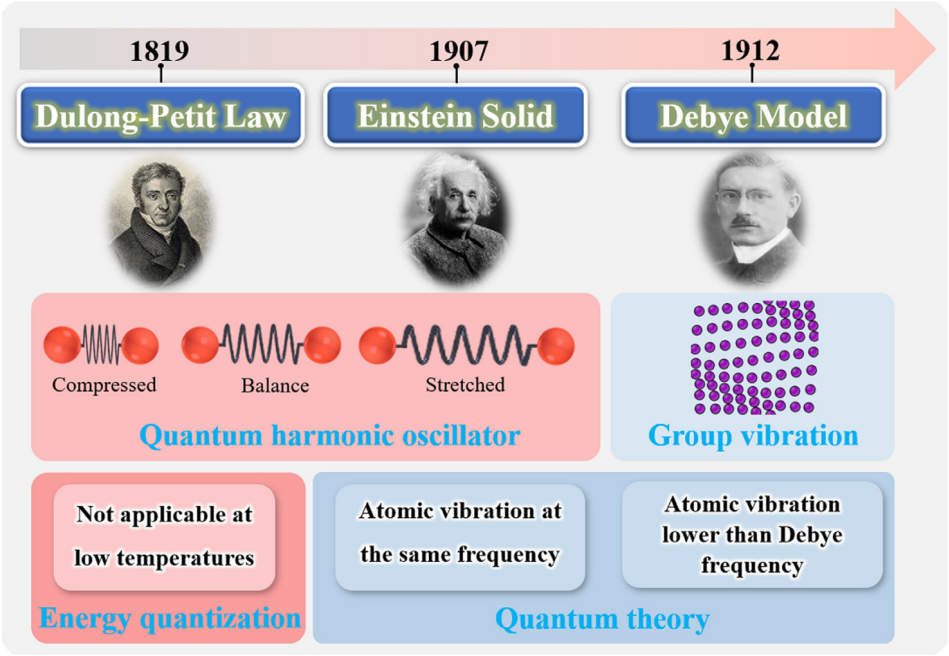

Fig. 12. Schematic diagram of the theoretical study progress on specific heat capacity of solid nanomaterials.

iodine molecule-decorated CNT fibers [62] by directly measuring k and α using the 3ω method. All of the results suggest that the c_p values of the decorated fibers are around 685 J/kg K, which is close to that of the pristine fibers (780 J/kg K) and reports from other researchers [50,222]. A big step for thermal characterization of the assembled fiber structure is the latest work by Qiu et al. [224], which points out the real radiation is only correlated with the outmost few layers of bundles on the CNT fiber surface. Based on the experimental observations, they developed a novel theoretical model which used the true circumference of the fiber surface to replace the fiber diameter. This progress is significant for the accurate evaluation of the thermophysical properties of assembled nanostructures.

Ftouni et al. [225] developed a 3ω-Völklein method for the c_p measurement of SiN nanofilms. Völklein geometry [226] refers to a structure that is elongated and suspended, which is used to design the sensors. They combined this geometry with the 3ω method and achieved high sensitivity measurement of ultra-thin nanofilms. Before the measurement, the researchers placed niobium nitride as a thermometer on SiN nanofilms with 50 nm and 100 nm thickness, respectively. During this measurement, the c_p did not show a significant difference for nanofilms with different thicknesses. The experimental results are in good agreement with the Debye-like c_p model above 100 K. The high sensitivity (4×10^{-6} J/kg K) of this method makes it valuable for the measurement of nanofilms.

2.3.2.2. AC-calorimetric technique. Notice that c_p has important research value for understanding lattice vibration, superconductivity and structural phase transition [227,228]. The AC-calorimetry technique was first developed in 1968 by Sullivan and Seidel to measure the c_p of samples with weight less than 200 mg [229]. In brief, the sample is heated by an alternating current with an angular frequency of $\omega/2$ passing through the heater, causing the temperature of the sample to periodically change with time, and then the current is amplified by a lock-in amplifier. Finally, the c_p of the sample can be determined by measuring the temperature of the system as a function of the current frequency.

The AC calorimetry method is a dynamic measurement method. That is, the c_p of the sample to be tested is measured during the dynamic heating process. Since the thermal equilibrium is difficult to achieve in the dynamic process, the c_p measurement accuracy is lower than that of the adiabatic method [230]. However, AC calorimetry is very suitable for the measurement of small samples, and the measurement sensitivity can reach 10^{-8}–10^{-12} J/K.

Zhang et al. [231] measured the slightly abnormal c_p of superconducting Sn nanowires at the superconducting transition using the AC calorimetry method. The results claim that the c_p of Sn nanowires are significantly different from that of the bulk Sn, which had two peaks at temperatures of 3.7 K and 5.5 K ascribed to the inner bulk contribution and the surface contribution, respectively [231]. Lee et al. [232] used this method to study the structural phase transition of Zr/B multilayer nanofilms, which can achieve low scan rate of less than 4000 K/s and thus minimize the heat loss [233]. Two exothermic peaks were found in the c_p versus temperature rise curve. The first peak is due to the non-uniform diffusion of Zr and B at low temperature to form amorphous Zr/B, and the second peak is due to crystallization at high temperature. Pradhan et al. [234] measured the c_p of randomly oriented SWCNT and MWCNT while using bulk graphite powder as a

reference sample. The results illustrate that the c_p values of the graphite powder and the MWCNT are the most consistent, while the c_p of MWCNT has the weakest temperature dependence, which is due to its macroscopic arrangement.

Since the AC calorimeter method is capable of measuring samples below 1 ng, Tress et al. [235] used this method to measure the glass transition of polystyrene nanofilms. This method was compared with broadband dielectric spectroscopy (BDS), spectroscopic vis-ellipsometry (SE), DSC and other methods. Studies pointed out that in multilayer molecular weight polystyrene, the glass transition temperature does not change by more than ± 3 K at a layer thickness of 5 nm. It was found that the c_p of nanomaterials obtained by the AC calorimetry method can explain the increase in the c_p compared to their bulk materials.

2.3.3. Experimental studies

2.3.3.1. Effect of size. Experimental reports studying the effect of solid size on the c_p are relatively limited. A representative example is a study by Novotny et al. [236], which reported that 27 Å and 37 Å lead particles (purity: 99.9999%) have higher c_p than bulk lead at ultra-low temperature (1.5–5 K). That phenomenon can be explained by the fact that small particles have a large specific surface area, which facilitates surface phonon softening. Since softening implies the attenuation of the vibration frequency, c_p, which depends on the vibration of the lowest frequency of the lattice, is therefore enhanced. Similarly, Rupp and Birringer [237] measured the c_p values of NC–Cu and polycrystalline Cu. The size effect brought about a 10% increase in c_p. Strukov et al. [238] performed c_p measurements of ultrathin ferroelectric $BaTiO_3$ films with different thicknesses using an ac-hot probe method. When the $BaTiO_3$ film thickness is less than 100 nm, the c_p does not increase abruptly near the ferroelectric phase transition temperature as observed with other sizes, owing to the large diffusion of the transition at the nanoscale. In marked contrast, in a study of a ternary nitrate eutectic [239], the effects of the addition of SiO_2 nanoparticles with different diameters (from 5 nm to 60 nm) on c_p were all basically the same. The c_p values were all about 1800 J/kg K, which represents a 13% boost compared to the counterpart without the nanoparticle addition. This indicates that the size of the nanoparticle additive has no effect on c_p for the eutectic material.

In a theoretical investigation, Singh et al. [240] calculated c_p values for metal nanowires and films. All the calculation results corroborated that the atomic vibration amplitude of the nano-solid surface is higher than that of the bulk material. As the size decreases, the atomic thermal vibration energy of the material surface increases, and the c_p is impacted accordingly. Wang et al. [241] studied the c_p of CuO nanoparticles with different sizes. At 325 K, the c_p increases from 0.49 kJ/kg K to 0.51 kJ/kg K as the particle size decreases from 12.5 nm to 3.4 nm. This observation was further corroborated in an experimental study, which found the softening of surface atom vibrations due to size effects causes an increase in c_p [240]. This conclusion was also found to be valid for the semiconductor materials [242].

2.3.3.2. Effect of grain boundary. Prior to talking about the effect of grain boundaries, we need to review the definition of NC materials because they are the main source of grain boundaries. Generally, NC materials are composed of nanometer-sized (1–10 nm) grains. The grain boundary is the interface between the grains with the same structure and orientation, which accounts for 50% or more in NC materials. The fractional and average grain size of grain boundaries in NC materials are inversely proportional [243]. Due to their small grain size and large specific surface area, the thermophysical properties of NC materials are significantly different from those of conventional crystals. For example, NC materials have a higher c_p. Therefore, nanopolycrystallization is an effective method for enhancing the thermal transport of solid nanomaterials.

Many scientists have studied the effect of grain boundaries on c_p. As for nanopolycrystalline metals and alloys, Tang et al. [244] studied the c_p in NC–Ni. It was found that NC–Ni has a higher c_p compared to conventional crystals due to the existence of grain boundaries. The excess isobaric specific heat capacity (the isobaric specific heat capacity difference between the NC materials and the bulk materials, Δc_p) is reduced at low temperature and high temperature, which is consistent with the results of previous experimental and MD simulations results [245,246]. Rojas et al. [247] confirmed by Raman spectroscopy that the c_p values of NC–Fe, Cu, Ni and $LaAl_2$ alloys are higher than those of the corresponding bulk materials. Besides, Δc_p at low temperatures had also been studied. The results found that the peak of Δc_p occurs at a low temperature range of 20–65 K. The reason is the softening of the phonons at the grain boundaries, that is, the atomic fraction increases significantly at the surface and the interface, and the decrease of the neighboring coordination number of the surface and interface atoms reduces the phonon frequency, which affects the phonon spectrum and Debye temperature of the NC materials, resulting in a decrease in c_p. Moreover, Li et al. [248] studied the effect of grain boundaries on the c_p of NC–Al at low temperatures, and the conclusion is in accordance with the above-mentioned results.

In addition, Adiga et al. [249] studied the effect of grain boundaries on the c_p of ultrananocrystalline diamond (UNCD). The results implied that the c_p of UNCD at RT is approximately 20% higher than that of single crystal diamond, and the Δc_p reaches a maximum in UNCD at about 350 K. The reason is that the vibrational density of the atoms increases at or around the grain boundary. These enhancements occur in the low frequency region of 5–20 Hz, and the contributions of the low and intermediate frequency phonons to the c_p become smaller at 350 K.

2.3.3.3. Effect of interfacial component. For the study of the c_p of nanoscale solid materials, we are more concerned with nanometer-sized crystalline materials, which are typically polycrystals with a crystal size of several nanometers. The polycrystals are usually composed of interfacial components formed by all atoms in the crystal lattice and all atoms located in the interface (grain boundary) between the crystallites. Therefore, in order to explore the effect of the interfacial components on c_p in crystalline materials, Rupp and Birringer [237] explored the c_p of nanometer-sized crystalline and polycrystalline Pb (crystal size is 6 nm) and Cu (crystal size is 8 nm) in 1987. The results revealed that the c_p value of both

Cu and Pb nanocrystals is slightly higher (10% and 40%) than that of the polycrystalline state in the temperature range of 150–300 K. This is mainly due to the relatively low density of Pb and the weak mutual coupling of atoms between the interfaces, which demonstrates that the interface interaction is also one of the factors that should be considered when determining c_p values. Bai et al. [250] studied the effect of the interfacial component on the c_p of NC–Fe with a grain size of 40 nm in an ultra-low temperature range of 1.8–26 K, and found that the increase in c_p at a relative high temperature ($\sim$26 K) is mainly caused by the Einstein oscillators due to the weak mutual coupling of atoms at the interface.

Lei et al. [251] also studied the effect of surface components on the c_p of metal NC materials. It is well known that the surface phonon softening causes the c_p of the metal nanocrystal material to be enhanced at low temperature, but the effect of the surface oxidation causes an unusual decrease in c_p. They used face centered cubic Al (fcc-Al) and amorphous Al_2O_3 (a-Al_2O_3) nanocrystals as the surface oxide layer around the NC–Al, and explained the phenomenon of c_p reduction by calculating the VDOS of fcc-Al and a-Al_2O_3 nanocrystals. The a-Al_2O_3@Al nanoparticles are composed of 1 nm thick a-Al_2O_3 shells encapsulating a fcc-Al core. According to the VDOS calculation results, the surface and volume VDOSs ($D(\omega)$) of the α-Al_2O_3 layer are different from the pure fcc-Al nanocrystals at low frequencies and $D(\omega)$ is scaled to $D(\omega) \sim\omega^{1.5}$. Furthermore, the c_p of a-Al_2O_3@Al nanoparticles demonstrated a different temperature dependence from pure metal nanocrystals at low temperatures.

2.3.3.4. Effect of temperature. In 1912, Debye proposed a formula for calculating the c_p of solids, which considered that the c_p is the sum of the atomic vibrations of various frequencies [252]. When the temperature is much lower than the Debye temperature, the c_p is proportional to T^3 in the 3-D case, to T^2 in the 2-D case and to T in the 1-D case, which is the well-known Debye's law [253]. When the temperature is much higher than the Debye temperature, the c_p of the solid conforms to the Dulong–Petit's law, which says the c_p is a constant independent of temperature [254]. Generally, the c_p of a solid is caused by the thermal vibration of the crystal lattice. As the temperature increases, the thermal vibration of the crystal lattice becomes stronger, and the c_p of the solid is larger. This section will discuss the effect of temperature on c_p of several common nanomaterials such as CNT, graphene, and nanocrystals.

For CNTs, Hone et al. [255] studied the temperature dependence of c_p on SWCNTs ropes at low temperatures. When the temperature is within 100–200 K, the c_p is linearly correlated with T. When the temperature is below 50 K, the c_p is proportional to T^2, which is in accordance with Debye's law. Similar results were reported by Li et al. [256]. In addition, some previous work reported that the c_p of both SWCNTs and MWCNTs renders a linear dependence on T at low temperatures [150,257], which is explained by the fact that the wall-to-wall coupling in MWCNTs is quite weak compared with graphite. A few research groups studied the c_p of double-walled carbon nanotubes (DWCNTs). For example, Xiang et al. [258] reported that the interaction between adjacent tubes and layers is not negligible for the c_p of DWCNTs in the low temperature of 0.3–30 K. The contribution of electrons to c_p in SWCNTs is much lower than that of phonons at low temperatures [256,259], and the relationship between c_p and T follows a cubic polynomial.

For graphene, Alofi et al. [260] studied the c_p of graphene under different acoustic branches as a function of T, such as the in-plane longitudinal mode (LA), the in-plane transverse mode (TA), and the out-of-plane or flexural mode (ZA). At low temperatures below 100 K, the c_p of the LA branches and the TA branches is proportional to T^2, while the c_p of the ZA branches was proportional to T, which is attributed to the quadratic dispersion in the ZA phonons. Therefore, the overall c_p of graphene is proportional to T at low temperatures. When $T > 2500$ K, the c_p is independent of T, which conforms to Dulong–Petit's law. Nika et al. [261] studied the phonon c_p of the single-layer, bilayer and twisted bilayer graphene, and the same conclusions as in Ref. [255] were obtained. That is, when the temperature is low, $T < 15$ K, the c_p and T relation is $c_p \sim T^{\,n}$: for single-layer graphene n = 1, for bilayer graphene n = 1.6, and for twisted bilayer graphene n = 1.3. The study of graphene c_p dependence on different layers offers the possibility of the selective thermal modulation based on graphene.

Many scholars have also studied the relationship between c_p and T for nanocrystals. For example, Zhang et al. [262] studied the relationship between the c_p and T of NC–Cu. According to the Debye formula, the relation between c_p and T of ideal crystalline Cu is $c_p \sim T^3$. However, it is found in their study that the c_p of NC–Cu was greater than that of the bulk Cu, and thus the relation deviates from the Debye law. The reason is that the atomic distribution in the grain boundary of NC–Cu is more chaotic, resulting in greater entropy and larger c_p.

So far, we have reviewed and summarized the theoretical analysis, experimental measurement techniques and key influencing factors for the thermophysical studies of solid nanomaterials in this section. Theoretical research has focused on how to define the c_p of solid nanomaterials through the Dulong–Petit law, Einstein model and Debye model, and analyzing the relationships and differences between the three models and their development processes. The most representative experimental techniques for thermophysical properties measurement of solid nanomaterials include the 3ω method and the AC-calorimetric technique. As to the size effect of c_p, we have concluded that particles have higher c_p than the bulk under ultra-low temperature. This phenomenon can be explained by the fact that the small size particles have a large specific surface area, which facilitates surface phonon softening. Furthermore, due to the small grain size and large specific surface area, the thermophysical properties of nanocrystal materials are significantly different from those of conventional crystals [237]. Due to differences in the interface components, the c_p value of nanocrystals is slightly higher than that of the polycrystalline state in the temperature range of 150–300 K. The c_p values of several typical nanomaterials have a different dependence on temperature over different temperature ranges.

3. Colloidal nanofluids

Nanofluids are an advanced colloid obtained by dispersing 1–100 nm nanoparticles in conventional liquids. Many studies have shown that nanofluids possess excellent thermophysical properties compared to conventional fluids. Therefore, it is necessary to examine parameters influencing nanofluids properties such as temperature, the morphology and volume fraction of nanoparticles, and type of base fluid. In this section, we summarize the latest studies on thermal conductivity, viscosity, density, and specific heat capacity of nanofluids. Thermophysical properties of nanofluids are investigated in four aspects including theoretical research, the development of models from classical to advanced level, measurement techniques, and the main elements affecting the properties.

3.1. Thermal conductivity

3.1.1. Theoretical models

Experimental results indicate that the thermal conductivity of nanofluids (k_{nf}) is usually higher than that of conventional fluids [10,14,263–265]. Fig. 13 schematically illustrates the development history of the classical thermal conductivity models for nanofluids and their characteristics. The first model has originated from Maxwell's theory [266] where a thermal conductivity model was proposed for solid–liquid mixtures. That model is based on a system of randomly dispersed spherical particles in suspension. The k_{eff} of the nanofluids is written as:

$$k_{nf} = \frac{k_p + 2k_{bf} + 2\Phi_p\left(k_p - k_{bf}\right)}{k_p + 2k_{bf} - \Phi_p\left(k_p - k_{bf}\right)} k_{bf} \tag{29}$$

where k_p and k_{bf} are the thermal conductivity of particles and the base fluid, respectively. Φ_p is the volume fraction of the nanoparticles. It is worthy to note that this model is rigorously valid for the case in which the value of k_p is close to k_{bf}. Hamilton [267] extended the Maxwell model to make it suitable for non-spherical particles as well. By considering the shape factor for particles, the modified Maxwell model can be written as:

$$k_{nf} = \frac{k_p + (n-1)k_{bf} + (n-1)\Phi_p\left(k_p - k_{bf}\right)}{k_p + (n-1)k_{bf} - \Phi_p\left(k_p - k_{bf}\right)} k_{bf} \tag{30}$$

where n is the empirical shape factor and defined as $n = 3/\Psi$, and Ψ is the ratio of the surface area of the particle with an arbitrary shape to that of a spherical particle with the same volume. For large volume fractions of spherical nanoparticles, the model of Bruggeman [268], which takes into account the interactions of the spherical particles, is more accurate:

$$\frac{k_{nf}}{k_{bf}} = \frac{\left(3\Phi_p - 1\right)\frac{k_p}{k_{bf}} + \left[3\left(1-\Phi_p\right) - 1\right] + \sqrt{\left\{\left(3\Phi_p - 1\right)\frac{k_p}{k_{bf}} + \left[3\left(1-\Phi_p\right) - 1\right]\right\}^2 + 8\frac{k_p}{k_{bf}}}}{4} \tag{31}$$

In fact, when nanoparticles are dispersed into a liquid, a thin layer is formed on the surface of nanoparticles which affects the magnitude of thermal conductivity. Yu and Choi [269] modified the Maxwell model by considering this nanolayer as follows:

$$k_{nf} = \frac{k_p + 2k_{bf} + 2\Phi_p\left(k_p - k_{bf}\right)(1+\beta)^3\Phi_p}{k_p + 2k_{bf} - \Phi_p\left(k_p - k_{bf}\right)(1+\beta)^3\Phi_p} k_{bf} \tag{32}$$

where β is obtained by the thickness of the nanolayer divided by the particle diameter. Compared to Maxwell model [266], it was approved that the nanolayer considered by Yu and Choi [269] can significantly ameliorate the k_{nf} when the diameter of nanoparticles is less than 10 nm. Similarly, Xue and Xu [270] considered the nanolayer on the particle surface and modified the model of Bruggeman [268]. The modified model is:

$$\left(1 - \frac{\Phi_p}{z}\right)\frac{k_{nf} - k_{bf}}{2k_{nf} + k_{bf}} + \frac{\Phi_p}{z}\frac{\left(k_{nf} - k_{is}\right)\left(2k_{is} + k_p\right) - z\left(k_p - k_{is}\right)\left(2\kappa_{is} + k_{nf}\right)}{\left(2k_{nf} + k_{is}\right)\left(2k_{is} + k_p\right) + 2z\left(k_p - k_{is}\right)\left(k_{is} - k_{nf}\right)} = 0 \tag{33}$$

$$z = \left[\frac{r_p/2}{r_p/2 + d_{is}}\right]^3 \tag{34}$$

where k_{is} denotes the k of the interfacial shell, d_{is} denotes the thickness of the interfacial shell, and r_p is the diameter of the nanoparticles. The shell and the nanoparticles can be regarded as composite nanoparticles and the volume fraction can be expressed as Φ_p/z. This model indicates that the k_{nf} depends on the nanoparticle size and the interfacial properties, which is in good agreement with the experimental data for CuO/ water and CuO/EG nanofluids.

The random motion of the nanoparticles in base fluid, which is called as Brownian motion, enhances the effective thermal conductivity [271]. Xuan et al. [272] proposed a modified Maxwell model taking into account the Brownian effect:

$$\frac{k_{nf}}{k_{bf}} = \frac{k_p + 2k_{bf} - 2\Phi_p\left(k_{bf}\Phi_P\right)}{k_p + 2k_{bf} + \Phi_p\left(k_{bf}\Phi_P\right)} + \frac{\rho_p\Phi_p c_p}{2k_{bf}}\sqrt{\frac{2k_B T}{3\pi r_{cl}\mu}} \tag{35}$$

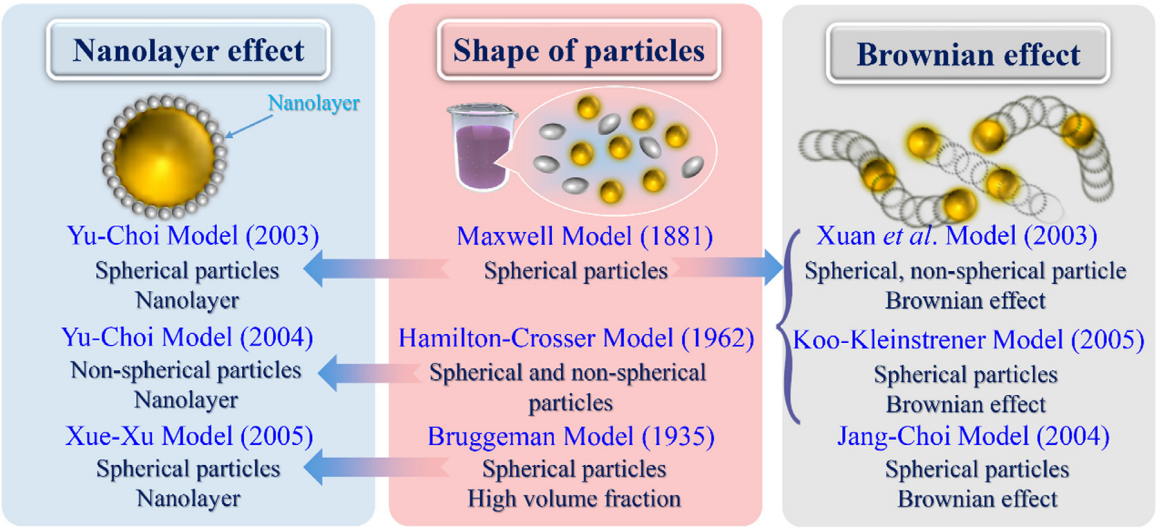

Fig. 13. Schematic diagram of the development history of the classical thermal conductivity models for nanofluids and their characteristics.

where k_B is the Boltzmann constant, μ is the dynamic viscosity of liquid, r_{cl} is defined as the apparent diameter of the cluster. Thus, this model is applicable to nanofluids in which the particles are randomly dispersed or even agglomerated. Koo and Kleinstreuer [273] presented a thermal conductivity model that considers the effect of nanoparticle size, concentration and temperature as well as particles Brownian motion. They captured the heat transfer caused by the fluid flow which was driven by the random movement of nanoparticles. The new thermal conductivity model is combined with the static part and Brownian motion part:

$$k_{nf} = k_{static} + k_{Brownian} = \frac{k_p + 2k_{bf} + 2\Phi_p\left(k_p\Phi_{bf}\right)}{k_p + 2k_{bf} + \Phi_p\left(k_p\Phi_{bf}\right)}k_{bf} + 5\times 10^4 f_1\Phi_p\rho_p c_p\sqrt{\frac{k_B T}{\rho_p r_p}}f_2\left(T, \Phi_p, \text{etc.}\right) \tag{36}$$

where f_1 and f_2 are both empirical functions obtained from experimental data, which are related to the particle volume fraction, particle shape and liquid temperature. At a higher temperature, Brownian motion is stronger and the model prediction is more accurate. Chon et al. [274] introduced the Reynolds number into the model based on the fitting of the experimental data of Al_2O_3/ water nanofluids, where the Reynolds number is a function of particles velocity. The model is described as:

$$\frac{k_{nf}}{k_{bf}} = 1 + 64.7\Phi_p^{0.74}\left(\frac{r_{bf}}{r_p}\right)^{0.369}\left(\frac{k_{bf}}{k_p}\right)^{0.747}\times \mathrm{Pr}^{0.9955}\times \mathrm{Re}^{1.2321} \tag{37}$$

$$\mathrm{Pr} = \frac{\mu_{bf}}{\rho_{bf}\alpha_{bf}},\quad \mathrm{Re} = \frac{\rho_{bf}v_p r_p}{\mu_{bf}} = \frac{\rho_{bf}k_B T}{3\pi\mu_{bf}^2\Lambda_{bf}} \tag{38}$$

where r_{bf} denotes the diameter of the base fluid molecule, Λ_{bf} refers to the mean free path of the base fluid molecules, and v_p is the Brownian motion velocity of the nanoparticles. The effect of the Brownian velocity of the nanoparticles on the k_f can be reflected from this model. In addition, Wang et al. [275] took the surface adsorption and size effects of nanoparticles into account, which gives:

$$\frac{k_{nf}}{k_{bf}} = \frac{\left(1-\Phi_p\right) + 3\Phi_p\int_0^\infty \frac{k_{cl}n}{k_{cl}+2k_{bf}}dr_p}{\left(1-\Phi_p\right) + 3\Phi_p\int_0^\infty \frac{k_{bf}n}{k_{cl}+2k_{bf}}dr_p} \tag{39}$$

In this model, it is considered that nanoparticles would form clusters due to surface adsorption, thus k_{cl} can be used to replace k_p. According to the fractal theory, the k_{nf} containing different particle cluster shapes can be fully considered. Jang and Choi [271] also considered collisions between base fluid molecules and the interaction between nanoparticles and base fluid. Their proposed model is:

$$k_{nf} = k_{bf}\left(1-\Phi_p\right) + k_p\Phi_p + 3C\frac{r_{bf}}{r_p}k_{bf}\mathrm{Re}_r^2\mathrm{Pr}\Phi_p \tag{40}$$

where C is an empirical constant. The above models embodied the vital role of Brownian motion in the thermal conduction of nanofluids.

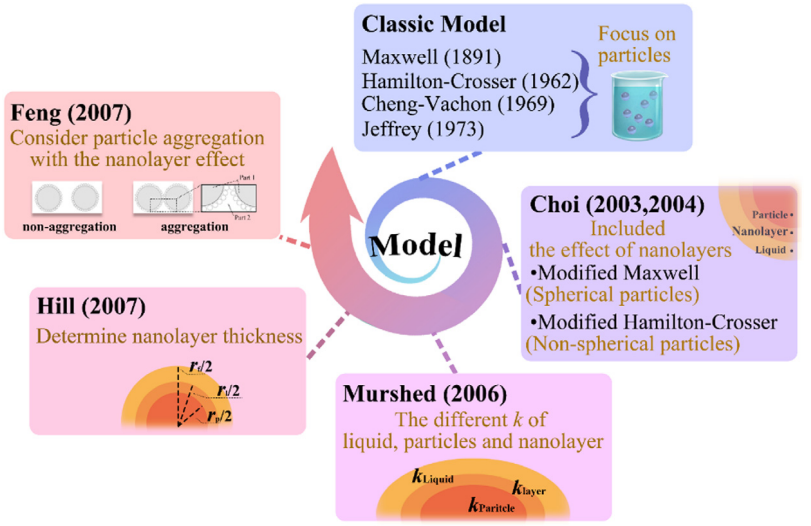

Fig. 14. Schematic diagram of the differences and ties among different models considering the effects of nanolayers.

3.1.1.1. Role of nanolayer thickness. The Hamilton–Crosser model [267] considered the effects of particle shape, the Cheng–Vachon model [276] included the particle distribution and the Jeffery model [277] focused on inter-particle interactions. The effect of the nanolayer on thermal transport cannot be neglected since the layered molecules always occur between the particle and liquid [278]. Hence, considering the effect of the nanolayer, Yu and Choi [269] proposed a modified Maxwell model (Eq. (32)) that is discussed in Section 3.1.1. Since the above-mentioned modified Maxwell model is only applicable to nanofluids with spherical nanoparticles, Yu and Choi [279] then proposed a modified Hamilton–Crosser model which could be applicable to the non-spherical nanoparticles by assuming the nanolayer is the confocal ellipsoid with the inner particles. The k_{eff} of this model is in good agreement with nanotube-in-oil suspensions, but it cannot predict the nonlinear k_{nf}.

Leong et al. proposed a new model which includes the effect of interfacial layer thickness with the assumption that there was no interaction between the particles and that the temperature fields are continuous in the fluid, particles and nanolayer with different k values [280]. This new model exhibits good agreement with available experimental data for different types of nanofluids [281]. Fig. 14 summarizes the differences and ties among various models considering the effects of nanolayers. However, there was a problem that had not been solved yet: How to determine the thickness of the nanolayer? To answer this question, Murshed et al. [281] proposed a series of models for determining the thickness of spherical and cylindrical nanoparticles through the manipulation of the heat conduction in the fluid, the particles and the nanolayer. Feng et al. [282] also studied the effect of non-aggregating particles and aggregating particles (clusters) on nanofluids following a study by Yu and Choi. [269]. They focused on the thermal transport of aggregating particles and proposed an expression for the effective thermal conductivity (k_{eff}): $k_{\text{eff}} = (1-y)k_{\text{m}} + yk_{\text{a}}$, where k_{eff} is the effective thermal conductivity, k_{m} is the predicted k from the modified Maxwell model, k_{a} is the thermal conductivity of the aggregation model and y is the ratio of aggregating particles to all nanoparticles. The particle distribution in this model is closer to experimental data.

3.1.1.2. Nanoparticle size effect. The enhancement of k_{nf} is attributed to the Brownian motion of the nanoparticles. Due to the small size of the nanoparticles and the strong Brownian motion, the size of the nanoparticles is an important factor affecting k_{nf} [283]. Xu et al. [284] considered the thermal convection caused by Brownian motion, and proposed a model for calculating k_{nf}:

$$\frac{k_{\text{nf}}}{k_{\text{bf}}} = \frac{k_{\text{p}} + 2k_{\text{bf}} - 2\Phi_{\text{p}}\left(k_{\text{bf}} - k_{\text{p}}\right)}{k_{\text{p}} + 2k_{\text{bf}} + \Phi_{\text{p}}\left(k_{\text{bf}} - k_{\text{p}}\right)} + \text{C}\frac{\text{Nu}\cdot r_{\text{bf}}}{\text{Pr}}\frac{(2-D_{\text{bf}})}{(1-D_{\text{bf}})^2}\frac{\left[\left(\frac{r_{\text{p,max}}}{r_{\text{p,min}}}\right)^{1-D_{\text{bf}}} - 1\right]^2}{\left(\frac{r_{\text{p,max}}}{r_{\text{p,min}}}\right)^{2-D_{\text{bf}}} - 1}\frac{1}{\bar{r}_{\text{p}}} \tag{41}$$

where C is an empirical constant, r_{bf} is the diameter of base fluid molecule, Nu is the Nusselt number, Pr is the Prandtl number, D_{bf} is the fractal dimension, $\bar{r}_{\text{p}}$ is an average size of the nanoparticles, and $r_{\text{p,min}}$ and $r_{\text{p,max}}$ are the minimum and maximum diameters of the nanoparticles, respectively. Experimental measurements of k of Al_2O_3/water and CuO/water nanofluids agree well with predictions of the theoretical model. However, this model is complex and consists of many empirical parameters.

Brownian motion is affected by the size of the nanoparticles [285]. Dong and Chen [286] considered the contributions of both particle size and Brownian motion to the k_{nf}. Brownian motion was assumed equivalent to the increase of the

radius of the particles. Finally, an improved thermal conductivity model was proposed. The relationship between the k_{eff} and the particle size was presented as:

$$k_{\text{nf}} = \frac{(\beta+1)\,k_{\text{bf}} + \beta k_{\text{p}} + 2\beta\Phi_{\text{p}}\left(k_{\text{p}} - k_{\text{bf}}\right)}{(\beta+1)\,k_{\text{bf}} + \beta k_{\text{p}} - \beta\Phi_{\text{p}}\left(k_{\text{p}} - k_{\text{bf}}\right)} k_{\text{bf}} \tag{42}$$

$$\Phi_{\text{p}} = \rho_{\text{s}} \frac{{r_{\text{eff}}}^3}{{r_{\text{p}}}^3} \tag{43}$$

where β is the coefficient, ρ_{s} is the density of the solid, and r_{eff} is the effective diameter, which is dependent on the Brownian velocity of the nanoparticles.

According to the previous studies, the Brownian motion-induced convection and the path of heat transfer are the two of the dominant factors that influence the heat transfer of nanofluids [287]. Ganesan et al. [288] studied the k of nanoclusters-based nanofluids with a very large particle size (115–530 nm). Considering the interfacial thermal resistance and the mixed convection of nanoparticles, the expression for k is:

$$\frac{k_{\text{nf}}}{k_{\text{bf}}} = \left(1 + A\text{Re}^{\gamma}\text{Pr}^{0.333}\Phi_{\text{p}}\right)\frac{1 + 2\beta\Phi_{\text{p}}}{1 - \beta\Phi_{\text{p}}} \tag{44}$$

where γ is the index determined by the system and A is a constant. The convection velocity is defined as the root mean square velocity υ_{p} of the nanoparticle:

$$\upsilon_{\text{p}} = \sqrt{\frac{18\text{k}_{\text{B}}T}{\pi\rho_{\text{p}}d^3}} \tag{45}$$

where k_{B} is the Boltzmann constant, T is the temperature, and ρ_{p} is the density of the particles. In general, k_{nf} decreases with increasing particle size.

3.1.1.3. Temperature influence. In addition to the factors mentioned above, k_{nf} also shows a strong dependence on temperature. It can be seen from the modified Maxwell model (Eq. (35)) proposed by Xuan et al. [272], it not only considers the effect of Brownian motion on k, but also involves the effect of temperature. In addition, Koo and Kleinstreuer [273] also considered the effect of temperature on k in Eq. (36). They believed that temperature can directly affect the Brownian motion of particles in the nanofluids, so in the second term of Eq. (36), it is a temperature-related function. At higher temperatures, Brownian motion is stronger and the model predicts more accurate. But it is only applicable for the temperature range 293–325 K. Vajjha and Das [289] obtained more extensive data based on this model, and proposed a thermal conductivity model for three EG-water based nanofluids containing Al_2O_3, ZnO, CuO nanoparticles, respectively. The k_{nf} is a temperature-dependent function similar to Eq. (39) and the empirical expression was given as:

$$f\left(T, \Phi_{\text{p}}\right) = \left(2.8217 \times 10^{-2}\Phi_{\text{p}} + 3.917 \times 10^{-3}\right)\left(\frac{T}{T_0}\right) + \left(-3.0669 \times 10^{-2}\Phi_{\text{p}} - 3.91123 \times 10^{-3}\right) \tag{46}$$

where Φ_{p} is the concentration of the nanoparticle. Compared with other models, this model is in better agreement with the experimental data.

In 2009, Moghadassi et al. [290] presented a model based on dimensionless groups considering the size and concentration of nanoparticles, thermal conductivity of both solid and liquid phases as well as the interfacial shell specifications. However, the effect of temperature was not considered in the model. Later on, Hosseini et al. [291] modified Moghadassi et al. [290] model by including temperature. Their dimensionless expression is:

$$\frac{k_{\text{nf}}}{k_{\text{bf}}} = 1 + \text{J}\left(\frac{\Phi_{\text{p}}^{\text{a}}}{r_{\text{p}}^{\text{b}}}\right)\left(\frac{T}{T_0}\right)^{\text{c}} \tag{47}$$

where J, a, b, and c are all constants depending on the type of nanofluid and are determined by experiments.

Based on information given in [292] on graphene-based composites and using Xuan et al. [272] model, Gao et al. [293] proposed a novel model for predicting the thermal conductivity of graphene nanofluids. This model includes the effect of interfacial thermal resistance, length, thickness, the average flatness ratio of the graphene nanoparticles and the Brownian motion. Based on the experimentally obtained k of the graphene nanofluid in the temperature range of 253–303 K, they proposed a mathematical expression as:

$$\frac{k_{\text{nf}}}{k_{\text{bf}}} = \frac{3 + 2\eta^2\Phi_{\text{p}}}{3 - \Phi_{\text{p}}} \Big/ k_{\text{bf}}\left(\frac{2R_{\text{k}}}{L_{\text{p}}} + 13.4\sqrt{t}\right) + \frac{\rho_{\text{p}}\Phi_{\text{p}}c_{\text{p,p}}}{2k_{\text{bf}}}\sqrt{\frac{2\text{k}_{\text{B}}T}{3\pi\mu r_{\text{c}}}} \tag{48}$$

where η is the average flatness ratio of the graphene, R_{k} is the interfacial thermal resistance, L_{p} is the length of particles, d_{p} is the thickness of the particles, ρ_{p} is the density of the particles, $c_{\text{p,p}}$ is the isobaric heat capacity of particles, μ is the dynamic viscosity, and r_{c} is the mean diameter of gyration, approximately half the graphene particle diameter $r_{\text{p,eq}}$. The first term on the right side of the equation is the effective k_{nf} for a static fluid, and the second term is the k_{nf} induced by

the Brownian motion of nanoparticles [294]. Non-spherical particles can be treated as spherical particles with the same volume, and thus the equivalent diameter is:

$$r_{p,eq} = \left(\frac{6V_{non-sph}}{\pi}\right)^{1/3} \tag{49}$$

3.1.1.4. Aggregation effect. The mechanisms of heat transfer enhancement of nanofluids have been studied by many researchers, who experimentally proved that besides Brownian motion, the aggregation of nanoparticles can also lead to the enhancement of k_{nf} [295,296].

Feng et al. [282] considered the aggregation effect of nanoparticles and proposed a new model for the k_{nf}. In this model the k_{nf} was related to the nanoparticle size, the nanoparticle volume fraction, the thickness of the interfacial nanolayer, the k of the nanoclusters and the base fluid, which can be expressed by:

$$\begin{aligned}\frac{k_{nf}}{k_{bf}} &= \left(1-\Phi_{p,eq}\right)\frac{k_{p,eq}+2k_{bf}+2\left(k_{p,eq}-k_{bf}\right)(1+\beta)^3\Phi_p}{\kappa_{p,eq}+2k_{bf}-\left(k_{p,eq}-k_{bf}\right)(1+\beta)^3\Phi_p} \\ &+ \Phi_{p,eq}\left[\left(1-\frac{3}{2}\Phi_{p,eq}\right)+\frac{3\Phi_{p,eq}}{\iota}\left[\frac{1}{\iota}\ln\frac{r_p/2+d_{is}}{\left(r_p/2+d_{is}\right)(1-\iota)}-1\right]\right]\end{aligned} \tag{50}$$

where $\iota = (1-k_{bf}/k_{p,eq})$, $k_{p,eq}$ is the equivalent thermal conductivity of the equivalent particles, Φ_p is the concentration of the particles in the nanofluid, $\Phi_{p,eq}$ is the equivalent volume fraction of equivalent particles, r_p is the particle diameter, and d_{is} is the interfacial shell thickness.

Pang et al. [297] considered the static and dynamic contributions to the amelioration of nanofluids thermal conductivity where the latter was partly attributed to nanoparticle aggregation. Therefore, the model of nanofluids can be presented as:

$$k_{nf} = 1+\frac{\Phi_a\left(k_a-k_{bf}\right)}{\left(1-\Phi_a\right)/n\left(k_a-k_{bf}\right)+k_{bf}}+\left[A_1\ln\left(A_2\Phi_a\mathrm{Re}^m\mathrm{Pr}^{0.333}\right)+A_3\right]\frac{1+2\Phi_a+2\left(1-\Phi_a\right)\alpha}{1-\Phi_a+\left(2+\Phi_a\right)\alpha} \tag{51}$$

where $\alpha = 2R_b{\cdot}k_{bf}/r_p$, R_b and r_p are the thermal resistance and particle diameter, respectively, Φ_a denotes the volume fraction of the aggregates in the nanofluid, k_a is the effective thermal conductivity of the aggregates based on composite theory [298], n is the shape effect factor, A_1, A_2, A_3 and m are constants determined by experiments, Nu is the Nusselt number, and Pr is the Prandtl number.

Xu et al. [299] introduced a new model for estimating k_{nf} based on fractal distributions of nanoparticles. By developing Hamilton [267] and Xu et al. [299] models, Wei et al. [300] proposed a model for k_{nf} based on fractal aggregation distribution by analyzing the relationship between the aggregate shape and the fractal dimension. The mathematical expression is:

$$\frac{k_{nf}}{k_{bf}} = \frac{m+(n-1)-(n-1)(1-m)\Phi_p}{m+(n-1)+(1-m)\Phi_p}+C\frac{\mathrm{Nu}\cdot r_{bf}}{\mathrm{Pr}}\frac{(2-D)D}{(1-D)^2}\frac{\left(\Phi_p^{\zeta_1}-1\right)^2}{\Phi_p^{\zeta_2}-1}\frac{1}{\overline{L_a}} \tag{52}$$

$$F = 3\frac{D}{D-1}\frac{3-D}{2-D}\frac{\Phi_e^{\zeta_2}-1}{\Phi_e^{-1}-1} \tag{53}$$

where $m = k_p/k_{bf}$, k_p is the k of the particles, n is the empirical shape factor determined by the Φ_p and the fractal dimension D, $\zeta_1 = (D-1)/(3-D)$, $\zeta_2 = (D-2)/(3-D)$, C is an empirical constant, r_{bf} denotes the diameter of base fluid molecules. and L_a denotes the average aggregation size. The two terms on the right contain the enhancement of k_{nf} induced by the size effect and Brownian motion effect.

3.1.1.5. Evolution of advanced models. With the deepening of thermal transport research for nanofluids, more and more factors have been considered, such as nanoparticle interaction, nanolayers, aggregation, Brownian motion and turbulent effects. Compared to classical models, the multi-parameter advanced models are much closer to reality. Here, we schematically illustrate the development history of the advanced k models for nanofluids and their characteristics (see Fig. 15). Taking into account the effect of the nanolayer, Murshed et al. [281] proposed two models of k_{nf} with spherical and cylindrical nanoparticles. For spherical nanoparticles, k_{nf} was defined as follows:

$$\begin{aligned}k_{nf} &= \left[\left(k_p-k_{nl}\right)\Phi_p k_{nl}\left(\gamma_1^2-\gamma^2+1\right)+\left(k_p+k_{nl}\right)\gamma_1^2\left(\Phi_p\gamma^2\left(k_{nl}-k_{bf}\right)+k_{bf}\right)\right] \\ &\cdot\left[\gamma_1^2\left(k_p+k_{nl}\right)-\left(k_p-k_{nl}\right)\Phi_p\left(\gamma_1^2+\gamma^2-1\right)\right]^{-1}\end{aligned} \tag{54}$$

As for cylindrical nanoparticles in nanofluids, it can be described as:

$$\begin{aligned}k_{nf} &= \left[\left(k_p-k_{nl}\right)\Phi_p k_{nl}\left(2\gamma_1^3-\gamma^3+1\right)+\left(k_p+2k_{nl}\right)\gamma_1^3\left(\Phi_p\gamma^3\left(k_{nl}-k_{bf}\right)+k_{bf}\right)\right] \\ &\cdot\left[\gamma_1^3\left(k_p+2k_{nl}\right)-\left(k_p-k_{nl}\right)\Phi_p\left(\gamma_1^3+\gamma^3-1\right)\right]^{-1}\end{aligned} \tag{55}$$

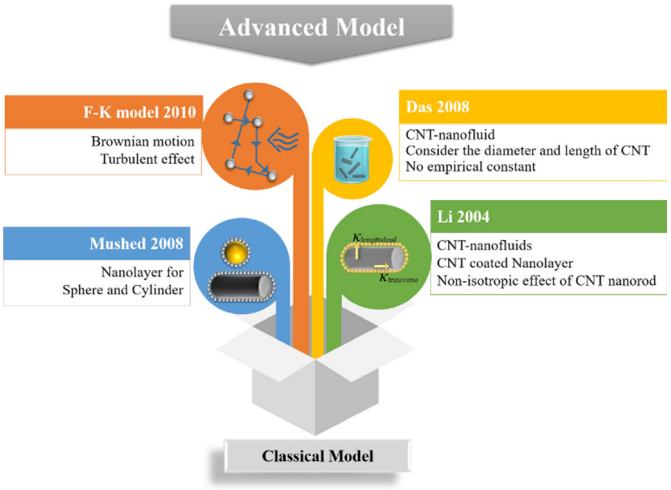

Fig. 15. Schematic diagram of the development history of the advanced thermal conductivity models for the nanofluids and their characteristics.

where k_{nf} denotes the k_{eff} of the nanofluid, k_p, k_{bf} and k_{nl} denotes the k of the particles, base fluid and nanolayer, respectively, Φ_p represents the volume fraction of particles, $1+\frac{2d_{nl}}{r_p}=\gamma$ and $1+\frac{d_{nl}}{r_p}=\gamma_1$, where d_{nl} denotes the nanolayer thickness, and r_p is the particle diameter. These models show a better agreement with the experimental results than other reported models at the time of their development.

In consideration of the particle's Brownian motion and turbulent effects, Feng and Kleinstreuer et al. [301] reported F–K model. Combined with the Maxwell model [266], this model was expressed as:

$$k_{nf}=k_{static}+k_{mm} \tag{56}$$

where k_{static} denotes the static part and k_{mm} denotes the micro-mixing part of the k_{nf}. The static part was given by Maxwell's model (Eq. (29)), and the micro-mixing part was given by:

$$k_{mm}=49500\cdot 38\cdot\frac{k_B\tau_p}{2m_p}\cdot(\rho c_p)_{nf}\cdot{\Phi_p}^2\cdot(T\ln T-T)\cdot\frac{\exp(-\xi\omega_n\tau_p)\sinh\left(\sqrt{\frac{(3\pi\mu_{bf}r_p)^2}{4m_p^2}-\frac{Q_{p-p}}{m_p}}\frac{m_p}{3\pi\mu_{bf}r_p}\right)}{\tau_p\sqrt{\frac{(3\pi\mu_{bf}r_p)^2}{4m_p^2}-\frac{K_{p-p}}{m_p}}} \tag{57}$$

where m_p represents the particle mass, r_p is the nanoparticles diameter, c_p is the isobaric heat capacity, Q_{p-p} is the particle–particle interaction intensity, and μ_f is the dynamic viscosity of the fluid. The damping coefficient ξ, the natural frequency ω_n and the characteristic time interval τ_p are defined as follows:

$$\xi=\frac{3\pi r_p\mu_{bf}}{2m_p\omega_n},\ \omega_n=\sqrt{\frac{Q_{P-P}}{m_p}},\ \tau_p=\frac{m_p}{3\pi\mu_{bf}r_p} \tag{58}$$

To tackle the inaccurate description issue of the CNT-contained nanofluids caused by the significant difference between the k_f and that of the particles, Das et al. [302] proposed a new model:

$$k_{nf}=k_{bf}\left[1+\frac{k_p\Phi_pL_{mol}}{k_{bf}\left(1-\Phi_p\right)r_{cnt}}\right] \tag{59}$$

where the L_{mol} denotes the molecule size and r_{cnt} is the average diameter of the CNTs. This model fits well with experimental data. The most prominent advantage is there is no need for any empirical constants in this model. Another advance in the field is Nan et al. [303] proposed a model which considers the non-isotropic issue of CNTs in nanofluids. This model explains the k enhancement of the CNT nanofluids by the sample function and concludes that the interfacial thermal resistance dominates the k of the CNT composites including CNT-containing nanofluids. For CNT-containing nanofluids, k_{nf} can be described as:

$$\frac{k_{nf}}{k_{bf}}=\frac{3+\Phi_p\left(\beta_T+\beta_L\right)}{3-\Phi_p\beta_T} \tag{60}$$

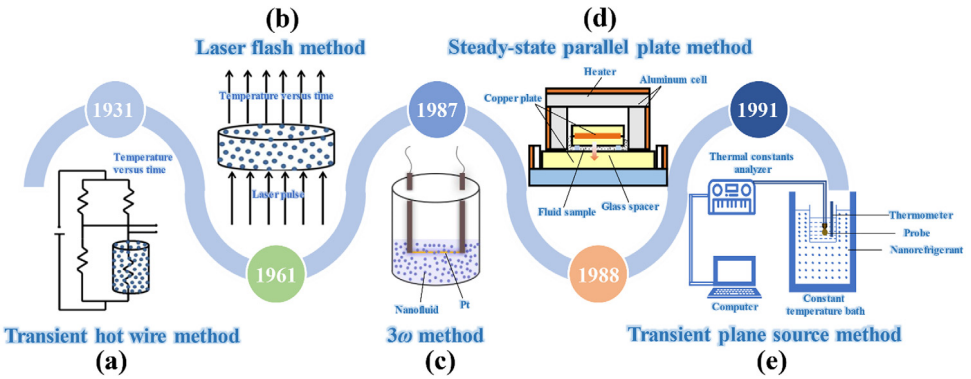

Fig. 16. Schematic diagram of thermal conductivity measurement principle (a) transient hot wire method [305], (b) laser flash method [305], (c) 3ω method, (d) steady-state parallel plate method [306] and (e) transient plane source method [307].

where:

$$\beta_T = \frac{2\left(k_T^{nf} - k_{bf}\right)}{k_T^{nf} + k_{bf}}, \beta_L = \frac{k_L^{nf}}{k_{bf}} - 1 \tag{61}$$

where k_T^{nf} and k_L^{nf} represent the transverse and longitudinal k of a nanofluid unit cell, respectively, which are given by:

$$k_T^{nf} = \frac{k_{nf}}{1 + \frac{2L_K}{r_{cnt}}\frac{k_{nf}}{k_{bf}}}, k_L^{nf} = \frac{k_{nf}}{1 + \frac{2L_K}{L_{cnt}}\frac{k_{nf}}{k_{bf}}} \tag{62}$$

where $L_K = R_K \cdot k_{bf}$. For nanotube composites, L_K is 16–40 nm when k_{bf} is 0.2–0.5 W/m K and R_K is 83×10^{-8} m^2 K/W, r_{cnt} is the CNT diameter, L_{cnt} is the CNT length.

Using experimental data, Corcione [304] proposed a model that can rapidly predict the k for a wide range of conditions (nanoparticle diameter: 10–150 nm, volume fraction: 0.002–0.09, temperature: 294–324 K). This model is expressed as:

$$\frac{k_{nf}}{k_{bf}} = 1 + 4.4\mathrm{Re}^{0.4}\mathrm{Pr}^{0.66}\left(\frac{T}{T_{fp}}\right)^{10}\left(\frac{k_p}{k_{bf}}\right)^{0.03}\Phi_p^{0.66} \tag{63}$$

where $\mathrm{Re} = \frac{2\rho_{bf}k_B T}{\pi\mu_{bf}^2 r_p}$ and T_{fp} is the freezing point of the base fluid.

3.1.2. Experimental measurement techniques

In the following section, we will turn to some classical and commonly used measurement methods for k_{nf}, including the most classical hot wire method, the widely used 3ω method, the most standardized laser flash method, the steady-state parallel method and the transient plate source method [305–307] (see Fig. 16).

3.1.2.1. Transient hot wire approach. The transient hot wire (THW) method (see Fig. 16a) is first proposed by Stalhane and Pyk in 1931. After several decades of development, the hot wire method has become one of the most accurate methods for measuring k_f [308–312]. The principle of the transient hot wire method is to immerse a wire (hot wire) which is heated at a constant power. The temperature of the hot wire rises and heat transfers to the surrounding liquid. The rate at which the hot wire temperature rises is related to the k of the surrounding liquid, so the k_f can be obtained by measuring the transient temperature rise. The hot wire method is generally measured indirectly using the bridge circuit [308]. The temperature rise curve of the hot wire is indirectly obtained by measuring the bridge voltage difference data.

The theoretical model of the hot wire method is based on two assumptions [308]: (i) The length of the hot wire is infinite, the diameter is also infinitely small, and is assumed to be placed vertically in an isotropic fluid to avoid the effects of free convection; (ii) the k of the hot wire is ideally infinite, so heat capacity can be approximated to zero. The k can be calculated according to the relationship between the rate of temperature rise of the hot wire and the k_f using this equation $k = \frac{q}{4\pi}\frac{d\ln t}{d\Delta T(t)}$, where q is heating power of the hot wire and t is time.

Antoniadis et al. [309] pointed out that in case of the fluids containing nanoparticles the solid phase is often polar or electrically conducting, so it may distort the electrical signal which leads to errors in *thermal* conductivity measurement. They suggested that the wire in this technique should be electrically insulated, a proposed use of the electrolytically oxidized tantalum wire to construct that kind of system. Guo et al. [308] studied the effect of particle size on the k_{nf} using the transient hot wire method. In their experiment, SiO_2 nanoparticles were added to DI water and ethylene glycol (EG), respectively. It was found that the k values of SiO_2/EG with a volume fraction of 0.5% and SiO_2/EG with a volume fraction of 1.0% were increased by 3.2% and 9.6%, respectively. Both were higher than that of DW-based nanofluids by

1.0% and 3.4%. Lee et al. [310] used an advanced hot wire system without the capacitance and natural convection effects to study the effect of particle size and volume fraction on the k_{eff} of Al_2O_3/EG nanofluids. The analysis implied that when the volume fraction was less than 0.25%, the effect of particle size is more pronounced than volume fraction. Specifically, the impact is more obvious at low volume fractions. When the volume fraction was over 0.2%, the particle number density was a key factor affecting the k_{nf} due to Brownian motion. Aparna et al. [311] compared the differences in k_{nf} measured by the hot wire method and the laser flash method. Interestingly, the nanoparticles exhibited a higher collision flux with the wall by the hot wire method than the laser flash method, resulting in a higher k.

3.1.2.2. 3ω method. As mentioned in the previous sections, the 3ω method (see Fig. 16c) is a powerful tool for the k characterization of solid nanomaterials, and it can also be used for nanofluids [267,313,314]. Oh et al. [313] measured the k of an aluminum oxide/deionized water (Al_2O_3/DI water) nanofluid using this method. The biggest advantage of their experimental setup was the home-made micro-device that only needs one drop of nanofluid to complete the k measurement. Turgut et al. [314] carried out the measurement of TiO_2/DI nanofluids with a volume fraction from 0.2% to 3.0% using the 3ω method. The results agreed well with that of the Hamilton–Crosser model [267] at volume fractions less than 1%. Qiu et al. [315] developed a so-called reusable freestanding sensor for the k measurement of conventional fluids (DI water, EG, ethanol, *etc.*) and nanofluids. The most classical test structure of nanofluids for the 3ω method is a metallic wire as the heater/thermometer immersed into the nanofluids. Karthik et al. [316] used a pure platinum wire to measure the k_{nf}. The k of 0.05 vol% CuO/DI water at RT and pH = 1 was reported as 0.666 W/m K with a very low measurement uncertainty less than 1.2%.

Han et al. [317] even developed a so-called extended 3ω-wire method to measure the k_{nf}. This method used a small temperature oscillation to ensure that the thermophysical properties of the nanofluids remained constant during the measurement. By means of phase-locking technology, the background noise was controlled, which enabled the authors to achieve the k measurement of poly-alpha-olefin (PAO) oil with dispersed composite carbon nanoparticles. The temperature-dependent k of nanorod-based nanofluids was also measured by this method [318], which confirmed that the 3ω method is powerful for the thermophysical measurement of nanofluids containing non-spherical particles. Choi et al. [319] successfully measured the k of a CNT/H_2O nanofluids by immersing a single platinum wire into the fluid. One may easily observe that the 3ω method detects the electrical signal in the frequency domain and needs to be averaged over a certain length of time, generally much longer than the characteristic time of the random motion of the nanoparticles in the fluid. This feature eliminates the spurious signals caused by the particle motion. It also proves the applicability of the 3ω method in the measurement of k of the nanofluid.

3.1.2.3. Laser flash method. The laser flash (LF) method (see Fig. 16b) first proposed by Parker et al. [174] is one of the most common methods for measuring k_{nf}. For colloidal nanofluids, the basic measurement principle is that the laser is used as the heating source to heat the bottom surface of nanofluids, and a thermometer on the top surface measures the temperature rise, so the α can be calculated based on the transient temperature response, then the k_{nf} is derived from the formula $k = \rho c_p \alpha$ [320]. As a standard transient method, the laser flash method has the advantage of short heating time, which minimizes the undesired influence of radiation and convection on the measurement accuracy [321]. Some nanofluids samples are transparent to infrared or visible light. Therefore, in order to reduce measurement errors, a metal film can be attached to both sides of the container preventing the flash from penetrating into the bottom surface and the infrared light from entering the sample on the top [322].

Harikrishnan et al. [323] measured the k of TiO_2/stearic acid nanofluids using the laser flash method, and proved that k_{nf} increases with increasing volume fraction of TiO_2 nanoparticles. Zhang et al. [324] also measured the k_{nf} with different Al_2O_3 nanoparticles sizes at high temperatures. The results emphasized that the k_{nf} was enhanced to different extent compared with the base fluids. Leena et al. [322] compared the k of TiO_2/EG-water with TiO_2/propylene glycol/water nanofluids using the same method, and calculated the theoretical value of k_{nf} using ultrasonic velocity, which was in agreement with experimental values.

It should be noted that the laser flash method would cause errors in measuring k_{nf}, especially for nanofluids with low k. Aparna et al. [311] used the laser flash method to measure the k of Al_2O_3/aqueous and Ag/aqueous nanofluids. Compared with other methods, the Brownian motion of the nanoparticles was limited due to the small liquid pool ($\sim$50 μL), so the k measured by the laser flash method was lower. Buonomo et al. [325] reported that the k of Al_2O_3/water nanofluids was increased by 4.95% according to the measurement results by the laser flash method. Beck et al. [283] measured the Al_2O_3/water nanofluids with the same nanoparticle size and volume fraction by the transient hot wire method, but results indicated that the k was increased by 16.5%, much higher than the values reported in [325]. Zagabathuni et al. [305] used a collision-mediated model to study the difference in k values by various experimental methods. It was found that the measurement results using the laser flash method were lower, which was attributed to the limitation of the Brownian motion and the reduction of the collision frequency of the nanoparticles. Kleinstreuer et al. [326] measured the k of polyalphaolefin (PAO)-based nanofluids by three methods, *i.e.* the laser flash method, the transient plane heat source method and the hot wire method. They concluded that the laser flash method lacks enough accuracy in measuring nanofluids with low k because their k is approximately the same as that of the liquid pool, resulting in the fact that heat flow through the liquid pool is not negligible. From the above analysis, as can be seen, the k measured by the laser flash method is lower than the other methods, but the difference is not significant for the pure fluid.

3.1.2.4. Steady-state parallel plate method. Steady-state parallel plate (SSPP) method (see Fig. 16d) is a basic experimental technique for measuring k_f. During the measurement, a small amount of the fluid is placed between two parallel copper round plates (99.9% purity) with thermocouples arranged. The k is determined according to the relationship between the heat flowing through the test structure and the temperature difference between the upper and lower copper plates [306]. For using this technique, it is important to avoid the heat loss from the sample, so the insulation system and heat controls system must be rigorous designed and controlled. Wang et al. [306] used this method to measure the k_{nf} with two kinds of nanoparticles (Al_2O_3 and CuO) dispersed in the same base fluid. The obtained k values were much higher than the predictions from the existing theoretical models. Li and Peterson [327] measured the k of Al_2O_3/H_2O nanofluids with two different particle diameters. They confirmed that the k_{nf} was boosted compared to the base fluid by 27% after the addition of nanoparticles with 36–47 nm diameters. Sridhara et al. [328] comprehensively compared the difference in results among various experimental measurement techniques. They pointed out that the steady-state parallel plate method is least affected by the nanoparticle aggregation phenomenon, owing to the small thickness of the liquid spreading on the plate.

The concentric cylindrical structure is another form for the steady-state method. The method derived from the above structure is named the steady-state coaxial cylinder method. Kurt et al. [329] employed this method to measure the k of EG-water fluids. Combined with artificial neural networks, accurate prediction of k_f was achieved. Barbés et al. [330] measured the k of CuO/water and CuO/EG nanofluids by using this method combined with microcalorimetry. Putra et al. [264] studied the effect of natural convection in nanofluids using a horizontally placed cylinder that was cooled at one end and heated at the other end. The measurement results suggested that for their prepared Al_2O_3/water nanofluid (concentration: 4%, average particle diameter 131 nm), k was enhanced by 24% compared to the base fluid. Notice that the apparatus of the steady state method is relatively simple and convenient, but still needs further developments to increase the measurement accuracy.

3.1.2.5. Transient plane-source method. The transient plane-source (TPS) method (see Fig. 16e) has become a commercial technique for measurement of k_{nf}. Generally, this method is implemented by hot disk technology where the hot disk is regarded as both the plane source and the temperature sensor. Once immersed in the colloidal materials, the heat loss from the hot disk is monitored by its electrical resistance change versus time, then the k of the colloidal materials is obtained [331–333]. The hot disk element consists of a continuous double spiral of electrically conducting nickel (Ni) metal and is sandwiched between two pieces of thin polyimide films. When the double spiral nickel strip is energized, its temperature rises rapidly and the heat spreads to the samples through the thin polyimide films. After a certain period, the k of the sample can be obtained based on the real-time recorded the temperature versus time curves [334].

Later, Harris et al. [335] proposed a modified transient plane source (MTPS) for the measuring of thermophysical properties of nanofluids in motion. By using a fast response sensor, minimal sample volume and low energy power flux, the modified method can distinguish the contribution from different heat transfer modes and eliminate the effect of heat convection. This method has been widely used for measurements of k_{nf}. Li et al. [336] measured Al_2O_3/water nanofluids in various conditions using the MTPS method to obtain the best thermal behavior. Compared with the base fluid, k_{nf} was enhanced by 10.1%. Peng et al. [307] also used the MTPS method to characterize the k_{nf} containing different shapes of CNTs, and concluded that the aspect ratio of CNTs is positively correlated with the k of CNT-based nano refrigerants.

3.1.3. Experimental studies

Several researchers have developed various experimental methods to measure k_{nf}. They found that the following seven factors strongly affect the obtained the k values during measurement:

1. nanoparticle concentration,
2. temperature,
3. nanoparticle size,
4. nanoparticle shape,
5. nanoparticle agglomeration,
6. pH,
7. sonication time.

Fig. 17 illustrates the intrinsic mechanisms of various factors on k_{nf}. How to scientifically control and modulate these factors is a big challenge. Thereafter, we will focus on the latest studies dealing with the effect of the above-mentioned factors on k_{nf}. We have summarized some significant experimental data of k of representative nanofluids reported by previous studies [10,274,281,283,306,313,314,327,336–393] (see Table 2).

3.1.3.1. Nanoparticle concentration effect. Nanoparticle concentration can significantly affect the k_{nf} [337–342]. The study of Esfe et al. [337] argued that increasing MgO nanoparticle concentration (from 0.5 vol% to 2 vol%) boosted Nu, which has a higher impact on the promotion of k. Their other studies also emphasized the significant nanoparticle concentration effect, when the concentration of ZnO–DWCNT nanoparticles reached the maximum (1.95 vol% for EG nanofluid and 1 vol% for water-EG nanofluid), the k could get boosted considerably: 24.9% promotion for ZnO–DWCNT/EG nanofluid and more than 32% promotion for ZnO–DWCNT/water-EG nanofluid [338,339]. Similar results were given by Rostamian et al. [340],

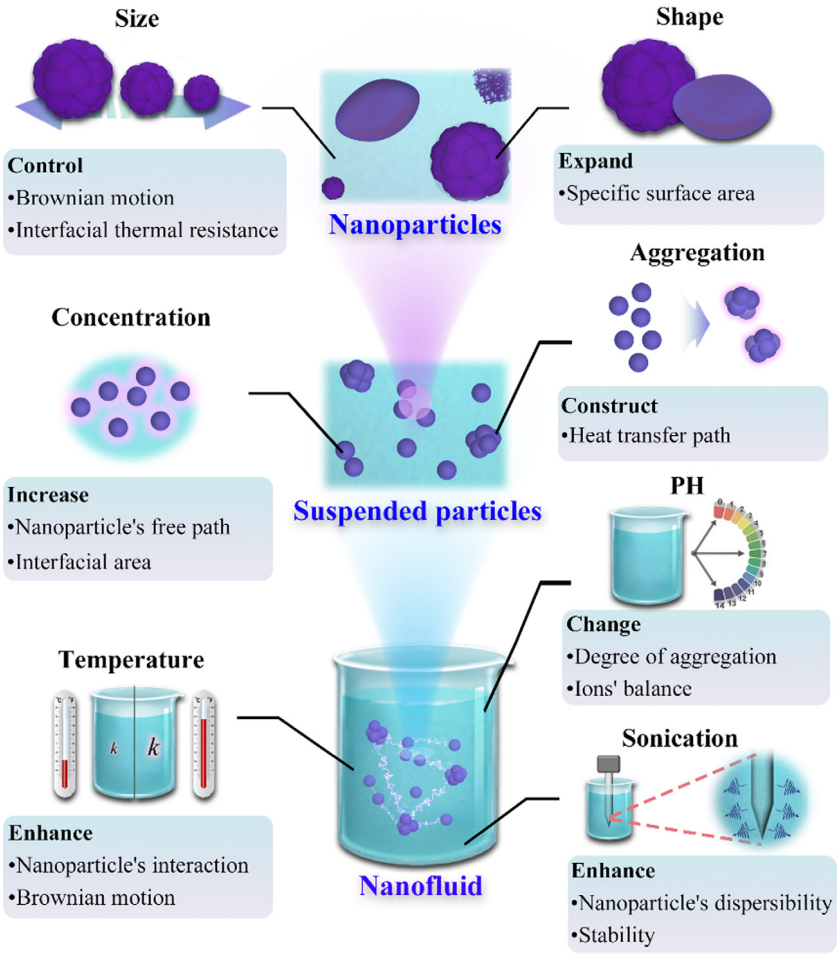

Fig. 17. The intrinsic mechanisms for the influence of various factors on the thermal conductivity of nanofluids.

when CuO nanoparticle concentration increased from 0.02 vol% to 0.75 vol%, the k of the CuO/water-EG nanofluid was improved by at least 28.9%. The increasing nanoparticle concentration could bring more positive results in nanofluids when also considering temperature effects, such as boosting k of SiC/EG nanofluids by 16.21% compared with the base EG nanofluids [341,342].

It is known that the addition of nanoparticles with high k has a positive influence on the overall heat transfer ability of nanofluids. Based on the above-mentioned work, the increasing nanoparticle concentration will further amplify this positive effect. In light of conclusions inferred by some researchers, the reason for the nanoparticle concentration effect could be the decreasing free path between nanoparticles due to the percolation effect, which increases the frequency of the lattice vibration [394,395]. In addition, the increasing interfacial area between nanoparticles and the base fluid [396] and the stronger heat transfer motion at enormous amounts of particles [397] also lead to the increase in k.

However, it is intriguing to note that k can obtain ideal improvement only under increasing nanoparticle concentration. The dispersion and stability of the nanoparticles inside the base fluid also affect the concentration effect [398,399], in which the dispersion depends on the sonication time as will be discussed later.

3.1.3.2. Temperature effect. Many studies have confirmed that temperature is one of the indispensable factors in studying k_{nf} [274,281,343,344,356,397,400–402]. Li and Peterson [344] used the steady-state method to obtain k of Al_2O_3/water nanofluids at different temperatures. The improvement of k_{eff} of Al_2O_3/water nanofluid compared with the base fluid was nearly three times when the temperature changed from 27.5 °C to 34.5 °C. It was believed that Brownian motion of the Al_2O_3 nanoparticles caused a micro-convection effect within the base fluid molecules, which was intensified by the increasing temperature and thus improved the heat transfer capacity of the nanofluid. This is consistent with the conclusion obtained by Chon et al. [274], who pointed out that the rise of temperature increased the Brownian velocity. Moreover, Mintsa et al. [343] experimentally proved the temperature-dependence of the k of CuO/water and Al_2O_3/water nanofluids. Duangthongsuk et al. [356] measured the k change with temperature for TiO_2/water nanofluids using the

Table 2
Summary of experimental data from research into the enhancement of the thermal conductivity of nanofluids (k_{nf}).

Particle type	Base fluid	k enhancement (%)	Volume concentration (%)	Size (nm)	Method	Year	Ref.
Al_2O_3	Water	31	18	41	THW	2009	[343]
		30	10	36	SSCB	2006	[344]
		28	6	36	SSCB	2007	[327]
		24	4	38.4	THW	2003	[345]
		22	14.6	20	TSHW	2007	[346]
		17.7	4	282	THW	2009	[283]
		14.4	4	40	Flash	2015	[347]
		10.1	4	15–50	TPS	2009	[336]
		9.7	3	43	THW	2010	[348]
		9	1	11	THW	2005	[274]
		8	3	38	SSCB	2007	[349]
		7.52	2	43	THW	2010	[348]
		7.1	0.08	10	THW	2018	[350]
		5.4	4	12	THW	2010	[351]
		4.7	0.05	10	THW	2018	[350]
		3.28	0.75	43	THW	2010	[348]
		3.1	0.04	10	THW	2018	[350]
		1.64	0.33	43	THW	2010	[348]
	EG	30	5	60.4	THW	2002	[352]
		22	0.08	10	THW	2018	[350]
		18	5	38	THW	1999	[353]
		17.3	0.06	10	THW	2018	[350]
		16.3	3	282	THW	2009	[283]
		14.3	4	12	THW	2010	[351]
		10.6	3	38	THW	2007	[349]
		9.7	4	45	3ω	2008	[313]
	EG/Water	12.6	2	13	THW	2015	[354]
		11.3	3	10	THW	2010	[351]
		10.4	3	50	THW	2010	[351]
		8.4	2	13	THW	2015	[354]
		16.2	2	13	THW	2015	[354]
	EO	30	7.4	28	SSPP	1999	[306]
	PO	38	5	60.4	THW	2002	[352]
		20	7.1	28	SSPP	1999	[306]
	Glycerol	27	5	60.4	THW	2002	[352]
	DI	13.3	4	45	3ω	2008	[313]
		4	1	48	THW	2007	[355]
TiO_2	Water	11.4	3	10	THW	2007	[349]
		8.7	3	34	THW	2007	[349]
		7	2	21	THW	2009	[356]
		6.5	2.6	40	THW	2007	[346]
		6.4	3	70	THW	2007	[349]
		4.2	2	20	THW	2007	[357]
	EG	19.52	7	5	THW	2016	[358]
		18	5	15	THW	2008	[281]
		14.4	3	10	THW	2007	[349]
		12.3	3	34	THW	2007	[349]
		7.5	3	70	THW	2007	[349]
	DI	33	5	Ø10×40	THW	2005	[359]
		30	5	15	THW	2005	[359]
		14.4	1	20.5	THW	2007	[355]
		7.2	3	21	3ω	2009	[314]

(*continued on next page*)

transient hot-wire method. All these researchers attributed the increase in k with increasing temperature to the effect of Brownian motion enhancement. Later, Godson et al. [400] indeed experimentally confirmed the change of Brownian velocity in nanofluids with temperature rise. They measured k of 0.9 vol% Ag/DI water nanofluids using the transient hot-wire method. When the temperature increased from 50 °C to 90 °C, the Brownian velocity enhanced from about 1.5×10^{-9} m/s to 2.1×10^{-9} m/s, and the k_{nf} was boosted from 0.8 W/m K to 1.6 W/m K. The effect of temperature on nanofluid heat transfer performance can be intuitively seen from the data. Li et al. [401] pointed out that the increase in temperature reduced the surface energy of the nanoparticles for agglomeration and improved the Brownian motion, leading to the improved k. Brownian motion is not only dependent on temperature. Harandi et al. [397] measured k of F–MWCNTs–Fe_3O_4/EG over the temperature range from 25 °C to 50 °C. The measured k demonstrated nearly linear

Table 2 (*continued*).

Particle type	Base fluid	k enhancement (%)	Volume concentration (%)	Size (nm)	Method	Year	Ref.
CuO	Water	52	6	29	SSCB	2006	[344]
		34	9.7	23	SSPP	1999	[306]
		32.3	7.5	25	THW	2012	[360]
		24	2	55–66	THW	2016	[361]
		16.5	4.68	33	TSHW	2007	[346]
		12	3.41	24	THW	1999	[353]
		5	1	33	THW	2007	[362]
	EG	54	14.8	23	SSPP	1999	[306]
		23	4	24	THW	1999	[353]
		21	2	55–66	THW	2016	[361]
		9	1	33	THW	2006	[363]
	MEG	21.3	7.5	25	THW	2012	[360]
	EO	14	2	55–66	THW	2016	[361]
CeO_2	EG	22	2.5	10–30	THW	2018	[364]
ZnO	Water	14.2	3	10	THW	2007	[349]
		7.3	3	60	THW	2007	[349]
	EG	21	3	30	THW	2007	[349]
		13	2.4	50	THW	2014	[365]
WO_3	EG	13.8	0.3	38	THW	2007	[355]
Fe_3O_4	Kerosene	34.6	1	15	THW	2010	[366]
	Water	11.5	3	15–23	THW	2010	[367]
		2.9	4.8	15–20	3ω	2019	[368]
		1.1	1	15–20	3ω	2019	[368]
$NiFe_2O_4$	DI	17.2	2	8	THW	2015	[369]
MgO	EG/Water	34.43	3	40	THW	2015	[370]
Cu	Oil	43	7.5	100	THW	2000	[10]
	Water	78	7.5	100	THW	2000	[10]
		23.8	0.1	75–100	THW	2006	[371]
	EG	40	0.3	<10	THW	2001	[372]
Au	Water	21	0.00026	10–20	THW	2003	[373]
	Toluene	8.8	0.011	10–20	THW	2003	[373]
		8	0.003	1.65	TSHW	2007	[346]
		1.4	0.024	2	MSBD	2006	[374]
	Ethanol	1.3	0.018	4	MSBD	2006	[374]
Ag	Water	20.8	1.7×10^{-5}	96	TWRC	2019	[375]
		16.5	0.001	10–20	THW	2003	[373]
		4	3.5×10^{-6}	96	TWRC	2019	[375]
	DI	16	0.5	5–25	THW	2015	[376]
Fe	EG	38.8	4	20	Theory	2018	[377]
		18	0.55	10	THW	2005	[378]
		16.5	0.3	10	THW	2007	[355]
		15.5	2	50	Theory	2018	[377]
Al	EG	45	5	80	THW	2008	[281]
MWCNT	Water	80	0.49	Ø40	THW	2006	[379]
		34	0.6	Ø130	THW	2005	[380]
		7	1	Ø10–30	THW	2007	[362]
		5	0.48	Ø10–30	THW	2016	[381]
	HTO	160	1	Ø25×50,000	THW	2001	[382]
		15	2	Ø5–20	THW	2012	[383]
	DI	7	1	Ø15×30,000	THW	2003	[384]
	EG	12.7	1	Ø15×30,000	THW	2003	[384]
		12.4	1	Ø20–50	THW	2005	[385]
	EO	8.5	1	Ø20–50	THW	2005	[385]
	DE	19.6	1	Ø15×30,000	THW	2003	[384]

(*continued on next page*)

dependence on the temperature, which could be ascribed to the enhancement of the interaction between nanoparticles due to the rising temperature.

Das et al. [345] also studied the temperature effect on the k of CuO/water and Al_2O_3/water nanofluids from both experimental and theoretical studies. The results indicated that their experimental observations were in good agreement with the Hamilton–Crosser thermal conductivity model above 50 °C. Murshed et al. [281] proved the strong positive

Table 2 (*continued*).

Particle type	Base fluid	k enhancement (%)	Volume concentration (%)	Size (nm)	Method	Year	Ref.
DWCNT	Water	8	1	Ø5	THW	2005	[380]
SWCNT	Water	16.2	0.48	Ø1-2×5000-30,000	THW	2016	[381]
		8.1	0.48	Ø1-2×1000–3000	THW	2016	[381]
	EG	15.5	0.21	100–600	THW	2012	[386]
Graphene	EG	86	0.05	0.7–1.3	TSHW	2011	[387]
Graphene Oxide	EG	61	0.05	0.7–1.4	TSHW	2011	[387]
C_{60}-C_{70} fullerenes	Toluene	0.816	0.378	–	MSBD	2006	[374]
	MO	6	5	10	THW	2007	[362]
SiC (sphere)	DI	15.8	4.2	26	THW	2002	[388]
		7.2	3	100	THW	2011	[389]
	EG	13	3.5	26	THW	2002	[388]
	DO	7.36	0.8	30	THW	2016	[390]
SiC (cylinder)	DI	22.9	4	600	THW	2002	[388]
	EG	23	4	600	THW	2002	[388]
SiO_2	Water	38.2	3	40–50	THW	2019	[391]
		3.2	1	12	THW	2007	[362]
		3	1	12	THW	2006	[363]
Ag/Au	PO	33	0.006	10	THW	2006	[392]
		15	0.003	10	THW	2006	[392]
Sn/SiO_2	TH66	13	5	50–100	THW	2013	[393]
DWCNT/ZnO	EG/Water	33	1	Ø3/10–30	THW	2015	[339]

influence of temperature on k_{nf} through experiments, and verified the strong agreement between theoretical models and experiments at high temperature. As can be seen, the influence of temperature on k is significant, and the higher the temperature, the greater the influence.

3.1.3.3. Nanoparticle size effect. As mentioned in the previous section, nanoparticle size is an important factor for k_{nf}. According to the classical Maxwell model, the k_{nf} without the influence of nanoparticle size is only a function of volume fraction [403], which is obviously unreasonable. Therefore, many theoretical models take into account the effect of nanoparticle size and the corresponding experimental evidence has been developed. The effect of nanoparticle size on k_{nf} is currently controversial. Many theoretical models and experimental results have contended that k_{nf} increases as the decreasing nanoparticle size. However, some other studies have reported the opposite conclusions, that the k increases as the increasing particle size.

The classical Maxwell model does not consider the Brownian motion of nanoparticles, so the model cannot predict the effective k_{nf} accurately enough. Dong and Chen [286] regarded both nanoparticle size and Brownian motion as two independent factors affecting k_{nf}. On the one hand, as the nanoparticle size decreased, the k_{nf} increased. On the other hand, Brownian motion was equivalent to an increase of the nanoparticle radius, resulting in an increase of the nanoparticle volume fraction, and thus k_{nf} was increased. Experimental results demonstrated that the effective k of Al_2O_3/water nanofluids decreased with the increase of nanoparticle size, which was in good agreement with the model prediction. Xu et al. [284] proposed a fractal model considering the thermal convection and the fractal distribution of nanoparticle size. They experimentally studied the k of Al_2O_3/DI water nanofluids as a function of nanoparticle size. The results indicated that the k_{eff} decreased with increasing nanoparticle size due to Brownian motion. Specifically, the smaller the nanoparticle size, the greater the Brownian motion velocity of these nanoparticles, and the higher k. Jang and Choi [404] experimentally verified that the k of oxide nanoparticle, metallic nanoparticle and CNT-based nanofluids all increased with the increasing nanoparticle/nanotube size. When the nanoparticle size was close to micrometers, the nanoparticles would not be suspended in the base liquid, and thus Brownian motion did not occur any longer and k_{nf} would not increase.

Some scholars have proposed the opposite conclusion. Timofeeva et al. [405] reported that the k of α-SiC/water nanofluids increased with increasing nanoparticle size in the range of 16–90 nm. The reason for this phenomenon was that the smaller nanoparticles had a larger surface area at the solid/liquid interface, which would become an obstacle to the heat flow, and thus k was smaller. Chen et al. [406] studied the relation between k and nanoparticle size for SiO_2/water nanofluids with nanoparticle sizes in the range of 10–30 nm. It was found that k_{nf} increased linearly with increasing nanoparticle size, owing to the reduced interfacial thermal resistance of the increased nanoparticle's size. Notice that this linear relationship was only valid in a small particle size range. Beck et al. [283] experimentally studied the effect of nanoparticle size (8–282 nm) on k of Al_2O_3/water or Al_2O_3/EG nanofluids. It was observed that Al_2O_3/water or Al_2O_3/EG nanofluids with larger nanoparticles had higher k, and the k remained constant when the diameter increased to 50 nm, which was consistent with the Maxwell equations. To further explore the effect of nanoparticle size on the k_{nf}, Ganesan et al. [288] studied k of nanoclusters-based Fe_3O_4 nanofluids with a very large particle size (115–530 nm). Although the

theoretical model predicated that k of Fe_3O_4 nanofluids increased by 5.3–12.6% with decreasing nanoparticle size, the experimental results were contrary to this trend, which might be attributed to the kinetic growth of nanoclusters into fractal like aggregates in the suspensions [407].

3.1.3.4. Nanoparticle shape effect. From the development of the k models, as can be seen that the shape of the nanoparticles is another non-negligible factor affecting k_{nf}. Xie et al. [388] measured k of SiC/water nanofluid using the transient hot-wire method. The results proposed that the nanofluid with spherical SiC particles had a remarkably lower k than that contained cylindrical particles at the same volume fraction. This was the first time that experimental evidence of the effect of particle shape on k_{nf} had been reported. After that, Murshed et al. [359] studied the k of TiO_2/DI water with spherical and rod nanoparticle shapes. Similarly, the k of TiO_2/DI water with spherical nanoparticles was lower than nanofluids containing the rod-shaped nanoparticles. Since the rod-shape nanoparticle renders a larger shape factor than the spherical counterpart, it can be known from the Hamilton and Crosser model (Eq. (30)) that the fluid with spherical particles has a smaller k than the other shapes. Besides cylindrical and spherical nanoparticles, Jeong et al. [408] also studied nanoparticles with nearly rectangular shape. In their study, the nanofluids with nearly rectangular shaped ZnO nanoparticles had a k that was 5.9% greater than that of a nanofluid with spherical nanoparticles. The authors attributed this result to the fact that the approximately rectangular nanoparticles had a larger effective agglomeration radius. Ferrouillat et al. [409] conducted an experimental study on the suspension of SiO_2 and ZnO nanoparticles with spherical and banana-shaped nanoparticles. For both nanofluids, the non-spherical nanoparticle-contained nanofluid exhibited a higher k than the spherical nanoparticle-contained nanofluid. The authors believed that the banana-type nanoparticles had a larger surface area, which resulted in a larger contact area of the nanoparticles with the base fluid that contributed to heat transfer.

In addition to the above-mentioned two shapes, Timofeeva et al. [410] studied alumina nanofluid containing four shapes, *i.e.*, platelets, blades, cylinders and bricks. The ability of the four shapes to enhance k ranking from high to low is: cylinders $>$ bricks $>$ blades $\approx$ platelets. This is because the decrease of the sphericity leads to the increase of the particle shape factor and the surface area, which has a positive influence on heat transfer. Here, the sphericity represented the ratio of the surface area of the spheres with the same volume as the particles to the surface area of the particles. Notice that the surface thermal resistance also increased at the same time. When the sphericity was less than 0.6, the surface effect would have a negative effect on k. Bhanushali et al. [411] compared the k values among different nanoparticle shapes: long nanowires, short nanowires, nanospheres and nanocubes. The results indicated that nanowire particles with a volume fraction of 0.25% increased k_{bf} by 40%, while nanosphere particles only increased k_{bf} by 9.3%. The authors pointed out that nanowire-shape particles had large aspect ratios, which reduced the adverse effects of interfacial thermal resistance on heat transfer. A large aspect ratio can excite thermal penetration, which also enhances k_{nf}. Similarly, Ghosh et al. [412] reported in their study that nanoparticles with large aspect ratios could increase the heat transfer rate and improve the k_{nf} during the nanoparticle collision. These experimental results verify that the influence of particle shape on k_{nf} is not negligible. Michaelides [265] has shown analytically why the shape and orientation of nanopartilces in the nanofluid would have a significant effect on k_{nf}.

3.1.3.5. Nanoparticles aggregation effect. Theoretical and experimental studies have illustrated that the aggregation of nanoparticles can significantly increase k_{nf}. When the aggregation of nanoparticles occurs, an effective heat transfer path is formed, which will greatly promote k_{nf} [413].

Based on Maxwell effective medium theory [287], Hong et al. [296] studied the effect of nanoparticle aggregation on k_{nf}. The experiments confirmed that k of Al_2O_3/DI water nanofluids increased with the increasing degree of aggregation, and the nanofluids with a volume fraction of 5% achieved a maximum k enhancement of 22%, which was much lower than the Maxwell upper limit. The degree of aggregation was quantified by measuring μ_{nf}. Pang et al. [297] also reported a new model for predicting k_{nf} based on the effective medium theory. Aggregation is consistently believed to make some non-negligible contributions to the enhancement of k_{nf}, especially at low concentrations. They compared the k_{eff} with different shapes of SiO_2/methanol aggregates at a concentration of 0.1%, including fiber, ellipsoid and spherical shapes. It was illustrated that for ellipsoid and fiber shapes, the greater the sphericity of the aggregation, the greater the k_{eff}. Moreover, the fiber shape had a greater enhancement of k_{nf} than the ellipsoid shape.

In addition, based on aggregation kinetics of the colloids, Prasher et al. [407] argued that k_{nf} first increased and then decreased with increasing volume fraction of aggregation, and reaches a maximum when the volume fraction is 0.35. Feng et al. [282] proposed a model for predicting the k of Al_2O_3/EG nanofluids with volume fractions of 0.03, 0.05 and 0.07 respectively, which considers the nanolayer and the aggregation of nanoparticles. The results indicated that the aggregation of the nanoparticles increases with decreases in nanoparticle size at the same volume fraction, and the larger the volume fraction of the nanoparticles, the more the nanoparticles aggregate. In order to further understand the influence of aggregation on the thermal properties of nanofluids, Wei et al. [300] proposed a fractal model which considers both the aggregate distribution and Brownian motion of nanoparticles. This model is in good agreement with the experimental data for k of SiO_2/ethanol nanofluids [275], Al_2Cu/water-EG nanofluids [414] and TiO_2/water nanofluids [359]. It was found that when the empirical shape factor $F < 6$, the shape of the aggregation is close to a circle, and the k_{nf} gradually decreases with increasing volume fraction. When the $F > 6$, the shape of the aggregation appears as a chain, so the k_{nf} increases with volume fraction much faster. F is the empirical shape factor related to the fractal dimension and volume fraction of the nanoparticles. Since the fractal dimension might be affected by the shape of aggregation, more experiments are needed for further analysis.

3.1.3.6. Effect of pH. Experimental studies have confirmed that modulating the pH values of the nanofluids can remarkably change the degree of nanoparticle aggregation, thereby affecting k_{nf}. Under a certain pH value, the nanoparticles and the base fluid reach a balance between the positive and negative ions, which is called the isoelectric point (IEP). Several scholars have carried out experiments in this area. Wang et al. [415] studied the dependence of k_{nf} on the pH value of Al_2O_3/water nanofluids and Cu/water nanofluids at a concentration of 0.1%. It was found that k_{nf} increases with the increasing pH value until it reaches the IEP and then decreases. The Al_2O_3/water nanofluids and the Cu/water nanofluids had an IEP of 7.5–8 and 9–9.5, respectively. The reason for this phenomenon is that the charge on the surface of the nanoparticles increases the IEP, resulting in an increase of the electrostatic repulsion force between the nanoparticles. The ensuing decreasing aggregation of the suspension and the increasing mobility of the nanoparticles lead to enhanced heat transfer of the nanofluids. Li et al. [416] proposed that surface charge provides a more efficient channel for heat transfer. They reported that the k_{nf} of CuO/DI water nanofluids increases with the increasing pH value in the 3–9.5 range. When the pH value is near the IEP of the CuO particles (∼8.5–9.5), more surface charge is attached onto the nanoparticles, which results in a more stable suspension and finally an optimum k_{nf} is reached. At a higher pH value, electrostatic repulsion between the nanoparticles is reduced and aggregation occurs, leading to a decrease in k_{nf}. Krishnakumar et al. [417] studied the change of k of Al_2O_3/ethanol nanofluids in the pH value range of 2.5 to 11. They observed the same trend in k_{nf} as in Ref. [416], which suggests that the k_{nf} increases to the maximum then decreases with increasing pH value. Under the optimum pH, $\approx$ 6.0, k of the Al_2O_3/ethanol nanofluids with 0.1 vol% and 0.5 vol% is increased by 11.2% and 15.5%, respectively. Habibzadeh et al. [418] studied the effect of pH on k of SnO_2/DI water nanofluids, and pointed out that with a pH value of 8.0, the SnO_2 nanoparticles have zero repulsive force. The suspension is stable enough, and k_{nf} reaches the maximum. Therefore, it is safe to conclude that under strong acidic or strong basic conditions, k_{nf} is lower.

However, Murshed et al. [419] reported that as the pH increased from 3.4 to 9, the enhancement of k for TiO_2/DI water nanofluids at a concentration of 0.2% decreased from 5.5% to 2.55%, indicating that when the pH is close to the IEP, the suspension became unstable and the nanoparticle aggregation results in a decrease of the k_{eff}, which can be explained by DLVO theory [420]. Xie et al. [421] experimentally studied the effect of pH on k of Al_2O_3/DI water nanofluids. The results imply that as the difference between the pH values of the suspension and that of the IEP (∼9.2) increases, k_{nf} becomes larger, while the k at the IEP is the smallest. The underlying mechanism is the repulsive force at the IEP is zero, and the resulting nanoparticle aggregation leads to a decrease in k_{nf}.

3.1.3.7. Sonication time effect. Ultrasonic dispersion is a common technique used in nanofluid preparation. Previous studies have illustrated that it is critical to perform adequate sonication of the sample to further increase k_{nf} [347,378,422–428]. Hong et al. [378] used the transient hot wire method to measure k of Fe/EG nanofluids for different sonication times. The results indicate that when the sonication time is less than 50 min, k_{nf} increases with time. When the time reaches 70 min, k_{nf} does not continue to increase with increasing sonication time.

Other researchers [422,423] studied the effect of sonication on k of CNT/water nanofluids. They observed an enhancement of k_{nf} as the sonication time increases, due to the improvement of dispersion uniformity. When the optimum sonication time (40 min) is exceeded, k_{nf} is reduced because the CNTs are broken and the aspect ratio is decreased. Kole and Dey [424] claimed the same trends in the study of ZnO/EG nanofluids. Specifically, at the optimum sonication time, k_{nf} can be increased from approximately 0.30 W/m K to 0.35 W/m K. Sonawane et al. [425] confirmed that sonication enhanced the Brownian motion of the nanoparticles in TiO_2/water, EG and paraffin oil nanofluids based on the improved interaction between the nanoparticles and the fluid. However, excessive sonication made the distance between the nanoparticles too close to aggregate, which led to the decrease in k_{nf}. Sundar et al. [426] attributed the increase of the k_{nf} to the prolonged sonication time which improved the nanoparticle uniformity and blocked nanoparticle sedimentation caused by sonication vibration. Buonomo et al. [347] studied the effect of sonication time on the k of Al_2O_3/water nanofluids by the nanoflash method for the first time. The results demonstrated that for different concentrations of nanofluids, k_{nf} varies greatly with increase in sonication time, but remains unchanged above the optimum time. Nemade et al. [427] achieved 18% enhancement in k of CuO/water nanofluids by selecting the appropriate sonication time during preparation. The study reported that the nanoparticle size depends strongly on the sonication time, and thus k_{nf} was influenced by the sonication.

In addition to the above conclusions, Asadi et al. [428] studied the effect of sonication time on surfactant-added $Mg(OH)_2$ nanofluids. In marked contrast to the above-mentioned surfactant-free nanofluids, k of surfactant-added $Mg(OH)_2$ nanofluids decreases immediately as the sonication time increases. This was because the sonication destroys the good stability of the surfactant in the nanofluids. In summary, the effect of sonication time on k_{nf} concentrates on its uniformity, stability, nanoparticle size and the interaction between nanoparticles and fluid molecules. A comprehensive review of the effect of sonication time on thermophysical properties of nanofluids has been done by Asadi et al. [428].

3.1.4. Hybrid nanofluids

There have been many studies on nanofluids containing only one type of nanoparticle, and many researchers have discovered and reported various thermophysical properties and important conclusions of such colloidal suspensions very well. However, research on nanofluids containing at least two types or more (hybrid nanofluids) is still in progress. In this section, our main purpose is to summarize and record the progress in the k of hybrid nanofluid (k_{hnf}) from both the theoretical and experimental point of views. Theoretically, a classical model that is suitable for hybrid nanofluids will be introduced. In experimental studies, the effects of various key factors on k_{hnf} are explored, such as nanoparticle type, size, shape and temperature.

3.1.4.1. Theory. Hybrid nanofluids are obtained by adding two or more different nanoparticles to the base fluids in order to increase k_{nf}, which generally renders higher k than observed in pure fluids or in single particle nanofluids. As to the theoretical studies, Takabi et al. [429] reported an improved Maxwell model to predict k_{hnf}:

$$\frac{k_{hnf}}{k_{bf}} = \frac{\frac{\Phi_{p1}k_{p1}+\Phi_{p2}k_{p2}}{\Phi_e} + 2k_{bf} + 2\left(\Phi_{p1}k_{p1} + \Phi_{p2}k_{p2}\right) - 2\Phi_e k_{bf}}{\frac{\Phi_{p1}k_{p1}+\Phi_{p2}k_{p2}}{\Phi_e} + 2k_{bf} - 2\left(\Phi_{p1}k_{p1} + \Phi_{p2}k_{p2}\right) + \Phi_e k_{bf}} \tag{64}$$

where k_{hnf} is the k_{eff} of the hybrid nanofluid, k_{bf} is the k of the base fluid, k_p denotes the k of the nanoparticles, Φ_e and Φ_p are the volume concentration of the hybrid nanofluids and nanoparticles, respectively. The comparison of this model with the experimental data was reported by Suresh et al. [430], who believe that k of Al_2O_3–Cu/water hybrid nanofluids cannot be accurately calculated using the improved Maxwell model, especially for hybrid nanofluids with high concentration.

Charab et al. [431] developed the extended Maxwell model (EMM) to predict the k_{hnf}. The EMM can be expressed as:

$$\frac{k_{nf}}{k_{bf}} = 1 + \frac{3\left(\frac{k_{p1}}{k_{bf}} - 1\right) \times \Phi_{FVC}^{p1}}{\left(\frac{k_{p1}}{k_{bf}} + 2\right) - \left(\frac{k_{p1}}{k_{bf}} - 1\right) \times \Phi_{FVC}^{p1}} + \frac{3\left(\frac{k_{p2}}{k_{bf}} - 1\right) \times \Phi_{FVC}^{p2}}{\left(\frac{k_{p2}}{k_{bf}} + 2\right) - \left(\frac{k_{p2}}{k_{bf}} - 1\right) \times \Phi_{FVC}^{p2}} \tag{65}$$

$$\Phi_{FVC}^{p1} = \Phi_e\left(\frac{V_{nf1}}{V_{nf1} + V_{nf2}}\right) \tag{66}$$

$$\Phi_{FVC}^{p2} = \Phi_e\left(\frac{V_{nf2}}{V_{nf1} + V_{nf2}}\right) \tag{67}$$

where V_{nf} is the nanofluid volume and Φ_{FVC} is the fractional volume concentration. The theoretical prediction differed greatly from the experimental results, and thus the particle mapping model (PMM) was proposed. This approach assumed that the heat transfer in the hybrid nanofluids was in series or in parallel, and k_{hnf} was calculated based on Fourier's law by using 2-D simulation. The results exhibited that the enhanced k_{nf} system was nonlinearly related to the volume fraction of the nanoparticles, probably caused by the stability of the nanoparticles and Brownian motion.

Based on the above studies, it is concluded that k_{hnf} can be significantly boosted compared with conventional fluids or nanofluids, and the boost is not linear with the concentration of different nanoparticles. Currently, more predictions about k_{hnf} are based on the correlations obtained from experimental data. Many researchers use artificial neural network (ANN) to study k_{hnf}, which can be expressed as a function of temperature, nanoparticle size and volume fraction [432–434]. However, theoretical models for the hybrid nanofluids still fail to achieve accurate prediction of k_{hnf}, and thus more improved models for the hybrid nanofluids need to be developed to meet practical requirements.

3.1.4.2. Experimental studies. A considerable number of experimental studies have confirmed that hybrid fluids have a significant enhancement effect compared to one-substance fluids, on k_{hnf}. It is obvious that the nanoparticle's type has an important influence on k_{hnf}. Botha et al. [435] measured k of Ag–SiO_2/oil hybrid nanofluids using the transient hot wire method and observed a 15% enhancement in k_{hnf}. The improvement of k_{hnf} is regarded as a result of the attachment of Ag nanoparticles onto the SiO_2, which causes shorter phonon transport distances between the nanoparticles. The study of Nine et al. [436] experimentally corroborated that Cu–Cu_2O nanofluids rendered a higher k than the Cu_2O nanofluids, which is related to the smaller size of the Cu–Cu_2O nanoparticles that enhance the collision between nanoparticles during Brownian motion. Aravind et al. [437] observed that a 10.5% enhancement in k_{hnf} occurs for graphene–MWCNTs hybrid nanofluids. Since MWCNTs possess a high aspect ratio, they can be tightly bound to graphene to reduce the interfacial resistance, and thus this hybrid nanofluid has a higher k than pure graphene nanofluids. Batmunkh et al. [438] proved that k of Ag–TiO_2 hybrid nanofluids is increased from 0.608 W/m K to 0.616 W/m K at RT after the addition of Ag nanoparticles. They concluded that both the relatively higher k of Ag nanoparticles themselves and the improved Ag/TiO_2 interface promote phonon conduction and thus increase the k_{nf}. Ho et al. [439] measured n-eicosane water-based fluid with Al_2O_3 nanoparticle addition. The results show that k_{hnf} is improved, because Al_2O_3 had a significantly higher k than n-eicosane particles. Madhesh et al. [440] found that when the concentration of Cu–TiO_2 nanoparticles in fluid was approximately 2%, k_{bf} is increased by 6%. They attributed this phenomenon to the configuration of Cu nanoparticles on the surface of Al_2O_3 nanoparticles, which facilitates the formation of a thermal interfacial network between the nanoparticles and the fluid, thereby promoting heat transfer.

However, there are also cases where k_{hnf} is lower than that of the base fluid. Jana et al. [398] studied CNT–Cu and CNT–Au hybrid nanofluids and the fluids with three components. The results indicate that the collaboration of Au and Cu nanoparticles with CNTs is not good, as expected, leading to excessive interfacial thermal resistance and obvious agglomeration, which causes k_{hnf} to not experience the expected enhancement. Baghbanzadeh et al. [441] compared k of the MWCNT fluids, spherical SiO_2 fluids and the MWCNT–SiO_2 hybrid fluids. Interestingly, their results demonstrate that k_{hnf} was between the two pure component fluids. They also pointed out that since the MWCNTs themselves have a large aspect ratio and a high k, the enhancement effect on k_{bf} is most pronounced. In the hybrid nanofluid, the mixing of SiO_2 and MWCNTs produced additional thermal resistance and thus the enhancement is weaker than MWCNTs but stronger than SiO_2 due to the lower k of SiO_2 than MWCNTs. Obviously, whether the hybrid nanofluids can render higher k or not is somewhat controversial. It seems that the specific nanoparticle constitution or namely the interfacial thermal

transport between the nanoparticles and the nanoparticle/fluid greatly affects the k of the resultant hybrid nanofluids. It is expected that future work on distinguishing the microscopic thermal transport behaviors in hybrid nanofluids would unravel this mystery.

Another important issue from experimental studies is what the key factors are and how they influence the k_{hnf}. Over the past decade, the concentration, size and shape of the nanoparticles and the temperature have been found to be the essential factors. Baghbanzadeh et al. [441] hold the point that the increased concentration of nanoparticles in the fluid contribute to the formation of a network which could enhance k_{hnf} and experimentally found the effective k_{hnf} is slightly boosted from 1.05 W/m K to 1.13 W/m K when the mass concentration changes from 0.1% to 1%. Baby and Sundara [442] confirmed the k of CuO decorated graphene/DI water hybrid nanofluids is improved by 28% if the concentration is boosted from 0.01% to 0.07%. Similarly, they ascribed this k boost to the enhanced percolation effect due to the increase in concentration. The percolation considerably reduces the distance between nanoparticles and promotes the contact between them, and thus enhances the lattice vibrations which increases k. Yarmand et al. [394] also gave experimental evidence which supported this view. Their study demonstrated that k of Ag-graphene/water nanofluids is positively linearly dependent on the addition concentration.

Some scientists have believed external factors, especially the temperature is a key factor influencing k_{hnf}. Sundar et al. [443] corroborated that k of MWCNT–Fe_3O_4/water nanofluids increased relative to the base fluid from 13.88% at 20 °C to 28.46% at 60 °C. They attribute this increase to the enhancement of Brownian motion. Harandi et al. [397] demonstrated that the k of functionalized MWCNT–Fe_3O_4/EG hybrid nanofluids increases with a rise of temperature, and they believe the enhanced interaction between the nanoparticles is the main reason. Esfahani et al. [444] also verified the improvement effect of k by studying ZnO–Ag (2 vol%)/water hybrid nanofluids with a temperature rise. They corroborated that k_{hnf} increases from 0.663 W/m K at 25 °C to 0.788 W/m K at 50 °C, which is also explained by enhanced Brownian motion.

Compared with the above-mentioned two dominant factors, the size and shape of the nanoparticles are subordinate factors that still influence k_{hnf}. Nine et al. [445] observed that cylindrical shaped nanoparticles in hybrid fluids have a slightly stronger enhancement effect on k_{bf} than the spherical nanoparticles at the time additional concentration level of 4 wt%. This is ascribed to the cylinder shape that typically have a larger aspect ratio, a favorable factor for the k boost. The study of Baghbanzadeh et al. [441] experimentally verified that if the nanoparticle size is larger, it is easy to form larger clusters with reduced specific area, which weakens the enhancement of k_{nf}. It can be seen from the above reports that the influence of various factors on the hybrid fluid is basically consistent with the influence on the common single-phase fluid. Table 2 summarizes the experimental data from research into the enhancement of k_{nf}, corresponding to different types of nanoparticles and base fluids, volume concentration, particle size, and measurement methods.

3.1.5. Molecular dynamic (MD) simulations

In general, most of the studies on k_{nf} are based on the experimental and theoretical results mentioned above, but some researchers have also studied the k_{nf} by means of MD simulation. Even though MD simulation is considerably difficult and requires much more computational time for the study on nanofluids, it is a good tool to study the behavior of thermal systems at small scales (atom and molecules level). Lu and Fan [446] proposed that k of Al_2O_3/water and Al_2O_3/EG nanofluids can be effectively analyzed by simplified MD simulation. How to choose the potential energy models between nanoparticles was the main target of the simplified MD simulation process, such as two-particles and multi-particle model [447,448]. Since some parameters in the multi-particles potential model are usually undetermined and computationally complex, the two-particle potential model is mainly used for MD simulation for nanofluids. Typically, the simulation results are in good agreement with experimental data, which proves they are reliable. In addition, simulation results reported that k of Al_2O_3/water and Al_2O_3/EG nanofluids increases significantly with an increase in the volume fraction of nanoparticles, and decreases with increasing nanoparticle size. Since the heat transfer orients mainly from the surface of the nanoparticles, which possess much larger surface area to volume ratios, k_{nf} increases. By using MD simulation, Rudyak et al. [449] studied the effect of the ratio of mass (m) and diameter (r) of different dispersed nanoparticles on the k_{eff} of nanofluids. They used the molecular models in base fluids and nanoparticles which are established by hard sphere systems of different diameters. It was demonstrated that k_{eff} of nanofluids always exceeds k_{bf} due to the presence of the nanoparticles, and the enhancement in k depends on the volume concentration, size and mass of the nanoparticles. In particular, the effect of mass will be more significant than that of nanoparticle size, which reveals that the ρ of the nanoparticles is also a key factor for k_{nf}.

Achhal and Jabraoui et al. [450] studied the dependence of k for Cu/Ar nanofluids on nanoparticle size and temperature by EMD simulation using the on Green–Kubo function. The interaction between Ar atoms was described by the well-known Lennard-Jones (L-J) potential, and the interaction between Cu atoms was described by the embedded atom method (EAM) potential. In their simulation process, a box consisting of Ar atoms arranged in a face-centered cubic (fcc) configuration was used as a model for nanofluids, and Cu atoms were used to replace the Ar atoms in the center of the box. The boundary conditions were set to be periodic boundaries, allowing the sample to relax under $T = 300$ K using the NVT ensemble for a period to ensure the presence of the fluid phase. The simulation results indicated that the relative enhancement of k increases from 0.19% to 7.66% with increasing volume fraction of nanoparticles, owing to the fact that more nanoparticles inhibit the condensation of the fluid around the nanoparticles. Another study by Javanmardi and Jafarpur [451] who also used the EDM method, found a nonlinear dependence of k_{eff} for SWCNT/water nanofluids on the

nanoparticle volume fraction. For their study, the SWCNTs were armchair with chiral vector (12, 0) and the interactions between the liquid water, SWCNTs, water and carbon were described by a TIP4P potential, Brenner's potential and L-J potential, respectively.

Mohebbi [452] developed a new EDM-NEDM combined simulation method to predict c_p and α of argon-based nanofluids respectively, where the boundary condition was set to a non-periodic boundary. The k_{nf} was further obtained by the well-known relation, $k = \alpha \rho c_p$. It was found that the k enhancements were 15% and 50% at 140 K and 107 K, respectively. It is clearly seen that the enhancement of k_{nf} was much more at low temperatures. Sankar et al. [453] also studied the temperature dependence of k for Pt/water nanofluids using the EMD method in which some water molecules are exchanged by the same number of Pt nanoparticles and the simulation was carried out under the NVT ensemble. The results revealed that k_{nf} enhances with temperature.

Keblinski et al. [454] first investigated the Brownian motion effect on heat transfer using the MD simulation in 2002. They used a heat flux autocorrelation function obtained by two different simulations in the same system. In the first simulation, the movements of all atoms were required to follow Newton's equation of motion, whereas in another simulation, the center of mass of all nanoparticles was fixed, so that the position of the nanoparticles was kept fixed all the time. It turned out that there is no difference in heat flux autocorrelation function using the two different simulation approaches. Since k is obtained by integrating the heat flux autocorrelation function, it was concluded that the Brownian motion does not affect k_{nf}. Meanwhile, Sun et al. [455] also demonstrated that the Brownian motion of nanoparticles has little effect on the enhancement of k_{nf}. In addition, Cui et al. [456] explored the effect of chaotic movements on heat transfer by applying different shear velocities (50 m/s and 0 m/s) to the nanoparticles and exploring the differences. They found that the chaotic movements of the nanoparticles affected the heat transfer process. The underlying mechanism of chaotic movements was mainly due to Brownian motion.

Besides the temperature and the volume fraction of nanoparticles, aggregation of nanoparticles is another important factor affecting the value of k_{nf} [454]. Kang et al. [457] calculated k of Cu/Ar nanofluids using the EMD method based with a Green–Kubo function. Unlike other MD simulations, in their study there were multiple nanoparticles in each simulated box with periodic boundary conditions, whose purpose was to create opportunities for the aggregation of nanoparticles. The results clearly show that aggregation of nanoparticles can effectively improve k_{nf}. Lee et al. [458] used the same method to explore the effect of nanoparticles aggregation and came to the same conclusion, where k_{nf} was calculated in two different states, *i.e.*, aggregated state and non-aggregated state. It was approved that in the aggregation case, the enhancement of k_{nf} is more pronounced, since more collisions happen in the system with more nanoparticles.

In addition, the influence of size [459], shape [459,460] and surrounding nanolayers [461] of nanoparticles have been investigated by researchers. Cui et al. [459] studied the effect of nanoparticle shape on thermal conductivity of nanofluids. They demonstrated that when the surface area to volume ratio for nanoparticles is larger, the rate of k enhancement is more. Liang and Tsai [461] showed that the increase in ρ of nanolayers will have a positive impact on k_{nf}. Despite extensive research on the enhancement of k_{nf} using the MD method, the understanding of the effects of various factors on k_{nf} is still incomplete. On the experimental side, it has been proven that the pH value of the nanofluid is another important factor, but there is no research on the influence of pH values by MD simulation. Therefore, we still need to pay more attention to MD simulation of nanofluids and make greater breakthroughs in the future.

Based on the above discussions, we have depicted the k enhancement of nanofluid suspensions formed by some common nanoparticles and base fluids in Fig. 18, wherein the nanoparticles comprise metal oxides: Al_2O_3 [283,313,348,350,351,355], and TiO_2 [281,314,349,355,357], and CuO [346,361–363], and ZnO [349,365], metals: Ag [376] and Fe [377], a non-metal oxide: SiO_2 [462,463], and advanced carbon nanomaterials: graphene oxide (GON) [464,465], graphene [387,466,467], CNT [363,386,468] and functionalized CNTs [469,470]. It is clearly seen from the figure that k of some carbon nanomaterials (CNT and graphene) based nanofluids exhibits a remarkably high boost compared to other metal- and metal oxide-based nanofluids.

3.2. Isobaric specific heat capacity

The isobaric specific heat capacity c_p is one of the important parameters describing the thermal properties of nanofluids. It is worth noting that most of the research on nanofluids is focused on the k, while the research on $c_{p,nf}$ only accounts for about 5% of studies [471]. Since 2008, researchers have begun to pay more attention to the study of c_p. In most cases, when nanoparticles are mixed with a liquid such as water, the effective isobaric specific heat capacity of the prepared nanofluid is reduced because the ratio of c_p of the nanoparticles to the base fluid is less than one. In this section, we will focus on $c_{p,nf}$ from both theoretical and experimental points of view, which includes the theoretical formula developed to predict $c_{p,nf}$ and the classical experimental measurement technique, *i.e.*, DSC. Finally, the theoretical calculations are compared with the experimental measurements, and their characteristics and advantages are also analyzed.

3.2.1. Theory

Pak et al. [472] first proposed a theoretical formula for predicting the $c_{p,nf}$ based on mixture rule:

$$c_{p,nf} = \left(1 - \Phi_p\right) c_{p,bf} + \Phi_p c_{p,p} \tag{68}$$

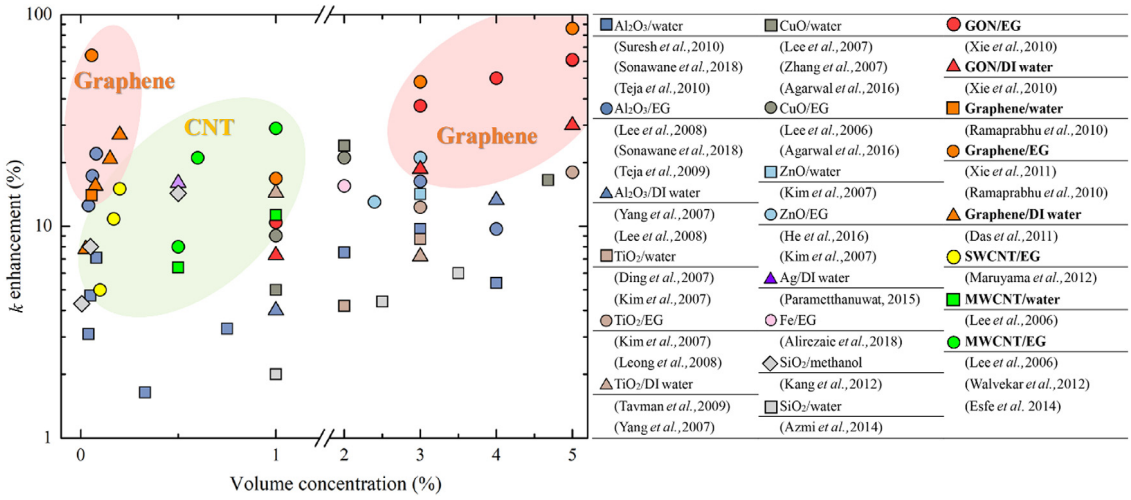

Fig. 18. Schematic diagram for the dependence of the thermal conductivity of nanofluids on volume concentration in various studies.

where $c_{p,nf}$, $c_{p,bf}$ and $c_{p,p}$ denote the effective isobaric specific heat capacity of the nanofluids, the base fluid and the nanoparticles, respectively, and Φ_p represents the volume fraction of the nanoparticles. This formula is only applicable to diluted suspensions, where the nanoparticle density is not much different from that of the base fluid. For nanoparticles with a large volume fraction, this formula would render a noticeable error. Xuan et al. [473] reported an improved c_p model, which assumes that the nanoparticles and the base fluid are in thermal equilibrium [474]:

$$c_{p,nf} = \frac{\left(1-\Phi_p\right)\rho_f c_{p,bf} + \Phi_p \rho_p c_{p,p}}{\left(1-\Phi_p\right)\rho_{bf} + \Phi_p \rho_p} \tag{69}$$

where ρ_{bf} and ρ_p denote the density of the base fluid and the nanoparticles, respectively. This equation has been widely quoted by many researchers and its reliability had been proven through experimental studies [348,475–477].

Sekhar et al. [478] developed a regression equation to predict $c_{p,nf}$ at any concentration by eighty-one sets of experimental data on water-based Al_2O_3, CuO, SiO_2 and TiO_2 nanofluids:

$$c_{p,nf} = 0.8429\left(1+\frac{T_{nf}}{50}\right)^{-0.3037}\left(1+\frac{r_p}{50}\right)^{0.4167}\left(1+\frac{\Phi_p}{100}\right)^{2.272} \tag{70}$$

where T_{nf} denotes the temperature range of the nanofluids (20–50 °C), r_p denotes the nanoparticles diameter (15–50 nm), and Φ_p denotes the volume fraction (0.01%–4%). The comparison between the calculated values and the experimental data indicates an average absolute deviations (AAD) of 8%–10%, which validates the reliability of Eq. (70). However, more experiments on a wide range of temperatures, particle sizes and volume fractions still need to be carried out. Vajjha et al. [479] proposed a correlation to predict $c_{p,nf}$:

$$\frac{c_{p,nf}}{c_{p,bf}} = \frac{A\left(T_{nf}/T_0\right) + B\left(c_{p,p}/c_{p,bf}\right)}{C+\Phi_p} \tag{71}$$

Here, $c_{p,nf}$ can be expressed as a function of temperature, nanoparticle volume fraction, nanoparticle isobaric specific heat capacity and the base fluid isobaric specific heat capacity. A, B and C are constants determined from experiments. The AAD of the experimental data were 0.5%–1.9% for the SiO_2, Al_2O_3 and CuO nanofluids with the same 2 vol% nanoparticle concentration, agreeing very well with Eq. (71). Then Cabaleiro et al. [480] reported a new correlation equation:

$$\frac{c_{p,bf}(T) - c_{p,nf}(T)}{c_{p,bf}(T)} = \frac{\Phi_p + A\frac{c_{p,p}(T)}{c_{p,bf}(T)}}{B+\Phi_p} \tag{72}$$

which is consistent with the experimental c_p results for five metal oxide nanofluids at high concentrations (AAD = 0.37–0.46%).

3.2.2. Experimental measurement techniques

The most classical experimental approach for studying the c_p of nanofluids is the DSC method. This technique involves the measurements of the amount of heat that is required to deliver to the sample and reference (with the well-defined heat capacity) to increase its' temperature. On the basis of those the heat capacity is calculated. Zhou and Ni [481] used this method to measure c_p of Al_2O_3/water nanofluids by analyzing the relation between the heat flow rate and the temperature

rise of the sample. It was reported that c_p is about 2.75 J/g K at a nanoparticle concentration of 15%, which is 1 J/g K lower than the nanofluid with a concentration of 10%. This result is consistent with the model proposed by Buongiorno [482]. Shin and Banerjee [483] measured c_p of SiO_2/melted carbonate crystal nanofluids at high temperatures (>400 °C) using DSC. They observed a 25% increase in $c_{p,bf}$ after the addition of SiO_2 nanoparticles which have high specific surface energy. They also measured the c_p of Al_2O_3/alkali salt nanofluids in the same way [484]. After adding Al_2O_3 nanoparticles, $c_{p,bf}$ is increased by 32%, which is believed to be associated with the formation of nanochain structures. Kumaresan et al. [485] used about 20 mg of CNT/water-EG nanofluids sample to measure c_p in the temperature range from −50 °C to 50 °C using the DSC method. When the concentration is 0.15% at RT, the measured c_p was 3.9 J/g K indicating the existing model still needed further improvement. Ho et al. [486] studied the change of c_p for Al_2O_3/molten Hitec salt nanofluids at different concentrations. The maximum enhancement of c_p (∼19.9%) occurs at a concentration of 0.063 wt%. Experimental studies by Raud et al. [487] on water-based metal oxides nanofluids further demonstrated the reliability of the DSC approach for c_p measurements. It was reported that c_p decreases as nanoparticle concentration increases.

Modulated temperature differential scanning calorimetry (MTDSC) is the advanced version of the traditional DSC method. It can provide higher sensitivity and resolution, which ensures the direct measurement of c_p by using modulated (usually sinusoidal) heating signals [488]. Robertis et al. [489] performed c_p measurements of Cu/EG nanofluids using this method, and reported a c_p value of 2.3 J/g K at RT. Cabaleiro et al. [480] measured c_p of MgO/EG, ZnO/EG and ZrO_2/EG nanofluids at various concentrations up to 15%. They found that under the same conditions, the c_p enhancement effect of ZnO and ZrO_2 on the base fluid is similar (∼30%). MTDSC was also used to examine the c_p of the nanofluids containing few nanometer sized nanodiamonds by Żyła et al. [490]. They measured EG based nanofluids with the mass concentration up to 10%, and two different purity nanodiamonds (87% and 97%) were adopted. They concluded that Xuan et al. model (Eq. (69)) could be applied to predict c_p of those nanofluids.

In addition to the above two methods, Murshed [491] used a transient double hot-wire technique to measure c_p of metal oxide particles (TiO_2, Al_2O_3) in deionized water, glycol and other base fluids. This new method is based on relatively simple equipment but has high precision with a measurement error within 2.77%. The results indicate that the effective c_p decreases significantly with increasing nanoparticle concentration. Based on the transient plane heat source method, Satti et al. [492] developed a novel thermal property analyzer to measure c_p for five kinds of metal oxide particles (Al_2O_3, ZnO, CuO, TiO_2, SiO_2)/propylene glycol nanofluids. All the experimental results for the five kinds of nanofluids suggest that the nanoparticle size has no effect on c_p, and the underlying mechanism still needs to explored.

3.2.3. Experiments vs. theory

Many literature reports have compared theoretical predictions with experimental data. Zhou and Ni [481] studied the c_p of Al_2O_3/water nanofluid using DSC and compared it with theoretical formula (Eqs. (68) and (69)). It was found that $c_{p,nf}$ decreased with an increasing volume fraction of the nanoparticles. The experimental data were very consistent with Eq. (69), but deviated significantly from the predictions of Eq. (68), whose results are larger than the experimental data. The results also corroborated the rationality of the prediction of Eq. (69). Barbés et al. [474] experimentally reported c_p of Al_2O_3/water and Al_2O_3/ethanol nanofluids as a function of volume fraction at 303.1 K and 330.4 K. The results indicate that c_p decreases with the increasing nanoparticle volume fraction, which agrees well with theoretical predictions of Eq. (69). Hanley et al. [493] studied c_p of SiO_2/water, Al_2O_3/water and CuO/water nanofluids with a volume fraction between 5 wt% and 50 wt%. They showed that Eq. (68) could accurately predict $c_{p,nf}$, while Eq. (69) failed to do so. They also found that with the increasing volume fraction of nanoparticles, the difference between the prediction results from Eqs. (68) and (69) becomes greater. Eq. (70) revealed that c_p was a function of the temperature, nanoparticle size and volume fraction. The theoretical values were in good agreement with the experimental data from different literature reports [389,494] and the AAD was 10∼−8%, which validated the reliability of Eq. (70).

Vajjha et al. [479] measured c_p of Al_2O_3, SiO_2 and ZnO nanofluids with a volume fraction of 2%, and obtained the correlation Eq. (71), where the AAD of the experimental data was 0.5%∼1.9%. Cabaleiro et al. [480] proposed a new model, Eq. (72), to correlate the c_p with the temperature as well as the volume fraction of the nanoparticles. The c_p of MgO/EG, ZnO/EG and ZrO_2/EG nanofluids, ZnO/EG-water and ZrO_2 EG-water mixture nanofluids were measured, with mass fraction up to 15%. The results indicate that the theoretical prediction and experiment data were in good agreement and the ADD was only 0.37∼0.46%.

By collating and comparing the data on $c_{p,nf}$ measurements from different literature, it can be clearly seen from the comparison results that c_p of conventional metal oxide-based [491,493] and non-metal oxide-based [493] nanofluids decreases as the loading of nanoparticles increases. This trend is quite different from the observed with CNTs/water [443,495] or graphene/water [496,497] nanofluids. For all CNT-loaded nanofluids, there is no obvious variation in c_p with an increase of CNT volume fraction, although graphene-loaded nanofluids show a slight downward trend (see Fig. 19). This difference is mainly ascribed to the fact that the c_p of conventional nanoparticles is much smaller (approximately one-tenth) than that of the base fluid, which is that of the base fluid, and CNTs and graphene exhibit higher c_p values than conventional nanoparticles. Hence, the c_p of CNTs and graphene-loaded nanofluids does not exhibit a significant decrease with the increasing nanoparticle loading.

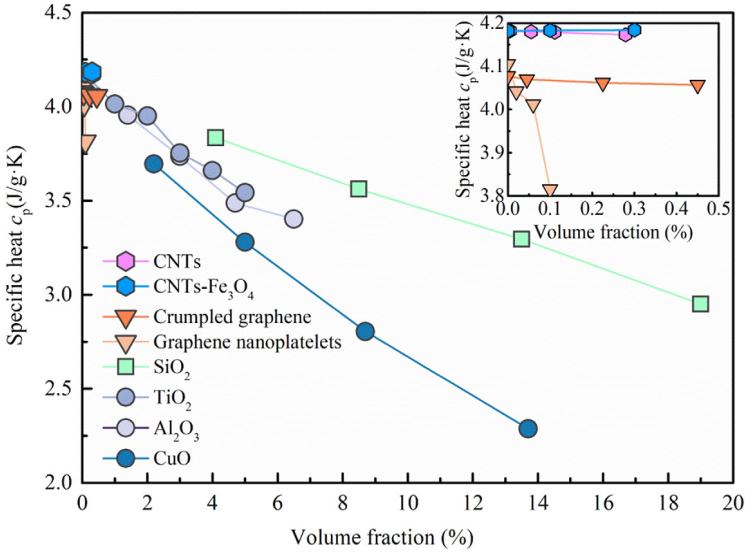

Fig. 19. A schematic diagram for the dependence of specific heat capacity on the volume fraction of nanoparticles in various studies, wherein the nanoparticles are dispersed in water.
Source: See Refs. [443,491,493,495–497].

3.3. Density

Throughout the research field of thermophysical properties of nanofluids, k_{nf} and μ_{nf} are the most studied thermophysical properties in the literature. Due to the wide application prospects of nanofluids, researchers are also interested in other thermophysical properties such as density of nanofluids (ρ_{nf}) and c_p. Although the study of ρ_{nf} is limited, we still summarize the existing research work, including theoretical modeling, experimental measurement techniques and some important results.

3.3.1. Theory

Density is one of the most basic physical properties of nanofluids, but theoretical research is limited. The most commonly used density model in current research is based on the physical rules that two substances follow when are mixed [263,498]:

$$\rho_{nf} = \left(\frac{m}{V}\right)_{nf} = \frac{m_{bf} + m_p}{V_{bf} + V_p} = \frac{\rho_{bf} V_{bf} + \rho_p V_p}{V_{bf} + V_p} = \left(1 - \Phi_p\right)\rho_{bf} + \Phi_p \rho_p \tag{73}$$

where $\Phi_p = \frac{V_p}{V_{bf}+V_p}$ denotes the volume fraction of nanoparticles. This linear theoretical method for density and volume fraction has been proven to be in good agreement with experimental results at RT [472,499]. Furthermore, in order to reflect the relationship between density and temperature, Khanafer and Vafai [263] proposed an empirical model based on experimental results by Ho et al. [499]. The model is shown as:

$$\rho_{nf} = 1001.064 + 2738.6191\Phi_p - 0.2095T \tag{74}$$

when Φ_p ranges from 0 to 4% and T is in the range of 5 °C to 40 °C, and the maximum relative error of the model is 0.22%.

The above model has been widely used in the calculation of ρ_{nf} [500–502], but Sharifpur et al. [503] found that experimental results were appreciably lower than those predicted by the model. They attributed this phenomenon to the fact that Eq. (73) ignores the effect of the gap between the nanoparticles and the base fluid, which is caused by the nanolayer on the particle surface. Therefore, on the basis of the above models, the authors took the nanolayer into consideration and developed the following model based on the experimental data:

$$\rho_{nf,\,new} = \frac{m_p + m_{bf}}{V_{bf} + V_p\left(r_p + d_{nl}\right)^3 / r_p^3} = \frac{\rho_{nf}}{\left(1 - \Phi_p\right) + \Phi_p\left(r_p + d_{nl}\right)^3 / r_p^3} \tag{75}$$

where r_p denotes the average particle diameter and d_{nl} denotes the nanolayer thickness, and the nanolayer is assumed to be a pure void. Moreover, according to the experimental data for the nanofluids obtained by dispersing oxide particles

(SiO_2, MgO, CuO) in base fluids (water, glycerol, EG), the authors gave an approximate function relation between the thickness and the average nanoparticle diameter as follows [503]:

$$d_{nl} = -0.0002833 \times {r_p}^2 + 0.0475 \times r_p - 0.1417 \tag{76}$$

It can be seen from Eq. (76) that the effect of the thickness of the nanolayer (equal to the gap) is closely related to the nanoparticle size. In their study, the model is in better agreement with the experimental results compared with the model given by Eq. (73). A density model with a more comprehensive adaptive range and more accurate predictions still needs further research.

3.3.2. Experimental measurement techniques

The density can directly affect the Re, friction coefficient, pressure loss and Nu during nanofluid flow and heat transfer processes. For measurement of ρ_{nf}, we will pay attention to some articles reporting measurements of the ρ_{nf}. Generally, the measurements of ρ_{nf} can be roughly divided into two methods. One is direct measurement by a density meter, and the other is calculation by the mass and a known volume of the nanofluid. Vajjha et al. [504] measured the ρ of three different nanofluids. An Anton-Paar digital density meter was chosen as the tool, and a circulating fluid temperature bath was used to ensure that the nanofluids retained a set temperature. Typically, a density meter consists of a U-shaped oscillating tube and a system comprising an electronic excitation device, a display device and a frequency counting device. Usually the U-shaped tubes are produced with the glass which has numerous advantages: (i) it is transparent and allows to check if inside the sample is air bubble, which may distort the results, (ii) it is chemically inert and easy to clean, (iii) it exhibits beneficial temperature deformation coefficient and sensitivity due its low specific weight. The experimental ρ values for Al_2O_3/EG-water and Sb_2O_5–SnO_2/EG-water nanofluids show good agreement with the Pak and Cho equations (Eq. (73)). For ZnO/EG-water nanofluids, the maximum deviation between the experimental results and the predicted values of Eq. (73) is approximately 8%. In addition, Pastoriza-Gallego et al. [505] and Mariano et al. [506] also used this type of density meter to measure ρ of different nanofluids, and the measured ρ values agreed within the range allowed by the experimental error.

Pandey et al. [507] measured the thermophysical properties of nanofluids, where the ρ is calculated from the mass and volume of the nanofluid. Kumaresan et al. [485] weighed 25 ml and 50 ml of MWCNT/DI water/EG nanofluids using a high-precision electronic balance, and repeated measurements three times, taking the average to calculate the ρ_{nf}. Pantzali et al. [508] also calculated ρ by weighing a known volume of nanofluid, with an estimated accuracy of about 5%.

3.3.3. Experiment vs. theory

Żyła et al. [16] experimentally measured the ρ of EG-based nanofluids containing various types of nitride nanoparticles, such as AlN, Si_3N_4 and TiN. A DMA 500 densimeter based on the U-type oscillation technique was used for ρ measurement. It was clearly shown that the ρ gradually decreases with an increase in the sample temperature, but increases with an increase in the nanoparticle fraction in the nanofluid. The measurement results at RT were then compared with theoretical predictions based on Eq. (73). The results clearly indicate that there is good agreement between the experimental measurement and the theoretical model prediction. For the EG-based nanofluids containing various nitride nanoparticles, the maximum AAD of ρ measurements at RT was less than 0.89%. In another study, Shoghl et al. [18] also proved the relation between ρ and the above-mentioned concentration and temperature. They experimentally obtained the ρ_{nf} at different concentrations and temperatures via a DMA-35N portable density meter. Compared with the mixed model predictions, the experimental results corroborated that Eq. (73) can accurately predict the ρ_{nf}. Ho et al. [499] also explored the dependence of ρ of Al_2O_3/water nanofluid on the volume fraction and temperature. It was found that the decline trend of ρ_{nf} is no longer significant with increasing temperature, which is attributed to the fact that the ρ of Al_2O_3 nanoparticles is not sensitive to changes in temperature, although the temperature is elevated. What is interesting is that the experimental data agrees very well with the data predicted by the mixing theory (Eq. (73)). In addition, Michaelides [498] calculated the corrections on the k data, because of the different expansion coefficients of liquids and nanoparticles and the variations of the ρ dues to temperature fluctuations. In summary, the above discussion and analysis indicate that we cannot ignore the effects of temperature and various parameters on ρ, and most of the experimental results have proved that the ρ_{nf} can be estimated very accurately using the classical mixed theory.

3.4. Viscosity

The estimation of dynamic viscosity (μ) of nanofluids is significant before its application in thermal systems due to its direct effect on pressure drop, pumping power and friction coefficient [26,27]. Therefore, large number of studies have been devoted to the experimental study of μ_{nf} and its dependence on various parameters, such as size, shape, concentration of nanoparticle, aggregation of nanoparticle, and temperature [508–535]. Besides experimental works, simulation approaches such as MD have also become popular for analyzing the effects of various parameters on μ_{nf} at atomic and molecular levels. This section provides a summary of latest developments on μ of mono and hybrid nanofluids, including the evolution of classical models and advanced models, experimental techniques and MD simulations.

3.4.1. Classical models

The equation proposed by Einstein [509] is known as the most classical equation presented for mixtures. Most of the other derivations are established on the evolution of Eq. (77).

3.4.1.1. Evolution of classical models. It is generally believed that the theoretical model related to μ_{nf} was first proposed by Einstein [509]. The model is suitable for nanofluids having spherical nanoparticles and a volume fraction lower than 2%, it is written as:

$$\mu_{nf} = \left(1 + 2.5\Phi_p\right)\mu_{bf} \tag{77}$$

The above model does not take into account the interaction between nanoparticles, and thus is only suitable for fluids with extremely low concentrations. Based on Eq. (77), Brinkman [510] presented a model for high-concentration nanofluids as:

$$\mu_{nf} = \frac{\mu_{bf}}{\left(1 - \Phi_p\right)^{2.5}} \tag{78}$$

Eqs. (77) and (78) are both valid for spherical nanoparticles and do not take nanoparticle motion into account. Batchelor [511] proposed a new model which reflects the Brownian motion of the nanoparticles:

$$\mu_{nf} = \left(1 + A\Phi_p + K_H{\Phi_p}^2\right)\mu_{bf} = \mu_{bf}\left(1 + 2.5\Phi_p + 6.2{\Phi_p}^2\right) \tag{79}$$

where K_H is the Huggins coefficient which describes the direct effect of Brownian motion on viscosity due to nanoparticle thermal motion and A is the coefficient from the Einstein dynamic viscosity model [509].

Saito considered the Brownian motion of spherical rigid particles, and developed a model to make it more adaptable to very small nanoparticles which their Brownian motion is more pronounced [512]. The model is:

$$\mu_{nf} = \left(1 + \frac{1.25\Phi_p}{1 - \Phi_p/0.87}\right)\mu_{bf} \tag{80}$$

Graham [513] introduced cell theory to study the relation between the μ and the concentration when the spherical nanoparticle concentration approached the maximum limit, it is expressed as:

$$\mu_{nf} = \left(1 + 2.5\Phi_p\right)\mu_{bf} + \left[\frac{4.5}{\left(2w/r_p\right)\cdot\left(1 + 2w/r_p\right)\cdot\left(1 + 2w/r_p\right)^2}\right]\mu_{bf} \tag{81}$$

where w denotes the minimum separate distance between the nanoparticles. The cell theory considers a nanoparticle in the host liquid that is surrounded by other nanoparticles. In the case of infinite dilution, this model is consistent with Eq. (77). Similarly, a model derived by Frankel and Acrivos [514] for nanofluids with evenly distributed nanoparticles at a concentration close to the maximum is expressed as:

$$\mu_{nf} = \frac{9}{8}\left[\frac{\left(\Phi_p/\Phi_{p,max}\right)^{1/3}}{1 - \left(\Phi_p/\Phi_{p,max}\right)^{1/3}}\right]\mu_{bf} \tag{82}$$

3.4.2. Advanced (recent) models

Einstein's classical model is not enough accurate to predict μ of most nanofluids, so some advanced and more realistic models have been proposed. Masoumi et al. [515] reported a new model for predicting μ_{nf}, which take into account the Brownian motion of nanoparticles, and demonstrates the effect of fluid temperature as well as size and density of the nanoparticles in the viscosity model. The developed model is:

$$\mu_{eff} = \mu_{bf} + \frac{\rho_p v_{BF} r_p^2}{72aw} \tag{83}$$

$$a = \mu_{bf}^{-1}\left[\left(c_1 r_p + c_2\right)\Phi_p + \left(c_3 r_p + c_4\right)\right] \tag{84}$$

where the μ_{bf} is the dynamic viscosity of the base fluid, the second term of Eq. (83) is the apparent dynamic viscosity, both the Brownian motion velocity v_{BF} and the correction factor a are functions of temperature, c_1, c_2, c_3 and c_4 are empirical constants determined by experiments, ρ_p, r_p and Φ_p represent the density, diameter and volume fraction of the nanoparticles, respectively. And w is the distance between the nanoparticles. It was observed that the theoretical predictions are in good agreement with the experimental results for CuO/water, CuO/EG, TiO_2/EG, CuO/EG-water and Al_2O_3/water nanofluids, and rendered a higher precision compared to other models [507,509,511].

Later, Hosseini et al. [516] proposed a dimensionless expression to predict the μ_{nf}:

$$\frac{\mu_{nf}}{\mu_{bf}} = \exp\left[a + c_1\left(\frac{T}{T_0}\right) + c_2\left(\Phi_p\right) + c_3\left(\frac{r_p}{1 + d_{nl}}\right)\right] \tag{85}$$

where a is the factor determined by the properties of the nanofluid, c_1, c_2 and c_3 are constants from the experimental data, T_0 and T are the reference and real temperatures of the nanofluid, respectively, d_{nl} is the thickness of the capping

Table 3
Summary of theoretical models for the prediction of the dynamic viscosity of nanofluids (μ_{nf}).

Model	Year	Equation	Features	Ref.
Einstein	1906	$\mu_{nf} = (1 + 2.5\Phi_p)\,\mu_{bf}$	Spherical nanoparticles, extremely low concentration	[509]
Saito	1950	$\mu_{nf} = \left(1 + \frac{1.25\Phi p}{1 - \Phi_p/0.87}\right)\mu_{bf}$	Spherical rigid nanoparticles, Brownian motion, small nanoparticles	[512]
Brinkman	1952	$\mu_{nf} = \frac{\mu_{bf}}{(1-\Phi p)^{2.5}}$	Spherical nanoparticles, high-concentration Continuous medium	[510]
Frankel and Acrivos	1967	$\mu_{nf} = \frac{9}{8}\left[\frac{(\Phi_p/\Phi_{max})^{1/3}}{1-(\Phi_p/\Phi_{max})^{1/3}}\right]\mu_{bf}$	Evenly distributed nanoparticles, maximum concentration limit	[514]
Batchelor	1977	$\mu_{nf} = \mu_{bf}(1 + 2.5\Phi p + 6.2\Phi p^2)$	Brownian motion	[511]
Graham	1981	$\mu_{nf} = (1 + 2.5\Phi_p)\,\mu_{bf} + \left[\frac{4.5}{(2w/d_p)\cdot(2+2w/d_p)\cdot(1+2w/d_p)^2}\right]\mu_{bf}$	Maximum concentration limit	[513]
Masoumi *et al.*	2009	$\mu_{nf} = \mu_{bf} + \frac{\rho_p}{72a}\left(\sqrt{\frac{18k_BT}{\pi\rho_P r_p}}\right)\left(\sqrt[3]{\frac{6\Phi_p}{\pi}}\right)$	Temperature, size and density of the nanoparticles Brownian motion	[515]
Chevalier	2009	$\frac{\mu_{nf}}{\mu_{bf}} = \left[1 - \frac{\varsigma}{\varsigma_m}\left(\frac{r_a}{r}\right)^{3-D_f}\right]^{-2}$	Agglomerate size	[517]
Hosseini	2010	$\frac{\mu_{nf}}{\mu_{bf}} = \exp\left[a + c_1\left(\frac{T}{T_0}\right) + c_2(\Phi_p) + c_3\left(\frac{r_p}{1+d_{nl}}\right)\right]$	Capping layer (nanolayer)	[516]
Chandrasekar	2010	$\mu_{eff} = 1 + m\left(\frac{\Phi_p}{1-\Phi_p}\right)^n$	Specific area, density and sphericity of the nanoparticles	[348]

layer (nanolayer). This model is consistent with the experimental results for Al_2O_3/water nanofluids, indicating that the dynamic viscosity of nanofluids varies nonlinearly with the volume fraction of nanoparticles.

Chevalier et al. [517] studied the μ of an aggregated suspension at high shear rates by fractal theory. The equation can be expressed as:

$$\frac{\mu_{nf}}{\mu_{bf}} = \left[1 - \frac{\varsigma}{\varsigma_m}\left(\frac{r_a}{r}\right)^{3-D_f}\right]^{-2} \tag{86}$$

where r_a is an average diameter of aggregates, ς is the crowding factor, and D_f is the fractal dimension which depends on the type of aggregation, the shape of the nanoparticles and the shear flow. For aggregated nanoparticles, D_f is usually set to be 1.8. This model agrees well with experimental results of the μ_{nf} with different volume fractions and nanoparticle sizes.

Chandrasekar et al. [348] developed a theoretical model for predicting μ of Al_2O_3/water nanofluids:

$$\mu_{eff} = 1 + m\left(\frac{\Phi_p}{1-\Phi_p}\right)^n \tag{87}$$

where the constants m and n are calculated by least squares regression, m is affected by the composition and properties of the fluid phase, and the specific area, density and sphericity of the nanoparticles. It was suggested that the theoretical results are in good agreement with the experimental measurements of Al_2O_3/water nanofluids by Nguyen et al. [518]. The μ is linear with the nanofluid concentration at low concentrations, but when particle loading exceeds 2% in volume fraction a non-linear behavior is observed, which is attributed to the interaction between the nanoparticles at high concentrations.

The aforementioned models are mostly suitable to predict the viscosity of nanofluids containing metal oxide nanoparticles at different temperatures and concentrations. There has been a lot of research work to achieve measurements of μ_{nf} through experimental approaches. In the next section, the typical measurement techniques for dynamic viscosity of nanofluids will be introduced in detail. Theoretical models for predicting the μ_{nf} are summarized in Table 3.

3.4.3. Experimental measurement techniques

Fig. 20 shows the most common approaches for measuring the viscosity of nanofluids. In this part we have a brief introduction to the measurement principles and advantages of these approaches.

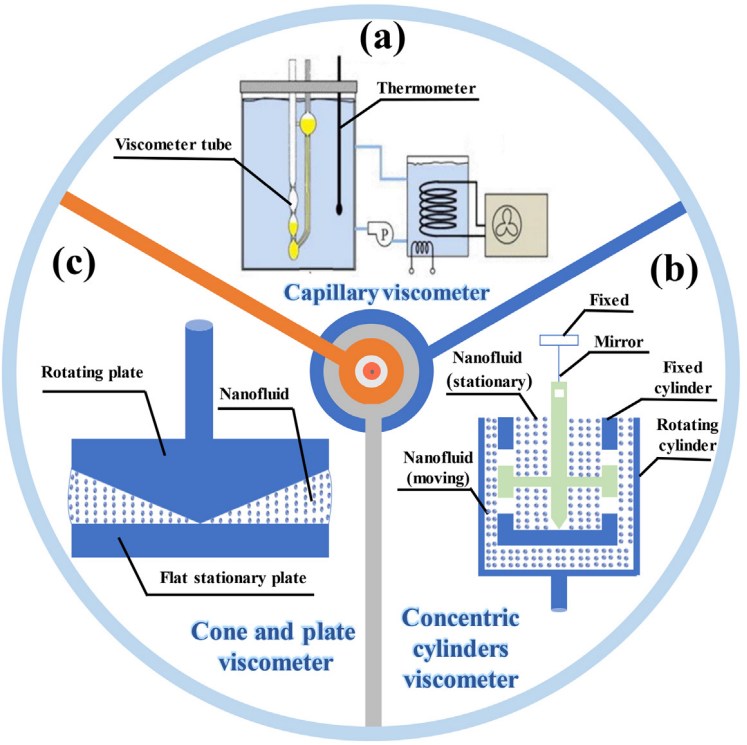

Fig. 20. Schematic diagram of the most common measurement techniques for the viscosity of nanofluids. (a) capillary viscometer [519] (Reprinted with permission from Elsevier), (b) concentric cylinder viscometer [520] and (c) cone and plate viscometer [520].

3.4.3.1. Capillary viscometer. Capillary viscometers (see Fig. 20a) have been widely used to measure μ_{nf} [519–526]. In brief, when the nanofluid flows through a capillary with a circular cross section, the axial pressure drop in the capillary and the volume rate of flow through the capillary driven by the pressure are measured, and the μ of the Newtonian nanofluid is determined by Hagen–Poiseuille's law. The ability to achieve relatively high shear rates is the most important advantage of this technique. In addition, it has the advantages of a simple structure and a low price.

Using this technique, Yiamsawas et al. [519] measured μ of TiO_2 and Al_2O_3 nanoparticles suspended in a mixture of EG and water. First, the viscometer tube was immersed in a transparent constant temperature water bath, and then a high-precision stopwatch was used to record the time at which the nanofluid flowed through the special position of the viscometer, and the temperature was measured by a thermometer with an accuracy of 0.1 °C. To ensure the accuracy of the measurements, each case with volume fractions of 1%, 2%, 3%, and 4% was repeated three times. It was concluded that nanofluids are Newtonian and classic models fail to predict the experimental data with high precision. Chevalier et al. [521] proposed the measurement of μ_{nf} by a capillary micro viscometers technique, which could also be used to evaluate the local pressure drop in a microchannel. Meanwhile, Jarahnejad et al. [522] measured μ of Al_2O_3/water and TiO_2/water nanofluids in the temperature range of 20–50 °C and concentrations between 3 and 14.3% in mass using a capillary viscometer. A thermostat bath setup was used to provide constant temperature during the measurement, and all experiments were carried out under atmospheric pressure. They analyzed the uncertainty of the setup by averaging the multiple measurement results of the samples, which exhibited good reliability with a maximum standard deviation lower than 1%. Moreover, the capillary viscometer approach has also been adopted in some researchers' work to explore μ_{nf} [408,409,523–526], and all the experimental results mentioned above demonstrate that the viscometer shows good reliability and accuracy.

3.4.3.2. Concentric cylinders. For rotational viscometers (concentric cylinder viscometers and cone and plate viscometers), the most popular form is the Couette concentric cylinder viscometer (see Fig. 20b) [520]. During measurements, the nanofluid is placed in a space between two coaxial cylinders, and the outer cylinder keeps rotating to drive the nanofluid to rotate around the axis, while the inner cylinder is stationary. The μ_{nf} can be obtained by using the radius of the inner and outer cylinders, the rotational speed ω and the torque per unit length of outer cylinder on the inner cylinder [527]. It is worthy to note that this technique is generally applicable to Newtonian nanofluids. For non-Newtonian nanofluids, there will be some deviation in the measurement results unless the space between the two cylinders is small enough [520].

To measure the dynamic viscosity of Ag/water-EG and graphene/water-EG nanofluids for volume concentrations of 0.01, 0.05, and 0.1%, Contreras et al. [527] used a rotational viscometer with concentric cylinders. They also compared

the experimental results with μ values predicted by the correlations of Einstein and Brinkman (Eqs. (77) and (78)). It was observed that for volume concentrations greater than 0.01, Einstein and Brinkman models the maximum deviation reaches 8% and 12%, respectively. Minakov et al. [528] also measured μ of CuO/DI water nanofluids using a rotational viscometer based on concentric cylinders, and demonstrated that the uncertainty of the measurement is approximately 1%. It was revealed that the viscosity of the nanofluids is strongly dependent on the shear rate. For Newtonian nanofluids, when a small nanoparticle concentration is suspended (0.25 vol%), the μ coefficient is no longer dependent on the shear rate.

3.4.3.3. Cone and plate approach. In general, a cone and plate viscometer is composed of a flat stationary plate and a rotating plate (see Fig. 20c), and the nanofluid is placed in the gap between the two plates [520]. The angle of the gap is usually very small ($< 4°$), so that the edge effect can be ignored. The rotating plate keeps rotating at an angular velocity of ω_0, and the torque can be calculated. The μ_{nf} can be calculated from the ω_0, the gap angle, the torque and the radius of the cone [348]. Unlike the other two viscometers mentioned above, the difference between Newton and non-Newtonian fluid measurement is not significant for the cone and plate viscometer, owing to the very small gap between the two plates. Hence, the cone and plate viscometer is also widely used for non-Newtonian fluids [520]. To understand why the cone-plate geometry could be used for the measurement of μ of non-Newtonian fluids, the definition of shear rate should be kept in mind. It is defined as the relationship between the decreasing flow velocity with thickness of the sample in laminar flow. In the cone-plate geometry, thickness of the sample is not constant, it changes from the middle (the smallest position) to the edge of the sample, and the linear velocity of the flow also changes [529]. The rotor that spins at a constant angular velocity causes the linear velocity of the flow depends on the distance from the axis of rotation (the smallest one in the middle). Therefore, a constant shear rate can be created in the whole volume of the sample by selecting the rotor angle and the measurement gap (ignoring the measurement error). This approach is useful for nanofluids that exhibit complex non-Newtonian rheological behavior and viscoelastic structures [529–531].

Chandrasekar et al. [348] studied μ for Al_2O_3/water nanofluids from both experimental and theoretical perspectives. In terms of experiments, the measurement of dynamic viscosity was achieved by a Brookfield cone and plate viscometer. The nanofluid sample was placed in a 0.013 mm gap between the cone and the plate. The measurement accuracy was found to be around 5% by measuring the base fluid at RT. In addition, the dynamic viscosity of the Ag–MgO/water hybrid nanofluid was also measured by a Brookfield cone and plate viscometer [532], and an electronic device was used to adjust the gap between the two plates to be 0.013 mm. The measurement of the viscous drag of the nanofluid to the spindle was achieved by calibrating the deflection of the spring. The authors concluded that theoretical models cannot predict the experimental data with high accuracy because the morphology of nanoparticles is not captured fully by these models. Asadi et al. [533] dispersed MWCNTs and ZnO in engine oil to form a stable suspension, and measured the dynamic viscosity of the MWCNTs–ZnO/engine oil hybrid nanofluids at different temperatures and concentrations using a cone and plate viscometer. The temperature of the nanofluids was set through the device in a short time to ensure that it remained stable during the measurement. Żyła et al. used a cone-plate geometry to study the non-Newtonian behavior of AlN/EG [531], Si_3N_4/EG [534] and EG based nanofluids containing mixture of graphite and nanodiamonds at constant temperature of 298.15 K [535].

3.4.3.4. Other measurement methods. Besides the methods mentioned above, there are two other techniques that are used to examine the viscosity of nanofluids, namely (i) Rheo-NMR and (ii) RheoScope. The first technique is a basically performing the rotational rheological measurements in the magnetic field, which allows use of the nuclear magnetic resonance (NMR) imaging to observe sample inside the system in real-time. This advanced equipment also allows for the detection of slippery effect between the sample and the measuring geometry (by comparing the linear velocity of the rotor surface and the laminar flow inside the nanofluid), which is impossible to achieve for other systems [536]. The advantage of the Rheo-NMR method is the possibility to determine the chemical structure changes during shearing of the sample. The second technique can be described as a rotational rheometer coupled with the optical microscope. This one allows observing the bottom (stationary) plate of the measurement geometry while performing a standard dynamic viscosity examination. Unfortunately, the magnification of the observations is limited. However, some large nanoparticle aggregates can still be observed when using an optical microscope (if they occur in the sample) [536].

Both techniques were used by Żyła et al. [536] to study the unexpected shape of μ curves of the $MgAl_2O_4$/DG nanofluids observed in their previous study to determine the rheological profile of those materials [537]. The Rheo-NMR method could be used to eliminate chemical changes occurring in the sample and slippage effects between the sample and the rotor. A series of experiments performed with RheoScope showed that the agglomeration and sedimentation of the particles are responsible for this strange behavior.

3.4.4. Experimental studies

The purpose of this section is to provide a comprehensive review of experimental progress and developments on the factors influencing the dynamic viscosity of nanofluids. The effects of several key factors such as temperature, concentration, size and shape of the NPs, pH and ultrasonication time are explicitly reviewed here. Fig. 21 clearly illustrates the intrinsic mechanism of various factors on μ_{nf}.

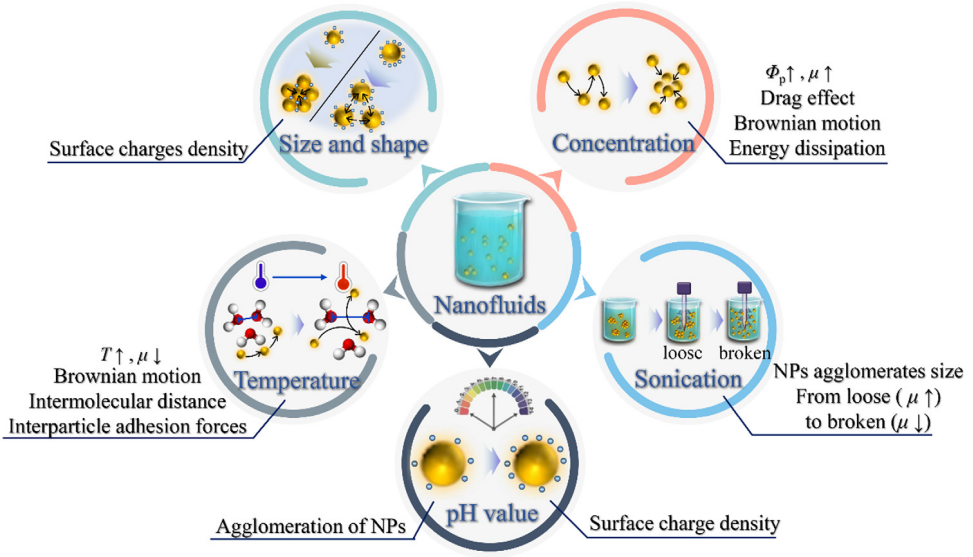

Fig. 21. Schematic diagram for the intrinsic mechanisms of various factors on the viscosity of nanofluids.

3.4.4.1. Effect of temperature. The effect of temperature on μ_{nf} is not negligible. Hence, many researchers have studied the effect of temperature on μ_{nf} [412,505,538–546]. The literature review indicates that an increase in temperature leads to the reduction of viscosity of nanofluids, and the amount of this reduction depends on the type of base fluid and nanoparticles. Esfe et al. [539] investigated the viscosity of nanofluids with Al_2O_3 nanoparticles dispersed in engine oil at different temperatures (5 °C–65 °C). They found that as the temperature of the nanofluid rises, μ_{nf} declines, which further indicates that the elevated temperature can effectively reduce the μ_{nf}. Meanwhile, Toghraie et al. [540] also confirmed the above conclusions by analyzing the evolution of μ of Fe_3O_4/water nanofluids with temperature. When the temperature is raised from 20 °C to 55 °C the viscosity continuously decreases, and this trend always occurs for nanofluids with different volume concentrations. Pastoriza-Gallego et al. [505] analyzed the effect of temperature on μ of CuO/water nanofluids in the temperature range of 10 °C–50 °C and concentration range of 1 to 10% in mass. The results revealed that the μ of the nanofluid with a mass fraction of 7% at 50 °C is virtually equal to water at 25 °C. Yang et al. [541] conducted a study on μ of viscoelastic-fluid-based nanofluids, in which Cu nanoparticles were homogeneously dispersed in a solution of cetyltrimethylammonium chloride (CTAC) and sodium salicylate (NaSal). It was also found that μ of viscoelastic nanofluids decreases with increasing temperature regardless of any shear rate.

The decrease of μ with temperature happens because when the nanofluid receives thermal energy (its temperature increases), the distance between molecules becomes more; therefore, interparticle adhesion forces and consequently the viscosity are reduced.

Moreover, some researchers studied the evolution of relative dynamic viscosity (ratio of nanofluid to base fluid dynamic viscosity, μ_{nf}/μ_{bf}) over varied temperature ranges (see for example [539,542,543]) Baratpour et al. [544] found from experimental data that the effect of temperature on the relative dynamic viscosity of SWCNT/EG nanofluids (tested for volume fractions up to 0.1%) is not significant in the range of 30 °C–60 °C for volume concentrations less than 0.025%. In addition to the conclusions obtained above, several researchers also demonstrated that the relative dynamic viscosity is not linearly increasing, and a slight reduction is observed with increasing temperature [410,540]. Murshed et al. [545] studied the viscosity of silicon oil based nanofluids containing two different types of nanoparticles i.e. TiO_2 and SiO_2. They remarked that when temperature increases from 20 to 59 °C, the viscosity lessens non-linearly.

3.4.4.2. Effect of nanoparticle concentration. So far, most studies have demonstrated that an increase in the volume fraction of nanoparticles directly leads to a significant increase in μ_{nf}. However, some exceptions have been also reported. For example, Chen et al. [547] developed a novel method to prepare a CNT/EG nanofluid that does not contain any surfactant, where the CNT was dispersed in the base fluid via mechanochemical reaction. For volume fractions less than 0.4 vol%, the μ of the CNT/EG nanofluid was recorded lower than that of the base fluid, which is ascribed to the lubrication of the nanoparticles. Furthermore, as the loading of nanoparticles increases, the relative dynamic viscosity also exhibits an increasing trend. Interestingly, this trend is even more pronounced when the temperature is above 55 °C. Later, the group further studied the μ changes of MWCNTs dispersed in different base fluids including water, EG, glycerin and silicone oils [548]. They found that both the MWCNT/silicone oil and MWCNT/glycerol nanofluids exhibited Newtonian behavior. For MWCNT/water nanofluids, the MWCNTs serve as a lubricant and cause the μ_{nf} to be lower than that of the base fluid at low volume fractions of MWCNTs. Żyła and Fal [549] examined the μ of SiO_2/EG nanofluids at a constant temperature

of 298.15 K, they found that μ_{nf} increases linearly with the volume fraction of particles and the value of enhancement is much higher than that predicted by the Einstein model.

In another study on the effect of nanoparticle volume concentration on μ, Al_2O_3/polyalkylene glycol nanofluids were prepared by Sharif et al. [550]. The μ of the Al_2O_3/polyalkylene glycol nanofluid in the range of 0.05–1 vol.% was analyzed, and the relative dynamic viscosity was found to vary linearly with concentration at 313.15 K. Furthermore, the dependence of μ on the concentration of SiC/DI water nanofluids was investigated by Lee et al. [389]. They found that the μ of SiC/DI water nanofluids rises with dispersing more nanoparticles in the host liquid. Corcione et al. [304] analyzed multi-group experimental data on the influence of various parameters on μ_{nf} in a wide range of literature. They focused on the effect of nanoparticle concentration on μ and found that μ increases linearly with the increasing concentration. In a recent study, Suganthi et al. [551] studied the rheological properties of ZnO/propylene glycol nanofluids. As a result, it was found that the hydrogen bond in the propylene glycol (that its formula is $C_3H_8O_2$) is weakened at a high temperature, which has a considerable contribution to the decrease of μ_{nf}. By loading ZnO nanoparticles, hydrogen bonds are further weakened. When this decrease trend completely exceeds the increase in μ due to the addition of nanoparticles, a decrease in the μ_{nf} will eventually occur.

3.4.4.3. Effect of nanoparticle size and shape. Nanoparticle's size and shape are also important factors that cannot be ignored in studying μ_{nf}, but the conclusions from different studies are not consistent [357,446,515,521,522,552–556]. He et al. [357] studied μ of TiO_2 nanofluids with nanoparticle sizes of 95, 145 and 210 nm, and found that the viscosity increases with an increase in nanoparticle size. Furthermore, the results of Nguyen et al. [553] for Al_2O_3/water nanofluids (where two different sizes of particles including 36 and 47 nm were used) indicated that the influence of nanoparticle size on viscosity is significant at higher concentrations while at low concentrations the effect is not significant. The authors attributed this difference to the molecular structure of nanofluids. Research on Al_2O_3/water nanofluids by Jarahnejad et al. [522] also revealed that a nanofluid with a nanoparticle size of 250 nm has a higher μ than the 200 nm counterpart, which is consistent with the above results, but viscosity of the nanofluid with a nanoparticle size of 250 nm is also higher than that with a 300 nm nanoparticle size. The inhomogeneity of the nanofluid can explain this contradictory result.

In addition, there are also some reports on μ_{nf} that decreases as nanoparticle size enlarges. The study of Al_2O_3/water by Anoope et al. [554] proved that using Al_2O_3 nanoparticles with a size of 45 nm leads to a greater viscosity compared a size of 150 nm, which is consistent with Einstein's theoretical prediction [509]. Kwek et al. [555] studied μ of Al_2O_3/water nanofluids where two sizes of nanoparticles including 10 and 150 nm were used. It was found that as the nanoparticle size increases, the relative μ_{nf} decreases from 1.9 to 1.5. This could be attributed to higher potential of nanoparticles with smaller size to aggregate due to lack of strong surface charges between them. This is in good agreement with the results of Masoumi et al. [515] and Lu et al. [446]. Apart from Al_2O_3 nanofluids, similar conclusions have been made regarding the study of SiO_2 nanofluids. The research of Chevalier [521] for three nanoparticle-size (35, 94 and 190 nm) in SiO_2/ethanol nanofluids also followed the trend of μ decreasing with increasing nanoparticle size. Namburu et al. [556] measured the μ of three nanoparticle-size (20, 50 and 100 nm) in SiO_2/water nanofluids. The nanofluid with 20 nm nanoparticles has the largest μ_{nf}, followed by the 50 nm-sized nanofluid. However, the difference in μ_{nf} caused by nanoparticle size gradually decreases as the temperature increases, indicating that the effect of nanoparticle size on μ_{nf} is not strong compared to other factors.

There are not many studies regarding the influence of nanoparticle shape on μ_{nf}. Among the limited studies, Timofeeva et al. [410,557] measured the μ of Al_2O_3/EG and Al_2O_3/water nanofluids and found slender or flat nanoparticles with lower sphericity generally have higher μ_{nf} than ideal spherical fluids at the same volume fraction. This is related to the structural limitations of nanoparticle rotation in Brownian motion. To get a nanofluid with low μ, it was suggested to use nanoparticles with lower aspect ratios.

3.4.4.4. Effect of pH. The values of pH can indirectly affect μ_{nf} by influencing the stability and dispersion of nanofluids. Therefore, in order to comprehensively analyze μ_{nf}, pH value is also one of the parameters that should be paid attention to. An experiment on the μ of SiO_2/water nanofluids with different particle sizes and pH values was carried out by Zhao et al. [558], in which the aggregation of nanoparticles was considered. A greater μ_{nf} was found in the pH range of 5–7 when the nanoparticle diameter is less than 20 nm. Then, the pH value no longer has a significant effect on the μ as the diameter of the nanoparticles increases, and it remains almost constant as the pH value changes. This is attributed to the existence of an electric double layer (EDL) over the nanoparticles and the change in the fractal dimension of the aggregates. Timofeeva et al. [410] investigated μ with various shapes of Al_2O_3 nanoparticles dispersed in EG/water mixture. It was found that adjusting the pH value of the suspension probably affects the surface charge over the nanoparticles. In their study the μ of the Al_2O_3/water nanofluid was successfully reduced by 31% without affecting k_{nf}. Notice that the surface charge of nanoparticles is another key parameter affecting μ_{nf}, and adjusting the pH value of the suspension is an effective parameter of modulating the surface charge of the nanoparticles.

Moreover, Wankam et al. [559] investigated the influences of pH on μ of heat transfer nanofluids. The rheological curves of 0.1 wt% ZrO_2 nanoparticles dispersed in water at different pH values (4, 6, 8, 10) were obtained, indicating that the μ of ZrO_2/water nanofluid is reduced by 20% for pH = 6 or 8 compared to pH = 4 or 10. In another work, Wang et al. [560] attained a strong repulsive force and reduced aggregation of nanoparticles by changing the pH of the suspension to achieve stable nanofluids. Similar increasing trends for viscosity of Al_2O_3/water and Cu/water nanofluids with pH value were obtained. There was an optimized pH value (pH_o) for the lowest viscosity of various nanofluids, e.g., $pH_o = 8$ for Al_2O_3/water nanofluid, $pH_o = 9.5$ for Cu/water nanofluids.

All the studies mentioned above emphasize that an optimized pH can effectively reduce μ_{nf}.

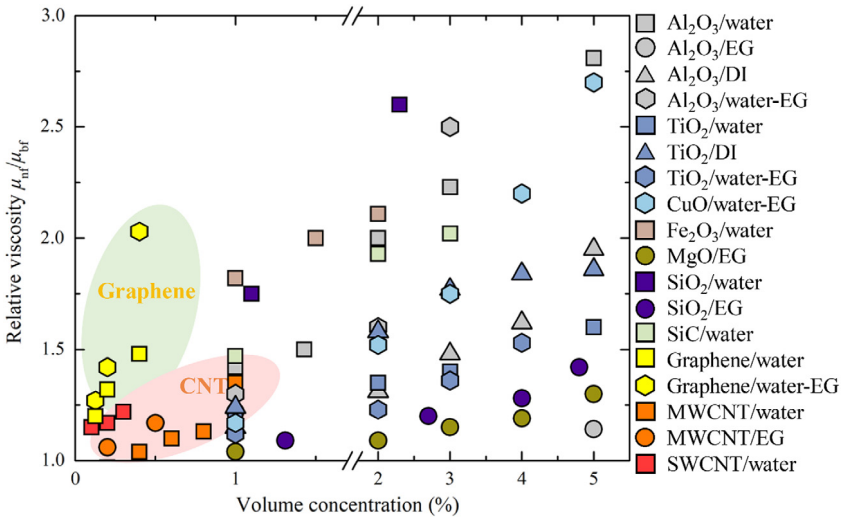

Fig. 22. A schematic diagram for the dependence of viscosity on the volume concentration of nanoparticles in various studies.

3.4.4.5. Sonication time effect. Ultrasonication is a commonly used method to change μ_{nf}, which can terminate agglomeration between particles and promote the uniform dispersion of nanoparticles in the base fluid [561]. Many researchers have studied ultrasonication duration effects on nanofluids, and concluded that generally μ_{nf} exhibits a tendency to decrease with ultrasonication duration. However, there is no uniform standard for optimal ultrasonication duration for nanofluids, which depends on the type of nanofluids.

Ruan et al. [562] studied the effect of ultrasonication time on μ of MWCNT/EG nanofluids at a concentration of 0.5 wt%. The results revealed that μ_{nf} increases with an increase of the ultrasonication time and reaches a maximum after 40 min, then it reduces with further sonication until it approaches the μ of pure EG after 1355 min. Moreover, the same experimental results were obtained at different shear rates. The reason for this phenomenon is that well-dispersed MWCNTs possess an extremely large specific surface area and thus have a higher μ_{nf}, while the reduction in the aspect ratio of the MWCNTs and the destruction of the 3-D network causes a lower μ_{nf}. Garg et al. [422] also reported the variation of μ of the CNT/water nanofluids with ultrasonication time. They observed that μ_{nf} increases to the maximum value and then decreases with ultrasonication time. Mahbubul et al. [563] analyzed the ultrasonication effect of the μ of Al_2O_3/water nanofluids at a concentration of 0.5 wt%. Their experimental results were similar to those of Ruan et al. and Garg et al. The optimal ultrasonication duration for the nanofluids in their study is approximately 40 min. After that, μ_{nf} keeps decreasing until it approaches μ_{bf} at 120 min. The reason was that the aggregation of the nanoparticles gradually decreases before 40 min, and after that the long-time ultrasonication destroys the aspect ratio of the nanoparticles, which reduces μ_{nf} [564].

The μ_{nf} also exhibited the same trend with the ultrasonication duration at different temperatures. Menbari et al. [565] studied the μ change of Al_2O_3–CuO/water nanofluids. It was found that as the ultrasonic time increases, μ_{nf} increases first and then decreases, and μ_{nf} reaches a maximum at an ultrasonication time of 100–120 min. Silambarasan et al. [566] reported the effect of ultrasonication time on μ of TiO_2/water nanofluids. Their results indicate that μ_{nf} decreases with increasing ultrasonication time, which is attributed to nanoparticle agglomeration and size reduction. Based on the above conclusions, the fact that μ_{nf} has a significant dependence on the duration of the ultrasound can guide the facile preparation of high-stability nanofluids.

In summary, Section 3.4.4 dealt with effect of key parameters such as particle's size and shape, concentration, pH, and sonication time on the viscosity magnitude of mono nanofluid. Researchers may focus more on the study of viscosity in high temperatures, for example higher than 70 °C, where the nanofluid can be used for high temperature applications such as parabolic collectors. Moreover, finding the optimal value of pH and sonication time is still a challenge in the evaluation of nanofluids viscosity. Size and shape of nanoparticles are other parameters that can be engineered to control the viscosity. Finally, concentration of nanoparticles has a key role to determine the behavior of nanofluid. The increase of concentration from a given value could change the nanofluid behavior from Newtonian to non-Newtonian. Since particle loading increase both thermal conductivity and viscosity (in general), therefore optimal concentration could be selected by heat transfer enhancement and pumping power indexes. Fig. 22 summarizes the effect of concentration on the viscosity of different types of nanofluids. It can be clearly seen from Fig. 22 that as the loading of nanoparticles increases, the μ of all types of nanofluids shows significant upward trends, such as Al_2O_3 [446,518,519,567,568], TiO_2 [281,314,519,568], CuO [569], Fe_2O_3 [570], MgO [571], SiO_2 [8,572] and SiC [389], graphene [534,573] and CNT [547,548,574] based nanofluids.

3.4.5. Hybrid nanofluids

The purpose of developing hybrid nanofluids is a trade-off between advantages and disadvantages of nanofluids made of one type of nanoparticles (mono nanofluids), which aims to obtain a medium with better heat transfer characteristics for practical engineering applications. There are many studies which have shown that hybrid nanofluids render better heat transfer performance, although further work is still needed to overcome the challenges in terms of stability and dispersion for practical applications [439,511,575–582]. It is also intriguing to note that μ is still one of the problems that cannot be ignored in hybrid nanofluids. In general, theoretical models fail to precisely predict dynamic viscosity of hybrid nanofluids (μ_{hnf}). Therefore, in order to accurately estimate μ_{hnf}, researchers have proposed new correlations (see Table 4), which are discussed below.

3.4.5.1. Theory. In Section 3.4.1.1, we already mentioned that Bachelor proposed a correlation Eq. (79) to predict μ of single-type nanoparticle suspensions with Brownian motion [511], and Ho et al. [439] has demonstrated that Eq. (79) can accurately predict μ_{hnf}. Afrand et al. [575] proposed SiO_2–MWCNT/engine oil hybrid nanofluids as heat engine coolants and lubricants, and explored the effect of temperature and solid volume fraction on μ. The experimental results revealed that there is a significant difference between experiments and the results predicted by model. Hence, they proposed a correlation that has been proven to accurately predict the μ_{hnf}. Its general form is as follows:

$$\frac{\mu_{nf}}{\mu_{bf}} = c_0 + c_1\Phi_p + c_2\Phi_p^2 + c_3\Phi_p^3 + c_4\Phi_p^4 \tag{88}$$

where μ_{nf} and μ_{bf} represent the dynamic viscosity of the nanofluid and base fluid, respectively, and c_0, c_1, c_2, c_3 and c_4 are coefficients for each temperature, whose values are given in Ref. [575]. It should be noted that Eq. (88) is valid only at temperatures ranging from 25 to 60 °C and solid concentration ranging from 0.05 vol% to 1 vol%.

Subsequently, Esfe et al. [576] also obtained a similar correlation to Eq. (88) for MWCNT–ZnO/engine oil hybrid nanofluids. Furthermore, the group proposed another dynamic viscosity model to predict the μ of Ag–MgO/water hybrid nanofluids by curve fitting the experimental data. The general form of the dynamic viscosity model is:

$$\mu_{nf} = \left(1 + 32.795\Phi_p - 7214\Phi_p^2 + 714600\Phi_p^3 - 0.1941 \times 10^8\Phi_p^4\right)\mu_{bf} \tag{89}$$

where $0 \le \Phi_p \le 0.02$. It is also found that the proposed model can precisely predict μ_{nf} under specific conditions [532].

Dardan et al. [577] also proposed a new correlation to predict μ of Al_2O_3–MWCNTs/engine oil hybrid nanofluids, which is a function in terms of nanoparticle volume concentration and temperature. The general form of the new correlation is:

$$\frac{\mu_{nf}}{\mu_{bf}} = 1.123 + 0.3251\Phi_p - 0.08994T + 0.002552T^2 - 0.00002386T^3 + 0.9695\left(\frac{T}{\Phi_p}\right)^{0.01719} \tag{90}$$

Subsequent comparison reveals that most of the experimentally obtained relative viscosity values are close to the predicted values, and the maximum deviation is only 2%. It further indicates that an excellent agreement between the measured data and predicted values exist, resulting in the proposed correlation being useful for engineering applications. Notice that Eq. (90) is valid for nanofluids with concentrations ranging from 0.0625 to 1 vol% and temperature from 25 to 50 °C.

Recently, an experimental study on the dynamic viscosity of MWCNT–ZnO/engine oil hybrid nanofluids was carried out by Asadi et al. [533], in which a new correlation to estimate μ_{nf} was proposed by fitting the experimental data. Similarly, it is also a function in terms of the solid volume concentration and temperature of the nanofluid. The exact description is:

$$\mu_{nf} = 796.8 + 76.26\Phi_p + 12.88T + 0.7695\Phi_pT + \frac{-196.9T - 16.53\Phi_pT}{\sqrt{T}} \tag{91}$$

It can be seen from comparison that the correlation is highly consistent with all experimental data. It should be noted that the above correlation is only suitable for temperature ranging from 5 °C to 55 °C and solid concentrations from 0.125 vol% to 1 vol%.

3.4.5.2. Experimental studies. Dynamic viscosity is a decisive factor in resisting the relative motion of nanofluids. In fact, hybrid nanofluids can further improve the heat transfer performance compared to mono nanofluids to some extent. At the same time as heat transfer is enhanced, μ_{hnf} should also be considered. Afrand et al. [575] studied the effects of temperature and solid volume fraction on μ_{hnf}. From the experimental data obtained, it can be found that the temperature rise has a positive effect on the μ_{hnf}, which is attributed to the increase in the temperature and weakening in the intermolecular interactions. As the solid volume fraction increases, the agglomeration of nanoparticles is more likely to occur, which further leads to a significant increase in μ_{hnf}, and thus the effect of temperature on μ_{hnf} becomes more pronounced. This trend has long been confirmed in the study of mono nanofluids. Furthermore, from the trend of relative viscosity with temperature and solid volume fraction, it can be observed that relative viscosity exhibits an increasing trend with respect to the increase of temperature and solid volume fraction, but the effect of solid volume fraction will be more significant. Soltani et al. [578] also studied the effects of temperature and particle concentration on μ_{hnf}. MgO–MWCNT/EG hybrid nanofluids were selected as the research object, and the final conclusions are consistent with

Table 4
Summary of theoretical models for the prediction of the dynamic viscosity of hybrid nanofluids (μ_{hnf}).

Model	Year	Equation	Features	Ref.
Afrand et al.	2016	$\frac{\mu_{nf}}{\mu_{bf}} = c_0 + c_1\Phi_p + c_2\Phi_p^2 + c_3\Phi_p^3 + c_4\Phi_p^4$	Valid only in temperature ranging from 25 to 60 °C and concentration ranging from 0.05 to 1 vol%	[575]
Esfe et al.	2017	$\mu_{nf} = \left(1 + 32.795\Phi_p - 7214\Phi_p^2 + 714600\Phi_p^3 - 0.1941 \times 10^8\Phi_p^4\right)\mu_{bf}$	Valid only in concentration ranging from 0 to 0.02 vol%	[576]
Dardan et al.	2016	$\frac{\mu_{nf}}{\mu_{bf}} = 1.123 + 0.3251\Phi_p - 0.08994T + 0.002552T^2 - 0.00002386T^3 + 0.9695\left(\frac{T}{\Phi_p}\right)^{0.01719}$	Valid only in concentration ranging from 0.0625 to 1 vol% and temperature ranging from 25 to 50 °C.	[577]
Asadi et al.	2016	$\mu_{nf} = 796.8 + 76.26\Phi_p + 12.88T + 0.7695\Phi_pT + \frac{-196.9T - 16.53\Phi_pT}{\sqrt{T}}$	Valid only in temperature ranging from 5 to 55 °C and concentration ranging from 0.125 to 1 vol%.	[533]

those mentioned above. The μ_{hnf} is positively correlated with the concentration of nanoparticles and negatively correlated with temperature. They found μ_{hnf} is slowly enhanced at a low volume fraction ($< 0.4\%$) while rapidly enhanced at high volume fractions (0.8% and 1%). They believed that this can be attributed to the MWCNT chains consequently formed via the interconnection of MWCNTs.

In another work, a study on thermophysical properties of SiO_2–CuO–C/EG-glycerol hybrid nanofluid was carried out by Akilu et al. [579]. Experimental results indicated that μ_{hnf} rises as the loading of nanoparticles increases, owing to the stronger interaction between the base fluid molecules and the nanoparticles. Finally, they compared the relative viscosity of the SiO_2–CuO–C/EG-glycerol hybrid nanofluid with the SiO_2/EG-glycerol nanofluid, and found that the μ_{hnf}/μ_{bf} was significantly lower than that of the μ_{nf}/μ_{bf} with a maximum difference of up to three times. This happened since the ρ of SiO_2 is much smaller than the ρ of the CuO–C hybrid nanoparticles, a smaller number of particles at the same weight favors the flow of the nanoparticles and reduces the flow resistance, consequently reducing μ_{hnf}.

A review of the aforementioned articles on μ_{hnf} reveals that all studies have reached a consistent conclusion. However, we have realized that in addition to a huge amount of research work examining the effects of temperature and concentration on μ_{hnf}, there are few reports on the influences of other key factors on μ_{hnf}. As a state-of-the-art high-performance heat transfer fluid, hybrid nanofluids need to be comprehensively analyzed and discussed. Therefore, it is necessary to analyze the influences of the size and shape of the nanoparticles, ultrasonication time and the pH of the base fluid. Whether the effect is identical to or different from the effects in mono nanofluids is unknown and much work remains for the future.

3.4.6. Molecular dynamic (MD) simulation

Although many studies have been done for evaluation of μ_{nf} experimentally, new techniques are constantly pursued [556,575–579]. In Section 3.1.5, we discussed that k_{nf} can be calculated by MD simulation methods, and the same method can also be applicable to study of μ_{nf}. Some pioneering researchers have adopted this method in the study of μ_{nf} and have made some new progress in this area. In MD simulation, both EMD and NEMD can be used to calculate μ_{nf}. In particular, the principle of EMD simulation is based on the Green–Kubo formula [580,581], while there are three unique methods used to calculate μ_{nf} in NEMD. However, most of the following studies have adopted the EMD method.

Recently, a study on the effect of different graphene nanosheet sizes (length: 10×10 nm and 20×20 nm) on the viscosity of nanofluids was carried out by Vakili-Nezhaad et al. [580]. All the water molecules' interactions were described using a L-J potential, Coulomb's law was used to model electrostatic interactions, a combination of L-J potential and Coulomb potential was employed to describe the interactions between atoms in graphene, while a rule of Lorentz–Berthelot combining was used to describe the interaction between the water molecules and the graphene nanosheets. In particular, μ_{nf} was determined via the Green–Kubo method based on the fluctuation–dissipation theorem and linear response theory. The results clearly demonstrated that all nanofluids have a higher μ than pure water, and μ exhibits a decreasing tendency with the increase in the size of the nanoparticles dispersed in the base fluid. Hence, there is a negative correlation between the size of the graphene nanosheets and μ_{nf}, which is mainly due to the stronger interaction between graphene and water molecules. This also confirms the conclusions that some researchers have reached experimentally [556], that is that the largest μ_{nf} values are observed in nanofluid with the smallest nanoparticle size.

Moreover, Rudyak et al. [581] also explored μ of different-sized nanoparticles dispersed in a base fluid using MD, where the nanofluids were formed by dispersing Al and Li nanoparticles in Ar. Similarly, the Green–Kubo method was used to calculate the shear viscosity, and L-J potential, RK potential and specially devised potentials are used to describe the interactions between molecules in the carrier medium, between the molecules and the nanoparticles, and between the nanoparticles, respectively. MD simulation results unambiguously demonstrate the dependence of μ_{nf} on nanoparticle size. If the volume concentration of the nanoparticles is constant, the finer the nanoparticles, the higher μ_{nf}.

The contribution to the increase in μ_{nf} is mainly due to the interaction of nanoparticles–molecule interactions and the correlations between molecules–molecules and nanoparticles–molecule interactions. Lou et al. [582] also confirmed that smaller nanoparticle sizes produce higher μ_{nf}, which can be explained by stronger interactions between water and Al_2O_3 nanoparticles. Another study on the effect on μ of SWCNT/ethanol nanofluids with SWCNT diameters of 0.54–1.08 nm yielded a lower μ_{nf} than μ_{bf} at any temperature with μ_{nf} decreasing with increasing SWCNT diameter. It has also been confirmed that the chirality of SWCNT has a slight impact on the shear viscosity [583].

MD simulation enables us to examine not only the effect of nanoparticle size on μ_{nf}, but also to explore the effects of various parameters such as temperature, volume fraction, and aggregation. In terms of the effect of nanoparticle volume fraction and temperature, Jabbari et al. [584] explored atomic and molecular level physical phenomena on SWCNT/water nanofluids. The results gained from the Green–Kubo relation indicate that the increase in volume fraction directly leads to a boost in μ_{nf}, which can be explained by the fact that as more and more water molecules are affected by the increase in the volume fraction of CNTs, stronger van der Waals forces are generated between them. The increase in temperature weakens the reaction between the water molecules and the bonds between the nanoparticles, thereby decreasing μ_{nf}. At the same time, that research group has also observed a positive relationship between the nanoparticle volume fraction and μ of CNT/water nanofluids [585]. In other words, as the volume fraction of nanoparticles increases, more water molecules will be affected by the nanoparticles, and the interactions between them hinder the momentum transfer between the nanofluid layers, consequently μ_{nf} increases. Conversely, the interaction between the nanoparticles and the base liquid molecules weakens as the temperature increases, which helps to increase the inter-molecular spacing and thus better dispersion is exhibited. Additionally, Zeroual et al. [586] studied μ of Cu/Ar nanofluids using the MD method, which attributed the effect of volume fraction on μ_{nf} to the presence of a dense nanolayer at the interface between the nanoparticles and the base fluid. In the MD simulation for μ of Al_2O_3/water nanofluids, Lou et al. [582] believe that under the joint control of concentration and temperature, which means that the interaction between nanoparticles and water molecules is the decisive factor influencing the μ_{nf}.

All MD simulations mentioned above have reached consistent conclusions, which validate the phenomena observed by some researchers experimentally. This also indicates that MD simulation can not only achieve the thermophysical results observed experimentally, but also enrich our understanding of nanofluid behaviors at the atomic and molecular levels. Despite the growing number of MD works reporting on nanofluids, there are still significant gaps to be explored.

4. Thermophysical properties and data mining

Since 2012, due to the rapid development of the Internet and information industry, the term "Big Data" has attracted more and more attention. It is defined as the massive data generated by the information explosion era. With the advent of the era, big data has quickly penetrated various industries of importance in today's society, including materials science, clean energy, fossil energy, environmental ecology, finance, military, communications and others [587–607]. Specifically, in the field of thermal physics, the thermophysical parameters are collected, analyzed and modeled by data mining, so that accurate prediction of the theoretical model can be achieved. In the future, data mining will play an important role and become one of the indispensable technical means in scientific research. For example, the application of data mining in materials science has been applied to solve many existing quantitative problems, such as simulated annealing, adaptive simulated annealing, and quantum annealing through highly complex and enormous data calculations [588].

Belianinov et al. [587] comprehensively summarized and analyzed data mining in scanning and electron microscopy. Among them, the application of data mining in scanning and electron microscopy is mainly to obtain some functions from multidimensional data sets. Generally, they are used to generate images to observe the molecular, atomic and nanoscale structural components inside the materials, and the data are collected, analyzed, and processed by computer-aided microscopy. At this stage, an accuracy of approximately a picometer has been achieved for determine the position of the atoms and the individual bond lengths and angles. Meanwhile, functional imaging can visualize multidimensional data sets and transform information into physical and chemical related information through multidimensional data processing analysis [587].

Data mining is one of the current academic focuses, and it may also have a vital impact on future scientific research and national social development. Data mining in the field of engineering thermophysics is a promising tool for developing this field. In terms of thermal properties of materials, different from previous theoretical and numerical simulation models, data-driven prediction models based on a large amount of experimental data could achieve more accurate predictions. At present, data-driven models have been studied and applied in the estimation of k_{nf} [589–607]. Training artificial neural networks (ANN) by mining a large amount of experimental data is the main technique for obtaining k_{nf}. The employed ANN for the k generally including multilayer perceptron artificial neural networks (MLP-ANN) [340,432,435,589–594,601–604], group methods of data handling (GMDH) [565,598], adaptive neuro fuzzy inference systems (ANFIS) [595–597,605], radial basis functions (RBF) [599,600] and enhanced artificial neural networks (EANN) [606,607]. Fig. 23 illustrates the research progress using artificial neural network based on data mining for accurate prediction of k. The application of these ANNs in thermophysical models will be discussed next.

MLP-ANN is one of the more widely studied ANNs with research studies covering single-type particles such Al_2O_3, TiO_2 and CuO and hybrid particles such as SWCNT/Al_2O_3 nanofluids. Since Hojjat et al. [589] first developed the MLP-ANN algorithm and obtained accurate k results for three nanofluids containing Al_2O_3, TiO_2 and CuO nanoparticles, respectively,

this marked a breakthrough in thermophysical modeling and data mining in heat transfer. Then for CNT-based nanofluids, Esfe et al. [590] combined MLP-ANN with the Back-Propagation (BP) algorithm and obtained more accurate k values for SWCNTs and MWCNTs in multi based fluids compared with classical models. Khosrojerdi et al. [591] and Esfe et al. [592] reported new MLP-ANN techniques which added the tangent sigmoid and pureline functions respectively, and Yousefi et al. [593] employed both tangent sigmoid transfer functions for hidden layers and pureline functions for output layers. In addition, Afrand et al. [594] reported the data-driven model for Fe_3O_4/water nanofluids which applied the Levenberg–Marquardt BP algorithm and the tangent sigmoid and pureline transfer functions, in order to reduce the predication errors of thermophysical properties using MLP-ANN.

For Al_2O_3/water nanofluids, Mehrabi et al. [595] employed the combination method of C-means clustering and ANFIS. By calculating the square error and the root mean square error between ANFIS and GMDH models and the same set of experimental results, they concluded that the C-ANFIS is better than GMDH. Esfahani et al. [596] studied nanofluids consisting of CuO, Ag and TiO_2 nanoparticle/oil nanofluids through the ANFIS method, indicating that the determination coefficient of the output k was higher than 0.97. Sadi et al. [597] focused on MWCNT/ionic liquid nanofluids and applied ANFIS with input parameters of temperature, volume fraction and molecular weight of the ionic liquid. This method is suitable for ionic liquid-based nanofluids with a determination coefficient 0.9959.

Combined with genetic algorithms, Mehrabi et al. [595] also used the GMDH approach to explore k of Al_2O_3/water nanofluids and the greatest difference between the model and experimental data is 6%. Shahsavar et al. [598] trained the same GMDH for Fe_3O_4/liquid paraffin nanofluids with the concentration range of 0.5%–3%, pointing out that the coefficient of determination of this model is 0.96.

The k of multi-nanoparticles in water, oil, and ethylene glycol based nanofluids has been obtained by Aminian [599] using the RBF method with tangent sigmoid transfer functions, and the input parameters are nanoparticle volume fraction, nanoparticle diameter, temperature, k of base fluid and the nanoparticle. The coefficient of determination of the model's output is 0.9309. Zhao et al. [600] predicted the k of Al_2O_3/water nanofluids using RBF with only two input parameters (temperature and volume fraction of the nanoparticles) by using 8 neurons in the hidden layer, which is enough accuracy with a coefficient of determination of up to 0.999944.

For the more complicated hybrid particle type nanofluids, the predicted k is mainly based on MLP-ANN, and there are also some studies based on ANFIS and EANN. Mechiri et al. [601] predicted k of Cu–Zn/Oil nanofluids using MLP-ANN with input parameters of nanoparticle volume fraction, nanoparticle diameter, temperature, and the k values of both the base fluid and the nanoparticles. Comparing with classical models such as multiple linear regression and the Hamilton and Crosser model, this method is more accurate with a coefficient of determination of 0.99379. Moreover, CNT-based nanofluids also have been researched using MLP-ANN by Esfe [602,603] for MWCNT–SiO_2/EG and SWCNTs–Al_2O_3/EG, respectively. The method with a maximum error of 1.94% is more reliable than transitional models. Similar to the case of single-type nanoparticle, the tangent sigmoid transfer function, pureline transfer function and BP algorithm have also been employed with MLP-ANN for hybrid particle nanofluids to obtain more accurate results [340,432,435,604]. In addition, Balla et al. [605] applied ANFIS to predict the k of Zn–Cu/water nanofluids based on the first-order Sugeno fuzzy inference system. The output of the model shows a high agreement with experimental results with the maximum deviation of 1%, which is very suitable for multi-metallic nanoparticles-based nanofluids. Karimipour et al. [606] and Bagherzadeh et al. [607] utilized EANN for $CuFe_2O_4$–SiO_2/water-EG and MWCNTs–Fe_3O_4/EG, respectively, and developed dissimilar training algorithms using Levenberg–Marquardt and Bayesian regularization backpropagations.

The emergence of data mining has opened a new gate for scientific research, and its importance has gradually emerged in research. The data driven models will be an indispensable part of model building in the future. In modeling of thermophysical properties using ANNs, the uncertainty of measured data is mostly ignored that affect the accuracy of predicted values.

5. Challenges and future works

The state-of-art on the thermophysical properties of the nanomaterials has been presented in the previous sections. In the following we focus on the challenges and needs of the further studies.

5.1. Solid state

As for solid nanomaterials, one of the main obstacles at this stage is cost. Synthesis techniques for nanomaterials are expensive, and the synthesized materials are usually contaminated or defective. Therefore, they need to be mass-produced at a lower cost. Due to size effects, the thermophysical properties of nanostructures are significantly different from those of the bulk materials because the characteristic lengths of the phonons are comparable to the size of the nanostructures. For typical 1-D and 2-D carbon nanomaterials, the presence of boundaries, defects, impurities and the enormous interfacial thermal resistance generated by phonon boundary scattering are the major obstacles to the improvement of thermophysical properties of nanomaterials. A key issue, currently being explored by many researchers is how to modify the interface structures to meet the requirement of ultrahigh thermal transport performance for nano-thermal interface materials (nTIMs). Experimentally, direct measurement of thermal transport properties of individual nanotubes is still challenging due to imperfect and poorly developed techniques for measuring nanoscale materials.

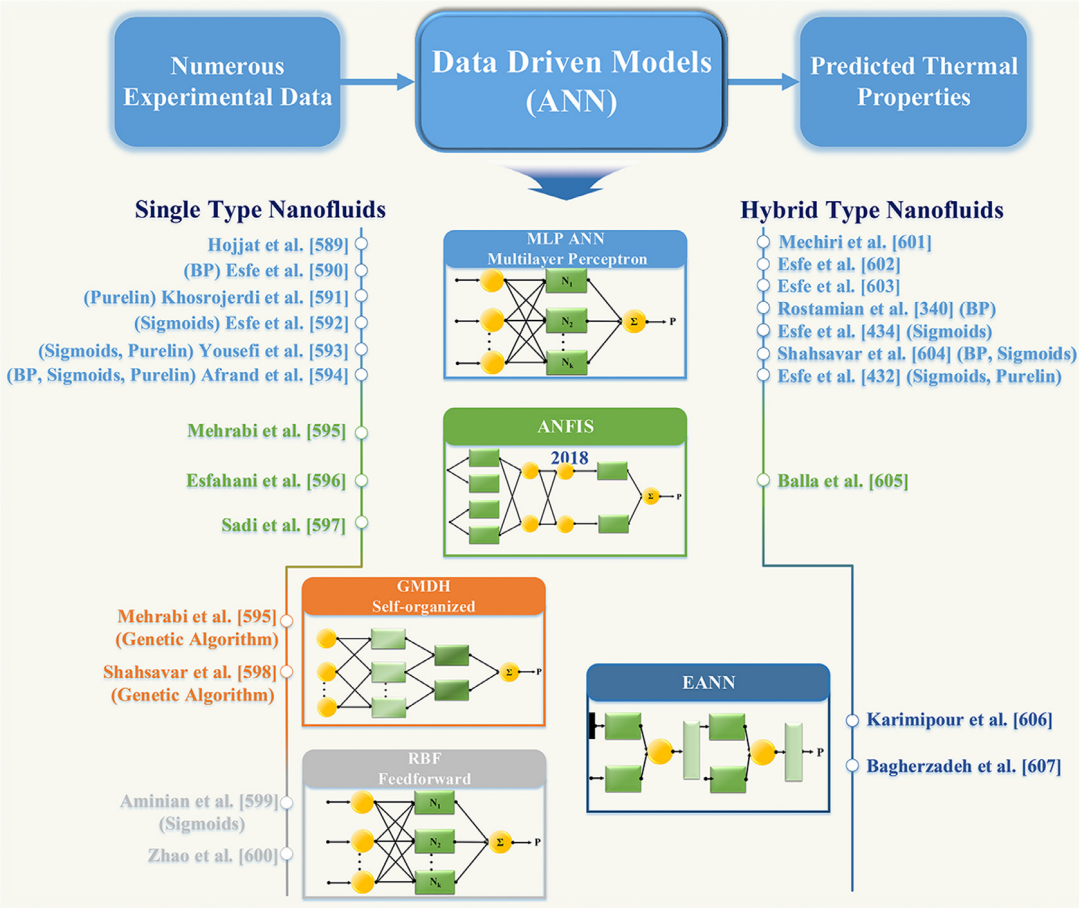

Fig. 23. Research progress of artificial neural network (ANN) based on data mining in accurate prediction of the thermal conductivity.

At the same time, there is a lack of characterization of the thermophysical properties of nanomaterials in extreme environments, such as high temperature and high-pressure conditions. It is necessary to establish a theory of abnormal heat transfer characteristics describing the interface of nanostructures, though how to establish transmission theory in the quantum system is still a big challenge. Therefore, the above challenges and gaps require experimental and theoretical joint efforts. Although research on nanomaterials has made significant progress in the past few decades, many important issues remain to be explored. Taking the well-known CNTs for an example, there are large differences among samples synthesized by different research groups, resulting in widely scattered thermophysical property values. This phenomenon stems from the difference in geometric parameters and quality, especially the unavoidable existence of defects that needs to be understood. There is no doubt that produced nanomaterials need to have identical and predictable thermophysical properties in order to satisfy many applications. Although the aforementioned theoretical advanced models and experiments have helped us understand thermal transport mechanisms for CNTs, there are still challenges regarding the transmission of vibration modes and the effects of near-interfacial defects and disorder.

As for composite nanomaterials, the challenge is how to add oriented nanomaterials to polymer composites, so as to effectively reduce the thermal contact resistance and improve the thermal transport performance. Additionally, the inherent properties of nanomaterials such as the CNT chirality, diameter, and defects will exert a great influence on the k of the composites. Functionalization of the nanomaterials is also a widely used approach to improve their thermal transport properties, while covalent functionalization can lead to structural damage to the nanomaterials. In marked contrast, the potential disadvantage of non-covalent functionalization is the weak bonding, so the effect on k of composite nanomaterials is more complicated.

5.2. Colloidal nanofluid

Although a large amount of research work on the thermophysical properties of nanofluids has been published and the research results show an exponentially increasing trend year by year, this does not mean that research on nanofluids is

mature enough. There are still many challenges and gaps to be filled with future works. For example, the high cost of nanofluid preparation is one of the most fundamental obstacles hindering application in industry. Whether producing nanofluids in one or two steps, there are many requirements in terms of hardware, and sophisticated instruments and equipment are essential. Thus, a comprehensive consideration of the preparation methods for nanofluids is also an effective method for improving the thermophysical properties of nanofluids. The following will systematically analyze the gaps and challenges in the research of thermophysical properties of nanofluids at this stage, and propose some constructive points based on the mentioned opportunities and challenges. It has been previously reviewed that nanoparticle aggregation is detrimental to the thermophysical properties of nanofluids, because aggregation nullifies the benefits of the high specific surface area of the nanoparticles. The long-term stability of nanoparticle-dispersed suspensions is an essential prerequisite for the application of nanofluids in industry. Generally, in the preparation process, aggregation of nanoparticles is unavoidable to a great extent due to the strong van der Waals interactions. In order to overcome this difficulty, researchers used to add the dispersion additives and surfactant into the base fluid while dispersing the nanoparticles. Although the problem of nanoparticle aggregation is solved, the surface properties of the nanoparticles become another uncertainty. This is due to the fact that the dispersant plays a major role as an impurity in the base fluid relative to the nanoparticles and inevitably has a non-negligible impact on the thermophysical properties of the nanofluids. Essentially, the thermophysical properties of nanofluids become ambiguous and unpredictable. An area that must be studied is how to use surfactants reasonably and bring certain benefits. Hence attention should also be paid to the effects of surfactants on the thermophysical properties of nanofluids in future study, whether in experimental or MD simulation work. Furthermore, unlike conventional nanofluids, hybrid nanofluids consist of two or above different nanoparticles as nanofillers, and their stability is also different from the conventional nanofluids.

In Section 3.2, we systematically reviewed trends relating to the $c_{p,nf}$. Based on the current literature the c_p of most nanofluids is lower than $c_{p,bf}$, and it further decreases with increases in the volume fraction of nanoparticles. This is not what most researchers and engineers wanted to obtain, because an excellent coolant should have a c_p value as high as possible so that it can carry more heat away from the high temperature area. Thus, the problem of relatively lower c_p values is also one of the barriers in the current research stage. Interestingly, CNT/graphene nanofluids avoid this problem to some extent because the c_p values of such nanofluids do not drop considerably with an increase in the volume fraction of nanoparticles. Therefore, CNT/graphene nanofluids are still one of the most promising heat transfer fluids in future research.

It is well known that, for the characterization of the thermophysical properties of nanofluids, most researchers focus on a comprehensive analysis of k_{nf} and μ_{nf}. For these two thermophysical parameters that directly affect the nanofluid performance in heat exchange equipment applications, we can conclude that k_{nf} and μ_{nf} are controlled by multiple factors, including temperature, concentration, shape and size of the nanoparticles and aggregation, etc. Therefore, theoretical models of k_{nf} and μ_{nf} have not been widely adopted since they do not fully consider the multiple factors of nanofluids, including the momentum conversion and charge distribution generated by the collision of nanoparticles. Although k_{nf} increases with increasing nanoparticle loading, the enhancement in μ_{nf} exhibits a steeper trend. As a result, the volume fraction of nanoparticles cannot be enhanced continuously — and some researchers have concluded that it is impractical to replace conventional fluids with nanofluids in industrial heat exchange equipment that require very high masses of heat transfer fluids.

These gaps and challenges provide extraordinary and significant guidance for the future development of nanomaterials. With the rapid development of nanotechnology and nanoscience, these problems will be fully solved, and some unprecedented discoveries will be made. This will further fuel the future efforts towards the application of nanomaterials to the fields of microelectronics and nano energy.

6. Conclusions

Inspired by their excellent properties and significant potential for employment in a wide range of advanced nanotechnology applications, recent research has made significant breakthroughs in improving our understanding of the thermophysical properties of nanomaterials. In this review, we have summarized the recent progress in understanding and controlling the thermophysical properties of solid-state to colloidal nanomaterials from theoretical, experimental and computational approaches. This began with an analysis of three important thermophysical properties of solid nanomaterials, *i.e.*, thermal conductivity, isobaric specific heat capacity and thermal diffusivity, followed by an analysis of four key thermophysical properties of nanofluids, *i.e.*, thermal conductivity, isobaric specific heat capacity, density and dynamic viscosity. In closing, current research opportunities and challenges are summarized, and promising future development directions are proposed.

For solid-state nanomaterials, a series of theoretical models such as the Callaway model, the Holland model, the BvKS model and a simple gray model have been proposed, through continuous improvement and modifications, for accurate and reliable predictions of the thermal conductivity of nanostructures. Research has suggested that the MFP distribution has a direct relationship and contributions to thermal conductivity. The difference between the bulk and the nanostructure is the remarkable MFP reduction owing to scattering at boundaries and interfaces. In addition, due to the limitation of the internal structure of nanomaterials, the thermal transport properties of the amorphous material are directly affected by the degree of disorder. Specifically, in amorphous nanomaterials with high disorder, the phonon velocity and polarization

direction inside the structure are not clear, and the concept of phonons cannot be used to evaluate their thermophysical properties.

We have also provided a comprehensive, state-of-the-art review of the mainstream experimental methods for the measurement of thermal conductivity of nanomaterials, including the well-known 3ω method and freestanding sensor-based 3ω method which can measure the thermophysical properties (k, c_p and α) of fibrous, powder, liquid and porous materials, the T-type probe method and their upgraded forms (combined 3ω-T type probe method and improved H-type probe method) which can measure thermal conductivity of single-layer graphene or nanofilms, the latest cutting-edge laser flash Raman spectroscopy method for 2-D graphene measurements, and the TDTR method with high accuracy and wide applicability for the measurement of the thermal conductivity of various nanostructured interfaces and materials. Grain size, grain boundaries, surface and interface interactions, doping, defects and temperature have a significant effect on thermal conductivity of nanomaterials. The following conclusions about the crystalline materials can be drawn: (i) the effect of grain size is more important than that of grain boundary, and the grain-boundary scattering short-wave phonons reduce the lattice thermal conductivity of the material in the low temperature region; (ii) the thermal transport performance can be improved by using noble metals (Au, Ag Pd, Pt) and adding small molecular halogens (I_2) between the interfaces, although their mechanisms are different; (iii) different doping and defect concentrations of nanomaterials cause an increase in phonon scattering; and (iv) the difference in the mass of the doping atoms is one of the key factors for the sharp decline in the observed thermal conductivity of relevant nanomaterials. It is worth noting that the effect of temperature is particularly complex, and there are significant differences in the dependence of thermal conductivity on temperature for different nanomaterials. The MD method with atomic-level simulation has proven its value in providing insight into the thermal behavior of nanomaterials, and thus has been widely adopted in research efforts focused on micro/nanoscale thermal transport.

Most of the popular methods for the measurement of thermal diffusivity of nanomaterials are transient, and generally divided into photothermal and electrothermal techniques. The former includes the classical laser-flash method, non-contact and non-destructive laser-flash Raman spectroscopy, the photothermal resistance technique for conductive and non-conductive materials, and infrared thermography. While the transient electrothermal technique (TET) is one of the most representative electrothermal techniques. Experimental studies have found that thermal diffusivity of nanomaterials dependents strongly on temperature, which is closely related to lattice wave, phonon transfer energy and free electron transfer energy. In conclusion, nanomaterials have excellent thermal conduction or insulation capabilities compared to traditional materials.

We also summarize three theoretical models used to define the isobaric specific heat capacity of nanomaterials, namely the Dulong–Petit law based on energy quantification, the Einstein solid model and the Debye model based on quantum theory. The principles of the models and their links and differences are also discussed. As to the effects of size and temperature on isobaric specific heat capacity, experiments have demonstrated that nanoparticles have higher isobaric specific heat capacity than their bulk counterparts at ultra-low temperatures, and there is a difference in temperature dependence at different temperature ranges. Moreover, the thermophysical properties of nanocrystal materials differ significantly from those of conventional large-scale crystals.

We paid special attention to the research progress in their theoretical models for the thermal conductivity of nanofluids. Researchers have attempted to involve the main parameters affecting the thermal conductivity of nanofluids including the thickness of the nanolayer, the aggregation and size of the nanoparticles and the temperature. In the experimental aspect, the measuring principles of the transient hot wire approach, the 3ω method, the laser flash method, the steady-state parallel plate method and the transient plane-source method are introduced in detail. Next, the effects of various factors on thermal conductivity are explored, due to the complexity of the internal mechanisms; many researchers have failed to reach a consensus conclusion on some factors. Most of them have concluded the following five rules: (1) increasing the concentration of nanoparticles will boost the thermal conductivity of the nanofluids, (2) the thermal conductivity of the nanofluids increases with the increasing temperature due to Brownian motion enhancement, (3) the effect of nanoparticle shape on the thermal conductivity of nanofluids is inconsistent; for most cases, with non-spherical it is higher than with spherical nanoparticles, (4) aggregation, which is closely related to the volume fraction and the shape of the aggregates, is generally advantageous, (5) both pH and ultrasonic time have a theoretically optimal values for different nanofluids.

As for the density and the specific heat capacity of nanofluids, we briefly reviewed relevant experimental and theoretical advances. Theoretical efforts have revealed that the isobaric specific heat capacity is essentially a monotonic function of temperature, nanoparticle diameter, and nanoparticle concentration, while experimental efforts are mainly based on common commercial DSC, from which experimental results agree very well with the theoretical predictions. Furthermore, since isobaric specific heat capacity of conventional nanoparticles are much smaller than the base fluid, isobaric specific heat capacity decreases as the volume fraction of the nanoparticles increases. However, this does not occur with nanofluids formed when advanced nanomaterials are used as fillers. Therefore, CNT and graphene nanofluids will remain research hotspots in the future.

We also reviewed representative theoretical models for the dynamic viscosity, beginning with the classical Einstein model, and then proceeding to advanced models that consider the effect of Brownian motion, nanolayers and nanoparticle aggregation, respectively. Three common techniques have been employed in experimental studies, including the use of a capillary viscometer, concentric cylinders, the cone and plate approach, and detailed analysis of the effects of various

factors on this property. It can be concluded that elevated temperatures increase the intermolecular distances, which is favorable for decreasing dynamic viscosity. Meanwhile, an increase in the nanoparticle volume fraction leads to a significant boost in dynamic viscosity due to an increase in the overall drag effect in the nanofluid, which further results in the energy dissipation of the nanofluid. Furthermore, an optimized pH and a long-time sonication are effective in reducing dynamic viscosity.

Future developments for solid nanomaterials are still striving for ultrahigh thermal conductivity or super thermal insulation performance. Promising future directions in the field of thermophysical properties of nanomaterials include: (i) phonon transport is the main thermal diffusion method for nanomaterials, so in-depth studies of phonon transport helps to develop and improve advanced thermal functional materials; (ii) interface thermal resistance is still the main bottleneck for development of high thermal conductivity materials; at present, technology for optimizing material interface resistance is still in its infancy, it is expected to improve in the future and is a hot spot for future work; and (iii) addressing the phonon scattering by boundaries, defects and impurities is an effective means of maximizing thermal conductivity of nanomaterials.

Further development of nanofluids with the following being needed work for the future: (i) attention should continue to be paid to the dispersion of nanoparticles, temperature, surfactants, pH adjustment, nanoparticle size, etc., because these features are still in the developing stage; (ii) the study of nanofluids dispersed by advanced nanomaterials, such as CNT and graphene still attracts a lot of attention, and new types of nanofluids with high thermal conductivity and low dynamic viscosity are needed to meet the requirements of advanced heat transfer applications; and (iii) in order to predict the effects of different parameters on the thermophysical properties of nanofluids more accurately, further efforts are needed to develop new models and correlations. In addition, the effects of nanoparticle Brownian motion, micro convection, clustering and pH on the thermophysical properties of hybrid nanofluids also deserve to be important future research directions.

Nomenclature

A	Isotope scattering coefficient	β	Layer thickness divided by particle diameter
b	Thermal effusivity	γ	Factor equal to $(1 + 2d_{\mathrm{nl}}/r_{\mathrm{p}})$
B_{type}	Function related to the ratio $\Lambda_{\mathrm{bu}}/L_{\mathrm{c}}$	δ	Dirac delta function
c_{p}	Isobaric specific heat capacity, J/kg K	ε	Degree of disorder
c_{v}	Isometric specific heat capacity, J/kg K	ζ	Porosity
$c(\omega)$	Spectral heat capacity per unit Phonon frequency, J/kg K	η	Average flatness ratio of the graphene
		θ_{D}	Debye temperature, K
C	Empirical constant	ι	Factor equal to $(1 - k_{\mathrm{f}}/k_{\mathrm{pe}})$
d	Thickness, m	μ	Dynamic viscosity, Pa s
D	Density of states	ξ_{ave}	Average thermal rectification factor
f	Heat capacity function	ρ	Density, kg/m^3
g_{BE}	Bose–Einstein distribution	σ	Electrical conductivity, S/m
G	Thermal conductance, W/K	τ	Relaxation time, s
h	Convective heat transfer coefficient, W/m^2 K	Φ	Volume fraction
I	Isotope scattering contribution	Ψ	Ratio of the surface area of different nanoparticles
k_{B}	Boltzmann constant, 1.38×10^{-23} J/K		
k	Thermal conductivity, W/m K	ω	Phonons frequency, Hz
k_2	Thermal conductivity correction term	ω_0	Phonons frequency parameter, Hz
k_Λ	Contribution to k per MFP	$\hbar$	Reduced Planck constant
K_{H}	Huggins coefficient	Λ	Mean free path, m
Kn	Knudsen number	ς_{m}	Crowding factor
L	Grain size, m		
L_{c}	Characteristic length, m	***Subscripts***	
ΔM	Atomic mass difference	acc	Accumulation function
n	Empirical shape factor	bf	Base fluid
Nu	Nusselt number	bu	Bulk
p	Polarizations	cl	Nanoparticle cluster
Pr	Prandtl number	D	Diffuson
q	Phonon wave vector, m^{-1}	De	Debye model
q_0	Phonon wave vector parameter, m^{-1}	eff	Effective
$Q_{\mathrm{p-p}}$	Particle–particle interaction intensity	eq	Equivalent
r	Diameter, m	E	Einstein model
R_{k}	Interfacial thermal resistance	f	Fluid
Re	Reynolds number	FVC	Fractional volume concentration
RT	Room temperature, K	Gr	Gray model
s_{s}	Sound speed, m/s	hnf	Hybrid nanofluid

S	Function representing the contribution to the heat flux of a phonon with MFP	Is	Interfacial shell
		L	Longitudinal
t	Time, s	mem	Membrane
T	Temperature, K	nano	Nanostructured material
V	System volume, m^3	nf	Nanofluid
v	Phonon group velocity, m/s	nl	Nanolayer
v_s	Average phonon velocity, m/s	np	Nanoparticle
v_{BF}	Brownian motion velocity, m/s	N	Normal three-phonon process
w	Nanoparticle spacing	p	Particle
y	Ratio of aggregating particles to all nanoparticles	P	Phonon
		RTA	Relaxation-time approximation
Greek symbols		T	Transverse
α	Thermal diffusivity, m^2/s	U	Umklapp process

Declaration of competing interest

The authors declare that they have no known competing financial interests or personal relationships that could have appeared to influence the work reported in this paper.

Acknowledgments

This work received financial support from Projects 51876008 and 51876007 supported by National Natural Science Foundation of China, Project 3202020 supported by Beijing Municipal Natural Science Foundation, and the Fundamental Research Funds for the Central Universities from University of Science and Technology Beijing (L. Qiu). This work was also supported by the UK Engineering and Physical Sciences Research Council (EPSRC) [grant number EP/P004709/1].

References

[1] S. Iijima, Helical microtubules of graphitic carbon, Nature 354 (1991) 56–58, http://dx.doi.org/10.1038/354056a0.
[2] A.L. Porter, Y. Jan, Where does nanotechnology belong in the map of science? Nat. Nanotechnol. 4 (2009) 534–536, http://dx.doi.org/10.1038/nnano.2009.207.
[3] Y.J. Chen, B. Groves, R.A. Muscat, G. Seelig, DNA nanotechnology from the test tube to the cell, Nat. Nanotechnol. 10 (2015) 748–760, http://dx.doi.org/10.1038/nnano.2015.195.
[4] Y. Huang, X. Dong, Y. Shi, C.M. Li, L.J. Li, P. Chen, Nanoelectronic biosensors based on CVD grown graphene, Nanoscale 2 (2010) 1485–1488, http://dx.doi.org/10.1039/c0nr00142b.
[5] L. Qiu, H. Zou, D. Tang, D. Wen, Y. Feng, X. Zhang, Inhomogeneity in pore size appreciably lowering thermal conductivity for porous thermal insulators, Appl. Therm. Eng. 130 (2018) 1004–1011, http://dx.doi.org/10.1016/j.applthermaleng.2017.11.066.
[6] I. Vukovic, G.T. Brinke, K. Loos, Block copolymer template-directed synthesis of well-ordered metallic nanostructures, Polymer 54 (2013) 2591–2605, http://dx.doi.org/10.1016/j.polymer.2013.03.013.
[7] M.M. Mariscal, J.A. Olmos-Asar, C. Gutierrez-Wing, A. Mayoral, M.J. Yacaman, On the atomic structure of thiol-protected gold nanoparticles: A combined experimental and theoretical study, Phys. Chem. Chem. Phys. 12 (2010) 11785–11790, http://dx.doi.org/10.1039/c004229c.
[8] H. Masuda, A. Ebata, K. Teramae, N. Hishinuma, Alteration of thermal conductivity and viscosity of liquid by dispersing ultra-fine particles. Dispersion of Al_2O_3, SiO_2 and TiO_2 ultra-fine particles, Netsu Bussei. 7 (1993) 227–233, http://dx.doi.org/10.2963/jjtp.7.227.
[9] S.U.S. Choi, Nanofluids: From vision to reality through research, J. Heat Transfer 131 (2009) 033106, http://dx.doi.org/10.1115/1.3056479.
[10] Y. Xuan, Q. Li, Heat transfer enhancement of nanofuids, Int. J. Heat Fluid Flow 21 (2000) 58–64, http://dx.doi.org/10.1016/S0142-727X(99)00067-3.
[11] S. Aman, I. Khan, Z. Ismail, M.Z. Salleh, Q.M. Al-Mdallal, Heat transfer enhancement in free convection flow of CNTs Maxwell nanofluids with four different types of molecular liquids, Sci. Rep. 7 (2017) 2445, http://dx.doi.org/10.1038/s41598-017-01358-3.
[12] J. Sui, L. Zheng, X. Zhang, Y. Chen, Z. Cheng, A novel equivalent agglomeration model for heat conduction enhancement in nanofluids, Sci. Rep. 6 (2016) 19560, http://dx.doi.org/10.1038/srep19560.
[13] M.U. Sajid, H.M. Ali, Thermal conductivity of hybrid nanofluids: A critical review, Int. J. Heat Mass Transfer 126 (2018) 211–234, http://dx.doi.org/10.1016/j.ijheatmasstransfer.2018.05.021.
[14] O. Mahian, L. Kolsi, M. Amani, P. Estellé, G. Ahmadi, C. Kleinstreuer, J.S. Marshall, M. Siavashi, R.A. Taylor, H. Niazmand, S. Wongwises, T. Hayat, A. Kolanjiyil, A. Kasaeian, I. Pop, Recent advances in modeling and simulation of nanofluid flows-Part I: Fundamentals and theory, Phys. Rep. 790 (2019) 1–48, http://dx.doi.org/10.1016/j.physrep.2018.11.004.
[15] L. Yang, J. Xu, K. Du, X. Zhang, Recent developments on viscosity and thermal conductivity of nanofluids, Powder Technol. 317 (2017) 348–369, http://dx.doi.org/10.1016/j.powtec.2017.04.061.
[16] G. Żyła, J.P. Vallejo, L. Lugo, Isobaric heat capacity and density of ethylene glycol based nanofluids containing various nitride nanoparticle types: An experimental study, J. Mol. Liq. 261 (2018) 530–539, http://dx.doi.org/10.1016/j.molliq.2018.04.012.
[17] A. Mariano, M.J. Pastoriza-Gallego, L. Lugo, L. Mussari, M.M. Piñeiro, Co_3O_4 ethylene glycol-based nanofluids: Thermal conductivity, viscosity and high pressure density, Int. J. Heat Mass Transfer 85 (2015) 54–60, http://dx.doi.org/10.1016/j.ijheatmasstransfer.2015.01.061.
[18] S.N. Shoghl, J. Jamali, M.K. Mostafa, Electrical conductivity, viscosity, and density of different nanofluids: An experimental study, Exp. Therm. Fluid Sci. 74 (2016) 339–346, http://dx.doi.org/10.1016/j.expthermflusci.2016.01.004.
[19] Y. He, T. Xie, Advances of thermal conductivity models of nanoscale silica aerogel insulation material, Appl. Therm. Eng. 81 (2015) 28–50, http://dx.doi.org/10.1016/j.applthermaleng.2015.02.013.
[20] D.P. Broom, K.M. Thomas, Gas adsorption by nanoporous materials: Future applications and experimental challenges, MRS Bull. 38 (2013) 412–421, http://dx.doi.org/10.1557/mrs.2013.105.
[21] L. Dai, D.W. Chang, J.B. Baek, W. Lu, Carbon nanomaterials for advanced energy conversion and storage, Small 8 (2012) 1130–1166, http://dx.doi.org/10.1002/smll.201101594.

[22] H. Jiang, Chemical preparation of graphene-based nanomaterials and their applications in chemical and biological sensors, Small 7 (2011) 2413–2427, http://dx.doi.org/10.1002/smll.201002352.
[23] S. Rashidi, O. Mahian, E.M. Languri, Applications of nanofluids in condensing and evaporating systems: A review, J. Therm. Anal. Calorim. 131 (2018) 2027–2039, http://dx.doi.org/10.1007/s10973-017-6773-7.
[24] S.S. Meibodi, A. Kianifar, O. Mahian, S. Wongwises, Second law analysis of a nanofluid-based solar collector using experimental data, J. Therm. Anal. Calorim. 126 (2016) 617–625, http://dx.doi.org/10.1007/s10973-016-5522-7.
[25] O. Mahian, A. Kianifar, S.Z. Heris, D. Wen, A.Z. Sahin, S. Wongwises, Nanofluids effects on the evaporation rate in a solar still equipped with a heat exchanger, Nano Energy 36 (2017) 134–155, http://dx.doi.org/10.1016/j.nanoen.2017.04.025.
[26] O. Mahian, A. Kianifar, A.Z. Sahin, S. Wongwises, Performance analysis of a minichannel-based solar collector using different nanofluids, Energy Convers. Manage. 88 (2014) 129–138, http://dx.doi.org/10.1016/j.enconman.2014.08.021.
[27] O. Mahian, A. Kianifar, S.A. Kalogirou, I. Pop, S. Wongwises, A review on the applications of nanofluids in solar energy field, Int. J. Heat Mass Transfer 57 (2013) 582–594, http://dx.doi.org/10.1016/j.ijheatmasstransfer.2012.10.037.
[28] O. Mahian, A. Kianifar, A.Z. Sahin, S. Wongwises, Heat transfer, pressure drop, and entropy generation in a solar collector using SiO_2/water nanofluids: Effects of nanoparticle size and pH, J. Heat Transfer 137 (2015) 061011, http://dx.doi.org/10.1115/1.4029870.
[29] N.A.C. Sidik, R. Mamat, A review on the application of nanofluids in vehicle engine cooling system, Int. Commun. Heat Mass Transfer 68 (2015) 85–90, http://dx.doi.org/10.1016/j.icheatmasstransfer.2015.08.017.
[30] A. Kasaeian, R. Daneshazarian, O. Mahian, L. Kolsi, A.J. Chamkha, S. Wongwises, I. Pop, Nanofluid flow and heat transfer in porous media : A review of the latest developments, Int. J. Heat Mass Transfer 107 (2017) 778–791, http://dx.doi.org/10.1016/j.ijheatmasstransfer.2016.11.074.
[31] O. Mahian, L. Kolsi, M. Amani, P. Estellé, G. Ahmadi, C. Kleinstreuer, J.S. Marshall, R.A. Taylor, H. Niazmand, S. Wongwises, T. Hayat, A. Kolanjiyil, A. Kasaeian, I. Pop, Recent advances in modeling and simulation of nanofluid flows—Part II: Applications, Phys. Rep. 791 (2019) 1–59, http://dx.doi.org/10.1016/j.physrep.2018.11.003.
[32] L. Yang, J. Chen, N. Yang, B. Li, Significant reduction of graphene thermal conductivity by phononic crystal structure, Int. J. Heat Mass Transfer 91 (2015) 428–432, http://dx.doi.org/10.1016/j.ijheatmasstransfer.2015.07.111.
[33] M.C. Wingert, J. Zheng, S. Kwon, R. Chen, Thermal transport in amorphous materials: a review, Semicond. Sci. Technol. 31 (2016) 113003, http://dx.doi.org/10.1088/0268-1242/31/11/113003.
[34] T. Zhu, E. Ertekin, Phonons, localization, and thermal conductivity of diamond nanothreads and amorphous graphene, Nano Lett. 16 (2016) 4763–4772, http://dx.doi.org/10.1021/acs.nanolett.6b00557.
[35] F. Yang, C. Dames, Mean free path spectra as a tool to understand thermal conductivity in bulk and nanostructures, Phys. Rev. B 87 (2013) 035437, http://dx.doi.org/10.1103/PhysRevB.87.035437.
[36] G. Chen, Nanoscale Energy Transport and Conversion: A Parallel Treatment of Electrons, Molecules, Phonons, and Photons, Oxford University Press, New York, 2005.
[37] J. Nakagawa, Y. Kage, T. Hori, J. Shiomi, M. Nomura, Crystal structure dependent thermal conductivity in two-dimensional phononic crystal nanostructures, Appl. Phys. Lett. 107 (2015) 023104, http://dx.doi.org/10.1063/1.4926653.
[38] Z. Wang, J.E. Alaniz, W. Jang, J.E. Garay, C. Dames, Thermal conductivity of nanocrystalline silicon: Importance of grain size and frequency-dependent mean free paths, Nano Lett. 11 (2011) 2206–2213, http://dx.doi.org/10.1021/nl1045395.
[39] Y. Hu, L. Zeng, A.J. Minnich, M.S. Dresselhaus, G. Chen, Spectral mapping of thermal conductivity through nanoscale ballistic transport, Nat. Nanotechnol. 10 (2015) 701–706, http://dx.doi.org/10.1038/nnano.2015.109.
[40] C. Dames, G. Chen, Thermoelectrics Handbook: Macro to Nano, Taylor & Francis, New York, 2005.
[41] J. Callaway, Model for lattice thermal conductivity at low temperatures, Phys. Rev. 113 (1959) 1046–1051, http://dx.doi.org/10.1103/PhysRev.113.1046.
[42] P.B. Allen, Improved Callaway model for lattice thermal conductivity, Phys. Rev. B 88 (2013) 144302, http://dx.doi.org/10.1103/PhysRevB.88.144302.
[43] M.G. Holland, Analysis of lattice thermal conductivity, Phys. Rev. 132 (1963) 2461–2471, http://dx.doi.org/10.1103/PhysRev.132.2461.
[44] G.A. Slack, S. Galginaitis, Thermal conductivity and phonon scattering by magnetic impurities in CdTe, Phys. Rev. 133 (1964) A253–A268, http://dx.doi.org/10.1103/PhysRev.133.A253.
[45] J. Cuffe, J.K. Eliason, A.A. Maznev, K.C. Collins, J.A. Johnson, A. Shchepetov, M. Prunnila, J. Ahopelto, C.M. Sotomayor Torres, G. Chen, K.A. Nelson, Reconstructing phonon mean-free-path contributions to thermal conductivity using nanoscale membranes, Phys. Rev. B 91 (2015) 245423, http://dx.doi.org/10.1103/PhysRevB.91.245423.
[46] A.A. Balandin, S. Ghosh, W. Bao, I. Calizo, D. Teweldebrhan, F. Miao, C.N. Lau, Superior thermal conductivity of single layer graphene, Nano Lett. 8 (2008) 902–907, http://dx.doi.org/10.1021/nl0731872.
[47] J.M. Larkin, A.J.H. McGaughey, Thermal conductivity accumulation in amorphous silica and amorphous silicon, Phys. Rev. B 89 (2014) 144303, http://dx.doi.org/10.1103/PhysRevB.89.144303.
[48] J.L. Feldman, M.D. Kluge, P.B. Allen, F. Wooten, Thermal conductivity and localization in glasses: Numerical study of a model of amorphous silicon, Phys. Rev. B 48 (1993) 12589–12602, http://dx.doi.org/10.1103/PhysRevB.48.12589.
[49] J.L. Feldman, P.B. Allen, S.R. Bickham, Numerical study of low-frequency vibrations in amorphous silicon, Phys. Rev. B 59 (1999) 3551–3559, http://dx.doi.org/10.1103/PhysRevB.59.3551.
[50] X. Zhang, S. Fujiwara, M. Fujii, Measurements of thermal conductivity and electrical conductivity of a single carbon fiber, Int. J. Thermophys. 21 (2000) 965–980, http://dx.doi.org/10.1023/A:1006674510648.
[51] J. Wang, M. Gu, X. Zhang, Y. Song, Thermal conductivity measurement of an individual fibre using a T type probe method, J. Phys. D Appl. Phys. 42 (2009) 105502, http://dx.doi.org/10.1088/0022-3727/42/10/105502.
[52] M. Fujii, X. Zhang, H. Xie, H. Ago, K. Takahashi, T. Ikuta, H. Abe, T. Shimizu, Measuring the thermal conductivity of a single carbon nanotube, Phys. Rev. Lett. 95 (2005) 065502, http://dx.doi.org/10.1103/PhysRevLett.95.065502.
[53] D.G. Cahill, R.O. Pohl, Thermal conductivity of amorphous solids above the plateau, Phys. Rev. B 35 (1987) 4067–4073, http://dx.doi.org/10.1103/PhysRevB.35.4067.
[54] D.G. Cahill, Thermal conductivity measurement from 30 to 750 K: The 3ω method, Rev. Sci. Instrum. 61 (1990) 802–808, http://dx.doi.org/10.1063/1.1141498.
[55] S. Ahmed, R. Liske, T. Wunderer, M. Leonhardt, R. Ziervogel, C. Fansler, T. Grotjohn, J. Asmussen, T. Schuelke, Extending the 3ω-method to the MHz range for thermal conductivity measurements of diamond thin films, Diam. Relat. Mater. 15 (2006) 389–393, http://dx.doi.org/10.1016/j.diamond.2005.08.041.
[56] B.W. Olson, S. Graham, K. Chen, A practical extension of the 3ω method to multilayer structures, Rev. Sci. Instrum. 76 (2005) 053901, http://dx.doi.org/10.1063/1.1896619.
[57] L. Qiu, X. Wang, G. Su, D. Tang, X. Zheng, J. Zhu, Z. Wang, P.M. Norris, P.D. Bradford, Y. Zhu, Remarkably enhanced thermal transport based on a flexible horizontally-aligned carbon nanotube array film, Sci. Rep. 6 (2016) 21014, http://dx.doi.org/10.1038/srep21014.
[58] L. Qiu, P. Guo, Q. Kong, C.W. Tan, K. Liang, J. Wei, J.N. Tey, Y. Feng, X. Zhang, B.K. Tay, Coating-boosted interfacial thermal transport for carbon nanotube array nano-thermal interface materials, Carbon 145 (2019) 725–733, http://dx.doi.org/10.1016/j.carbon.2019.01.085.

[59] L. Qiu, N. Zhu, H. Zou, Y. Feng, X. Zhang, D. Tang, Advances in thermal transport properties at nanoscale in China, Int. J. Heat Mass Transfer 125 (2018) 413–433, http://dx.doi.org/10.1016/j.ijheatmasstransfer.2018.04.087.
[60] L. Qiu, X. Wang, D. Tang, X. Zheng, P.M. Norris, D. Wen, J. Zhao, X. Zhang, Q. Li, Functionalization and densification of inter-bundle interfaces for improvement in electrical and thermal transport of carbon nanotube fibers, Carbon 105 (2016) 248–259, http://dx.doi.org/10.1016/j.carbon.2016.04.043.
[61] L. Qiu, H. Zou, X. Wang, Y. Feng, X. Zhang, J. Zhao, X. Zhang, Q. Li, Enhancing the interfacial interaction of carbon nanotubes fibers by Au nanoparticles with improved performance of the electrical and thermal conductivity, Carbon 141 (2019) 497–505, http://dx.doi.org/10.1016/j.carbon.2018.09.073.
[62] L. Qiu, H. Zou, N. Zhu, Y. Feng, X. Zhang, X. Zhang, Iodine nanoparticle-enhancing electrical and thermal transport for carbon nanotube fibers, Appl. Therm. Eng. 141 (2018) 913–920, http://dx.doi.org/10.1016/j.applthermaleng.2018.06.049.
[63] L. Qiu, Y. Ouyang, Y. Feng, X. Zhang, Note: Thermal conductivity measurement of individual porous polyimide fibers using a modified wire-shape 3ω method, Rev. Sci. Instrum. 89 (2018) 096112, http://dx.doi.org/10.1063/1.5052692.
[64] L. Qiu, X. Zheng, P. Yue, J. Zhu, D. Tang, Y. Dong, Y. Peng, Adaptable thermal conductivity characterization of microporous membranes based on freestanding sensor-based 3ω technique, Int. J. Therm. Sci. 89 (2015) 185–192, http://dx.doi.org/10.1016/j.ijthermalsci.2014.11.005.
[65] L. Qiu, K. Scheider, S.A. Radwan, L.A.S. Larkin, C.B. Saltonstall, Y. Feng, X. Zhang, P.M. Norris, Thermal transport barrier in carbon nanotube array nano-thermal interface materials, Carbon 120 (2017) 128–136, http://dx.doi.org/10.1016/j.carbon.2017.05.037.
[66] L. Qiu, P. Guo, H. Zou, Y. Feng, X. Zhang, S. Pervaiz, D. Wen, Extremely low thermal conductivity of graphene nanoplatelets using nanoparticle decoration, ES Energy Environ. 2 (2018) 66–72, http://dx.doi.org/10.30919/esee8c139.
[67] W. Ma, T. Miao, X. Zhang, K. Takahashi, T. Ikuta, B. Zhang, Z. Ge, A T-type method for characterization of the thermoelectric performance of an individual free-standing single crystal Bi_2S_3 nanowire, Nanoscale 8 (2016) 2704–2710, http://dx.doi.org/10.1039/C5NR05946A.
[68] X. Zhang, X. Shi, W. Ma, Development of multi-physical properties comprehensive measurement system for micro/nanoscale filamentary materials, Sci. Sin. Technol. 48 (2018) 403–414, http://dx.doi.org/10.1360/N092018-00018.
[69] H. Wang, S. Hu, K. Takahashi, X. Zhang, H. Takamatsu, J. Chen, Experimental study of thermal rectification in suspended monolayer graphene, Nature Commun. 8 (2017) 15843, http://dx.doi.org/10.1038/ncomms15843.
[70] J. Hone, M. Whitney, C. Piskoti, A. Zettl, Thermal conductivity of single-walled carbon nanotubes, Phys. Rev. B 59 (1999) R2514–R2516, http://dx.doi.org/10.1103/PhysRevB.59.R2514.
[71] E. Pop, D. Mann, Q. Wang, K. Goodson, H. Dai, Thermal conductance of an individual single-wall carbon nanotube above room temperature, Nano Lett. 6 (2006) 96–100, http://dx.doi.org/10.1021/nl052145f.
[72] S. Ghosh, I. Calizo, D. Teweldebrhan, E.P. Pokatilov, D.L. Nika, A.A. Balandin, W. Bao, F. Miao, C.N. Lau, Extremely high thermal conductivity of graphene: Prospects for thermal management applications in nanoelectronic circuits, Appl. Phys. Lett. 92 (2008) 151911, http://dx.doi.org/10.1063/1.2907977.
[73] C. Faugeras, B. Faugeras, M. Orlita, M. Potemski, R.R. Nair, A.K. Geim, Thermal conductivity of graphene in corbino membrane geometry, ACS Nano 4 (2010) 1889–1892, http://dx.doi.org/10.1021/nn9016229.
[74] S. Chen, A.L. Moore, W. Cai, J.W. Suk, J. An, C. Mishra, C. Amos, C.W. Magnuson, J. Kang, L. Shi, R.S. Ruoff, Raman measurements of thermal transport in suspended monolayer graphene of variable sizes in vacuum and gaseous environments, ACS Nano 5 (2010) 321–328, http://dx.doi.org/10.1021/nn102915x.
[75] W. Cai, A.L. Moore, Y. Zhu, X. Li, S. Chen, L. Shi, R.S. Ruoff, Thermal transport in suspended and supported monolayer graphene grown by chemical vapor deposition, Nano Lett. 10 (2010) 1645–1651, http://dx.doi.org/10.1021/nl9041966.
[76] R. Yan, J.R. Simpson, S. Bertolazzi, J. Brivio, M. Watson, X. Wu, A. Kis, T. Luo, A.R. Hight Walker, H.G. Xing, Thermal conductivity of monolayer molybdenum disulfide obtained from temperature-dependent Raman spectroscopy, ACS Nano 8 (2014) 986–993, http://dx.doi.org/10.1021/nn405826k.
[77] G.S. Doerk, C. Carraro, R. Maboudian, Single nanowire thermal conductivity measurements by Raman thermography, ACS Nano 4 (2010) 4908–4914, http://dx.doi.org/10.1021/nn1012429.
[78] R.M. Costescu, M.A. Wall, D.G. Cahill, Thermal conductance of epitaxial interfaces, Phys. Rev. B 67 (2003) 054302, http://dx.doi.org/10.1103/PhysRevB.67.054302.
[79] D.G. Cahill, Analysis of heat flow in layered structures for time-domain thermoreflectance, Rev. Sci. Instrum. 75 (2004) 5119–5122, http://dx.doi.org/10.1063/1.1819431.
[80] B.C. Gundrum, D.G. Cahill, R.S. Averback, Thermal conductance of metal–metal interfaces, Phys. Rev. B 72 (2005) 245426, http://dx.doi.org/10.1103/PhysRevB.72.245426.
[81] H.K. Lyeo, D.G. Cahill, Thermal conductance of interfaces between highly dissimilar materials, Phys. Rev. B 73 (2006) 144301, http://dx.doi.org/10.1103/PhysRevB.73.144301.
[82] M. Li, J.S. Kang, Y. Hu, Anisotropic thermal conductivity measurement using a new Asymmetric-Beam Time-Domain Thermoreflectance (AB-TDTR) method, Rev. Sci. Instrum. 89 (2018) 084901, http://dx.doi.org/10.1063/1.5026028.
[83] P. Jiang, B. Huang, Y.K. Koh, Accurate measurements of cross-plane thermal conductivity of thin films by dual-frequency time-domain thermoreflectance (TDTR), Rev. Sci. Instrum. 87 (2016) 075101, http://dx.doi.org/10.1063/1.4954969.
[84] B. Sun, Y.K. Koh, Understanding and eliminating artifact signals from diffusely scattered pump beam in measurements of rough samples by time-domain thermoreflectance (TDTR), Rev. Sci. Instrum. 87 (2016) 064901, http://dx.doi.org/10.1063/1.4952579.
[85] H. Jang, J.D. Wood, C.R. Ryder, M.C. Hersam, D.G. Cahill, Anisotropic thermal conductivity of exfoliated black phosphorus, Adv. Mater. 27 (2015) 8017–8022, http://dx.doi.org/10.1002/adma.201503466.
[86] P. Jiang, X. Qian, R. Yang, Time-domain thermoreflectance (TDTR) measurements of anisotropic thermal conductivity using a variable spot size approach, Rev. Sci. Instrum. 88 (2017) 074901, http://dx.doi.org/10.1063/1.4991715.
[87] J. Wang, M. Gu, X. Zhang, G. Wu, Measurements of thermal effusivity of a fine wire and contact resistance of a junction using a T type probe, Rev. Sci. Instrum. 80 (2009) 076107, http://dx.doi.org/10.1063/1.3159863.
[88] J. Liu, H. Wang, Y. Hu, W. Ma, X. Zhang, Laser flash-Raman spectroscopy method for the measurement of the thermal properties of micro/nano wires, Rev. Sci. Instrum. 86 (2015) 014901, http://dx.doi.org/10.1063/1.4904868.
[89] E.E. Michaelides, Transport properties of nanofluids. A critical review, J. Non-Equilib. Thermodyn. 38 (2013) 1–79, http://dx.doi.org/10.1515/jnetdy-2012-0023.
[90] N. Savvides, H.J. Goldsmid, Boundary scattering of phonons in fine-grained hot-pressed Ge-Si alloys. I. the dependence of lattice thermal conductivity on grain size and porosity, J. Phys. C Solid State Phys. 13 (1980) 4657–4670, http://dx.doi.org/10.1088/0022-3719/13/25/009.
[91] Q. Zhang, B. Cao, X. Zhang, M. Fujii, K. Takahashi, Size effects on the thermal conductivity of polycrystalline platinum nanofilms, J. Phys. Condens. Matter. 18 (2006) 7937–7950, http://dx.doi.org/10.1088/0953-8984/18/34/007.
[92] H. Dong, B. Wen, R. Melnik, Relative importance of grain boundaries and size effects in thermal conductivity of nanocrystalline materials, Sci. Rep. 4 (2014) 7037, http://dx.doi.org/10.1038/srep07037.

[93] G. Soyez, J.A. Eastman, L.J. Thompson, G.R. Bai, P.M. Baldo, A.W. McCormick, R.J. DiMelfi, A.A. Elmustafa, M.F. Tambwe, D.S. Stone, Grain-size-dependent thermal conductivity of nanocrystalline yttria-stabilized zirconia films grown by metal–organic chemical vapor deposition, Appl. Phys. Lett. 77 (2000) 1155–1157, http://dx.doi.org/10.1063/1.1289803.
[94] L. Qiu, X. Zheng, J. Zhu, G. Su, D. Tang, The effect of grain size on the lattice thermal conductivity of an individual polyacrylonitrile-based carbon fiber, Carbon 51 (2013) 265–273, http://dx.doi.org/10.1016/j.carbon.2012.08.052.
[95] K. Watari, K. Hirao, M. Toriyama, K. Ishizaki, Effect of grain size on the thermal conductivity of si_3n_4, J. Am. Ceram. Soc. 82 (1999) 777–779, http://dx.doi.org/10.1111/j.1151-2916.1999.tb01835.x.
[96] Y. Ohishi, J. Xie, Y. Miyazaki, Y. Aikebaier, H. Muta, K. Kurosaki, S. Yamanaka, N. Uchida, T. Tada, Thermoelectric properties of heavily boron- and phosphorus-doped silicon, Japan. J. Appl. Phys. 54 (2015) 071301, http://dx.doi.org/10.7567/JJAP.54.071301.
[97] M. Mohr, L. Daccache, S. Horvat, K. Brühne, T. Jacob, H.J. Fecht, Influence of grain boundaries on elasticity and thermal conductivity of nanocrystalline diamond films, Acta Mater. 122 (2017) 92–98, http://dx.doi.org/10.1016/j.actamat.2016.09.042.
[98] J. Anaya, S. Rossi, M. Alomari, E. Kohn, L. Tóth, B. Pécz, K.D. Hobart, T.J. Anderson, T.I. Feygelson, B.B. Pate, M. Kuball, Control of the in-plane thermal conductivity of ultra-thin nanocrystalline diamond films through the grain and grain boundary properties, Acta Mater. 103 (2016) 141–152, http://dx.doi.org/10.1016/j.actamat.2015.09.045.
[99] Y. Li, A. Wei, D. Datta, Thermal characteristics of graphene nanoribbons endorsed by surface functionalization, Carbon 113 (2017) 274–282, http://dx.doi.org/10.1016/j.carbon.2016.11.067.
[100] M.D. Losego, M.E. Grady, N.R. Sottos, D.G. Cahill, P.V. Braun, Effects of chemical bonding on heat transport across interfaces, Nature Mater. 11 (2012) 502–506, http://dx.doi.org/10.1038/nmat3303.
[101] P.J. O'Brien, S. Shenogin, J. Liu, P.K. Chow, D. Laurencin, P.H. Mutin, M. Yamaguchi, P. Keblinski, G. Ramanath, Bonding-induced thermal conductance enhancement at inorganic heterointerfaces using nanomolecular monolayers, Nature Mater. 12 (2013) 118–122, http://dx.doi.org/10.1038/nmat3465.
[102] S. Majumdar, J.A. Sierra-Suarez, S.N. Schiffres, W.L. Ong, C.F. Higgs, A.J.H. McGaughey, J.A. Malen, Vibrational mismatch of metal leads controls thermal conductance of self-assembled monolayer junctions, Nano Lett. 15 (2015) 2985–2991, http://dx.doi.org/10.1021/nl504844d.
[103] K. Zheng, F. Sun, J. Zhu, Y. Ma, X. Li, D. Tang, F. Wang, X. Wang, Enhancing the thermal conductance of polymer and sapphire interface via self-assembled monolayer, ACS Nano 10 (2016) 7792–7798, http://dx.doi.org/10.1021/acsnano.6b03381.
[104] N. Behabtu, C.C. Young, D.E. Tsentalovich, O. Kleinerman, X. Wang, A.W. Ma, E.A. Bengio, R.F. Waarbeek, J.J. Jong, R.E. Hoogerwerf, S.B. Fairchild, J.B. Ferguson, B. Maruyama, J. Kono, Y. Talmon, Y. Cohen, M.J. Otto, M. Pasquali, Strong, light, Multifunctional fibers of carbon nanotubes with ultrahigh conductivity, Science 339 (2013) 182–186, http://dx.doi.org/10.1126/science.1228061.
[105] A.A. Balandin, Thermal properties of graphene and nanostructured carbon materials, Nature Mater. 10 (2011) 569–581, http://dx.doi.org/10.1038/nmat3064.
[106] S. Hu, J. Chen, N. Yang, B. Li, Thermal transport in graphene with defect and doping: Phonon modes analysis, Carbon 116 (2017) 139–144, http://dx.doi.org/10.1016/j.carbon.2017.01.089.
[107] B. Mortazavi, S. Ahzi, Molecular dynamics study on the thermal conductivity and mechanical properties of boron doped graphene, Solid State Commun. 152 (2012) 1503–1507, http://dx.doi.org/10.1016/j.ssc.2012.04.048.
[108] E.K. Goharshadi, S.J. Mahdizadeh, Thermal conductivity and heat transport properties of nitrogen-doped graphene, J. Mol. Graph. Model. 62 (2015) 74–80, http://dx.doi.org/10.1016/j.jmgm.2015.09.008.
[109] T. Zhang, J. Li, Y. Cao, L. Zhu, G. Chen, Tailoring thermal transport properties of graphene by nitrogen doping, J. Nanopart. Res. 19 (2017) 48, http://dx.doi.org/10.1007/s11051-017-3749-2.
[110] W. Lee, K.D. Kihm, H.G. Kim, W. Lee, S. Cheon, S. Yeom, G. Lim, K.R. Pyun, S.H. Ko, S. Shin, Two orders of magnitude suppression of graphene's thermal conductivity by heavy dopant (Si), Carbon 138 (2018) 98–107, http://dx.doi.org/10.1016/j.carbon.2018.05.064.
[111] J. Li, L. Porter, S. Yip, Atomistic modeling of finite-temperature properties of crystalline β-SiC II. Thermal conductivity and effects of point defects, J. Nucl. Mater. 255 (1998) 139–152, http://dx.doi.org/10.1016/S0022-3115(98)00034-8.
[112] H. Malekpour, P. Ramnani, S. Srinivasan, G. Balasubramanian, D.L. Nika, A. Mulchandani, R.K. Lake, A.A. Balandin, Thermal conductivity of graphene with defects induced by electron beam irradiation, Nanoscale 8 (2016) 14608–14616, http://dx.doi.org/10.1039/C6NR03470E.
[113] J. Haskins, A. Kinaci, C. Sevik, H. Sevinçli, G. Cuniberti, T. Çağin, Control of thermal and electronic transport in defect-engineered graphene nanoribbons, ACS Nano 5 (2011) 3779–3787, http://dx.doi.org/10.1021/nn200114p.
[114] H. Zhang, G. Lee, K. Cho, Thermal transport in graphene and effects of vacancy defects, Phys. Rev. B 84 (2011) 115460, http://dx.doi.org/10.1103/PhysRevB.84.115460.
[115] T. Feng, X. Ruan, Z. Ye, B. Cao, Spectral phonon mean free path and thermal conductivity accumulation in defected graphene: The effects of defect type and concentration, Phys. Rev. B 91 (2015) 224301, http://dx.doi.org/10.1103/PhysRevB.91.224301.
[116] J. Hu, S. Schiffli, A. Vallabhaneni, X. Ruan, Y.P. Chen, Tuning the thermal conductivity of graphene nanoribbons by edge passivation and isotope engineering: A molecular dynamics study, Appl. Phys. Lett. 97 (2010) 133107, http://dx.doi.org/10.1063/1.3491267.
[117] S.K. Chien, Y.T. Yang, C.K. Chen, Influence of chemisorption on the thermal conductivity of graphene nanoribbons, Carbon 50 (2012) 421–428, http://dx.doi.org/10.1016/j.carbon.2011.08.056.
[118] K. Chen, W. Li, W. Duan, Z. Shuai, B. Gu, Effect of defects on the thermal conductivity in a nanowire, Phys. Rev. B 72 (2005) 045422, http://dx.doi.org/10.1103/PhysRevB.72.045422.
[119] T.H. Fang, Z.W. Lee, W.J. Chang, C.C. Huang, Determining porosity effect on the thermal conductivity of single-layer graphene using a molecular dynamics simulation, Phys. E 106 (2019) 90–94, http://dx.doi.org/10.1016/j.physe.2018.10.017.
[120] E. Pop, V. Varshney, A.K. Roy, Thermal properties of graphene: Fundamentals and applications, MRS Bull. 37 (2012) 1273–1281, http://dx.doi.org/10.1557/mrs.2012.203.
[121] Z.W. Tan, J.S. Wang, C.K. Gan, First-principles study of heat transport properties of graphene nanoribbons, Nano Lett. 11 (2011) 214–219, http://dx.doi.org/10.1021/nl103508m.
[122] J.D. Renteria, S. Ramirez, H. Malekpour, B. Alonso, A. Centeno, A. Zurutuza, A.I. Cocemasov, D.L. Nika, A.A. Balandin, Strongly anisotropic thermal conductivity of free-standing reduced graphene oxide films annealed at high temperature, Adv. Funct. Mater. 25 (2015) 4664–4672, http://dx.doi.org/10.1002/adfm.201501429.
[123] T. Xie, Y. He, Z. Hu, Theoretical study on thermal conductivities of silica aerogel composite insulating material, Int. J. Heat Mass Transfer 58 (2013) 540–552, http://dx.doi.org/10.1016/j.ijheatmasstransfer.2012.11.016.
[124] T.P. Teng, C.M. Cheng, C.P. Cheng, Performance assessment of heat storage by phase change materials containing MWCNTs and graphite, Appl. Therm. Eng. 50 (2013) 637–644, http://dx.doi.org/10.1016/j.applthermaleng.2012.07.002.
[125] M. Li, A nano-graphite/paraffin phase change material with high thermal conductivity, Appl. Energy 106 (2013) 25–30, http://dx.doi.org/10.1016/j.apenergy.2013.01.031.
[126] L. Fan, X. Fang, X. Wang, Y. Zeng, Y. Xiao, Z. Yu, X. Xu, Y. Hu, K. Cen, Effects of various carbon nanofillers on the thermal conductivity and energy storage properties of paraffin-based nanocomposite phase change materials, Appl. Energy 110 (2013) 163–172, http://dx.doi.org/10.1016/j.apenergy.2013.04.043.

[127] T. Ma, Z. Liu, J. Wen, Y. Gao, X. Ren, H. Chen, C. Jin, X.L. Ma, N. Xu, H.M. Cheng, W. Ren, Tailoring the thermal and electrical transport properties of graphene films by grain size engineering, Nature Commun. 8 (2017) 14486, http://dx.doi.org/10.1038/ncomms14486.
[128] C. Yu, L. Shi, Z. Yao, D. Li, A. Majumdar, Thermal conductance and thermopower of an individual single-wall carbon nanotube, Nano Lett. 5 (2005) 1842–1846, http://dx.doi.org/10.1021/nl051044e.
[129] X.D. Din, E.E. Michaelides, Kinetic theory and molecular dynamics simulations of microscopic flows, Phys. Fluids 9 (1997) 3915–3925, http://dx.doi.org/10.1063/1.869490.
[130] Z. Xu, M.J. Buehler, Nanoengineering heat transfer performance at carbon nanotube interfaces, ACS Nano 3 (2009) 2767–2775, http://dx.doi.org/10.1021/nn9006237.
[131] V. Varshney, S.S. Patnaik, A.K. Roy, G. Froudakis, B.L. Farmer, P. Architectures, V. Varshney, S.S. Patnaik, A.K. Roy, G. Froudakis, B.L. Farmer, Modeling of thermal transport in pillared-graphene architectures, ACS Nano 4 (2010) 1153–1161, http://dx.doi.org/10.1021/nn901341r.
[132] N. Yang, G. Zhang, B. Li, Violation of Fourier's law and anomalous heat diffusion in silicon nanowires, Nano Today 5 (2010) 85–90, http://dx.doi.org/10.1016/j.nantod.2010.02.002.
[133] Y. Zhou, X. Zhang, M. Hu, Nonmonotonic diameter dependence of thermal conductivity of extremely thin Si nanowires: Competition between hydrodynamic phonon flow and boundary scattering, Nano Lett. 17 (2017) 1269–1276, http://dx.doi.org/10.1021/acs.nanolett.6b05113.
[134] A. Soleimani, H. Araghi, Z. Zabihi, A. Alibakhshi, A comparative study of molecular dynamics simulation methods for evaluation of the thermal conductivity and phonon transport in Si nanowires, Comput. Mater. Sci. 142 (2018) 346–354, http://dx.doi.org/10.1016/j.commatsci.2017.10.024.
[135] R.J. Stevens, L.V. Zhigilei, P.M. Norris, Effects of temperature and disorder on thermal boundary, Int. J. Heat Mass Transfer 50 (2007) 3977–3989, http://dx.doi.org/10.1016/j.ijheatmasstransfer.2007.01.040.
[136] Z. Liang, H.L. Tsai, Reduction of solid–solid thermal boundary resistance by inserting an interlayer, Int. J. Heat Mass Transfer 55 (2012) 2999–3007, http://dx.doi.org/10.1016/j.ijheatmasstransfer.2012.02.019.
[137] S. Merabia, K. Termentzidis, Thermal conductance at the interface between crystals using equilibrium and nonequilibrium molecular dynamics, Phys. Rev. B 86 (2012) 094303, http://dx.doi.org/10.1103/PhysRevB.86.094303.
[138] K. Termentzidis, S. Merabia, P. Chantrenne, P. Keblinski, Cross-plane thermal conductivity of superlattices with rough interfaces using equilibrium and non-equilibrium molecular dynamics, Int. J. Heat Mass Transfer 54 (2011) 2014–2020, http://dx.doi.org/10.1016/j.ijheatmasstransfer.2011.01.001.
[139] A. Majumdar, P. Reddy, Role of electron–phonon coupling in thermal conductance of metal–nonmetal interfaces, Appl. Phys. Lett. 84 (2004) 4768–4770, http://dx.doi.org/10.1063/1.1758301.
[140] Y. Wang, X. Ruan, A.K. Roy, Two-temperature nonequilibrium molecular dynamics simulation of thermal transport across metal-nonmetal interfaces, Phys. Rev. B 85 (2012) 205311, http://dx.doi.org/10.1103/PhysRevB.85.205311.
[141] P. Singh, M. Seong, S. Sinha, Detailed consideration of the electron–phonon thermal conductance at metal–dielectric interfaces, Appl. Phys. Lett. 102 (2013) 181906, http://dx.doi.org/10.1063/1.4804383.
[142] C.W. Chang, A.M. Fennimore, A. Afanasiev, D. Okawa, T. Ikuno, H. Garcia, D. Li, A. Majumdar, A. Zettl, Isotope effect on the thermal conductivity of boron nitride nanotubes, Phys. Rev. Lett. 97 (2006) 085901, http://dx.doi.org/10.1103/PhysRevLett.97.085901.
[143] L. Lindsay, D.A. Broido, N. Mingo, Diameter dependence of carbon nanotube thermal conductivity and extension to the graphene limit, Phys. Rev. B 82 (2010) 161402, http://dx.doi.org/10.1103/PhysRevB.82.161402.
[144] J. Che, T. Çagin, W.A. Goddard III, Thermal conductivity of carbon nanotubes, Nanotechnology 11 (2000) 65–69, http://dx.doi.org/10.1088/0957-4484/11/2/305.
[145] S. Berber, Y.K. Kwon, D. Tománek, Unusually high thermal conductivity of carbon nanotubes, Phys. Rev. Lett. 84 (2000) 4613–4616, http://dx.doi.org/10.1103/PhysRevLett.84.4613.
[146] D. Donadio, G. Galli, Thermal conductivity of isolated and interacting carbon nanotubes: Comparing results from molecular dynamics and the Boltzmann transport equation, Phys. Rev. Lett. 99 (2007) 255502, http://dx.doi.org/10.1103/PhysRevLett.99.255502.
[147] I. Ivanov, A. Puretzky, G. Eres, H. Wang, Z. Pan, H. Cui, R. Jin, J. Howe, D.B. Geohegan, Fast and highly anisotropic thermal transport through vertically aligned carbon nanotube arrays, Appl. Phys. Lett. 89 (2006) 2004–2007, http://dx.doi.org/10.1063/1.2397008.
[148] D. Yang, Q. Zhang, G. Chen, S.F. Yoon, J. Ahn, S. Wang, Q. Zhou, Q. Wang, J. Li, Thermal conductivity of multiwalled carbon nanotubes, Phys. Rev. B 66 (2002) 165440, http://dx.doi.org/10.1103/PhysRevB.66.165440.
[149] R. Jin, Z. Zhou, D. Mandrus, I.N. Ivanov, G. Eres, J.Y. Howe, A.A. Puretzky, D.B. Geohegan, The effect of annealing on the electrical and thermal transport properties of macroscopic bundles of long multi-wall carbon nanotubes, Phys. B 388 (2007) 326–330, http://dx.doi.org/10.1016/j.physb.2006.06.135.
[150] W. Yi, L. Lu, D. Zhang, Z. Pan, S. Xie, Linear specific heat of carbon nanotubes, Phys. Rev. B 59 (1999) R9015–R9018, http://dx.doi.org/10.1103/PhysRevB.59.R9015.
[151] A.E. Aliev, M.H. Lima, E.M. Silverman, R.H. Baughman, Thermal conductivity of multi-walled carbon nanotube sheets: Radiation losses and quenching of phonon modes, Nanotechnology 21 (2010) 035709, http://dx.doi.org/10.1088/0957-4484/21/3/035709.
[152] J.E. Fischer, W. Zhou, J. Vavro, M.C. Llaguno, C. Guthy, R. Haggenmueller, M.J. Casavant, D.E. Walters, R.E. Smalley, Magnetically aligned single wall carbon nanotube films: Preferred orientation and anisotropic transport properties, J. Appl. Phys. 93 (2003) 2157–2163, http://dx.doi.org/10.1063/1.1536733.
[153] T.S. Gspann, S.M. Juckes, J.F. Niven, M.B. Johnson, J.A. Elliott, M.A. White, A.H. Windle, High thermal conductivities of carbon nanotube films and micro-fibres and their dependence on morphology, Carbon 114 (2017) 160–168, http://dx.doi.org/10.1016/j.carbon.2016.12.006.
[154] J. Hone, M.C. Llaguno, N.M. Nemes, A.T. Johnson, J.E. Fischer, D.A. Walters, M.J. Casavant, J. Schmidt, R.E. Smalley, Electrical and thermal transport properties of magnetically aligned single wall carbon nanotube films, Appl. Phys. Lett. 77 (2000) 666–668, http://dx.doi.org/10.1063/1.127079.
[155] E. Muñoz, J. Lu, B.I. Yakobson, Ballistic thermal conductance of graphene ribbons, Nano Lett. 10 (2010) 1652–1656, http://dx.doi.org/10.1021/nl904206d.
[156] Z. Han, A. Fina, Thermal conductivity of carbon nanotubes and their polymer nanocomposites: A review, Prog. Polym. Sci. 36 (2011) 914–944, http://dx.doi.org/10.1016/j.progpolymsci.2010.11.004.
[157] X. Jiang, Q. Weng, X. Wang, X. Li, J. Zhang, D. Golberg, Y. Bando, Recent progress on fabrications and applications of boron nitride nanomaterials: A review, J. Mater. Sci. Technol. 31 (2015) 589–598, http://dx.doi.org/10.1016/j.jmst.2014.12.008.
[158] V. Guerra, C. Wan, T. McNally, Thermal conductivity of 2d nano-structured boron nitride (BN) and its composites with polymers, Prog. Mater. Sci. 100 (2019) 170–186, http://dx.doi.org/10.1016/j.pmatsci.2018.10.002.
[159] X. Zheng, L. Qiu, G. Su, D. Tang, Y. Liao, Y. Chen, Thermal conductivity and thermal diffusivity of SiO_2 nanopowder, J. Nanopart. Res. 13 (2011) 6887–6893, http://dx.doi.org/10.1007/s11051-011-0596-4.
[160] L.W. Hrubesh, Aerogel applications, J. Non-Cryst. Solids 225 (1998) 335–342, http://dx.doi.org/10.1016/S0022-3093(98)00135-5.
[161] E.T. Afriyie, P. Karami, P. Norberg, K. Gudmundsson, Textural and thermal conductivity properties of a low density mesoporous silica material, Energy Build. 75 (2014) 210–215, http://dx.doi.org/10.1016/j.enbuild.2014.02.012.
[162] J. Wang, J. Kuhn, X. Lu, Monolithic silica aerogel insulation doped with TiO_2 powder and ceramic fibers, J. Non-Cryst. Solids 186 (1995) 296–300, http://dx.doi.org/10.1016/0022-3093(95)00068-2.

[163] F. Tian, B. Song, X. Chen, N.K. Ravichandran, Y. Lv, K. Chen, S. Sullivan, J. Kim, Y. Zhou, T.H. Liu, M. Goni, Z. Ding, J. Sun, G. Amila, G.U. Gamage, H. Sun, H. Ziyaee, S. Huyan, L. Deng, J. Zhou, A.J. Schmidt, S. Chen, C.W. Chu, P.Y. Huang, D. Broido, L. Shi, G. Chen, Z. Ren, High thermal conductivity in cubic boron arsenide crystals, Science 361 (2018) 582–585.
[164] P. Yue, L. Qiu, X. Zheng, D. Tang, The effective thermal conductivity of porous polymethacrylimide foams, Key Eng. Mater. 609–610 (2014) 196–200, http://dx.doi.org/10.4028/www.scientific.net/KEM.609-610.196.
[165] J. Li, J. Yin, T. Ji, Y. Feng, Y. Liu, H. Zhao, Y. Li, C. Zhu, D. Yue, B. Su, X. Liu, Microstructure evolution effect on high-temperature thermal conductivity of LDPE/BNNS investigated by in-situ SAXS, Mater. Lett. 234 (2019) 74–78, http://dx.doi.org/10.1016/j.matlet.2018.09.061.
[166] G. Kalaprasad, P. Pradeep, G. Mathew, C. Pavithran, S. Thomas, Thermal conductivity and thermal diffusivity analyses of low-density polyethylene composites reinforced with sisal, glass and intimately mixed sisal/glass fibres, Compos. Sci. Technol. 60 (2000) 2967–2977, http://dx.doi.org/10.1016/S0266-3538(00)00162-7.
[167] F. Mashali, E.M. Languri, J. Davidson, D. Kerns, W. Johnson, K. Nawaz, G. Cunningham, Thermo-physical properties of diamond nanofluids: A review, Int. J. Heat Mass Transfer 129 (2019) 1123–1135, http://dx.doi.org/10.1016/j.ijheatmasstransfer.2018.10.033.
[168] J. Guo, X. Wang, T. Wang, Thermal characterization of microscale conductive and nonconductive wires using transient electrothermal technique, J. Appl. Phys. 101 (2007) 063537, http://dx.doi.org/10.1063/1.2714679.
[169] A.M. Papadopoulos, State of the art in thermal insulation materials and aims for future developments, Energy Build. 37 (2005) 77–86, http://dx.doi.org/10.1016/j.enbuild.2004.05.006.
[170] H. Xie, A. Cai, X. Wang, Thermal diffusivity and conductivity of multiwalled carbon nanotube arrays, Phys. Lett. A 369 (2007) 120–123, http://dx.doi.org/10.1016/j.physleta.2007.02.079.
[171] Q. Li, X. Zhang, K. Takahashi, Variable-spot-size laser-flash Raman method to measure in-plane and interfacial thermal properties of 2D van der Waals heterostructures, Int. J. Heat Mass Transfer 125 (2018) 1230–1239, http://dx.doi.org/10.1016/j.ijheatmasstransfer.2018.05.011.
[172] J. Hou, X. Wang, C. Liu, H. Cheng, Development of photothermal-resistance technique and its application to thermal diffusivity measurement of single-wall carbon nanotube bundles, Appl. Phys. Lett. 88 (2006) 181910, http://dx.doi.org/10.1063/1.2199614.
[173] L.I. Giri, S. Tuli, M. Sharma, P. Bugnon, H. Berger, A. Magrez, Thermal diffusivity measurements of templated nanocomposite using infrared thermography, Mater. Lett. 115 (2014) 106–108, http://dx.doi.org/10.1016/j.matlet.2013.10.042.
[174] W.J. Parker, R.J. Jenkins, C.P. Butler, G.L. Abbott, Flash method of determining thermal diffusivity, heat capacity, and thermal conductivity, J. Appl. Phys. 32 (1961) 1679–1684, http://dx.doi.org/10.1063/1.1728417.
[175] J. Blumm, A. Lindemann, S. Min, Thermal characterization of liquids and pastes using the flash technique, Thermochim. Acta 455 (2007) 26–29, http://dx.doi.org/10.1016/j.tca.2006.11.023.
[176] W. Lin, J. Shang, W. Gu, C.P. Wong, Parametric study of intrinsic thermal transport in vertically aligned multi-walled carbon nanotubes using a laser flash technique, Carbon 50 (2012) 1591–1603, http://dx.doi.org/10.1016/j.carbon.2011.11.038.
[177] M. Akoshima, K. Hata, D.N. Futaba, K. Mizuno, T. Baba, M. Yumura, Thermal diffusivity of single-walled carbon nanotube forest measured by laser flash method, Japan. J. Appl. Phys. 48 (2009) 05EC07, http://dx.doi.org/10.1143/JJAP.48.05EC07.
[178] X. Zhang, D. Sun, Y. Li, G.H. Lee, X. Cui, D. Chenet, Y. You, T.F. Heinz, J.C. Hone, Measurement of lateral and interfacial thermal conductivity of single- and bilayer MoS_2 and $MoSe_2$ using refined optothermal Raman technique, ACS Appl. Mater. Interfaces 7 (2015) 25923–25929, http://dx.doi.org/10.1021/acsami.5b08580.
[179] P. Thiyagarajan, Z. Yan, J.C. Yoon, M.W. Oh, J.H. Jang, Thermal conductivity reduction in three dimensional graphene-based nanofoam, RSC Adv. 5 (2015) 99394–99397, http://dx.doi.org/10.1039/c5ra19130k.
[180] Q. Li, W. Ma, X. Zhang, Laser flash Raman spectroscopy method for characterizing thermal diffusivity of supported 2D nanomaterials, Int. J. Heat Mass Transfer 95 (2016) 956–963, http://dx.doi.org/10.1016/j.ijheatmasstransfer.2015.12.065.
[181] C. Xing, T. Munro, C. Jensen, H. Ban, C.G. Copeland, R.V. Lewis, Thermal characterization of natural and synthetic spider silks by both the 3ω and transient electrothermal methods, Mater. Des. 119 (2017) 22–29, http://dx.doi.org/10.1016/j.matdes.2017.01.057.
[182] C. Xing, T. Munro, C. Jensen, H. Ban, Analysis of the electrothermal technique for thermal property characterization of thin fibers, Meas. Sci. Technol. 24 (2013) 105603, http://dx.doi.org/10.1088/0957-0233/24/10/105603.
[183] X. Feng, X. Wang, Thermophysical properties of free-standing micrometer-thick poly(3-hexylthiophene) films, Thin Solid Films 519 (2011) 5700–5705, http://dx.doi.org/10.1016/j.tsf.2011.03.043.
[184] X. Huang, J. Wang, G. Eres, X. Wang, Thermophysical properties of multi-wall carbon nanotube bundles at elevated temperatures up to 830 K, Carbon 49 (2011) 1680–1691, http://dx.doi.org/10.1016/j.carbon.2010.12.053.
[185] X. Huang, G. Liu, X. Wang, New secrets of spider silk: Exceptionally high thermal conductivity and its abnormal change under stretching, Adv. Mater. 24 (2012) 1482–1486, http://dx.doi.org/10.1002/adma.201104668.
[186] J. Hou, X. Wang, J. Guo, Thermal characterization of micro/nanoscale conductive and non-conductive wires based on optical heating and electrical thermal sensing, J. Phys. D Appl. Phys. 39 (2006) 3362–3370, http://dx.doi.org/10.1088/0022-3727/39/15/021.
[187] J. Hou, X. Wang, L. Zhang, Thermal characterization of submicron polyacrylonitrile fibers based on optical heating and electrical thermal sensing, Appl. Phys. Lett. 89 (2006) 152504, http://dx.doi.org/10.1063/1.2358952.
[188] C.S. Welch, D.M. Heath, W.P. Winfree, Remote measurement of in-plane diffusivity components in plates, J. Appl. Phys. 61 (1987) 895–898, http://dx.doi.org/10.1063/1.338140.
[189] A. Mendioroz, R. Fuente-Dacal, E. Apianiz, A. Salazar, Thermal diffusivity measurements of thin plates and filaments using lock-in thermography, Rev. Sci. Instrum. 80 (2009) 074904, http://dx.doi.org/10.1063/1.3176467.
[190] K. Sakai, Y. Kobayashi, T. Saito, A. Isogai, Partitioned airs at microscale and nanoscale: Thermal diffusivity in ultrahigh porosity solids of nanocellulose, Sci. Rep. 6 (2016) 20434, http://dx.doi.org/10.1038/srep20434.
[191] M.M.S. Wahsh, R.M. Khattab, N.M. Khalil, F. Gouraud, M. Huger, T. Chotard, Fabrication and technological properties of nanoporous spinel/forsterite/zirconia ceramic composites, Mater. Des. 53 (2014) 561–567, http://dx.doi.org/10.1016/j.matdes.2013.07.059.
[192] M. Venkataraman, R. Mishra, J. Militky, L. Hes, Aerogel based nanoporous fibrous materials for thermal insulation, Fibers Polym. 15 (2014) 1444–1449, http://dx.doi.org/10.1007/s12221-014-1444-9.
[193] Y. Hirata, Y. Kinoshita, T. Shimonosono, T. Chaen, Theoretical and experimental analyses of thermal properties of porous polycrystalline mullite, Ceram. Int. 43 (2017) 9973–9978, http://dx.doi.org/10.1016/j.ceramint.2017.05.009.
[194] G. Mayr, B. Plank, J. Sekelja, G. Hendorfer, Active thermography as a quantitative method for non-destructive evaluation of porous carbon fiber reinforced polymers, NDT E Int. 44 (2011) 537–543, http://dx.doi.org/10.1016/j.ndteint.2011.05.012.
[195] E. Wu, M. Li, Q. Gao, A. Mandelis, Effect of porosity on thermal diffusivity of woven carbon fiber reinforced polymers, Laser Opt. Prog. 11 (2017) 326–331, http://dx.doi.org/10.3788/LOP54.111601.
[196] J. Renteria, D. Nika, A. Balandin, Graphene thermal properties: Applications in thermal management and energy storage, Appl. Sci. 4 (2014) 525–547, http://dx.doi.org/10.3390/app4040525.
[197] T.W. Pan, W.S. Kuo, N.H. Tai, Tailoring anisotropic thermal properties of reduced graphene oxide/multi-walled carbon nanotube hybrid composite films, Compos. Sci. Technol. 151 (2017) 44–51, http://dx.doi.org/10.1016/j.compscitech.2017.07.015.
[198] R.E. Hummel, Electronic Properties of Materials, Springer Science & Business Media, New York, 2011.

[199] W.H. Tuan, T.T. Chou, C.T. Kao, S.Y. Wang, B.J. Weng, Thermal diffusivity of graphite paper and its joint with alumina substrate, J. Eur. Ceram. Soc. 38 (2018) 187–191, http://dx.doi.org/10.1016/j.jeurceramsoc.2017.07.029.
[200] E.M. Jackson, P.E. Laibinis, W.E. Collins, A. Ueda, C.D. Wingard, B. Penn, Development and thermal properties of carbon nanotube-polymer composites, Composites B 89 (2016) 362–373, http://dx.doi.org/10.1016/j.compositesb.2015.12.018.
[201] K. Voges, M. Vadala, D.C. Lupascu, Dense nanopowder composites for thermal insulation, Phys. Status Solidi Appl. Mater. Sci. 212 (2015) 439–442, http://dx.doi.org/10.1002/pssa.201431551.
[202] G. Zhan, A.K. Mukherjee, Carbon nanotube reinforced alumina-based ceramics with novel mechanical, electrical, and thermal properties, Int. J. Appl. Ceram. Technol. 1 (2004) 161–171, http://dx.doi.org/10.1111/j.1744-7402.2004.tb00166.x.
[203] T. Borca-Tasciuc, S. Vafaei, D.A. Borca-Tasciuc, B.Q. Wei, R. Vajtai, P.M. Ajayan, Anisotropic thermal diffusivity of aligned multiwall carbon nanotube arrays, J. Appl. Phys. 98 (2005) 054309, http://dx.doi.org/10.1063/1.2034079.
[204] Q. Gong, Z. Li, X. Bai, D. Li, Y. Zhao, J. Liang, Thermal properties of aligned carbon nanotube/carbon nanocomposites, Mater. Sci. Eng. A 384 (2004) 209–214, http://dx.doi.org/10.1016/j.msea.2004.06.006.
[205] Y. Yue, X. Huang, X. Wang, Thermal transport in multiwall carbon nanotube buckypapers, Phys. Lett. A 374 (2010) 4144–4151, http://dx.doi.org/10.1016/j.physleta.2010.08.034.
[206] Y. Xie, T. Wang, B. Zhu, C. Yan, P. Zhang, X. Wang, G. Eres, 19-Fold thermal conductivity increase of carbon nanotube bundles toward high-end thermal design applications, Carbon 139 (2018) 445–458, http://dx.doi.org/10.1016/j.carbon.2018.07.009.
[207] T. Wang, X. Wang, J. Guo, Z. Luo, K. Cen, Characterization of thermal diffusivity of micro/nanoscale wires by transient photo-electro-thermal technique, Appl. Phys. A 87 (2007) 599–605, http://dx.doi.org/10.1007/s00339-007-3879-y.
[208] L. Kumari, T. Zhang, G.H. Du, W.Z. Li, Q.W. Wang, A. Datye, K.H. Wu, Thermal properties of CNT-Alumina nanocomposites, Compos. Sci. Technol. 68 (2008) 2178–2183, http://dx.doi.org/10.1016/j.compscitech.2008.04.001.
[209] H. Lin, S. Xu, X. Wang, N. Mei, Significantly reduced thermal diffusivity of freestanding two-layer graphene in graphene foam, Nanotechnology 24 (2013) 415706, http://dx.doi.org/10.1088/0957-4484/24/41/415706.
[210] P. Goli, H. Ning, X. Li, C.Y. Lu, K.S. Novoselov, A.A. Balandin, Thermal properties of graphene-copper-graphene heterogeneous films, Nano Lett. 14 (2014) 1497–1503, http://dx.doi.org/10.1021/nl404719n.
[211] Z. Hou, W. Song, P. Wang, M.J. Meziani, C.Y. Kong, A. Anderson, H. Maimaiti, G.E. Lecroy, H. Qian, Y.P. Sun, Flexible graphene-graphene composites of superior thermal and electrical transport properties, ACS Appl. Mater. Interfaces 6 (2014) 15026–15032, http://dx.doi.org/10.1021/am502986j.
[212] S.N. Goyanes, J.D. Marconi, P.G. König, G.H. Rubiolo, C.L. Matteo, A.J. Marzocca, Analysis of thermal diffusivity in aluminum (particle)-filled PMMA compounds, Polymer 42 (2001) 5267–5274, http://dx.doi.org/10.1016/S0032-3861(00)00877-6.
[213] A. Prasad, A. Ambirajan, Criteria for accurate measurement of thermal diffusivity of solids using the Angstrom method, Int. J. Therm. Sci. 134 (2018) 216–223, http://dx.doi.org/10.1016/j.ijthermalsci.2018.08.007.
[214] B. Weidenfeller, M. Höfer, F.R. Schilling, Thermal conductivity, thermal diffusivity, and specific heat capacity of particle filled polypropylene, Composites A 35 (2004) 423–429, http://dx.doi.org/10.1016/j.compositesa.2003.11.005.
[215] M. Wiener, G. Reichenauer, S. Braxmeier, F. Hemberger, H.P. Ebert, Carbon aerogel-based high-temperature thermal insulation, Int. J. Thermophys. 30 (2009) 1372–1385, http://dx.doi.org/10.1007/s10765-009-0595-1.
[216] J. Feng, J. Feng, C. Zhang, Thermal conductivity of low density carbon aerogels, J. Porous Mater. 19 (2012) 551–556, http://dx.doi.org/10.1007/s10934-011-9504-7.
[217] Y. Xie, S. Xu, Z. Xu, H. Wu, C. Deng, X. Wang, Interface-mediated extremely low thermal conductivity of graphene aerogel, Carbon 98 (2016) 381–390, http://dx.doi.org/10.1016/j.carbon.2015.11.033.
[218] J.P. Holman, Heat Transfer, Tata McGraw-Hill Education, New York, 2002.
[219] A.T. Petit, P.L. Dulong, Study on the measurement of specific heat of solids, Ann. Chim. Phys. 10 (1819) 395–413.
[220] A. Einstein, Die plancksche theorie der strahlung und die theorie der spezifischen waerme, Ann. Phys.-Berlin 327 (1907) 180–190, http://dx.doi.org/10.1002/andp.19063270110.
[221] P. Debye, Zur theorie der spezifischen wärmen, Ann. Phys.-Berlin 344 (1912) 789–839, http://dx.doi.org/10.1002/andp.19123441404.
[222] L. Lu, W. Yi, D. Zhang, 3ω method for specific heat and thermal conductivity measurements, Rev. Sci. Instrum. 72 (2001) 2996–3003, http://dx.doi.org/10.1063/1.1378340.
[223] X.J. Hu, A.A. Padilla, J. Xu, T.S. Fisher, K.E. Goodson, 3-Omega measurements of vertically oriented carbon nanotubes on silicon, J. Heat Transfer-T ASME 128 (2006) 1109–1113, http://dx.doi.org/10.1115/1.2352778.
[224] L. Qiu, P. Guo, X. Yang, Y. Ouyang, Y. Feng, X. Zhang, J. Zhao, X. Zhang, Q. Li, Electro curing of oriented bismaleimide between aligned carbon nanotubes for high mechanical and thermal performances, Carbon 145 (2019) 650–657, http://dx.doi.org/10.1016/j.carbon.2019.01.074.
[225] H. Ftouni, D. Tainoff, J. Richard, K. Lulla, J. Guidi, E. Collin, O. Bourgeois, Specific heat measurement of thin suspended SiN membrane from 8 K to 300 K using the 3ω-Völklein method, Rev. Sci. Instrum. 84 (2013) 094902, http://dx.doi.org/10.1063/1.4821501.
[226] F. Völklein, H. Reith, A. Meier, Measuring methods for the investigation of in-plane and cross-plane thermal conductivity of thin films, Phys. Status Solidi 210 (2013) 106–118, http://dx.doi.org/10.1002/pssa.201228478.
[227] J.M. Schliesser, B.F. Woodfield, Lattice vacancies responsible for the linear dependence of the low-temperature heat capacity of insulating materials, Phys. Rev. B 91 (2015) 024109, http://dx.doi.org/10.1103/PhysRevB.91.024109.
[228] Q. Shi, L. Zhang, M.E. Schlesinger, J. Boerio-Goates, B.F. Woodfield, Low temperature heat capacity study of Fe_3PO_7 and $Fe_4(P_2O_7)_3$, J. Chem. Thermodyn. 62 (2013) 86–91, http://dx.doi.org/10.1016/j.jct.2013.02.023.
[229] T.H.K. Barron, G.K. White, Heat Capacity and Thermal Expansion At Low Temperatures, Springer Science & Business Media, Berlin, 2012.
[230] Q. Shi, Z. Tan, N. Yin, Low temperature calorimetry and its application in material research, Chin. Sci. Bull. 61 (2016) 3100–3114, http://engine.scichina.com/doi/10.1360/N972016-00550.
[231] Y. Zhang, C.H. Wong, J. Shen, S.T. Sze, B. Zhang, H. Zhang, Y. Dong, H. Xu, Z. Yan, Y. Li, X. Hu, R. Lortz, Dramatic enhancement of superconductivity in single-crystalline nanowire arrays of Sn, Sci. Rep. 6 (2016) 32963, http://dx.doi.org/10.1038/srep32963.
[232] D. Lee, G.D. Sim, K. Xiao, Y. Seok Choi, J.J. Vlassak, Scanning AC nanocalorimetry study of Zr/B reactive multilayers, J. Appl. Phys. 114 (2013) 214902, http://dx.doi.org/10.1063/1.4833572.
[233] K. Xiao, J.M. Gregoire, P.J. McCluskey, J.J. Vlassak, A scanning AC calorimetry technique for the analysis of nano-scale quantities of materials, Rev. Sci. Instrum. 83 (2012) 114901, http://dx.doi.org/10.1063/1.4763571.
[234] N.R. Pradhan, H. Duan, J. Liang, G.S. Iannacchione, The specific heat and effective thermal conductivity of composites containing single-wall and multi-wall carbon nanotubes, Nanotechnology 20 (2009) 245705, http://dx.doi.org/10.1088/0957-4484/20/24/245705.
[235] M. Tress, M. Erber, E.U. Mapesa, H. Huth, J. Müller, A. Serghei, C. Schick, K.J. Eichhorn, B. Voit, F. Kremer, Glassy dynamics and glass transition in nanometric thin layers of polystyrene, Macromolecules 43 (2010) 9937–9944, http://dx.doi.org/10.1021/ma102031k.
[236] V. Novotny, P.P.M. Meincke, J.H.P. Watson, Effect of size and surface on the specific heat of small lead particles, Phys. Rev. Lett. 28 (1972) 901–903, http://dx.doi.org/10.1103/PhysRevLett.28.901.
[237] J. Rupp, R. Birringer, Enhanced specific-heat-capacity (c_p) measurements (150 300 K) of nanometer-sized crystalline materials, Phys. Rev. B 36 (1987) 7888–7890, http://dx.doi.org/10.1103/PhysRevB.36.7888.

[238] B.A. Strukov, S.T. Davitadze, S.N. Kravchun, S.A. Taraskin, M. Goltzman, V.V. Lemanov, S.G. Shulman, Specific heat and heat conductivity of $BaTiO_3$ polycrystalline films in the thickness range, J. Phys. Condens. Matter 15 (2003) 4331–4340, http://dx.doi.org/10.1088/0953-8984/15/25/304.
[239] J. Seo, D. Shin, Size effect of nanoparticle on specific heat in a ternary nitrate ($LiNO_3$-$NaNO_3$-KNO_3) salt eutectic for thermal energy storage, Appl. Therm. Eng. 102 (2016) 144–148, http://dx.doi.org/10.1016/j.applthermaleng.2016.03.134.
[240] M. Singh, S. Lara, S. Tlali, Effects of size and shape on the specific heat, melting entropy and enthalpy of nanomaterials, J. Taibah Univ. Sci. 11 (2017) 922–929, http://dx.doi.org/10.1016/j.jtusci.2016.09.011.
[241] B. Wang, L. Zhou, X. Peng, Surface and size effects on the specific heat capacity of nanoparticles, Int. J. Thermophys. 27 (2006) 139–151, http://dx.doi.org/10.1007/s10765-006-0022-9.
[242] N. Arora, D.P. Joshi, U. Pachauri, Effect of size and dimension dependent specific heat on thermal conductivity of nanostructured semiconductors, Mater. Chem. Phys. 217 (2018) 235–241, http://dx.doi.org/10.1016/j.matchemphys.2018.05.071.
[243] A.I. Gusev, Effects of the nanocrystalline state in solids, Usp.Fiz. Nauk 41 (1998) 49–76, http://dx.doi.org/10.1070/PU1998v041n01ABEH000329.
[244] J.F. Tang, X.S. Li, W.Y. Long, Y. Wang, Vibrational properties in nanocrystalline nickels: Temperature effects and composite model for thermodynamics, Phys. Status Solidi 245 (2008) 1527–1533, http://dx.doi.org/10.1002/pssb.200743160.
[245] D. Wolf, J. Wang, S.R. Phillpot, H. Gleiter, Phonon-induced anomalous specific heat of a nanocrystalline model material by computer simulation, Phys. Rev. Lett. 74 (1995) 4686–4689, http://dx.doi.org/10.1103/PhysRevLett.74.4686.
[246] N. Sun, K. Lu, Heat-capacity comparison among the nanocrystalline, amorphous, and coarse-grained polycrystalline states in element selenium, Phys. Rev. B 54 (1996) 6058–6061, http://dx.doi.org/10.1103/PhysRevB.54.6058.
[247] D.P. Rojas, L. Fernández Barquín, J. Rodríguez Fernández, L. Rodríguez Fernández, J. Gonzalez, Phonon softening on the specific heat of nanocrystalline metals, Nanotechnology 21 (2010) 445702, http://dx.doi.org/10.1088/0957-4484/21/44/445702.
[248] Y. Li, J. Luo, Y. Yi, H. Zhu, Z. Gan, X. Ji, H. Lei, Study on low temperature specific heat capacity of Aluminum nanocrystalline, J. Synth. Cryst. 43 (2014) 676–681, http://dx.doi.org/10.16553/j.cnki.issn1000-985x.2014.03.015.
[249] S.P. Adiga, V.P. Adiga, R.W. Carpick, D.W. Brenner, Vibrational properties and specific heat of ultrananocrystalline diamond: Molecular dynamics simulations, J. Phys. Chem. C 115 (2011) 21691–21699, http://dx.doi.org/10.1021/jp207424m.
[250] H.Y. Bai, J.L. Luo, D. Jin, J.R. Sun, Particle size and interfacial effect on the specific heat of nanocrystalline Fe, J. Appl. Phys. 79 (1996) 361–364, http://dx.doi.org/10.1063/1.360838.
[251] H. Lei, J. Luo, J. Li, F. Dai, M. Yang, J. Zhang, J. Zhang, Anomalous specific heats of metallic nanocrystals induced by surface oxidation, Appl. Phys. Lett. 109 (2016) 213106, http://dx.doi.org/10.1063/1.4968815.
[252] R.C. Zeller, R.O. Pohl, Thermal conductivity and specific heat of noncrystalline solids, Phys. Rev. B 4 (1971) 2029–2041, http://dx.doi.org/10.1103/PhysRevB.4.2029.
[253] D. Gerlich, B. Abeles, R.E. Miller, High-temperature specific heats of Ge, Si, and Ge-Si alloys, J. Appl. Phys. 36 (1965) 76–79, http://dx.doi.org/10.1063/1.1713926.
[254] J.M. Ziman, Electrons and Phonons: The Theory of Transport Phenomena in Solids, Oxford university press, London, 2001.
[255] J. Hone, B. Batlogg, Z. Benes, A.T. Johnson, J.E. Fischer, Quantized phonon spectrum of single-wall carbon nanotubes, Science 289 (2000) 1730–1733, http://dx.doi.org/10.1126/science.289.5485.1730.
[256] Y. Li, X. Qiu, Y. Yin, F. Yang, Q. Fan, The specific heat of carbon nanotube networks and their potential applications, J. Phys. D: Appl. Phys. 42 (2009) 155405, http://dx.doi.org/10.1126/10.1088/0022-3727/42/15/155405.
[257] V.N. Popov, Low-temperature specific heat of nanotube systems, Phys. Rev. B 66 (2002) 153408, http://dx.doi.org/10.1103/PhysRevB.66.153408.
[258] B. Xiang, C.B. Tsai, C.J. Lee, D.P. Yu, Y.Y. Chen, Low-temperature specific heat of double wall carbon nanotubes, Solid State Commun. 138 (2006) 516–520, http://dx.doi.org/10.1016/j.ssc.2006.04.022.
[259] J.C. Lasjaunias, K. Biljaković, Z. Benes, J.E. Fischer, P. Monceau, Low-temperature specific heat of single-wall carbon nanotubes, Phys. Rev. B 65 (2002) 113409, http://dx.doi.org/10.1103/PhysRevB.65.113409.
[260] A. Alofi, G.P. Srivastava, Phonon conductivity in graphene, J. Appl. Phys. 112 (2012) 013517, http://dx.doi.org/10.1063/1.4733690.
[261] D.L. Nika, A.I. Cocemasov, A.A. Balandin, Specific heat of twisted bilayer graphene: Engineering phonons by atomic plane rotations, Appl. Phys. Lett. 105 (2014) 031904, http://dx.doi.org/10.1063/1.4890622.
[262] H. Zhang, H. Lei, Y. Tang, J. Luo, K. Li, X. Deng, Thermal capacity of nanocrystalline copper at low temperatures, Acta Phys. Sin. 59 (2010) 471–475, http://dx.doi.org/10.7666/d.y1820142.
[263] K. Khanafer, K. Vafai, A critical synthesis of thermophysical characteristics of nanofluids, Int. J. Heat Mass Transfer 54 (2011) 4410–4428, http://dx.doi.org/10.1016/j.ijheatmasstransfer.2011.04.048.
[264] N. Putra, W. Roetzel, S.K. Das, Natural convection of nano-fluids, Heat Mass Transfer 39 (2003) 775–784, http://dx.doi.org/10.1007/s00231-002-0382-z.
[265] E.E. Michaelides, Nanofluidics: Thermodynamic and Transport Properties, Springer, New York, 2014.
[266] J.C. Maxwell, A Treatise on Electricity and Magnetism, Clarendon Press, Oxford, 1873.
[267] R.L. Hamilton, Thermal conductivity of heterogeneous two-component systems, Ind. Eng. Chem. Fundam. 1 (1962) 187–191, http://dx.doi.org/10.1021/i160003a005.
[268] D.A.G. Bruggeman, Berechnung verschiedener physikalischer Konstanten von heterogenen substanzen. I. Dielektrizitätskonstanten und leitfähigkeiten der mischkörper aus isotropen substanzen, Ann. Phys. 416 (1935) 636–664, http://dx.doi.org/10.1002/andp.19354160705.
[269] W. Yu, S.U.S. Choi, The role of interfacial layers in the enhanced thermal conductivity of nanofluids: A renovated Maxwell model, J. Nanopart. Res. 5 (2003) 167–171, http://dx.doi.org/10.1023/A:1024438603801.
[270] Q. Xue, W. Xu, A model of thermal conductivity of nanofluids with interfacial shells, Mater. Chem. Phys. 90 (2005) 298–301, http://dx.doi.org/10.1016/j.matchemphys.2004.05.029.
[271] S.P. Jang, S.U.S. Choi, Role of Brownian motion in the enhanced thermal conductivity of nanofluids, Appl. Phys. Lett. 84 (2004) 4316–4318, http://dx.doi.org/10.1063/1.1756684.
[272] Y. Xuan, Q. Li, W. Hu, Aggregation structure and thermal conductivity of nanofluids, AIChE J. 49 (2003) 1038–1043, http://dx.doi.org/10.1002/aic.690490420.
[273] J. Koo, C. Kleinstreuer, A new thermal conductivity model for nanofluids, J. Nanopart. Res. 6 (2004) 577–588, http://dx.doi.org/10.1007/s11051-004-3170-5.
[274] C.H. Chon, K.D. Kihm, S.P. Lee, S.U.S. Choi, Empirical correlation finding the role of temperature and particle size for nanofluid (Al_2O_3) thermal conductivity enhancement, Appl. Phys. Lett. 87 (2005) 153107, http://dx.doi.org/10.1063/1.2093936.
[275] B. Wang, L. Zhou, X. Peng, A fractal model for predicting the effective thermal conductivity of liquid with suspension of nanoparticles, Int. J. Heat Mass Transfer 46 (2003) 2665–2672, http://dx.doi.org/10.1016/S0017-9310(03)00016-4.
[276] S.C. Cheng, R.I. Vachon, The prediction of the thermal conductivity of two and three phase solid heterogeneous mixtures, Int. J. Heat Mass Transfer 12 (1969) 249–264, http://dx.doi.org/10.1016/0017-9310(69)90009-X.
[277] D.J. Jeffrey, Conduction through a random suspension of spheres, Proc. R. Soc. Lond. Ser. A Math. Phys. Eng. Sci. 335 (1973) 355–367, http://dx.doi.org/10.1098/rspa.1973.0130.

[278] C.J. Yu, A.G. Richter, A. Datta, M.K. Durbin, P. Dutta, Molecular layering in a liquid on a solid substrate: An X-ray reflectivity study, Phys. B 283 (2000) 27–31, http://dx.doi.org/10.1016/S0921-4526(99)01885-2.
[279] W. Yu, S.U.S. Choi, The role of interfacial layers in the enhanced thermal conductivity of nanofluids: A renovated Hamilton-Crosser model, J. Nanopart. Res. 6 (2004) 355–361, http://dx.doi.org/10.1007/s11051-004-2601-7.
[280] K.C. Leong, C. Yang, S.M.S. Murshed, A model for the thermal conductivity of nanofluids-the effect of interfacial layer, J. Nanopart. Res. 8 (2006) 245–254, http://dx.doi.org/10.1007/s11051-005-9018-9.
[281] S.M.S. Murshed, K.C. Leong, C. Yang, Investigations of thermal conductivity and viscosity of nanofluids, Int. J. Therm. Sci. 47 (2008) 560–568, http://dx.doi.org/10.1016/j.ijthermalsci.2007.05.004.
[282] Y. Feng, B. Yu, P. Xu, M. Zou, The effective thermal conductivity of nanofluids based on the nanolayer and the aggregation of nanoparticles, J. Phys. D: Appl. Phys. 40 (2007) 3164–3171, http://dx.doi.org/10.1088/0022-3727/40/10/020.
[283] M.P. Beck, Y. Yuan, P. Warrier, A.S. Teja, The effect of particle size on the thermal conductivity of alumina nanofluids, J. Nanopart. Res. 11 (2009) 1129–1136, http://dx.doi.org/10.1007/s11051-008-9500-2.
[284] J. Xu, B. Yu, M. Zou, P. Xu, A new model for heat conduction of nanofluids based on fractal distributions of nanoparticles, J. Phys. D: Appl. Phys. 39 (2006) 4486–4490, http://dx.doi.org/10.1088/0022-3727/41/13/139801.
[285] K.D. Kihm, C.H. Chon, J.S. Lee, S.U.S. Choi, A new heat propagation velocity prevails over brownian particle velocities in determining the thermal conductivities of nanofluids, Nanoscale Res. Lett. 6 (2011) 361, http://dx.doi.org/10.1186/1556-276X-6-361.
[286] S. Dong, X. Chen, An improved model for thermal conductivity of nanofluids with effects of particle size and Brownian motion, J. Therm. Anal. Calorim. 129 (2017) 1255–1263, http://dx.doi.org/10.1007/s10973-017-6256-x.
[287] J. Eapen, R. Rusconi, R. Piazza, S. Yip, The classical nature of thermal conduction in nanofluids, J. Heat Transfer-T ASME 132 (2010) 102402, http://dx.doi.org/10.1115/1.4001304.
[288] V. Ganesan, C. Louis, S.P. Damodaran, Novel nanofluids based on magnetite nanoclusters and investigation on their cluster size-dependent thermal conductivity, J. Phys. Chem. C 122 (2018) 6918–6929, http://dx.doi.org/10.1021/acs.jpcc.7b12043.
[289] R.S. Vajjha, D.K. Das, Experimental determination of thermal conductivity of three nanofluids and development of new correlations, Int. J. Heat Mass Transfer 52 (2009) 4675–4682, http://dx.doi.org/10.1016/j.ijheatmasstransfer.2009.06.027.
[290] A.R. Moghadassi, S.M. Hosseini, D. Henneke, A. Elkamel, A model of nanofluids effective thermal conductivity based on dimensionless groups, J. Therm. Anal. Calorim. 96 (2009) 81–84, http://dx.doi.org/10.1007/s10973-008-9843-z.
[291] S.M. Hosseini, M.R. Safaei, M. Goodarzi, A.A.A.A. Alrashed, T.K. Nguyen, New. temperature, New temperature interfacial shell dependent dimensionless model for thermal conductivity of nanofluids, Int. J. Heat Mass Transfer 114 (2017) 207–210, http://dx.doi.org/10.1016/j.ijheatmasstransfer.2017.06.061.
[292] K. Chu, W. Li, F. Tang, Flatness-dependent thermal conductivity of graphene-based composites, Phys. Lett. A 377 (2013) 910–914, http://dx.doi.org/10.1016/j.physleta.2013.02.009.
[293] Y. Gao, H. Wang, A.P. Sasmito, A.S. Mujumdar, Measurement and modeling of thermal conductivity of graphene nanoplatelet water and ethylene glycol base nanofluids, Int. J. Heat Mass Transfer 123 (2018) 97–109, http://dx.doi.org/10.1016/j.ijheatmasstransfer.2018.02.089.
[294] X.Q. Wang, A.S. Mujumdar, Heat transfer characteristics of nanofluids: a review, Int. J. Therm. Sci. 46 (2007) 1–19, http://dx.doi.org/10.1016/j.ijthermalsci.2006.06.010.
[295] J. Fan, L. Wang, Review of heat conduction in nanofluids, J. Heat Transfer-T ASME. 133 (2011) 040801, http://dx.doi.org/10.1115/1.4002633.
[296] J. Hong, D. Kim, Effects of aggregation on the thermal conductivity of alumina/water nanofluids, Thermochim. Acta 542 (2012) 28–32, http://dx.doi.org/10.1016/j.tca.2011.12.019.
[297] C. Pang, J.Y. Jung, Y.T. Kang, Aggregation based model for heat conduction mechanism in nanofluids, Int. J. Heat Mass Transfer 72 (2014) 392–399, http://dx.doi.org/10.1016/j.ijheatmasstransfer.2013.12.055.
[298] C.W. Nan, R. Birringer, D.R. Clarke, H. Gleiter, Effective thermal conductivity of particulate composites with interfacial thermal resistance, J. Appl. Phys. 81 (1997) 6692–6699, http://dx.doi.org/10.1063/1.365209.
[299] J. Xu, B. Yu, M. Zou, P. Xu, A new model for heat conduction of nanofluids based on fractal distributions of nanoparticles, J. Phys. D: Appl. Phys. 39 (2006) 4486–4490, http://dx.doi.org/10.1088/0022-3727/39/20/028.
[300] W. Wei, J. Cai, X. Hu, Q. Han, S. Liu, Y. Zhou, Fractal analysis of the effect of particle aggregation distribution on thermal conductivity of nanofluids, Phys. Lett. A 380 (2016) 2953–2956, http://dx.doi.org/10.1016/j.physleta.2016.07.005.
[301] Y. Feng, C. Kleinstreuer, Nanofluid convective heat transfer in a parallel-disk system, Int. J. Heat Mass Transfer 53 (2010) 4619–4628, http://dx.doi.org/10.1016/j.ijheatmasstransfer.2010.06.031.
[302] H.E. Patel, K.B. Anoop, T. Sundararajan, S.K. Das, Model for thermal conductivity of CNT-nanofluids, Bull. Mater. Sci. 31 (2008) 387–390, http://dx.doi.org/10.1007/s12034-008-0060-y.
[303] C. Nan, G. Liu, Y. Lin, M. Li, Interface effect on thermal conductivity of carbon nanotube composites, Appl. Phys. Lett. 85 (2004) 3549–3551, http://dx.doi.org/10.1063/1.1808874.
[304] M. Corcione, Empirical correlating equations for predicting the effective thermal conductivity and dynamic viscosity of nanofluids, Energy Convers. Manage. 52 (2011) 789–793, http://dx.doi.org/10.1016/j.enconman.2010.06.072.
[305] A. Zagabathuni, S. Ghosh, S.K. Pabi, The difference in the thermal conductivity of nanofluids measured by different methods and its rationalization, Beilstein J. Nanotechnol. 7 (2016) 2037–2044, http://dx.doi.org/10.3762/BJNANO.7.194.
[306] X. Wang, X. Xu, S.S.U. Choi, Thermal conductivity of nanoparticle-fluid mixture, J. Thermophys. Heat Transfer 13 (1999) 474–480, http://dx.doi.org/10.2514/2.6486.
[307] W. Jiang, G. Ding, H. Peng, Measurement and model on thermal conductivities of carbon nanotube nanorefrigerants, Int. J. Therm. Sci. 48 (2009) 1108–1115, http://dx.doi.org/10.1016/j.ijthermalsci.2008.11.012.
[308] W. Guo, G. Li, Y. Zheng, C. Dong, Measurement of the thermal conductivity of SiO_2 nanofluids with an optimized transient hot wire method, Thermochim. Acta. 661 (2018) 84–97, http://dx.doi.org/10.1016/j.tca.2018.01.008.
[309] K.D. Antoniadis, G.J. Tertsinidou, M.J. Assael, W.A. Wakeham, Necessary conditions for accurate, transient hot-wire measurements of the apparent thermal conductivity of nanofluids are seldom satisfied, Int. J. Thermophys. 37 (2016) 78, http://dx.doi.org/10.1007/s10765-016-2083-8.
[310] J. Lee, H. Lee, Y.J. Baik, J. Koo, Quantitative analyses of factors affecting thermal conductivity of nanofluids using an improved transient hot-wire method apparatus, Int. J. Heat Mass Transfer 89 (2015) 116–123, http://dx.doi.org/10.1016/j.ijheatmasstransfer.2015.05.064.
[311] Z. Aparna, M.M. Michael, S.K. Pabi, S. Ghosh, Diversity in thermal conductivity of aqueous Al_2O_3- and Ag-nanofluids measured by transient hot-wire and laser flash methods, Exp. Therm. Fluid Sci. 94 (2018) 231–245, http://dx.doi.org/10.1016/j.expthermflusci.2018.02.005.
[312] M.H. Esfe, S. Saedodin, O. Mahian, S. Wongwises, Thermal conductivity of Al_2O_3/water nanofluids: Measurement, correlation, sensitivity analysis, and comparisons with literature reports, J. Therm. Anal. Calorim. 117 (2014) 675–681, http://dx.doi.org/10.1016/10.1007/s10973-014-3771-x.
[313] D.W. Oh, A. Jain, J.K. Eaton, K.E. Goodson, J.S. Lee, Thermal conductivity measurement and sedimentation detection of aluminum oxide nanofluids by using the 3ω method, Int. J. Heat Fluid Flow 29 (2008) 1456–1461, http://dx.doi.org/10.1016/j.ijheatfluidflow.2008.04.007.
[314] A. Turgut, I. Tavman, M. Chirtoc, H.P. Schuchmann, C. Sauter, S. Tavman, Thermal conductivity and viscosity measurements of water-based TiO_2 nanofluids, Int. J. Thermophys. 30 (2009) 1213–1226, http://dx.doi.org/10.1007/s10765-009-0594-2.

[315] L. Qiu, X. Zheng, G. Su, D. Tang, Design and application of a freestanding sensor based on 3ω technique for thermal-conductivity measurement of solids, liquids, and nanopowders, Int. J. Thermophys. 34 (2013) 2261–2275, http://dx.doi.org/10.1007/s10765-011-1075-y.
[316] R. Karthik, R. Harish Nagarajan, B. Raja, P. Damodharan, Thermal conductivity of CuO-DI water nanofluids using 3-ω measurement technique in a suspended micro-wire, Exp. Therm. Fluid Sci. 40 (2012) 1–9, http://dx.doi.org/10.1016/j.expthermflusci.2012.01.006.
[317] Z. Han, B. Yang, S.H. Kim, M.R. Zachariah, Application of hybrid sphere/carbon nanotube particles in nanofluids, Nanotechnology 18 (2007) 105701, http://dx.doi.org/10.1088/0957-4484/18/10/105701.
[318] B. Yang, Z.H. Han, Temperature-dependent thermal conductivity of nanorod-based nanofluids, Appl. Phys. Lett. 89 (2006) 2004–2007, http://dx.doi.org/10.1063/1.2338424.
[319] T.Y. Choi, M.H. Maneshian, B. Kang, W.S. Chang, C.S. Han, D. Poulikakos, Measurement of the thermal conductivity of a water-based single-wall carbon nanotube colloidal suspension with a modified 3-ω method, Nanotechnology 20 (2009) http://dx.doi.org/10.1088/0957-4484/20/31/315706.
[320] X. Yang, C. Liang, T. Ma, Y. Guo, J. Kong, J. Gu, M. Chen, J. Zhu, A review on thermally conductive polymeric composites: classification, measurement, model and equations, mechanism and fabrication methods, Adv. Compos. Hybrid Mater. 1 (2018) 207–230, http://dx.doi.org/10.1007/s42114-018-0031-8.
[321] M.J. Assael, M. Dix, K. Gialou, L. Vozar, W.A. Wakeham, Application of the transient hot-wire technique to the measurement of the thermal conductivity of solids, Int. J. Thermophys. 23 (2002) 615–633, http://dx.doi.org/10.1023/A:1015494802462.
[322] M. Leena, S. Srinivasan, A comparative study on thermal conductivity of TiO_2/ethylene glycol–water and TiO_2/propylene glycol–water nanofluids, J. Therm. Anal. Calorim. 131 (2018) 1987–1998, http://dx.doi.org/10.1007/s10973-017-6616-6.
[323] S. Harikrishnan, S. Magesh, S. Kalaiselvam, Preparation and thermal energy storage behaviour of stearic acid-TiO_2 nanofluids as a phase change material for solar heating systems, Thermochim. Acta. 565 (2013) 137–145, http://dx.doi.org/10.1016/j.tca.2013.05.001.
[324] Z. Zhang, Y. Yuan, L. Ouyang, Q. Sun, X. Cao, S. Alelyani, Enhanced thermal properties of Li_2CO_3–Na_2CO_3–K_2CO_3 nanofluids with nanoalumina for heat transfer in high-temperature CSP systems, J. Therm. Anal. Calorim. 128 (2017) 1783–1792, http://dx.doi.org/10.1007/s10973-016-6050-1.
[325] B. Buonomo, L. Colla, L. Fedele, O. Manca, L. Marinelli, A comparison of nanofluid thermal conductivity measurements by flash and hot disk techniques, J. Phys. Conf. Ser. 547 (2014) 012046, http://dx.doi.org/10.1088/1742-6596/547/1/012046.
[326] C. Kleinstreuer, Y. Feng, Experimental and theoretical studies of nanofluid thermal conductivity enhancement: A review, Nanoscale Res. Lett. 6 (2011) 229, http://dx.doi.org/10.1186/1556-276X-6-229.
[327] C.H. Li, G.P. Peterson, The effect of particle size on the effective thermal conductivity of Al_2O_3-water nanofluids, J. Appl. Phys. 101 (2007) 044312, http://dx.doi.org/10.1063/1.2436472.
[328] V. Sridhara, L.N. Satapathy, Al_2O_3-based nanofluids: a review, Nanoscale Res. Lett. 6 (2011) 456, http://dx.doi.org/10.1186/1556-276X-6-456.
[329] H. Kurt, M. Kayfeci, Prediction of thermal conductivity of ethylene glycol-water solutions by using artificial neural networks, Appl. Energy 86 (2009) 2244–2248, http://dx.doi.org/10.1016/j.apenergy.2008.12.020.
[330] B. Barbés, R. Páramo, E. Blanco, C. Casanova, Thermal conductivity and specific heat capacity measurements of CuO nanofluids, J. Therm. Anal. Calorim. 115 (2014) 1883–1891, http://dx.doi.org/10.1007/s10973-013-3518-0.
[331] S.E. Gustafsson, E. Karawacki, M.N. Khan, Transient hot-strip method for simultaneously measuring thermal conductivity and thermal diffusivity of solids and fluids, J. Phys. D: Appl. Phys. 12 (1979) 1411–1421, http://dx.doi.org/10.1088/0022-3727/12/9/003.
[332] S.E. Gustafsson, Transient plane source techniques for thermal conductivity and thermal diffusivity measurements of solid materials, Rev. Sci. Instrum. 62 (1991) 797–804, http://dx.doi.org/10.1063/1.1142087.
[333] M. Gustavsson, S.E. Gustafsson, Thermal conductivity as an indicator of fat content in milk, Thermochim. Acta 442 (2006) 1–5, http://dx.doi.org/10.1016/j.tca.2005.11.037.
[334] V. Bohac, M.K. Gustavsson, L. Kubicar, S.E. Gustafsson, Parameter estimations for measurements of thermal transport properties with the hot disk thermal constants analyzer, Rev. Sci. Instrum. 71 (2000) 2452–2455, http://dx.doi.org/10.1063/1.1150635.
[335] A. Harris, S. Kazachenko, R. Bateman, J. Nickerson, M. Emanuel, Measuring the thermal conductivity of heat transfer fluids via the modified transient plane source (MTPS), J. Therm. Anal. Calorim. 116 (2014) 1309–1314, http://dx.doi.org/10.1007/s10973-014-3811-6.
[336] D. Zhu, X. Li, N. Wang, X. Wang, J. Gao, H. Li, Dispersion behavior and thermal conductivity characteristics of Al_2O_3-H_2O nanofluids, Curr. Appl. Phys. 9 (2009) 131–139, http://dx.doi.org/10.1016/j.cap.2007.12.008.
[337] M.H. Esfe, S. Saedodin, Turbulent forced convection heat transfer and thermophysical properties of MgO-water nanofluid with consideration of different nanoparticles diameter, an empirical study, J. Therm. Anal. Calorim. 119 (2015) 1205–1213, http://dx.doi.org/10.1007/s10973-014-4197-1.
[338] M.H. Esfe, S. Esfandeh, M. Afrand, M. Rejvani, S.H. Rostamian, Experimental evaluation, new correlation proposing and ANN modeling of thermal properties of EG based hybrid nanofluid containing zno-DWCNT nanoparticles for internal combustion engines applications, Appl. Therm. Eng. 133 (2018) 452–463, http://dx.doi.org/10.1016/j.applthermaleng.2017.11.131.
[339] M.H. Esfe, W.M. Yan, M. Akbari, A. Karimipour, M. Hassani, Experimental study on thermal conductivity of DWCNT-ZnO/water-EG nanofluids, Int. Commun. Heat Mass Transfer 68 (2015) 248–251, http://dx.doi.org/10.1016/j.icheatmasstransfer.2015.09.001.
[340] S.H. Rostamian, M. Biglari, S. Saedodin, M.H. Esfe, An inspection of thermal conductivity of CuO-SWCNTs hybrid nanofluid versus temperature and concentration using experimental data, ANN modeling and new correlation, J. Mol. Liq. 231 (2017) 364–369, http://dx.doi.org/10.1016/j.molliq.2017.02.015.
[341] X. Li, C. Zou, X. Lei, W. Li, Stability and enhanced thermal conductivity of ethylene glycol-based SiC nanofluids, Int. J. Heat Mass Transfer 89 (2015) 613–619, http://dx.doi.org/10.1016/j.ijheatmasstransfer.2015.05.096.
[342] L. Yang, W. Ji, J. Huang, G. Xu, An updated review on the influential parameters on thermal conductivity of nano-fluids, J. Mol. Liq. (2019) 111780, http://dx.doi.org/10.1016/j.molliq.2019.111780.
[343] H.A. Mintsa, G. Roy, C.T. Nguyen, D. Doucet, New temperature dependent thermal conductivity data for water-based nanofluids, Int. J. Therm. Sci. 48 (2009) 363–371, http://dx.doi.org/10.1016/j.ijthermalsci.2008.03.009.
[344] C.H. Li, G.P. Peterson, Experimental investigation of temperature and volume fraction variations on the effective thermal conductivity of nanoparticle suspensions (nanofluids), J. Appl. Phys. 99 (2006) 084314, http://dx.doi.org/10.1063/1.2191571.
[345] S.K. Das, N. Putra, P. Thiesen, W. Roetzel, Temperature dependence of thermal conductivity enhancement for nanofluids, J. Heat Transfer-T ASME 125 (2003) 567–574, http://dx.doi.org/10.1115/1.1571080.
[346] X. Zhang, H. Gu, M. Fujii, Effective thermal conductivity and thermal diffusivity of nanofluids containing spherical and cylindrical nanoparticles, Exp. Therm. Fluid Sci. 31 (2007) 593–599, http://dx.doi.org/10.1016/j.expthermflusci.2006.06.009.
[347] B. Buonomo, O. Manca, L. Marinelli, S. Nardini, Effect of temperature and sonication time on nanofluid thermal conductivity measurements by nano-flash method, Appl. Therm. Eng. 91 (2015) 181–190, http://dx.doi.org/10.1016/j.applthermaleng.2015.07.077.
[348] M. Chandrasekar, S. Suresh, A. Chandra Bose, Experimental investigations and theoretical determination of thermal conductivity and viscosity of Al_2O_3/water nanofluid, Exp. Therm. Fluid Sci. 34 (2010) 210–216, http://dx.doi.org/10.1016/j.expthermflusci.2009.10.022.
[349] S.H. Kim, S.R. Choi, D. Kim, Thermal conductivity of metal-oxide nanofluids: Particle size dependence and effect of laser irradiation, J. Heat Transfer 129 (2007) 298, http://dx.doi.org/10.1115/1.2427071.

[350] N. Kumar, S.S. Sonawane, S.H. Sonawane, Experimental study of thermal conductivity, heat transfer and friction factor of Al_2O_3 based nanofluid, Int. Commun. Heat Mass Transfer 90 (2018) 1–10, http://dx.doi.org/10.1016/j.icheatmasstransfer.2017.10.001.
[351] M.P. Beck, Y. Yuan, P. Warrier, A.S. Teja, The thermal conductivity of alumina nanofluids in water, ethylene glycol, and ethylene glycol+water mixtures, J. Nanopart. Res. 12 (2010) 1469–1477, http://dx.doi.org/10.1007/s11051-009-9716-9.
[352] H. Xie, J. Wang, T. Xi, Y. Liu, F. Ai, Q. Wu, Thermal conductivity enhancement of suspensions containing nanosized alumina particles, J. Appl. Phys. 91 (2002) 4568–4572, http://dx.doi.org/10.1063/1.1454184.
[353] S. Lee, S.U.S. Choi, S. Li, J.A. Eastman, Measuring thermal conductivity of fluids containing oxide nanoparticles, J. Heat Transfer 121 (1999) 280–289, http://dx.doi.org/10.1115/1.2825978.
[354] N.A. Usri, W.H. Azmi, R. Mamat, K.A. Hamid, G. Najafi, Thermal conductivity enhancement of Al_2O_3 nanofluid in ethylene glycol and water mixture, Energy Procedia 79 (2015) 397–402, http://dx.doi.org/10.1016/j.egypro.2015.11.509.
[355] D.H. Yoo, K.S. Hong, H.S. Yang, Study of thermal conductivity of nanofluids for the application of heat transfer fluids, Thermochim. Acta 455 (2007) 66–69, http://dx.doi.org/10.1016/j.tca.2006.12.006.
[356] W. Duangthongsuk, S. Wongwises, Measurement of temperature-dependent thermal conductivity and viscosity of TiO_2-water nanofluids, Exp. Therm. Fluid Sci. 33 (2009) 706–714, http://dx.doi.org/10.1016/j.expthermflusci.2009.01.005.
[357] Y. He, Y. Jin, H. Chen, Y. Ding, D. Cang, H. Lu, Heat transfer and flow behaviour of aqueous suspensions of TiO_2 nanoparticles (nanofluids) flowing upward through a vertical pipe, Int. J. Heat Mass Transfer 50 (2007) 2272–2281, http://dx.doi.org/10.1016/j.ijheatmasstransfer.2006.10.024.
[358] R.S. Khedkar, N. Shrivastava, S.S. Sonawane, K.L. Wasewar, Experimental investigations and theoretical determination of thermal conductivity and viscosity of TiO_2-ethylene glycol nanofluid, Int. Commun. Heat Mass Transfer 73 (2016) 54–61, http://dx.doi.org/10.1016/j.icheatmasstransfer.2016.02.004.
[359] S.M.S. Murshed, K.C. Leong, C. Yang, Enhanced thermal conductivity of TiO_2-water based nanofluids, Int. J. Therm. Sci. 44 (2005) 367–373, http://dx.doi.org/10.1016/j.ijthermalsci.2004.12.005.
[360] R.S. Khedkar, S.S. Sonawane, K.L. Wasewar, Influence of CuO nanoparticles in enhancing the thermal conductivity of water and monoethylene glycol based nanofluids, Int. Commun. Heat Mass Transfer 39 (2012) 665–669, http://dx.doi.org/10.1016/j.icheatmasstransfer.2012.03.012.
[361] R. Agarwal, K. Verma, N.K. Agrawal, R.K. Duchaniya, R. Singh, Synthesis, characterization, thermal conductivity and sensitivity of CuO nanofluids, Appl. Therm. Eng. 102 (2016) 1024–1036, http://dx.doi.org/10.1016/j.applthermaleng.2016.04.051.
[362] Y. Hwang, J.K. Lee, C.H. Lee, Y.M. Jung, S.I. Cheong, C.G. Lee, B.C. Ku, S.P. Jang, Stability and thermal conductivity characteristics of nanofluids, Thermochim. Acta 455 (2007) 70–74, http://dx.doi.org/10.1016/j.tca.2006.11.036.
[363] Y.J. Hwang, Y.C. Ahn, H.S. Shin, C.G. Lee, G.T. Kim, H.S. Park, J.K. Lee, Investigation on characteristics of thermal conductivity enhancement of nanofluids, Curr. Appl. Phys. 6 (2006) 1068–1071, http://dx.doi.org/10.1016/j.cap.2005.07.021.
[364] M. Keyvani, M. Afrand, D. Toghraie, M. Reiszadeh, An experimental study on the thermal conductivity of cerium oxide/ethylene glycol nanofluid: Developing a new correlation, J. Mol. Liq. 266 (2018) 211–217, http://dx.doi.org/10.1016/j.molliq.2018.06.010.
[365] H. Li, L. Wang, Y. He, Y. Hu, J. Zhu, B. Jiang, Experimental investigation of thermal conductivity and viscosity of ethylene glycol based ZnO nanofluids, Appl. Therm. Eng. 88 (2014) 363–368, http://dx.doi.org/10.1016/j.applthermaleng.2014.10.071.
[366] W. Yu, H. Xie, L. Chen, Y. Li, Enhancement of thermal conductivity of kerosene-based Fe_3O_4 nanofluids prepared via phase-transfer method, Colloids Surf. A 355 (2010) 109–113, http://dx.doi.org/10.1016/j.colsurfa.2009.11.044.
[367] M. Abareshi, E.K. Goharshadi, S.M. Zebarjad, H.K. Fadafan, A. Youssefi, Fabricationcharacterization and measurement of thermal conductivity of Fe_3O_4 nanofluids, J. Magn. Magn. Mater. 322 (2010) 3895–3901, http://dx.doi.org/10.1016/j.jmmm.2010.08.016.
[368] S. Doganay, A. Turgut, L. Cetin, Magnetic field dependent thermal conductivity measurements of magnetic nanofluids by 3ω method, J. Magn. Magn. Mater. 474 (2019) 199–206, http://dx.doi.org/10.1016/j.jmmm.2018.10.142.
[369] A. Karimi, M.A.A. Sadatlu, B. Saberi, H. Shariatmadar, M. Ashjaee, Experimental investigation on thermal conductivity of water based nickel ferrite nanofluids, Adv. Powder Technol. 26 (2015) 1529–1536, http://dx.doi.org/10.1016/j.apt.2015.08.015.
[370] M.H. Esfe, M. Afrand, A. Karimipour, W.M. Yan, N. Sina, An experimental study on thermal conductivity of mgo nanoparticles suspended in a binary mixture of water and ethylene glycol, Int. Commun. Heat Mass Transfer 67 (2015) 173–175, http://dx.doi.org/10.1016/j.icheatmasstransfer.2015.07.009.
[371] M.S. Liu, M.C.C. Lin, C.Y. Tsai, C.C. Wang, Enhancement of thermal conductivity with Cu for nanofluids using chemical reduction method, Int. J. Heat Mass Transfer 49 (2006) 3028–3033, http://dx.doi.org/10.1016/j.ijheatmasstransfer.2006.02.012.
[372] J.A. Eastman, S.U.S. Choi, S. Li, W. Yu, L.J. Thompson, Anomalously increased effective thermal conductivities of ethylene glycol-based nanofluids containing copper nanoparticles, Appl. Phys. Lett. 78 (2001) 718–720, http://dx.doi.org/10.1063/1.1341218.
[373] H.E. Patel, S.K. Das, T. Sundararajan, A. Sreekumaran Nair, B. George, T. Pradeep, Thermal conductivities of naked and monolayer protected metal nanoparticle based nanofluids: Manifestation of anomalous enhancement and chemical effects, Appl. Phys. Lett. 83 (2003) 2931–2933, http://dx.doi.org/10.1063/1.1602578.
[374] S.A. Putnam, D.G. Cahill, P.V. Braun, Thermal conductivity of nanoparticle suspensions, J. Appl. Phys. 99 (2006) 084308, http://dx.doi.org/10.1063/1.2189933.
[375] R. Carbajal-Valdéz, A. Rodríguez-Juárez, J.L. Jiménez-Pérez, J.F. Sánchez-Ramírez, A. Cruz-Orea, Z.N. Correa-Pacheco, M. Macias, J.L. Luna-Sánchez, Experimental investigation on thermal properties of Ag nanowire nanofluids at low concentrations, Thermochim. Acta 671 (2019) 83–88, http://dx.doi.org/10.1016/j.tca.2018.11.015.
[376] T. Parametthanuwat, N. Bhuwakietkumjohn, S. Rittidech, Y. Ding, Experimental investigation on thermal properties of silver nanofluids, Int. J. Heat Fluid Flow 56 (2015) 80–90, http://dx.doi.org/10.1016/j.ijheatfluidflow.2015.07.0.
[377] A. Alirezaie, M.H. Hajmohammad, M.R. Hassani Ahangar, M. Hemmat Esfe, Price-performance evaluation of thermal conductivity enhancement of nanofluids with different particle sizes, Appl. Therm. Eng. 128 (2018) 373–380, http://dx.doi.org/10.1016/j.applthermaleng.2017.08.143.
[378] T.K. Hong, H.S. Yang, C.J. Choi, Study of the enhanced thermal conductivity of Fe nanofluids, J. Appl. Phys. 97 (2005) 064311, http://dx.doi.org/10.1063/1.1861145.
[379] Y. Ding, H. Alias, D. Wen, R.A. Williams, Heat transfer of aqueous suspensions of carbon nanotubes (CNT nanofluids), Int. J. Heat Mass Transfer 49 (2006) 240–250, http://dx.doi.org/10.1016/j.ijheatmasstransfer.2005.07.009.
[380] M.J. Assael, I.N. Metaxa, J. Arvanitidis, D. Christofilos, C. Lioutas, Thermal conductivity enhancement in aqueous suspensions of carbon multi-walled and double-walled nanotubes in the presence of two different dispersants, Int. J. Thermophys. 26 (2005) 647–664, http://dx.doi.org/10.1007/s10765-005-5569-3.
[381] M. Xing, J. Yu, R. Wang, Experimental investigation and modelling on the thermal conductivity of CNTs based nanofluids, Int. J. Therm. Sci. 104 (2016) 404–411, http://dx.doi.org/10.1016/j.ijthermalsci.2016.01.024.
[382] S.U.S. Choi, Z.G. Zhang, W. Yu, F.E. Lockwood, E.A. Grulke, Anomalous thermal conductivity enhancement in nanotube suspensions, Appl. Phys. Lett. 79 (2001) 2252–2254, http://dx.doi.org/10.1063/1.1408272.
[383] M.F. Pakdaman, M.A. Akhavan-Behabadi, P. Razi, An experimental investigation on thermo-physical properties and overall performance of MWCNT/heat transfer oil nanofluid flow inside vertical helically coiled tubes, Exp. Therm. Fluid Sci. 40 (2012) 103–111, http://dx.doi.org/10.1016/j.expthermflusci.2012.02.005.

[384] H. Xie, H. Lee, W. Youn, M. Choi, Nanofluids containing multiwalled carbon nanotubes and their enhanced thermal conductivities, J. Appl. Phys. 94 (2003) 4967–4971, http://dx.doi.org/10.1063/1.1613374.
[385] M.S. Liu, M.C.C. Lin, I.T. Huang, C.C. Wang, Enhancement of thermal conductivity with carbon nanotube for nanofluids, Int. Commun. Heat Mass Transfer 32 (2005) 1202–1210, http://dx.doi.org/10.1016/j.icheatmasstransfer.2005.05.005.
[386] S. Harish, K. Ishikawa, E. Einarsson, S. Aikawa, S. Chiashi, J. Shiomi, S. Maruyama, Enhanced thermal conductivity of ethylene glycol with single-walled carbon nanotube inclusions, Int. J. Heat Mass Transfer 55 (2012) 3885–3890, http://dx.doi.org/10.1016/j.ijheatmasstransfer.2012.03.001.
[387] W. Yu, H. Xie, X. Wang, X. Wang, Significant thermal conductivity enhancement for nanofluids containing graphene nanosheets, Phys. Lett. A 375 (2011) 1323–1328, http://dx.doi.org/10.1016/j.physleta.2011.01.040.
[388] H. Xie, J. Wang, T. Xi, Y. Liu, Thermal conductivity of suspensions containing nanosized SiC particles, Int. J. Thermophys. 23 (2002) 571–580, http://dx.doi.org/10.1023/A:1015121805842.
[389] S.W. Lee, S.D. Park, S. Kang, I.C. Bang, J.H. Kim, Investigation of viscosity and thermal conductivity of SiC nanofluids for heat transfer applications, Int. J. Heat Mass Transfer 54 (2011) 433–438, http://dx.doi.org/10.1016/j.ijheatmasstransfer.2010.09.026.
[390] X. Li, C. Zou, L. Zhou, A. Qi, Experimental study on the thermo-physical properties of diathermic oil based SiC nanofluids for high temperature applications, Int. J. Heat Mass Transfer 97 (2016) 631–637, http://dx.doi.org/10.1016/j.ijheatmasstransfer.2016.02.056.
[391] R. Ranjbarzadeh, A. Moradikazerouni, R. Bakhtiari, A. Asadi, M. Afrand, An experimental study on stability and thermal conductivity of water/silica nanofluid: Eco-friendly production of nanoparticles, J. Clean. Prod. 206 (2019) 1089–1100, http://dx.doi.org/10.1016/j.jclepro.2018.09.205.
[392] A. Ceylan, K. Jastrzembski, S.I. Shah, Enhanced solubility Ag–Cu nanoparticles and their thermal transport properties, Metall. Mater. Trans. A 37 (2006) 2033–2038, http://dx.doi.org/10.1007/BF02586123.
[393] S. Cingarapu, D. Singh, E.V. Timofeeva, M.R. Moravek, Nanofluids with encapsulated tin nanoparticles for advanced heat transfer and thermal energy storage, Int. J. Energy Res. 38 (2013) 51–59, http://dx.doi.org/10.1002/er.3041.
[394] H. Yarmand, S. Gharehkhani, G. Ahmadi, S.F.S. Shirazi, S. Baradaran, E. Montazer, M.N.M. Zubir, M.S. Alehashem, S.N. Kazi, M. Dahari, Graphene nanoplatelets-silver hybrid nanofluids for enhanced heat transfer, Energy Convers. Manage. 100 (2015) 419–428, http://dx.doi.org/10.1016/j.enconman.2015.05.023.
[395] H. Yarmand, S. Gharehkhani, S.F.S. Shirazi, M. Goodarzi, A. Amiri, W.S. Sarsam, M.S. Alehashem, M. Dahari, S.N. Kazi, Study.of. synthesis, Study of synthesis stability and thermo-physical properties of graphene nanoplatelet/platinum hybrid nanofluid, Int. Commun. Heat Mass Transfer 77 (2016) 15–21, http://dx.doi.org/10.1016/j.icheatmasstransfer.2016.07.010.
[396] L.S. Sundar, E. Venkata Ramana, M.P.F. Graça, M.K. Singh, A.C.M. Sousa, Nanodiamond-Fe_3O_4 nanofluids: Preparation and measurement of viscosity, electrical and thermal conductivities, Int. Commun. Heat Mass Transfer 73 (2016) 62–74, http://dx.doi.org/10.1016/j.icheatmasstransfer.2016.02.013.
[397] S.S. Harandi, A. Karimipour, M. Afrand, M. Akbari, A. D'Orazio, An experimental study on thermal conductivity of F-MWCNTs-Fe_3O_4/EG hybrid nanofluid: Effects of temperature and concentration, Int. Commun. Heat Mass Transfer 76 (2016) 171–177, http://dx.doi.org/10.1016/j.icheatmasstransfer.2016.05.029.
[398] S. Jana, A. Salehi-Khojin, W.H. Zhong, Enhancement of fluid thermal conductivity by the addition of single and hybrid nano-additives, Thermochim. Acta 462 (2007) 45–55, http://dx.doi.org/10.1016/j.tca.2007.06.009.
[399] S.M. Abbasi, A. Rashidi, A. Nemati, K. Arzani, The effect of functionalisation method on the stability and the thermal conductivity of nanofluid hybrids of carbon nanotubes/gamma alumina, Ceram. Int. 39 (2013) 3885–3891, http://dx.doi.org/10.1016/j.ceramint.2012.10.232.
[400] L. Godson, B. Raja, D.M. Lal, S. Wongwises, Experimental investigation on the thermal conductivity and viscosity of silver-deionized water nanofluid, Exp. Heat Transfer 23 (2010) 317–332, http://dx.doi.org/10.1080/08916150903564796.
[401] Y. Li, W. Qu, J. Feng, Temperature dependence of thermal conductivity of nanofluids, Chin. Phys. Lett. 25 (2008) 3319–3322, http://dx.doi.org/10.1088/0256-307X/25/9/060.
[402] L. Yang, W. Ji, Z. Zhang, X. Jin, Thermal conductivity enhancement of water by adding graphene nano-sheets: Consideration of particle loading and temperature effects, Int. Commun. Heat Mass Transfer 109 (2019) 104353, http://dx.doi.org/10.1016/j.icheatmasstransfer.2019.104353.
[403] S. Kakaç, A. Pramuanjaroenkij, Review of convective heat transfer enhancement with nanofluids, Int. J. Heat Mass Transfer 52 (2009) 3187–3196, http://dx.doi.org/10.1016/j.ijheatmasstransfer.2009.02.006.
[404] S.P. Jang, S.U.S. Choi, Effects of various parameters on nanofluid thermal conductivity, J. Heat Transfer-T ASME 129 (2007) 617–623, http://dx.doi.org/10.1115/1.2712475.
[405] E.V. Timofeeva, D.S. Smith, W. Yu, D.M. France, D. Singh, J.L. Routbort, Particle size and interfacial effects on thermo-physical and heat transfer characteristics of water-based α-SiC nanofluids, Nanotechnology 21 (2010) 215703, http://dx.doi.org/10.1088/0957-4484/21/21/215703.
[406] G. Chen, W. Yu, D. Singh, D. Cookson, J. Routbort, Application of SAXS to the study of particle-size-dependent thermal conductivity in silica nanofluids, J. Nanopart. Res. 10 (2008) 1109–1114, http://dx.doi.org/10.1007/s11051-007-9347-y.
[407] R. Prasher, P.E. Phelan, P. Bhattacharya, Effect of aggregation kinetics on the thermal conductivity of nanoscale colloidal solutions (nanofluid), Nano Lett. 6 (2006) 1529–1534, http://dx.doi.org/10.1021/nl060992s.
[408] J. Jeong, C. Li, Y. Kwon, J. Lee, S.H. Kim, R. Yun, Particle shape effect on the viscosity and thermal conductivity of zno nanofluids, Int. J. Refrig. 36 (2013) 2233–2241, http://dx.doi.org/10.1016/j.ijrefrig.2013.07.024.
[409] S. Ferrouillat, A. Bontemps, O. Poncelet, O. Soriano, J.A. Gruss, Influence of nanoparticle shape factor on convective heat transfer and energetic performance of water-based SiO_2 and ZnO nanofluids, Appl. Therm. Eng. 51 (2013) 839–851, http://dx.doi.org/10.1016/j.applthermaleng.2012.10.020.
[410] E.V. Timofeeva, J.L. Routbort, D. Singh, Particle shape effects on thermophysical properties of alumina nanofluids, J. Appl. Phys. 106 (2009) 014304, http://dx.doi.org/10.1063/1.3155999.
[411] S. Bhanushali, N.N. Jason, P. Ghosh, A. Ganesh, G.P. Simon, W. Cheng, Enhanced thermal conductivity of copper nanofluids: The effect of filler geometry, ACS Appl. Mater. Interfaces 9 (2017) 18925–18935, http://dx.doi.org/10.1021/acsami.7b03339.
[412] M.M. Ghosh, S. Ghosh, S.K. Pabi, Effects of particle shape and fluid temperature on heat-transfer characteristics of nanofluids, J. Mater. Eng. Perform. 22 (2013) 1525–1529, http://dx.doi.org/10.1007/s11665-012-0441-7.
[413] D. Song, D. Jing, W. Ma, X. Zhang, Effect of particle aggregation on thermal conductivity of nanofluids: Enhancement of phonon MFP, J. Appl. Phys. 125 (2019) 015103, http://dx.doi.org/10.1063/1.5062600.
[414] M. Chopkar, S. Sudarshan, P.K. Das, I. Manna, Effect of particle size on thermal conductivity of nanofluid, Metall. Mater. Trans. A 39 (2008) 1535–1542, http://dx.doi.org/10.1007/s11661-007-9444-7.
[415] X. Wang, X. Li, S. Yang, Influence of pH and SDBS on the stability and thermal conductivity of nanofluids, Energy Fuels 23 (2009) 2684–2689, http://dx.doi.org/10.1021/ef800865a.
[416] X. Li, D. Zhu, X. Wang, N. Wang, J. Gao, H. Li, Thermal conductivity enhancement dependent ph and chemical surfactant for Cu-H_2O nanofluids, Thermochim. Acta 469 (2008) 98–103, http://dx.doi.org/10.1016/j.tca.2008.01.008.
[417] T.S. Krishnakumar, S.P. Viswanath, S.M. Varghese, J.M. Prakash, Experimental studies on thermal and rheological properties of Al_2O_3–ethylene glycol nanofluid, Int. J. Refrig. 89 (2018) 122–130, http://dx.doi.org/10.1016/j.ijrefrig.2018.03.008.

[418] S. Habibzadeh, A. Kazemi-Beydokhti, A.A. Khodadadi, Y. Mortazavi, S. Omanovic, M. Shariat-Niassar, Stability and thermal conductivity of nanofluids of tin dioxide synthesized via microwave-induced combustion route, Chem. Eng. J. 156 (2010) 471–478, http://dx.doi.org/10.1016/j.cej.2009.11.007.
[419] S.M.S. Murshed, K.C. Leong, C. Yang, Characterization of electrokinetic properties of nanofluids, J. Nanosci. Nanotechnol. 8 (2008) 5966–5971, http://dx.doi.org/10.1166/jnn.2008.329.
[420] H.J. Kim, S.H. Lee, J.H. Lee, S.P. Jang, Effect of particle shape on suspension stability and thermal conductivities of water-based bohemite alumina nanofluids, Energy 90 (2015) 1290–1297, http://dx.doi.org/10.1016/j.energy.2015.06.084.
[421] H. Xie, W. Yu, Y. Li, L. Chen, Discussion on the thermal conductivity enhancement of nanofluids, Nanoscale Res. Lett. 6 (2011) 124, http://dx.doi.org/10.1186/1556-276X-6-124.
[422] P. Garg, J.L. Alvarado, C. Marsh, T.A. Carlson, D.A. Kessler, K. Annamalai, An experimental study on the effect of ultrasonication on viscosity and heat transfer performance of multi-wall carbon nanotube-based aqueous nanofluids, Int. J. Heat Mass Transfer 52 (2009) 5090–5101, http://dx.doi.org/10.1016/j.ijheatmasstransfer.2009.04.029.
[423] R. Sadri, G. Ahmadi, H. Togun, M. Dahari, S.N. Kazi, E. Sadeghinezhad, N. Zubir, An experimental study on thermal conductivity and viscosity of nanofluids containing carbon nanotubes, Nanoscale Res. Lett. 9 (2014) 151, http://dx.doi.org/10.1186/1556-276X-9-151.
[424] M. Kole, T.K. Dey, Thermophysical and pool boiling characteristics of ZnO-ethylene glycol nanofluids, Int. J. Therm. Sci. 62 (2012) 61–70, http://dx.doi.org/10.1016/j.ijthermalsci.2012.02.002.
[425] S.S. Sonawane, R.S. Khedkar, K.L. Wasewar, Effect of sonication time on enhancement of effective thermal conductivity of nano TiO_2–water, ethylene glycol, and paraffin oil nanofluids and models comparisons, Exp. Nanosci. 10 (2015) 310–322, http://dx.doi.org/10.1080/17458080.2013.832421.
[426] L.S. Sundar, E. Venkata Ramana, M.K. Singh, A.C.M. Sousa, Thermal conductivity and viscosity of stabilized ethylene glycol and water mixture Al_2O_3 nanofluids for heat transfer applications: An experimental study, Int. Commun. Heat Mass Transfer 56 (2014) 86–95, http://dx.doi.org/10.1016/j.icheatmasstransfer.2014.06.009.
[427] K. Nemade, S. Waghuley, A novel approach for enhancement of thermal conductivity of CuO/H_2O based nanofluids, Appl. Therm. Eng. 95 (2016) 271–274, http://dx.doi.org/10.1016/j.applthermaleng.2015.11.053.
[428] A. Asadi, M. Asadi, M. Siahmargoi, T. Asadi, M. Gholami Andarati, The effect of surfactant and sonication time on the stability and thermal conductivity of water-based nanofluid containing $Mg(OH)_2$ nanoparticles: An experimental investigation, Int. J. Heat Mass Transfer 108 (2017) 191–198, http://dx.doi.org/10.1016/j.ijheatmasstransfer.2016.12.022.
[429] B. Takabi, S. Salehi, Augmentation of the heat transfer performance of a sinusoidal corrugated enclosure by employing hybrid nanofluid, Adv. Mech. Eng. 6 (2014) 147059, http://dx.doi.org/10.1155/2014/147059.
[430] S. Suresh, K.P. Venkitaraj, P. Selvakumar, M. Chandrasekar, Synthesis of Al_2O_3-Cu/water hybrid nanofluids using two step method and its thermo physical properties, Colloids Surf. A 388 (2011) 41–48, http://dx.doi.org/10.1016/j.colsurfa.2011.08.005.
[431] A.A. Charab, S. Movahedirad, R. Norouzbeigi, Thermal conductivity of Al_2O_3+TiO_2/water nanofluid: Model development and experimental validation, Appl. Therm. Eng. 119 (2017) 42–51, http://dx.doi.org/10.1016/j.applthermaleng.2017.03.059.
[432] M.H. Esfe, S. Wongwises, A. Naderi, A. Asadi, M.R. Safaei, H. Rostamian, M. Dahari, A. Karimipour, Thermal conductivity of Cu/TiO_2-water/EG hybrid nanofluid: Experimental data and modeling using artificial neural network and correlation, Int. Commun. Heat Mass Transfer 66 (2015) 100–104, http://dx.doi.org/10.1016/j.icheatmasstransfer.2015.05.014.
[433] M. Vafaei, M. Afrand, N. Sina, R. Kalbasi, F. Sourani, H. Teimouri, Evaluation of thermal conductivity of MgO-MWCNTs/EG hybrid nanofluids based on experimental data by selecting optimal artificial neural networks, Phys. E 85 (2017) 90–96, http://dx.doi.org/10.1016/j.physe.2016.08.020.
[434] M.H. Esfe, S. Esfandeh, S. Saedodin, H. Rostamian, Experimental evaluation, sensitivity analyzation and ANN modeling of thermal conductivity of ZnO-MWCNT/EG-water hybrid nanofluid for engineering applications, Appl. Therm. Eng. 125 (2017) 673–685, http://dx.doi.org/10.1016/j.applthermaleng.2017.06.077.
[435] S.S. Botha, P. Ndungu, B.J. Bladergroen, Physicochemical properties of oil-based nanofluids containing hybrid structures of silver nanoparticles supported on silica, Ind. Eng. Chem. Res. 50 (2011) 3071–3077, http://dx.doi.org/10.1021/ie101088x.
[436] M.J. Nine, B. Munkhbayar, M.S. Rahman, H. Chung, H. Jeong, Highly productive synthesis process of well dispersed Cu_2O and Cu/Cu_2O nanoparticles and its thermal characterization, Mater. Chem. Phys. 141 (2013) 636–642, http://dx.doi.org/10.1016/j.matchemphys.2013.05.032.
[437] S.S.J. Aravind, S. Ramaprabhu, Graphene-multiwalled carbon nanotube-based nanofluids for improved heat dissipation, RSC Adv. 3 (2013) 4199–4206, http://dx.doi.org/10.1039/C3RA22653K.
[438] M. Batmunkh, M.R. Tanshen, M.J. Nine, M. Myekhlai, H. Choi, H. Chung, H. Jeong, Thermal conductivity of TiO_2 nanoparticles based aqueous nanofluids with an addition of a modified silver particle, Ind. Eng. Chem. Res. 53 (2014) 8445–8451, http://dx.doi.org/10.1021/ie403712f.
[439] C.J. Ho, J.B. Huang, P.S. Tsai, Y.M. Yang, Preparation and properties of hybrid water-based suspension of Al_2O_3 nanoparticles and MEPCM particles as functional forced convection fluid, Int. Commun. Heat Mass Transfer 37 (2010) 490–494, http://dx.doi.org/10.1016/j.icheatmasstransfer.2009.12.007.
[440] D. Madhesh, R. Parameshwaran, S. Kalaiselvam, Experimental investigation on convective heat transfer and rheological characteristics of Cu-TiO_2 hybrid nanofluids, Exp. Therm. Fluid Sci. 52 (2014) 104–115, http://dx.doi.org/10.1016/j.expthermflusci.2013.08.026.
[441] M. Baghbanzadeh, A. Rashidi, D. Rashtchian, R. Lotfi, A. Amrollahi, Synthesis of spherical silica/multiwall carbon nanotubes hybrid nanostructures and investigation of thermal conductivity of related nanofluids, Thermochim. Acta 549 (2012) 87–94, http://dx.doi.org/10.1016/j.tca.2012.09.006.
[442] T.T. Baby, R. Sundara, Synthesis and transport properties of metal oxide decorated graphene dispersed nanofluids, J. Phys. Chem. C 115 (2011) 8527–8533, http://dx.doi.org/10.1021/jp200273g.
[443] L.S. Sundar, M.K. Singh, A.C.M. Sousa, Enhanced heat transfer and friction factor of MWCNT-Fe_3O_4/water hybrid nanofluids, Int. Commun. Heat Mass Transfer 52 (2014) 73–83, http://dx.doi.org/10.1016/j.icheatmasstransfer.2014.01.012.
[444] N.N. Esfahani, D. Toghraie, M. Afrand, A new correlation for predicting the thermal conductivity of ZnO–Ag (50%–50%)/water hybrid nanofluid: An experimental study, Powder Technol. 323 (2018) 367–373, http://dx.doi.org/10.1016/j.powtec.2017.10.025.
[445] M.J. Nine, M. Batmunkh, J.H. Kim, H.S. Chung, H.M. Jeong, Investigation of Al_2O_3-MWCNTs hybrid dispersion in water and their thermal characterization, J. Nanosci. Nanotechnol. 12 (2012) 4553–4559, http://dx.doi.org/10.1166/jnn.2012.6193.
[446] W. Lu, Q. Fan, Study for the particle's scale effect on some thermophysical properties of nanofluids by a simplified molecular dynamics method, Eng. Anal. Bound. Elem. 32 (2008) 282–289, http://dx.doi.org/10.1016/j.enganabound.2007.10.006.
[447] R.J. Sadus, Molecular Simulation of Fluids (Theory, Algorithms and Object-Orientation), Elsevier, New York, 1999.
[448] D.K. Dysthe, A.H. Fuchs, B. Rousseau, Prediction of fluid mixture transport properties by molecular dynamics, Int. J. Thermophys. 19 (1998) 437–448, http://dx.doi.org/10.1023/A:1022513411043.
[449] V.Y. Rudyak, A.A. Belkin, E.A. Tomilina, On the thermal conductivity of nanofluids, Tech. Phys. Lett. 36 (2010) 660–662, http://dx.doi.org/10.1134/S1063785010070229.

[450] E.M. Achhal, H. Jabraoui, S. Zeroual, H. Loulijat, A. Hasnaoui, S. Ouaskit, Modeling and simulations of nanofluids using classical molecular dynamics: Particle size and temperature effects on thermal conductivity, Adv. Powder Technol. 29 (2018) 2434–2439, http://dx.doi.org/10.1016/j.apt.2018.06.023.
[451] M.J. Javanmardi, K. Jafarpur, A molecular dynamics simulation for thermal conductivity evaluation of carbon nanotube-water nanofluids, J. Heat Transfer 135 (2013) 042401, http://dx.doi.org/10.1115/1.4022997.
[452] A. Mohebbi, Prediction of specific heat and thermal conductivity of nanofluids by a combined equilibrium and non-equilibrium molecular dynamics simulation, J. Mol. Liq. 175 (2012) 51–58, http://dx.doi.org/10.1016/j.molliq.2012.08.010.
[453] N. Sankar, N. Mathew, C.B. Sobhan, Molecular dynamics modeling of thermal conductivity enhancement in metal nanoparticle suspensions, Int. Commun. Heat Mass Transfer 35 (2008) 867–872, http://dx.doi.org/10.1016/j.icheatmasstransfer.2008.03.006.
[454] P. Keblinski, S.R. Phillpot, S.U.S. Choi, J.A. Eastman, Mechanisms of heat flow in suspensions of nano-sized particles (nanofluids), Int. J. Heat Mass Transfer 45 (2002) 855–863, http://dx.doi.org/10.1016/S0017-9310(01)00175-2.
[455] C. Sun, W. Lu, B. Bai, J. Liu, Anomalous enhancement in thermal conductivity of nanofluid induced by solid walls in a nanochannel, Appl. Therm. Eng. 31 (2011) 3799–3805, http://dx.doi.org/10.1016/j.applthermaleng.2011.07.021.
[456] W. Cui, Z. Shen, J. Yang, S. Wu, Effect of chaotic movements of nanoparticles for nanofluid heat transfer augmentation by molecular dynamics simulation, Appl. Therm. Eng. 76 (2015) 261–271, http://dx.doi.org/10.1016/j.applthermaleng.2014.11.030.
[457] H. Kang, Y. Zhang, M. Yang, L. Li, Molecular dynamics simulation on effect of nanoparticle aggregation on transport properties of a nanofluid, J. Nanotechnol. Eng. Med. 3 (2012) 021001, http://dx.doi.org/10.1115/1.4007044.
[458] S.L. Lee, R. Saidur, M.F.M. Sabri, T.K. Min, Molecular dynamic simulation on the thermal conductivity of nanofluids in aggregated and non-aggregated states, Numer. Heat Transfer A 68 (2015) 432–453, http://dx.doi.org/10.1080/10407782.2014.986366.
[459] W. Cui, Z. Shen, J. Yang, S. Wu, M. Bai, Influence of nanoparticle properties on the thermal conductivity of nanofluids by molecular dynamics simulation, RSC Adv. 4 (2014) 55580–55589, http://dx.doi.org/10.1039/c4ra07736a.
[460] W. Cui, M. Bai, J. Lv, G. Li, X. Li, On the influencing factors and strengthening mechanism for thermal conductivity of nanofluids by molecular dynamics simulation, Ind. Eng. Chem. Res. 50 (2011) 13568–13575, http://dx.doi.org/10.1021/ie201307w.
[461] Z. Liang, H.L. Tsai, Thermal conductivity of interfacial layers in nanofluids, Phys. Rev. E 83 (2011) 041602, http://dx.doi.org/10.1103/PhysRevE.83.041602.
[462] C. Pang, J.Y. Jung, J.W. Lee, Y.T. Kang, Thermal conductivity measurement of methanol-based nanofluids with Al_2O_3 and SiO_2 nanoparticles, Int. J. Heat Mass Transfer 55 (2012) 5597–5602, http://dx.doi.org/10.1016/j.ijheatmasstransfer.2012.05.048.
[463] W.H. Azmi, K.V. Sharma, P.K. Sarma, R. Mamat, G. Najafi, Heat transfer and friction factor of water based TiO_2 and SiO_2 nanofluids under turbulent flow in a tube, Int. Commun. Heat Mass Transfer 59 (2014) 30–38, http://dx.doi.org/10.1016/j.icheatmasstransfer.2014.10.007.
[464] W. Yu, H. Xie, D. Bao, Enhanced thermal conductivities of nanofluids containing graphene oxide nanosheets, Nanotechnology 21 (2010) http://dx.doi.org/10.1088/0957-4484/21/5/055705.
[465] W. Yu, H. Xie, W. Chen, Experimental investigation on thermal conductivity of nanofluids containing graphene oxide nanosheets, J. Appl. Phys. 107 (2010) 094317, http://dx.doi.org/10.1063/1.3372733.
[466] T.T. Baby, S. Ramaprabhu, Investigation of thermal and electrical conductivity of graphene based nanofluids, J. Appl. Phys. 108 (2010) 124308, http://dx.doi.org/10.1063/1.3516289.
[467] S.S. Gupta, V.M. Siva, S. Krishnan, T.S. Sreeprasad, P.K. Singh, T. Pradeep, S.K. Das, Thermal conductivity enhancement of nanofluids containing graphene nanosheets, J. Appl. Phys. 110 (2011) 084302, http://dx.doi.org/10.1063/1.3650456.
[468] R. Walvekar, I.A. Faris, M. Khalid, Thermal conductivity of carbon nanotube nanofluid-Experimental and theoretical study, Heat Transfer Res. 41 (2012) 145–163, http://dx.doi.org/10.1002/htj.20405.
[469] M.H. Esfe, S. Saedodin, O. Mahian, S. Wongwises, Thermophysical properties, heat transfer and pressure drop of COOH-functionalized multi walled carbon nanotubes/water nanofluids, Int. Commun. Heat Mass Transfer 58 (2014) 176–183, http://dx.doi.org/10.1016/j.icheatmasstransfer.2014.08.037.
[470] M.H. Esfe, S. Saedodin, O. Mahian, S. Wongwises, Heat transfer characteristics and pressure drop of COOH-functionalized DWCNTs/water nanofluid in turbulent flow at low concentrations, Int. J. Heat Mass Transfer 73 (2014) 186–194, http://dx.doi.org/10.1016/j.ijheatmasstransfer.2014.01.069.
[471] R. Taylor, S. Coulombe, T. Otanicar, P. Phelan, A. Gunawan, W. Lv, G. Rosengarten, R. Prasher, H. Tyagi, Small particles, big impacts: A review of the diverse applications of nanofluids, J. Appl. Phys. 113 (2013) 011301, http://dx.doi.org/10.1063/1.4754271.
[472] B.C. Pak, Y.I. Cho, Hydrodynamic and heat transfer study of dispersed fluids with submicron metallic oxide particles, Exp. Heat Transfer 11 (1998) 151–170, http://dx.doi.org/10.1080/08916159808946559.
[473] Y. Xuan, W. Roetzel, Conceptions for heat transfer correlation of nanofluids, Int. J. Heat Mass Transfer 43 (2000) 3701–3707, http://dx.doi.org/10.1016/S0017-9310(99)00369-5.
[474] B. Barbés, R. Páramo, E. Blanco, M.J. Pastoriza-Gallego, M.M. Piñeiro, J.L. Legido, C. Casanova, Thermal conductivity and specific heat capacity measurements of Al_2O_3 nanofluids, J. Therm. Anal. Calorim. 111 (2013) 1615–1625, http://dx.doi.org/10.1007/s10973-012-2534-9.
[475] A.T. Utomo, H. Poth, P.T. Robbins, A.W. Pacek, Experimental and theoretical studies of thermal conductivity, viscosity and heat transfer coefficient of titania and alumina nanofluids, Int. J. Heat Mass Transfer 55 (2012) 7772–7781, http://dx.doi.org/10.1016/j.ijheatmasstransfer.2012.08.003.
[476] D. Shin, D. Banerjee, Enhancement of specific heat capacity of high-temperature silica-nanofluids synthesized in alkali chloride salt eutectics for solar thermal-energy storage applications, Int. J. Heat Mass Transfer 54 (2011) 1064–1070, http://dx.doi.org/10.1016/j.ijheatmasstransfer.2010.11.017.
[477] A.K. Starace, J.C. Gomez, J. Wang, S. Pradhan, G.C. Glatzmaier, Nanofluid heat capacities, J. Appl. Phys. 110 (2011) 093123, http://dx.doi.org/10.1063/1.3672685.
[478] Y.R. Sekhar, K.V. Sharma, Study of viscosity and specific heat capacity characteristics of water-based Al_2O_3 nanofluids at low particle concentrations, J. Exp. Nanosci. 10 (2015) 86–102, http://dx.doi.org/10.1080/17458080.2013.796595.
[479] R.S. Vajjha, D.K. Das, A review and analysis on influence of temperature and concentration of nanofluids on thermophysical properties, heat transfer and pumping power, Int. J. Heat Mass Transfer 55 (2012) 4063–4078, http://dx.doi.org/10.1016/j.ijheatmasstransfer.2012.03.048.
[480] D. Cabaleiro, C. Gracia-Fernández, J.L. Legido, L. Lugo, Specific heat of metal oxide nanofluids at high concentrations for heat transfer, Int. J. Heat Mass Transfer 88 (2015) 872–879, http://dx.doi.org/10.1016/j.ijheatmasstransfer.2015.04.107.
[481] S. Zhou, R. Ni, Measurement of the specific heat capacity of water-based Al_2O_3 nanofluid, Appl. Phys. Lett. 92 (2008) 093123, http://dx.doi.org/10.1063/1.2890431.
[482] J. Buongiorno, Convective transport in nanofluids, J. Heat Transfer 128 (2006) 240–250, http://dx.doi.org/10.1115/1.2150834.
[483] D. Shin, D. Banerjee, Enhanced specific heat of silica nanofluid, J. Heat Transfer 133 (2010) 024501, http://dx.doi.org/10.1115/1.4002600.
[484] D. Shin, D. Banerjee, Specific heat of nanofluids synthesized by dispersing alumina nanoparticles in alkali salt eutectic, Int. J. Heat Mass Transfer 74 (2014) 210–214, http://dx.doi.org/10.1016/j.ijheatmasstransfer.2014.02.066.
[485] V. Kumaresan, R. Velraj, Experimental investigation of the thermo-physical properties of water-ethylene glycol mixture based CNT nanofluids, Thermochim. Acta 545 (2012) 180–186, http://dx.doi.org/10.1016/j.tca.2012.07.017.

[486] M.X. Ho, C. Pan, Optimal concentration of alumina nanoparticles in molten hitec salt to maximize its specific heat capacity, Int. J. Heat Mass Transfer 70 (2014) 174–184, http://dx.doi.org/10.1016/j.ijheatmasstransfer.2013.10.078.
[487] R. Raud, B. Hosterman, A. Diana, T.A. Steinberg, G. Will, Experimental study of the interactivity, specific heat, and latent heat of fusion of water based nanofluids, Appl. Therm. Eng. 117 (2017) 164–168, http://dx.doi.org/10.1016/j.applthermaleng.2017.02.033.
[488] Z. Jiang, C.T. Imrie, J.M. Hutchinson, An introduction to temperature modulated differential scanning calorimetry (TMDSC): A relatively non-mathematical approach, Thermochim. Acta 387 (2002) 75–93, http://dx.doi.org/10.1016/S0040-6031(01)00829-2.
[489] E. De Robertis, E.H.H. Cosme, R.S. Neves, A.Y. Kuznetsov, A.P.C. Campos, S.M. Landi, C.A. Achete, Application of the modulated temperature differential scanning calorimetry technique for the determination of the specific heat of copper nanofluids, Appl. Therm. Eng. 41 (2012) 10–17, http://dx.doi.org/10.1016/j.applthermaleng.2012.01.003.
[490] G. Żyła, J.P. Vallejo, J. Fal, L. Lugo, Nanodiamonds–Ethylene Glycol nanofluids: Experimental investigation of fundamental physical properties, Int. J. Heat Mass Transfer 121 (2018) 1201–1213, http://dx.doi.org/10.1016/j.ijheatmasstransfer.2018.01.073.
[491] S.M.S. Murshed, Determination of effective specific heat of nanofluids, J. Exp. Nanosci. 6 (2011) 539–546, http://dx.doi.org/10.1080/17458080.2010.498838.
[492] J.R. Satti, D.K. Das, D. Ray, Specific heat measurements of five different propylene glycol based nanofluids and development of a new correlation, Int. J. Heat Mass Transfer 94 (2016) 343–353, http://dx.doi.org/10.1016/j.ijheatmasstransfer.2015.11.065.
[493] H. O'Hanley, J. Buongiorno, T. McKrell, L.W. Hu, Measurement and model validation of nanofluid specific heat capacity with differential scanning calorimetry, Adv. Mech. Eng. 4 (2012) 181079, http://dx.doi.org/10.1155/2012/181079.
[494] S.P. Jang, J.H. Lee, K.S. Hwang, S.U.S. Choi, Particle concentration and tube size dependence of viscosities of Al_2O_3-water nanofluids flowing through micro- and minitubes, Appl. Phys. Lett. 91 (2007) 243112, http://dx.doi.org/10.1063/1.2824393.
[495] S. Halelfadl, T. Maré, P. Estellé, Efficiency of carbon nanotubes water based nanofluids as coolants, Exp. Therm. Fluid Sci. 53 (2014) 104–110, http://dx.doi.org/10.1016/j.expthermflusci.2013.11.010.
[496] A. Amiri, G. Ahmadi, M. Shanbedi, M. Etemadi, M.N.M. Zubir, B.T. Chew, S.N. Kazi, Heat transfer enhancement of water-based highly crumpled few-layer graphene nanofluids, RSC Adv. 6 (2016) 105508–105527, http://dx.doi.org/10.1039/c6ra22365f.
[497] H. Yarmand, S. Gharehkhani, S.F.S. Shirazi, A. Amiri, M.S. Alehashem, M. Dahari, S.N. Kazi, Experimental investigation of thermo-physical properties, convective heat transfer and pressure drop of functionalized graphene nanoplatelets aqueous nanofluid in a square heated pipe, Energy Convers. Manag. 114 (2016) 38–49, http://dx.doi.org/10.1016/j.enconman.2016.02.008.
[498] E.E. Michaelides, Variation of the expansion coefficient of nanofluids with temperature: A correction for conductivity data, J. Nanotechnol. Eng. Med. 3 (2013) 044502, http://dx.doi.org/10.1115/1.4024100.
[499] C.J. Ho, W.K. Liu, Y.S. Chang, C.C. Lin, Natural convection heat transfer of alumina-water nanofluid in vertical square enclosures: An experimental study, Int. J. Therm. Sci. 49 (2010) 1345–1353, http://dx.doi.org/10.1016/j.ijthermalsci.2010.02.013.
[500] S.Z. Heris, M.N. Esfahany, S.G. Etemad, Experimental investigation of convective heat transfer of Al_2O_3/water nanofluid in circular tube, Int. J. Heat Fluid Flow 28 (2007) 203–210, http://dx.doi.org/10.1016/j.ijheatfluidflow.2006.05.001.
[501] J. Li, C. Kleinstreuer, Thermal performance of nanofluid flow in microchannels, Int. J. Heat Fluid Flow 29 (2008) 1221–1232, http://dx.doi.org/10.1016/j.ijheatfluidflow.2008.01.005.
[502] B. Raei, F. Shahraki, M. Jamialahmadi, S.M. Peyghambarzadeh, Experimental study on the heat transfer and flow properties of γ-Al_2O_3/water nanofluid in a double-tube heat exchanger, J. Therm. Anal. Calorim. 127 (2017) 2561–2575, http://dx.doi.org/10.1007/s10973-016-5868-x.
[503] M. Sharifpur, S. Yousefi, J.P. Meyer, A new model for density of nanofluids including nanolayer, Int. Commun. Heat Mass Transfer 78 (2016) 168–174, http://dx.doi.org/10.1016/j.icheatmasstransfer.2016.09.010.
[504] R.S. Vajjha, D.K. Das, B.M. Mahagaonkar, Density measurement of different nanofluids and their comparison with theory, Pet. Sci. Technol. 27 (2009) 612–624, http://dx.doi.org/10.1080/10916460701857714.
[505] M.J. Pastoriza-Gallego, C. Casanova, J.L. Legido, M.M. Piñeiro, CuO in water nanofluid: Influence of particle size and polydispersity on volumetric behaviour and viscosity, Fluid Phase Equilib. 300 (2011) 188–196, http://dx.doi.org/10.1016/j.fluid.2010.10.015.
[506] A. Mariano, M.J. Pastoriza-Gallego, L. Lugo, A. Camacho, S. Canzonieri, M.M. Piñeiro, Thermal conductivity, rheological behaviour and density of non-Newtonian ethylene glycol-based SnO_2 nanofluids, Fluid Phase Equilib. 337 (2013) 119–124, http://dx.doi.org/10.1016/j.fluid.2012.09.029.
[507] S.D. Pandey, V.K. Nema, Experimental analysis of heat transfer and friction factor of nanofluid as a coolant in a corrugated plate heat exchanger, Exp. Therm. Fluid Sci. 38 (2012) 248–256, http://dx.doi.org/10.1016/j.expthermflusci.2011.12.013.
[508] M.N. Pantzali, A.G. Kanaris, K.D. Antoniadis, A.A. Mouza, S.V. Paras, Effect of nanofluids on the performance of a miniature plate heat exchanger with modulated surface, Int. J. Heat Fluid Flow 30 (2009) 691–699, http://dx.doi.org/10.1016/j.ijheatfluidflow.2009.02.005.
[509] A. Einstein, Eine neue bestimmung der molekuldimensionen, Ann. Phys. 19 (1906) 289–306, http://dx.doi.org/10.1002/andp.19063240204.
[510] H.C. Brinkman, The viscosity of concentrated suspensions and solutions, J. Chem. Phys. 20 (1952) 571, http://dx.doi.org/10.1063/1.1700493.
[511] G.K. Batchelor, The effect of Brownian motion on the bulk stress in a suspension of spherical particles, J. Fluid Mech. 83 (1977) 97–117, http://dx.doi.org/10.1017/S0022112077001062.
[512] N. Saito, Concentration dependence of the viscosity of high polymer solutions. I, J. Phys. Soc. Japan 5 (1950) 4–8, http://dx.doi.org/10.1143/JPSJ.5.4.
[513] A.L. Graham, On the viscosity of suspensions of solid spheres, Chem. Eng. 37 (1981) 275–286, http://dx.doi.org/10.1007/bf00951252.
[514] N.A. Frankel, A. Acrivos, On the viscosity of a concentrated suspension of solid spheres, Chem. Eng. Sci. 22 (1967) 847–853, http://dx.doi.org/10.1016/0009-2509(67)80149-0.
[515] N. Masoumi, N. Sohrabi, A. Behzadmehr, A new model for calculating the effective viscosity of nanofluids, J. Phys. D. Appl. Phys. 42 (2009) 055501, http://dx.doi.org/10.1088/0022-3727/42/5/055501.
[516] S.M. Hosseini, A.R. Moghadassi, D.E. Henneke, A new dimensionless group model for determining the viscosity of nanofluids, J. Therm. Anal. Calorim. 100 (2010) 873–877, http://dx.doi.org/10.1007/s10973-010-0721-0.
[517] J. Chevalier, O. Tillement, F. Ayela, Structure and rheology of SiO_2 nanoparticle suspensions under very high shear rates, Phys. Rev. E 80 (2009) 051403, http://dx.doi.org/10.1103/PhysRevE.80.051403.
[518] C.T. Nguyen, F. Desgranges, N. Galanis, G. Roy, T. Maré, S. Boucher, H.A. Mintsa, Viscosity data for Al_2O_3-water nanofluid-hysteresis: is heat transfer enhancement using nanofluids reliable? Int. J. Therm. Sci. 47 (2008) 103–111, http://dx.doi.org/10.1016/j.ijthermalsci.2007.01.033.
[519] T. Yiamsawas, O. Mahian, A.S. Dalkilic, S. Kaewnai, S. Wongwises, Experimental studies on the viscosity of TiO_2 and Al_2O_3 nanoparticles suspended in a mixture of ethylene glycol and water for high temperature applications, Appl. Energy 111 (2013) 40–45, http://dx.doi.org/10.1016/j.apenergy.2013.04.068.
[520] K. Walters, W.M. Jones, Measurement of viscosity, in: W. Boyes (Ed.), Instrum. Ref. B, fourth ed., Elsevier, 2010, pp. 69–75.
[521] J. Chevalier, O. Tillement, F. Ayela, Rheological properties of nanofluids flowing through microchannels, Appl. Phys. Lett. 91 (2007) 233103, http://dx.doi.org/10.1063/1.2821117.
[522] M. Jarahnejad, E.B. Haghighi, M. Saleemi, N. Nikkam, R. Khodabandeh, B. Palm, M.S. Toprak, M. Muhammed, Experimental investigation on viscosity of water-based Al_2O_3 and TiO_2 nanofluids, Rheol. Acta 54 (2015) 411–422, http://dx.doi.org/10.1007/s00397-015-0838-y.
[523] J. Chen, J. Jia, Experimental study of TiO_2 nanofluid coolant for automobile cooling applications, Mater. Res. Innov. 21 (2017) 177–181, http://dx.doi.org/10.1080/14328917.2016.1198549.

[524] A.S. Dalkilic, B.O Küçükyıldırım, A. Akdogan Eker, A. Çebi, S. Tapan, C. Jumpholkul, S. Wongwises, Experimental investigation on the viscosity of Water-CNT and Antifreeze-CNT nanofluids, Int. Commun. Heat Mass Transfer 80 (2017) 47–59, http://dx.doi.org/10.1016/j.icheatmasstransfer.2016.11.011.
[525] E.V. Timofeeva, A.N. Gavrilov, J.M. McCloskey, Y.V. Tolmachev, S. Sprunt, L.M. Lopatina, J.V. Selinger, Thermal conductivity and particle agglomeration in alumina nanofluids: Experiment and theory, Phys. Rev. E 76 (2007) 28–39, http://dx.doi.org/10.1103/PhysRevE.76.061203.
[526] M.M. Heyhat, F. Kowsary, A.M. Rashidi, S. Alem Varzane Esfehani, A. Amrollahi, Experimental investigation of turbulent flow and convective heat transfer characteristics of alumina water nanofluids in fully developed flow regime, Int. Commun. Heat Mass Transfer 39 (2012) 1272–1278, http://dx.doi.org/10.1016/j.icheatmasstransfer.2012.06.024.
[527] E.M.C. Contreras, G.A. Oliveira, E.P. Bandarra Filho, Experimental analysis of the thermohydraulic performance of graphene and silver nanofluids in automotive cooling systems, Int. J. Heat Mass Transfer 132 (2019) 375–387, http://dx.doi.org/10.1016/j.ijheatmasstransfer.2018.12.014.
[528] A.V. Minakov, V.Y. Rudyak, D.V. Guzei, A.S. Lobasov, Measurement of the heat transfer coefficient of a nanofluid based on water and copper oxide particles in a cylindrical channel, High Temp. 53 (2015) 246–253, http://dx.doi.org/10.1134/S0018151X15020169.
[529] G. Żyła, J. Fal, P. Estellé, Thermophysical and dielectric profiles of ethylene glycol based titanium nitride (TiN–EG) nanofluids with various size of particles, Int. J. Heat Mass Transfer 113 (2017) 1189–1199, http://dx.doi.org/10.1016/j.ijheatmasstransfer.2017.06.032.
[530] M.J. Pastoriza-Gallego, L. Lugo, J.L. Legido, M.M. Piñeiro, Rheological non-Newtonian behaviour of ethylene glycol-based Fe_2O_3 nanofluids, Nanoscale Res. Lett. 6 (2011) 560, http://dx.doi.org/10.1186/1556-276X-6-560.
[531] G. Żyła, J. Fal, Experimental studies on viscosity, thermal and electrical conductivity of aluminum nitride-ethylene glycol (AlN-EG) nanofluids, Thermochim. Acta 637 (2016) 11–16, http://dx.doi.org/10.1016/j.tca.2016.05.006.
[532] M.H. Esfe, A.A.A. Arani, M. Rezaie, W.M. Yan, A. Karimipour, Experimental determination of thermal conductivity and dynamic viscosity of Ag-MgO/water hybrid nanofluid, Int. Commun. Heat Mass Transfer 66 (2015) 189–195, http://dx.doi.org/10.1016/j.icheatmasstransfer.2015.06.003.
[533] M. Asadi, A. Asadi, Dynamic viscosity of MWCNT/ZnO-engine oil hybrid nanofluid: An experimental investigation and new correlation in different temperatures and solid concentrations, Int. Commun. Heat Mass Transfer 76 (2016) 41–45, http://dx.doi.org/10.1016/j.icheatmasstransfer.2016.05.019.
[534] G. Żyła, J. Fal, S. Bikić, M. Wanic, Ethylene glycol based silicon nitride nanofluids: An experimental study on their thermophysical, electrical and optical properties, Phys. E Low-Dimens. Syst. Nanostruct. 104 (2018) 82–90, http://dx.doi.org/10.1016/j.physe.2018.07.023.
[535] G. Żyła, J. Fal, P. Estellé, The influence of ash content on thermophysical properties of ethylene glycol based graphite/diamonds mixture nanofluids, Diam. Relat. Mater. 74 (2017) 81–89, http://dx.doi.org/10.1016/j.diamond.2017.02.008.
[536] G. Żyła, M. Cholewa, On unexpected behavior of viscosity of diethylene glycol-based $MgAl_2O_4$ nanofluids, RSC Adv. 4 (2014) 26057–26062, http://dx.doi.org/10.1039/c4ra03143a.
[537] G. Żyła, M. Cholewa, A. Witekb, Rheological properties of diethylene glycol-based $MgAl_2O_4$ nanofluid, RSC Adv. 3 (2013) 6429–6434, http://dx.doi.org/10.1039/c3ra40187a.
[538] T. Yiamsawas, A.S. Dalkilic, O. Mahian, S. Wongwises, Measurement and correlation of the viscosity of water-based Al_2O_3 and TiO_2 nanofluids in high temperatures and comparisons with literature reports, J. Dispers. Sci. Technol. 34 (2013) 1697–1703, http://dx.doi.org/10.1080/01932691.2013.764483.
[539] M.H. Esfe, M. Afrand, S. Gharehkhani, H. Rostamian, D. Toghraie, M. Dahari, An experimental study on viscosity of alumina-engine oil: Effects of temperature and nanoparticles concentration, Int. Commun. Heat Mass Transfer 76 (2016) 202–208, http://dx.doi.org/10.1016/j.icheatmasstransfer.2016.05.013.
[540] D. Toghraie, S.M. Alempour, M. Afrand, Experimental determination of viscosity of water based magnetite nanofluid for application in heating and cooling systems, J. Magn. Magn. Mater. 417 (2016) 243–248, http://dx.doi.org/10.1016/j.jmmm.2016.05.092.
[541] J. Yang, F. Li, W. Zhou, Y. He, B. Jiang, Experimental investigation on the thermal conductivity and shear viscosity of viscoelastic-fluid-based nanofluids, Int. J. Heat Mass Transfer 55 (2012) 3160–3166, http://dx.doi.org/10.1016/j.ijheatmasstransfer.2012.02.052.
[542] M. Sharifpur, S.A. Adio, J.P. Meyer, Experimental investigation and model development for effective viscosity of Al_2O_3-glycerol nanofluids by using dimensional analysis and GMDH-NN methods, Int. Commun. Heat Mass Transfer 68 (2015) 208–219, http://dx.doi.org/10.1016/j.icheatmasstransfer.2015.09.002.
[543] N. Ahammed, L.G. Asirvatham, S. Wongwises, Effect of volume concentration and temperature on viscosity and surface tension of graphene-water nanofluid for heat transfer applications, J. Therm. Anal. Calorim. 123 (2016) 1399–1409, http://dx.doi.org/10.1007/s10973-015-5034-x.
[544] M. Baratpour, A. Karimipour, M. Afrand, S. Wongwises, Effects of temperature and concentration on the viscosity of nanofluids made of single-wall carbon nanotubes in ethylene glycol, Int. Commun. Heat Mass Transfer 74 (2016) 108–113, http://dx.doi.org/10.1016/j.icheatmasstransfer.2016.02.008.
[545] S.M.S. Murshed, F.J.V. Santos, C.A. de Castro, Investigations of viscosity of silicone oil-based semiconductor nanofluids, J. Nanofluids 2 (2013) 261–266, http://dx.doi.org/10.1166/jon.2013.1062.
[546] K. Bashirnezhad, S. Bazri, M.R. Safaei, M. Goodarzi, M. Dahari, O. Mahian, A.S. Dalkiliça, S. Wongwises, Viscosity of nanofluids: A review of recent experimental studies, Int. Commun. Heat Mass Transfer 73 (2016) 114–123, http://dx.doi.org/10.1016/j.icheatmasstransfer.2016.02.005.
[547] L. Chen, H. Xie, Y. Li, W. Yu, Nanofluids containing carbon nanotubes treated by mechanochemical reaction, Thermochim. Acta 477 (2008) 21–24, http://dx.doi.org/10.1016/j.tca.2008.08.001.
[548] L. Chen, H. Xie, W. Yu, Y. Li, Rheological behaviors of nanofluids containing multi-walled carbon nanotube, J. Dispers. Sci. Technol. 32 (2011) 550–554, http://dx.doi.org/10.1080/01932691003757223.
[549] G. Żyła, J. Fal, Viscosity, thermal and electrical conductivity of silicon dioxide–ethylene glycol transparent nanofluids: An experimental studies, Thermochim. Acta 650 (2017) 106–113, http://dx.doi.org/10.1016/j.tca.2017.02.001.
[550] M.Z. Sharif, W.H. Azmi, A.A.M. Redhwan, R. Mamat, Investigation of thermal conductivity and viscosity of Al_2O_3/PAG nanolubricant for application in automotive air conditioning system, Int. J. Refrig. 70 (2016) 93–102, http://dx.doi.org/10.1016/j.ijrefrig.2016.06.025.
[551] K.S. Suganthi, N. Anusha, K.S. Rajan, Low viscous ZnO-propylene glycol nanofluid: A potential coolant candidate, J. Nanopart. Res. 15 (2013) 1986, http://dx.doi.org/10.1007/s11051-013-1986-6.
[552] J.P. Meyer, S.A. Adio, M. Sharifpur, P.N. Nwosu, The viscosity of nanofluids: A review of the theoretical, empirical, and numerical models, Heat Transfer Eng. 37 (2016) 387–421, http://dx.doi.org/10.1080/01457632.2015.1057447.
[553] C.T. Nguyen, F. Desgranges, G. Roy, N. Galanis, T. Maré, S. Boucher, H.A. Mintsa, Temperature and particle-size dependent viscosity data for water-based nanofluids-hysteresis phenomenon, Int. J. Heat Fluid Flow 28 (2007) 1492–1506, http://dx.doi.org/10.1016/j.ijheatfluidflow.2007.02.004.
[554] K.B. Anoop, T. Sundararajan, S.K. Das, Effect of particle size on the convective heat transfer in nanofluid in the developing region, Int. J. Heat Mass Transfer 52 (2009) 2189–2195, http://dx.doi.org/10.1016/j.ijheatmasstransfer.2007.11.063.
[555] D. Kwek, A. Crivoi, F. Duan, Effects of temperature and particle size on the thermal property measurements of Al_2O_3-water nanofluids, J. Chem. Eng. 55 (2010) 5690–5695, http://dx.doi.org/10.1021/je1006407.

[556] P.K. Namburu, D.P. Kulkarni, A. Dandekar, D.K. Das, Experimental investigation of viscosity and specific heat of silicon dioxide nanofluids, Micro Nano Lett. 2 (2007) 27–71, http://dx.doi.org/10.1049/mnl:20070037.
[557] E.V. Timofeeva, W. Yu, D.M. France, D. Singh, J.L. Routbort, Nanofluids for heat transfer: An engineering approach, Nanoscale Res. Lett. 6 (2011) 182, http://dx.doi.org/10.1186/1556-276X-6-182.
[558] J. Zhao, Z. Luo, M. Ni, K. Cen, Dependence of nanofluid viscosity on particle size and pH value, Chin. Phys. Lett. 26 (2009) 066202, http://dx.doi.org/10.1088/0256-307X/26/6/066202.
[559] C.T. Wamkam, M.K. Opoku, H. Hong, P. Smith, Effects of pH on heat transfer nanofluids containing ZrO_2 and TiO_2 nanoparticles, J. Appl. Phys. 109 (2011) 024305, http://dx.doi.org/10.1063/1.3532003.
[560] X. Wang, X. Li, Influence of pH on nanofluids' viscosity and thermal conductivity, Chin. Phys. Lett. 26 (2009) 056601, http://dx.doi.org/10.1088/0256-307X/26/5/056601.
[561] Babita, S.K. Sharma, S.M. Gupta, Preparation and evaluation of stable nanofluids for heat transfer application: A review, Exp. Therm. Fluid Sci. 79 (2016) 202–212, http://dx.doi.org/10.1016/j.expthermflusci.2016.06.029.
[562] B. Ruan, A.M. Jacobi, Ultrasonication effects on thermal and rheological properties of carbon nanotube suspensions, Nanoscale Res. Lett. 7 (2012) 127, http://dx.doi.org/10.1186/1556-276X-7-127.
[563] I.M. Mahbubul, T.H. Chong, S.S. Khaleduzzaman, I.M. Shahrul, R. Saidur, B.D. Long, M.A. Amalina, Effect of ultrasonication duration on colloidal structure and viscosity of alumina-water nanofluid, Ind. Eng. Chem. Res. 53 (2014) 6677–6684, http://dx.doi.org/10.1021/ie500705j.
[564] Y. Yang, E.A. Grulke, Z.G. Zhang, G. Wu, Thermal and rheological properties of carbon nanotube-in-oil dispersions, J. Appl. Phys. 99 (2006) 114307, http://dx.doi.org/10.1063/1.2193161.
[565] A. Menbari, A.A. Alemrajabi, Y. Ghayeb, Investigation on the stability, viscosity and extinction coefficient of CuO-Al_2O_3/Water binary mixture nanofluid, Exp. Therm. Fluid Sci. 74 (2016) 122–129, http://dx.doi.org/10.1016/j.expthermflusci.2015.11.025.
[566] M. Silambarasan, S. Manikandan, K.S. Rajan, Viscosity and thermal conductivity of dispersions of sub-micron TiO_2 particles in water prepared by stirred bead milling and ultrasonication, Int. J. Heat Mass Transfer 55 (2012) 7991–8002, http://dx.doi.org/10.1016/j.ijheatmasstransfer.2012.08.030.
[567] W. Williams, J. Buongiorno, L.W. Hu, Experimental investigation of turbulent convective heat transfer and pressure loss of Alumina/water and Zirconia/water nanoparticle colloids (nanofluids) in horizontal tubes, J. Heat Transfer 130 (2008) 042412, http://dx.doi.org/10.1115/1.2818775.
[568] S. Murshed, K. Leong, C. Yang, Thermophysical properties of nanofluids, in: K.D. Sattler (Ed.), Handb. Nanophysics Nanoparticles Quantum Qots, CRC press, Boca Raton, 2010, p. 32, (1–14).
[569] P.K. Namburu, D.P. Kulkarni, D. Misra, D.K. Das, Viscosity of copper oxide nanoparticles dispersed in ethylene glycol and water mixture, Exp. Therm. Fluid Sci. 32 (2007) 397–402, http://dx.doi.org/10.1016/j.expthermflusci.2007.05.001.
[570] L.S. Sundar, M.K. Singh, A.C.M. Sousa, Investigation of thermal conductivity and viscosity of Fe_3O_4 nanofluid for heat transfer applications, Int. Commun. Heat Mass Transfer 44 (2013) 7–14, http://dx.doi.org/10.1016/j.icheatmasstransfer.2013.02.014.
[571] H. Xie, W. Yu, W. Chen, MgO nanofluids: Higher thermal conductivity and lower viscosity among ethylene glycol-based nanofluids containing oxide nanoparticles, J. Exp. Nanosci. 5 (2010) 463–472, http://dx.doi.org/10.1080/17458081003628949.
[572] V.Y. Rudyak, S.V. Dimov, V.V. Kuznetsov, S.P. Bardakhanov, Measurement of the viscosity coefficient of an ethylene glycol-based nanofluid with silicon-dioxide particles, Dokl. Phys. 58 (2013) 173–176, http://dx.doi.org/10.1134/s1028335813050042.
[573] M. Kole, T.K. Dey, Investigation of thermal conductivity, viscosity, and electrical conductivity of graphene based nanofluids, J. Appl. Phys. 113 (2013) 084307, http://dx.doi.org/10.1063/1.4793581.
[574] S. Harish, K. Ishikawa, E. Einarsson, S. Aikawa, T. Inoue, P. Zhao, M. Watanabe, S. Chiashi, J. Shiomi, S. Maruyama, Temperature Dependent Thermal Conductivity increase of aqueous nanofluid with single walled carbonnanotube inclusion, Mater. Express 2 (2012) 213–223, http://dx.doi.org/10.1166/mex.2012.1074.
[575] M. Afrand, K.N. Najafabadi, M. Akbari, Effects of temperature and solid volume fraction on viscosity of SiO_2-MWCNTs/SAE40 hybrid nanofluid as a coolant and lubricant in heat engines, Appl. Therm. Eng. 102 (2016) 45–54, http://dx.doi.org/10.1016/j.applthermaleng.2016.04.002.
[576] M.H. Esfe, M. Afrand, S.H. Rostamian, D. Toghraie, Examination of rheological behavior of MWCNTs/ZnO-SAE40 hybrid nano-lubricants under various temperatures and solid volume fractions, Exp. Therm. Fluid Sci. 80 (2017) 384–390, http://dx.doi.org/10.1016/j.expthermflusci.2016.07.011.
[577] E. Dardan, M. Afrand, A.H. Meghdadi Isfahani, Effect of suspending hybrid nano-additives on rheological behavior of engine oil and pumping power, Appl. Therm. Eng. 109 (2016) 524–534, http://dx.doi.org/10.1016/j.applthermaleng.2016.08.103.
[578] O. Soltani, M. Akbari, Effects of temperature and particles concentration on the dynamic viscosity of MgO-MWCNT/ethylene glycol hybrid nanofluid: Experimental study, Phys. E Low-Dimens. Syst. Nanostruct. 84 (2016) 564–570, http://dx.doi.org/10.1016/j.physe.2016.06.015.
[579] S. Akilu, A.T. Baheta, M.A.M. Said, A.A. Minea, K.V. Sharma, Properties of glycerol and ethylene glycol mixture based SiO_2-CuO/C hybrid nanofluid for enhanced solar energy transport, Sol. Energy Mater. Sol. Cells 179 (2018) 118–128, http://dx.doi.org/10.1016/j.solmat.2017.10.027.
[580] G.R. Vakili-Nezhaad, M. Mohammadi, A.M. Gujarathi, M. Al-Wadhahi, R. Al-Maamari, Molecular dynamics simulation of water–graphene nanofluid, SN Appl. Sci. 1 (2019) 214, http://dx.doi.org/10.1007/s42452-019-0224-y.
[581] V.Y. Rudyak, S.L. Krasnolutskii, Simulation of the nanofluid viscosity coefficient by the molecular dynamics method, Tech. Phys. 60 (2015) 798–804, http://dx.doi.org/10.1134/S1063784215060237.
[582] Z. Lou, M. Yang, Molecular dynamics simulations on the shear viscosity of Al_2O_3 nanofluids, Comput. Fluids 117 (2015) 17–23, http://dx.doi.org/10.1016/j.compfluid.2015.05.006.
[583] G.R. Vakili-Nezhaad, M. Al-Wadhahi, A.M. Gujrathi, R. Al-Maamari, M. Mohammadi, Effect of temperature and diameter of narrow single-walled carbon nanotubes on the viscosity of nanofluid: A molecular dynamics study, Fluid Phase Equilib. 434 (2017) 193–199, http://dx.doi.org/10.1016/j.fluid.2016.11.032.
[584] F. Jabbari, A. Rajabpour, S. Saedodin, Viscosity of carbon nanotube/water nanofluid, J. Therm. Anal. Calorim. 135 (2019) 1787–1796, http://dx.doi.org/10.1007/s10973-018-7458-6.
[585] F. Jabbari, S. Saedodin, A. Rajabpour, Experimental investigation and molecular dynamics simulations of viscosity of CNT-water nanofluid at different temperatures and volume fractions of nanoparticles, J. Chem. Eng. Data 64 (2019) 262–272, http://dx.doi.org/10.1021/acs.jced.8b00783.
[586] S. Zeroual, H. Loulijat, E. Achehal, P. Estellé, A. Hasnaoui, S. Ouaskit, Viscosity of Ar-Cu nanofluids by molecular dynamics simulations: Effects of nanoparticle content, temperature and potential interaction, J. Mol. Liq. 268 (2018) 490–496, http://dx.doi.org/10.1016/j.molliq.2018.07.090.
[587] A. Belianinov, R. Vasudevan, E. Strelcov, C. Steed, S.M. Yang, A. Tselev, S. Jesse, M. Biegalski, G. Shipman, C. Symons, A. Borisevich, R. Archibald, S. Kalinin, Big data and deep data in scanning and electron microscopies: deriving functionality from multidimensional data sets, Adv. Struct. Chem. Imaging 1 (2015) 6, http://dx.doi.org/10.1186/s40679-015-0006-6.
[588] L.A. Wilson, Survey on Big Data gathers input from materials community, MRS Bull. 38 (2013) 751–753, http://dx.doi.org/10.1557/mrs.2013.225.
[589] M. Hojjat, S.G. Etemad, R. Bagheri, J. Thibault, Thermal conductivity of non-Newtonian nanofluids: Experimental data and modeling using neural network, Int. J. Heat Mass Transfer 54 (2011) 1017–1023, http://dx.doi.org/10.1016/j.ijheatmasstransfer.2010.11.039.
[590] M.H. Esfe, M. Afrand, S. Wongwises, A. Naderi, A. Asadi, S. Rostami, M. Akbari, Applications of feedforward multilayer perceptron artificial neural networks and empirical correlation for prediction of thermal conductivity of $Mg(OH)_2$-EG using experimental data, Int. Commun. Heat Mass Transfer 67 (2015) 46–50, http://dx.doi.org/10.1016/j.icheatmasstransfer.2015.06.015.

[591] S. Khosrojerdi, M. Vakili, M. Yahyaei, K. Kalhor, Thermal conductivity modeling of graphene nanoplatelets/deionized water nanofluid by MLP neural network and theoretical modeling using experimental results, Int. Commun. Heat Mass Transfer 74 (2016) 11–17, http://dx.doi.org/10.1016/j.icheatmasstransfer.2016.03.010.
[592] M.H. Esfe, W.M. Yan, M. Afrand, M. Sarraf, D. Toghraie, M. Dahari, Estimation of thermal conductivity of Al_2O_3/water (40%)-ethylene glycol (60%) by artificial neural network and correlation using experimental data, Int. Commun. Heat Mass Transfer 74 (2016) 125–128, http://dx.doi.org/10.1016/j.icheatmasstransfer.2016.02.002.
[593] F. Yousefi, S. Mohammadiyan, H. Karimi, Application of artificial neural network and PCA to predict the thermal conductivities of nanofluids, Heat Mass Transfer 52 (2016) 2141–2154, http://dx.doi.org/10.1007/s00231-015-1730-0.
[594] M. Afrand, D. Toghraie, N. Sina, Experimental study on thermal conductivity of water-based Fe_3O_4 nanofluid: Development of a new correlation and modeled by artificial neural network, Int. Commun. Heat Mass Transfer 75 (2016) 262–269, http://dx.doi.org/10.1016/j.icheatmasstransfer.2016.04.023.
[595] M. Mehrabi, M. Sharifpur, J.P. Meyer, Application of the FCM-based neuro-fuzzy inference system and genetic algorithm-polynomial neural network approaches to modelling the thermal conductivity of alumina-water nanofluids, Int. Commun. Heat Mass Transfer 39 (2012) 971–977, http://dx.doi.org/10.1016/j.icheatmasstransfer.2012.05.017.
[596] J.A. Esfahani, M.R. Safaei, M. Goharimanesh, L.R. de Oliveira, M. Goodarzi, S. Shamshirband, E.P.B. Filho, Comparison of experimental data, modelling and non-linear regression on transport properties of mineral oil based nanofluids, Powder Technol. 317 (2017) 458–470, http://dx.doi.org/10.1016/j.powtec.2017.04.034.
[597] M. Sadi, Prediction of thermal conductivity and viscosity of ionic liquid-based nanofluids using adaptive neuro fuzzy inference system, Heat Transfer Eng. 38 (2017) 1561–1572, http://dx.doi.org/10.1080/01457632.2016.1262720.
[598] A. Shahsavar, S. Khanmohammadi, A. Karimipour, M. Goodarzi, A novel comprehensive experimental study concerned synthesizes and prepare liquid paraffin-Fe_3O_4 mixture to develop models for both thermal conductivity & viscosity: A new approach of GMDH type of neural network, Int. J. Heat Mass Transfer 131 (2019) 432–441, http://dx.doi.org/10.1016/j.ijheatmasstransfer.2018.11.069.
[599] A. Aminian, Predicting the effective thermal conductivity of nanofluids for intensification of heat transfer using artificial neural network, Powder Technol. 301 (2016) 288–309, http://dx.doi.org/10.1016/j.powtec.2016.05.040.
[600] N. Zhao, Z. Li, Experiment and artificial neural network prediction of thermal conductivity and viscosity for Alumina-water nanofluids, Mater. (Basel) 10 (2017) 552, http://dx.doi.org/10.3390/ma10050552.
[601] S.K. Mechiri, V. Vasu, G.A. Venu, S.R. Babu, Thermal conductivity of Cu-Zn hybrid newtonian nanofluids: Experimental data and modeling using neural network, Procedia Eng. 127 (2015) 561–567, http://dx.doi.org/10.1016/j.proeng.2015.11.345.
[602] M.H. Esfe, M. Rejvani, R. Karimpour, A.A. Abbasian Arani, Estimation of thermal conductivity of ethylene glycol-based nanofluid with hybrid suspensions of SWCNT–Al_2O_3 nanoparticles by correlation and ANN methods using experimental data, J. Therm. Anal. Calorim. 128 (2017) 1359–1371, http://dx.doi.org/10.1007/s10973-016-6002-9.
[603] M.H. Esfe, P.M. Behbahani, A.A.A. Arani, M.R. Sarlak, Thermal conductivity enhancement of SiO_2–MWCNT (85:15%)–EG hybrid nanofluids, J. Therm. Anal. Calorim. 128 (2016) 249–258, http://dx.doi.org/10.1007/s10973-016-5893-9.
[604] A. Shahsavar, M. Bahiraei, Experimental investigation and modeling of thermal conductivity and viscosity for non-Newtonian hybrid nanofluid containing coated CNT/Fe_3O_4 nanoparticles, Powder Technol. 318 (2017) 441–450, http://dx.doi.org/10.1016/j.powtec.2017.06.023.
[605] H.H. Balla, S. Abdullah, W.M.F. Wanmahmood, M. Abdul Razzaq, R. Zulkifli, K. Sopian, Modelling and measuring the thermal conductivity of multi-metallic Zn/Cu nanofluid, Res. Chem. Intermed. 39 (2013) 2801–2815, http://dx.doi.org/10.1007/s11164-012-0799-z.
[606] A. Karimipour, S.A. Bagherzadeh, M. Goodarzi, A.A. Alnaqi, M. Bahiraei, M.R. Safaei, M.S. Shadloo, Synthesized $CuFe_2O_4/SiO_2$ nanocomposites added to water/EG: Evaluation of the thermophysical properties beside sensitivity analysis & EANN, Int. J. Heat Mass Transfer 127 (2018) 1169–1179, http://dx.doi.org/10.1016/j.ijheatmasstransfer.2018.08.112.
[607] S.A. Bagherzadeh, A. D'Orazio, A. Karimipour, M. Goodarzi, Q.V. Bach, A novel sensitivity analysis model of EANN for F-MWCNTs-Fe_3O_4/EG nanofluid thermal conductivity: Outputs predicted analytically instead of numerically to more accuracy and less costs, Physica A 521 (2019) 406–415, http://dx.doi.org/10.1016/j.physa.2019.01.048.